A STABLE ISOTOPE STUDY OF WATER AND CHLORIDE MOVEMENT IN NATURAL DESERT SOILS

By

Robert G. Knowlton, Jr.

Submitted in Partial Fulfillment of the
Requirements for the Degree of Doctor of Philosophy
in Geoscience (Hydrology)

New Mexico Institute of Mining and Technology

Socorro, New Mexico

May 1990

ABSTRACT

The quantification of recharge in arid regions is very important to scientists, engineers, and water resource planners for agricultural irrigation, drinking water supply, and economic development. Arid environments have been suggested for hazardous waste disposal applications. An understanding of soil-water and solute transport processes in natural, unsaturated desert soils is essential for quantifying recharge. This study presents the results of an effort in which existing theory was modified and applied to an arid site to estimate the liquid- and vapor-phase fluxes. Experimental results thus obtained enhance our current understanding of these processes.

A mathematical model developed by C.Barnes and G.Allison was used as the basis for a numerical model which is capable of quantifying the liquid and vapor-flux portions of soil-water movement in the vadose zone. The model is based on the lower volatility of $H_2{}^{16}O$ compared to $H_2{}^{18}O$ and $HD^{16}O$, and therefore the distribution of ^{2}H (or D) and ^{18}O can be used as tracers for evaporation and water-vapor movement. Through a non-linear least-squares approach, the non-isothermal, quasi-steady state model response is matched to an observed isotope profile by optimizing the values of the following input parameters: the recharge rate, the liquid tortuosity factor, and the vapor tortuosity factor. The fitted parameters are then used in solving numerically for the liquid and vapor fluxes as a function of depth. This method of estimating soil-water flow is fairly robust because the relative diffusivities of the isotopic species vary little with water content.

A new vacuum distillation technique for extraction of soil water was developed during this project. Samples extracted by this method are reproducible within $\pm$ 0.15 $^{\circ}/_{oo}$ (permil) for $\delta^{18}O$ and $\pm$ 1.2 $^{\circ}/_{oo}$ for δD.

Experimental data was collected at a research site in a desert lowland in central New Mexico for use with the numerical stable-isotope model. A comparison of summer and winter model results suggests that there is a net annual downward vapor flux of soil water within the top meter of the profile. During the summer months, below a depth of about 0.1 meters, the vapor flux portion of soil-water movement is downward in response to a temperature induced vapor-pressure gradient. Simultaneously, the liquid flux is upward from about 0.3 meters in depth in response to capillary pressure gradients brought about by the evaporative demand at the land surface. Therefore, between 0.1 and 0.3 meters conservative solutes will move upward and volatile constituents will move downward, simultaneously. This phenomenon leads to markedly different distributions of conservative versus volatile solutes. The distribution of bomb-pulse ^{36}Cl and tritium (^{3}H) was measured in a previous study at the same research site. That study found that the bulk of the ^{36}Cl, a conservative solute, was located in the top meter of the profile, whereas the majority of the tritium

ABSTRACT
(continued)

was located within the two to three meter depth range; this distribution of conservative and volatile tracers is consistent with the liquid- and vapor-flux patterns indicated by the stable-isotope data from this study.

The stable-isotope model used in this study may be applied to estimate the recharge rate. According to the model, the recharge rate is approximately 0.9 cm/yr, or about 4 percent of the average annual precipitation. This compares favorably with independent estimates at the same site by previous investigators.

TABLE OF CONTENTS

TABLE OF CONTENTS
(Continued)

LIST OF FIGURES

LIST OF FIGURES
(continued)

LIST OF FIGURES
(continued)

LIST OF FIGURES
(continued)

LIST OF FIGURES
(continued)

LIST OF TABLES

ACKNOWLEDGMENTS

Dr. Fred M. Phillips has my utmost respect and gratitude for serving as my advisor. His encouragement and guidance has been invaluable. I am also indebted to the other members of my committee for their help and support: Dr. Andrew Campbell for his expertise in the laboratory; Dr. Daniel B. Stephens for his input on soil physics; Dr. John L. Wilson for his views on heat and moisture flow; and Dr. Peter Wierenga for his knowledge of heat flow, and for the use of the line-source thermal conductivity probe. Dr. Bill Rison has been very patient directing me in constructing several electronic components that he designed, which were essential tools in my research. The numerous other staff members, graduate and undergraduate students who have assisted me in both the laboratory and field are specially commended, given the amount of patience they must have had.

I would like to thank the staff of the Sevilleta National Wildlife Refuge for all their support and cooperation. Mr. Ted Stans has been especially helpful through the years of research carried out at the site.

The New Mexico Water Resources Research Institute funded most of this research and my graduate stipend through grants on project number 1345644. I am indebted to this organization, and hope that this type of support continues for others.

The most important thanks of all goes to my wife, Jan Quigley. Without her love and support throughout these years I would not have made this accomplishment. I am truly grateful for all that she has given me, and hope that I can now do the same for her. My parents and family have also given me the confidence and support needed to pursue this degree, and I am sincerely grateful.

1. INTRODUCTION

Ground water constitutes the sole water supply in much of New Mexico. Long-term availability of ground water is thus the primary limitation to economic development in many cases. This hydrologic reality has long been recognized by New Mexico water law through its control of ground-water withdrawal in basins which are threatened by overdraft. The goal of the legal regulation of pumping is to provide the maximum sustainable long-term water yield. This long-term yield is dependent not only on pumping rates, but also on the groundwater recharge rate. Knowledge of the recharge rate thus has important implications for the economic development of the state.

Many authors (e.g., Falconer et al., 1982; Mann, 1976) have maintained that there is no direct recharge of ground water by infiltration of precipitation through the vadose zone of arid regions. Although this concept may be valid for some circumstances, localities exist in arid (and even hyperarid) environments which act as aquifer recharge areas due to incident precipitation (Verhagen et al., 1979; Dincer et al., 1974; Bergstrom and Aten, 1965). The extent and importance of this type of recharge has probably been obscured due to misunderstanding of the behavior of soil water in desert regions. Recent, detailed investigations in New Mexico (Stephens et al., 1985; Stephens and Knowlton, 1986; Mattick et al., 1986; Phillips et al., 1988; Stone and McGurk,

1985) have shown that direct recharge does take place in the arid portions of this state, and have shed light on the nature of the recharge process. Phillips et al. (1988) found that bomb-pulse chlorine-36 (^{36}Cl) and tritium (^{3}H) have significantly different travel time characteristics in the vadose zone at two arid sites in New Mexico. They theorized that the movement of tritium was enhanced in the profile due to vapor transport. A solute such as ^{36}Cl would only travel in the liquid phase of water, and, therefore, would appear to be retarded with respect to the tritium movement. The majority of the tritiated soil water appeared to be greater than twice as deep in the profile as the bulk of the ^{36}Cl at the SNWR study site. The soil-water movement in the upper portion of the profile is thus assumed to be enhanced by a vapor-phase flux of water. This vapor flux should not extend to the water table and contribute directly to recharge because the vapor pressure gradient would diminish with depth. The vapor flux could, however, enhance movement of soil water at shallower depths, thus contributing to the overall movement of soil water which eventually becomes recharge. Therefore, from a water resources planning perspective, vapor-phase contributions to ground-water recharge may be important. Also, from a hazardous waste siting perspective, if vapor-phase movement of soil water is significant, then volatile pollutants may travel more rapidly through the vadose zone to an underlying aquifer than the dissolved constituents in the liquid phase. Hence, non-volatile solutes may appear to be retarded relative to the movement of volatile constituents. Therefore, it may be important for engineers and water

resource planners to quantify both the liquid and vapor flux in designing a hazardous waste facility.

This study uses the stable isotopes of hydrogen and oxygen, deuterium (^{2}H or D) and oxygen-18 (^{18}O), in the water molecule, to evaluate the processes that contribute to soil-water movement in natural desert soils. A method to quantify the liquid- and vapor-phase contributions to soil-water movement is presented and should aid in evaluating the hypotheses presented by Phillips et al. (1988). In addition, the model presented in this study may be used specifically to estimate the recharge rate. Enhanced understanding of the recharge process resulting from this research should allow more accurate estimation of ground--water recharge in New Mexico. It should also permit evaluation of methods for enhancing natural recharge in the state.

2. RELATED RESEARCH

Recent estimates of recharge rates in New Mexico under arid or semiarid conditions have been made by several investigators (Stephens et al., 1985; Stephens and Knowlton, 1986; Mattick et al., 1986; Phillips et al., 1988; Stone and McGurk, 1985). Stephens and Knowlton (1986) applied soil-physics techniques to quantify the amount of areal recharge through the vadose zone. They concluded that the recharge flux might be on the order of a few percent of the precipitation rate. This result is quite significant, considering that many previous studies in other arid environments have concluded that recharge is negligible. However, the soil-physics techniques employed in the Stephens and Knowlton (1986) study to quantify the recharge rate have statistical measurement errors as large as an order of magnitude.

Phillips et al. (1988) investigated the same site as that used by Stephens and Knowlton (1986). Phillips et al. (1988) used bomb-pulse ^{36}Cl and tritium as thirty-year tracers for the estimation of water and conservative solute movement. One of their most interesting results was the relative positions of the bomb-^{36}Cl and bomb-tritium peaks in the soil profiles. Bomb ^{36}Cl and bomb tritium were both released by atmospheric nuclear weapons tests; the bomb-^{36}Cl fallout peaking in about 1958 and the tritium fallout in 1964. The bomb ^{36}Cl was incorporated in precipitation and dry deposition and has been infiltrating slowly

through the soil dissolved in the liquid soil water (Phillips et al., 1983; Phillips et al., 1984). The bomb tritium was incorporated into atmospheric water vapor (as the molecule HTO) and has also been moving downward with the soil water. If piston displacement is assumed, one would expect to find the bomb-tritium peak in the soil water at a slightly shallower depth than the bomb-^{36}Cl peak, due to the timing of the fallout peaks. This has not proved to be the case.

Figure 1 shows the positions of the tritium and ^{36}Cl peaks for one soil profile measured at the Sevilleta National Wildlife Refuge research site, near Socorro. The bomb-^{36}Cl peak is found at a depth of about one meter, whereas the bomb-tritium peak is located at almost two meters. Thus, although the tritium entered the soil after the ^{36}Cl, the majority of the tritium has penetrated deeper. Figure 1 also contains a graph of depth versus chloride age, based upon chloride mass-balance calculations (Phillips et al., 1988). The chloride mass-balance appears to accurately predict the depth of the bomb-^{36}Cl peak. Limitations of the radioisotope approach have been discussed by Phillips et al. (1988).

These results lead to the conclusion that tritiated water is moving downward faster than chloride. Two hypotheses offer likely explanations: (1) chloride is retarded relative to water by interaction with soil grains during liquid flow, and (2) the tritium moves faster than the chloride because it is transported in both liquid and vapor phases whereas the chloride can travel only in the liquid phase.

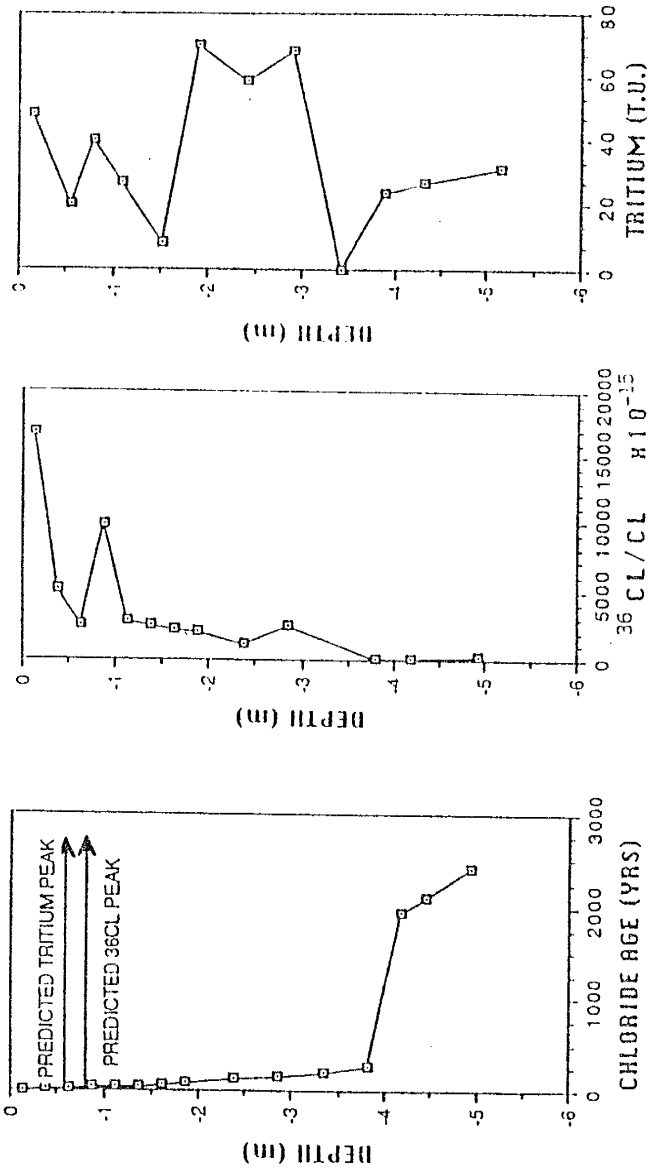

Figure 1 - Predicted position of the bomb-^{36}Cl and ^{3}H peaks compared to the observed position. Chloride age is calculated by the chloride mass balance method. (after Phillips et al., 1988)

Laboratory column experiments were devised by Mattick et al. (1986) to test the first hypothesis. The experimental conditions were designed so that only liquid flow of water and chloride was allowed and vapor transport was prevented by maintaining a zero vapor-pressure gradient. The chloride was observed to move relatively uniformly along with the moisture, indicating that the tracer had little chemical interaction with the porous media.

The second hypothesis is based on the fact that water (both H_2O and the isotopically labeled HTO) is volatile and can thus move as a gas, whereas chloride is not volatile and thus can be transported only when it is dissolved in liquid water. Net water vapor transport in the soil (due to gradients of partial pressure of water vapor) could, in turn, result from gradients of temperature, matric potential, osmotic potential, or a combination of these. Preliminary calculations suggest that average temperature and osmotic potential gradients are, by themselves, not sufficient to account for the observed difference between the ^{3}H and ^{36}Cl peaks. The matric potential gradients may work together with seasonally fluctuating temperature gradients to enhance downward vapor movement and restrict upward movement.

A recent laboratory study conducted by Grismer et al. (1986) has suggested that at low to moderate moisture contents the vapor-phase component of water flow may be significant. If the inferences made in Grismer's study, along with the radionuclide tracer work described above, are borne out, they will imply that in arid regions vapor-phase movement is at least as important as liquid-phase movement in transporting soil water below the root zone, where it

can become groundwater recharge. In general, such a major role for vapor transport has not been previously recognized, and it has important implications for determining ground-water recharge in desert soils. Commonly-used methods of measuring recharge, based on Darcy's law, normally only involve liquid-phase flux calculations. The often-used chloride mass-balance method (Stone and McGurk, 1985) also accounts only for liquid flow. Thus, actual recharge amounts may be larger than those determined by these methods, by at least a factor of two.

Differentiation of liquid and vapor fluxes by standard physical measurements is quite difficult, due to the large variation of matric potential with water content at high soil-water suctions. This is not the case when applying direct tracing techniques using the stable isotopes of hydrogen and oxygen in the water molecule. This technique takes advantage of the fact that the diffusivities of the isotopic species vary little with water content (unlike hydraulic conductivity) and the method is thus more robust at low water content than calculations based on Darcy's law (Barnes and Allison, 1984).

The systematics of oxygen and hydrogen isotope variation in precipitation (Dansgaard, 1964) have been understood for over twenty years. However, understanding of the isotopic systematics in soils has lagged considerably. The foundations were laid by Zimmerman et al. (1967). The basic mathematical formulations they developed are still used, however, they limited their theory and experiments to evaporation from saturated soils. More recent investigations in humid climates by Thoma et al. (1979), Bath et al. (1982), and Saxena (1984)

have been able to apply the theory of Zimmerman et al. (1967) with little modification.

The much more difficult problem of isotope distribution in dry, desert soils was not addressed until the work of Allison (1982). Since then, this topic has been further treated by a formal theoretical description for isothermal soils (Barnes and Allison, 1983), laboratory experiments involving dry soils (Allison et al., 1983), field investigations in a semiarid region (Allison and Hughes, 1983), bi-modal transport in desert soils (Sharma and Hughes, 1985), and a theoretical development for non-isothermal soils (Barnes and Allison, 1984). The last citation is most pertinent to the study presented here, inasmuch as the theory allows for downward diffusion of water vapor under temperature gradients. This phenomenon may have been observed under laboratory and field conditions (Allison, 1982; Bath et al., 1982; Allison and Hughes, 1983), but these investigators were unable to analyze their results for non-isothermal conditions due to a lack of temperature data. Examples of the application of these stable-isotope techniques in field situations can be found in Allison et al. (1984) and Allison et al. (1985). Most of this previous work has concentrated on quantifying evaporation rates from the soil surface, and not the downward flux of vapor through the profile. Hence, our goals require an advance in the application of these techniques.

3. SITE DESCRIPTION

The field site comprises an area of about 1.3 square kilometers in the Sevilleta National Wildlife Refuge about 24 kilometers north of Socorro, NM (Figure 2). The site lies within the Rio Grande drainage basin on the south side of the Rio Salado, an ephemeral, braided tributary to the mainstream. The area receives about 20 cm of precipitation per year and the gross annual lake evaporation is about 178 cm (U.S. Department of Agriculture, 1972).

The surficial geology has been mapped by Machette (1978), and consists mostly of fluvial sands and dune sand (Figure 3). A few discontinuous, thin silt and clay layers exist beneath parts of the area. Vegetation is relatively sparse, consisting of salt cedar along the ephemeral drainage, saltbush, creosote, juniper and grasses on the ancient flood plain, and only a few juniper near the edges of the sand dune. Greater vegetation density is suggested where a shallow low-permeable layer is beneath the sand-covered, ancient, flood plain. The predominant vegetation around our sampling locations are saltbush and grasses. Depth of saltbush rooting appears to be limited to the upper 1.0 to 1.5 meters (Stephens et al., 1985); however, quantification studies are needed. The topography varies from moderate slopes near the sand dunes (Qsa) and sandstone outcrop (QTsa) to nearly flat lands on the ancestral flood plain (Qab).

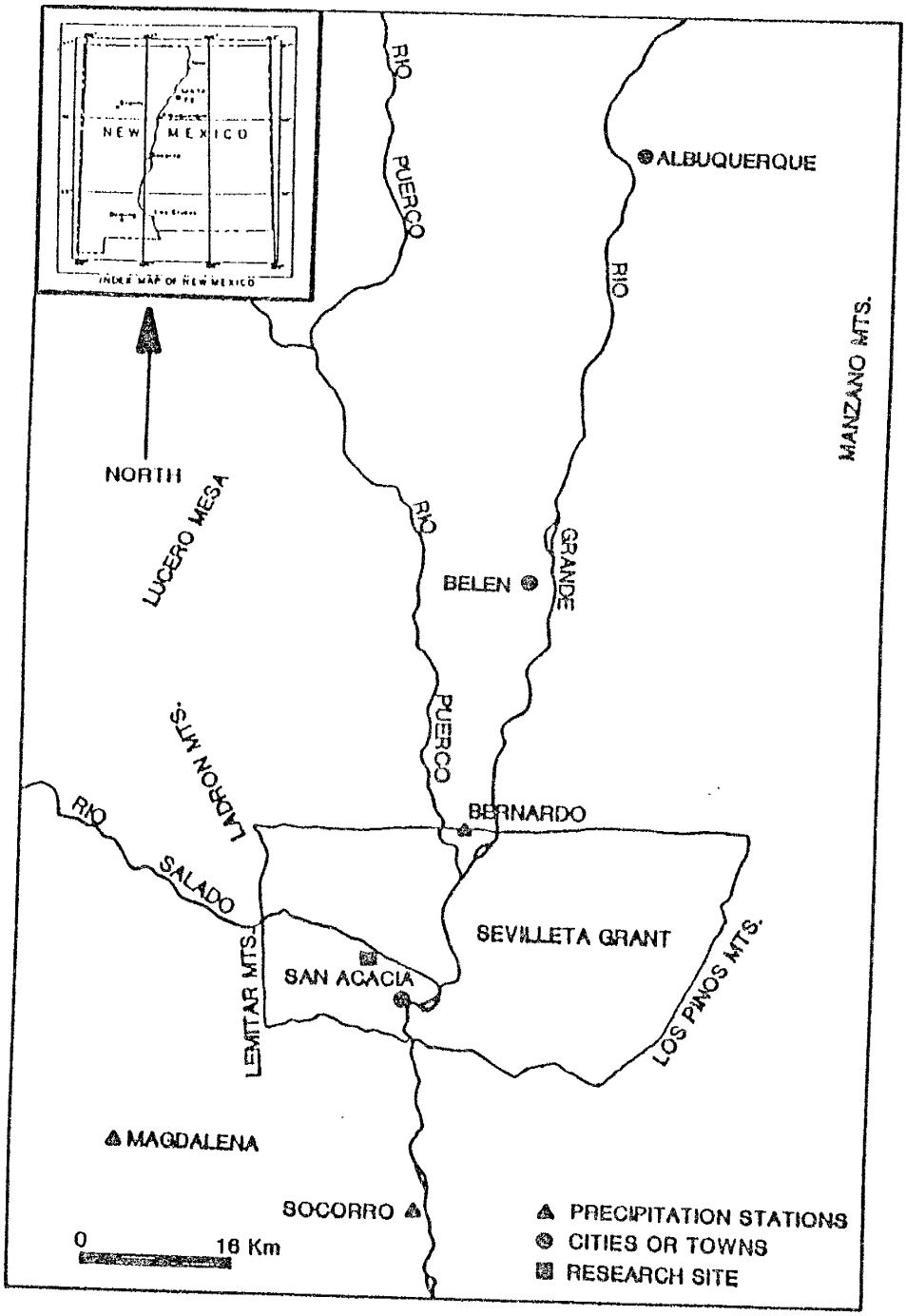

Figure 2 - Site location map (after Stephens et al., 1985)

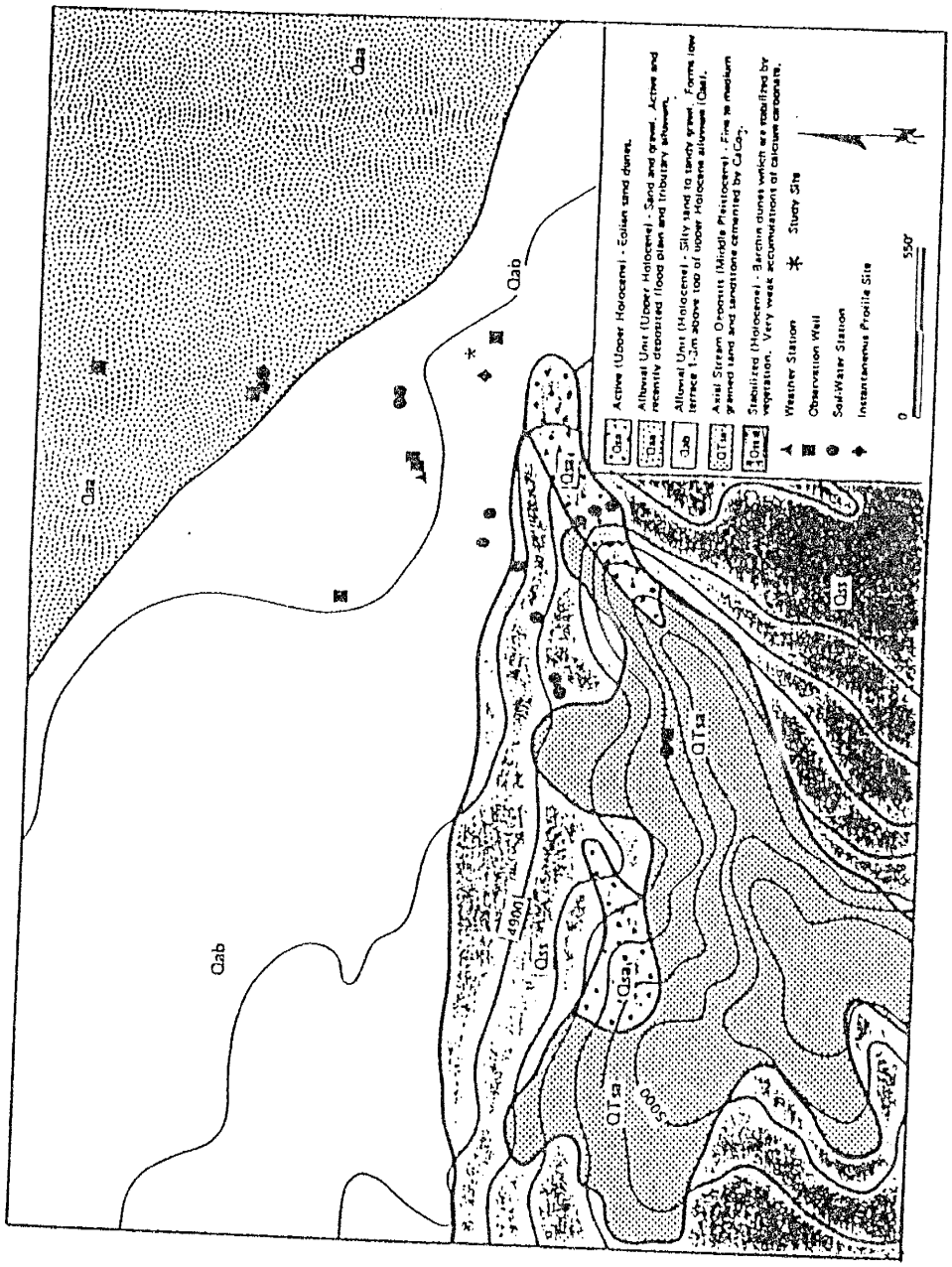

Figure 3 - Instrument locations and geologic map, with topography contours in feet above mean sea level. (after Stephens et al., 1985)

In the lowland areas, the depth to less permeable Pleistocene sediments is about 17 meters and the depth to ground water is only about 3 meters. Near soil-moisture station 1 (see Stephens et al., 1985 for complete instrumentation description) the depth to ground water is approximately 6 meters. The aquifer consists mostly of unconsolidated sand with some cobbles. The hydraulic gradient is eastward in the direction of the grade of the Rio Salado channel.

The Rio Salado flows mostly during August and September in response to intense thunderstorms in the mountains to the west. Approximately half of the annual rain and snow falls during the winter. No evidence of runoff from the sampling site has been observed since monitoring began in November 1982 (Stephens et al., 1985). The lack of runoff is due to the favorable infiltration characteristics of the sandy surficial deposits (Stephens et al., 1985).

The monitoring network that exists at the site includes a weather station; a number of observation wells, some with continuous recorders; and fifteen soil-water monitoring stations. For a more detailed discussion of this instrumentation see Stephens et al. (1985). The radioisotope work conducted by Mattick et al. (1986) was done in close proximity to soil-moisture station 1. Work carried out in this study was also performed within 15 meters of this station. Figure 4 is a map of the locations of each of these research sites.

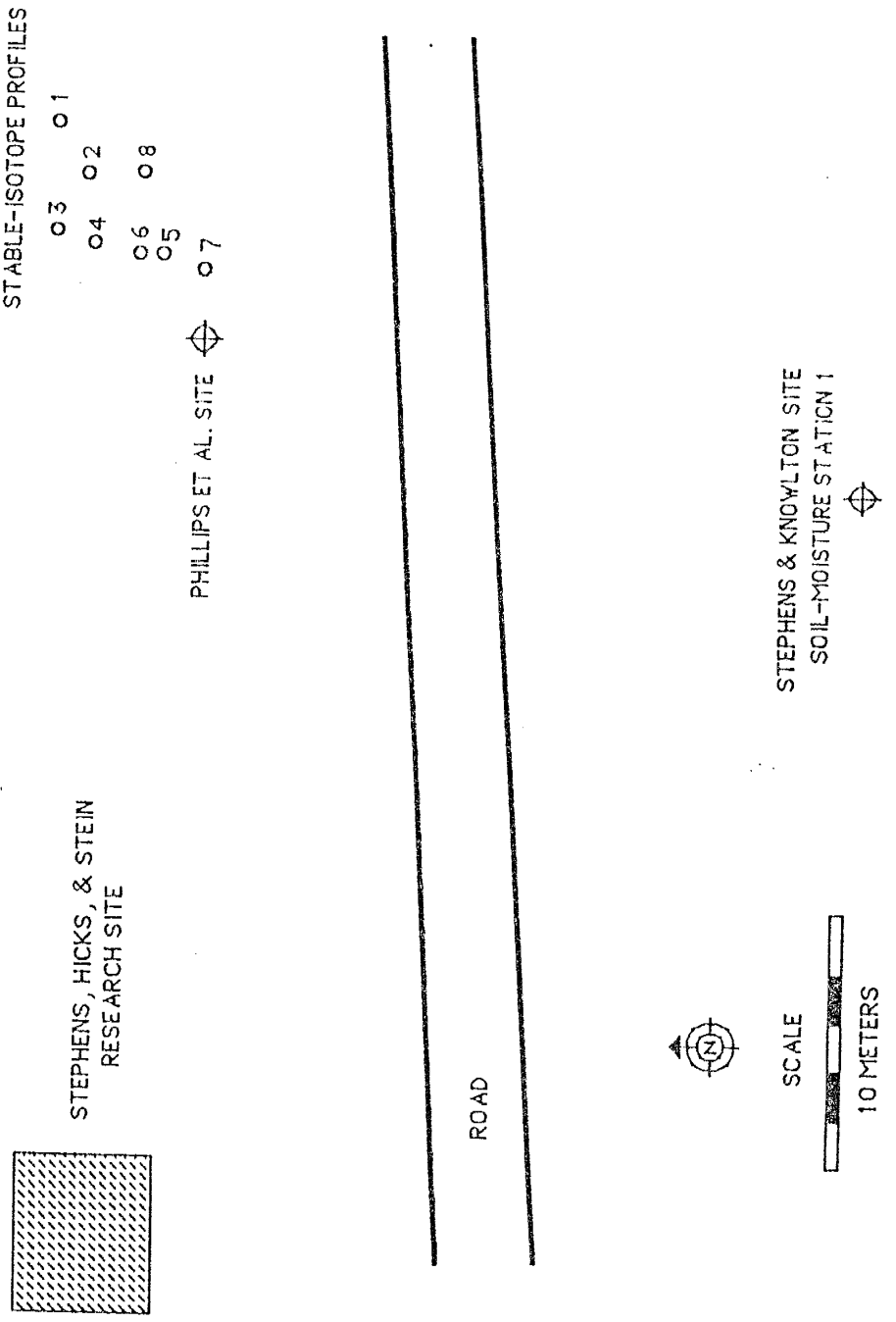

Figure 4 - Location of sampling and research sites at the Sevilleta site

4. METHODS AND PROCEDURES

4.1 Field and Laboratory Methods

4.1.1 Field Sampling. Eight coreholes were drilled at the Sevilleta National Wildlife Refuge in the course of this study. Two methods were employed to obtain soil samples: rotary hollow-stem augering with a drill rig, and hand augering. The first two coreholes drilled at the site used a drill rig, a Mobile B-60, owned by the State of New Mexico, Environmental Improvement Division (NMEID). A continuous profile of soil samples was obtained from the coreholes by sampling with shelby tubes just ahead of the auger. The samples collected ranged from land surface to 5.0 meters in depth. The shelby tubes were sealed to prevent evaporation and transported back to the laboratory. In the laboratory these samples were sectioned immediately into smaller subintervals. The soil samples were then sealed in glass jars to prevent evaporation of the soil water. The jars were refrigerated to minimize any biological activity.

A hand augering technique was also used to obtain continuous soil sampling. Once the soil was removed from the corehole, the sample was immediately placed in a glass canning jar and sealed to prevent evaporation. At each depth interval sampled, a thermistor was lowered to the bottom of the hole and temperature recorded for potential use in numerical modeling. Depth of sampling was generally from land surface to approximately 4.5 meters.

4.1.2 Distillation Techniques. Three techniques are now available for distilling soil water from a soil sample without appreciable isotopic fractionation. One of these procedures was developed for this research project. These techniques are discussed in the next chapter, which is a paper submitted to the journal Isotope Geoscience entitled 'A Quantitative Evaluation of a Vacuum Distillation Technique to Extract Soil Water for Stable-isotope Analyses'. A hierarchical analysis of variance, or components-of-variance analysis, is presented in this paper to quantify errors involved in the distillation technique, gas preparation procedures, and mass spectrometric analyses.

4.1.3 CO_2/H_2O Equilibration Technique. The majority of ratio mass spectrometers in use today cannot handle direct injection of a water sample in order to analyze its isotopic composition. Instead, to analyze a water sample for its $^{18}O/^{16}O$ ratio, the water must be equilibrated with CO_2, and the CO_2 analyzed on a mass spectrometer. The CO_2/H_2O equilibration technique used in this study was not previously used at the New Mexico Institute of Mining and Technology Stable Isotope Laboratory. Therefore, the equilibration setup for this technique was constructed during this project.

The apparatus and procedures for this equilibration technique were outlined by Roether (1970). Roether's procedure is a variation of the standard technique employed by Epstein and Mayeda (1953). The technique involves equilibrating a CO_2 gas of known isotopic composition with the water sample of interest in a special glass equilibration vessel. Water volumes of 1 to 10 milliliters are generally applicable. The equilibration vessel is placed in a

constant temperature shaker bath. This step is not included in the Epstein and Mayeda technique. The shaker bath must be capable of shaking at a frequency greater than the resonance frequency of water, about 3.8 cycles/sec, to optimize the equilibration time. Typically, the frequency of the shaker bath is set at 5.0 cycles/sec. Equilibration times for the Roether technique are therefore on the order of 2 hours, as compared to several days with the Epstein and Mayeda technique. The equilibrated CO_2 gas is then purified and transferred to a sample bottle on an extraction line. That sample bottle is then mounted directly on the inlet system of the mass spectrometer for isotopic ratio analysis. Appendix A presents a more detailed methodology for the CO_2/H_2O equilibration technique. Also included in appendix A is a method to calibrate the mercury manometer on the vacuum line for determination of CO_2 yield.

4.1.4 H_2 Reduction Technique. To determine the $^2H/H$ ratio of the water, a reduction technique was employed to generate hydrogen gas from the water sample. A relatively newly developed zinc reduction technique has been set up for this project (Kendall and Coplen, 1985; Coleman et al., 1982).

The hydrogen reduction technique involves the heating of the soil water in a reaction vessel in the presence of zinc. Special reaction vessels and an aluminum block heater are needed, as outlined by Kendall and Coplen (1985). The zinc used in this reduction procedure must have special additives in order to reduce the water sample without fractionation. The altered zinc is considered to be 'optimally contaminated'. A sample of 'optimally contaminated' zinc, obtained from Indiana University, is placed in the bottom of a reaction vessel.

Approximately 0.25 grams of zinc is used with a water sample of 5 microliters. At the start of the procedure, the vessel is sealed and pumped on by a high vacuum system. The zinc is heated with a heat gun to drive off any adsorbed atmospheric water vapor. The vessel is attached to a special port on the line which allows the syringe injection of the water sample through a septum. A dewar of liquid nitrogen is placed around the base of the vessel, covering the zinc. When the water is injected into the apparatus, it is condensed down to the zinc. A heat gun is used to speed the transfer process. The vessel is then sealed and removed from the vacuum line. It is then placed in the aluminum block heater at a temperature of 500 °C for 30 minutes. Almost immediately after entering the heater, zinc oxide and hydrogen gas are formed. The vessel is then ready for direct connection to the inlet system of the mass spectrometer for analysis. Appendix A presents a more detailed methodology for this hydrogen reduction technique.

4.1.5 Mass Spectrometry. Several laboratories have been employed to measure the isotopic compositions of the gases prepared from these soil samples. Samples have been analyzed at Yale University, the U.S. Geological Survey Laboratory in Reston, VA, the University of Missouri at Columbia, the University of New Mexico, and recently at the New Mexico Institute of Mining and Technology. Disappointingly, problems with inter-laboratory calibrations, toluene contamination, early vacuum distillation procedures, and mass spectrometry analyses resulted in the exclusion of the data from labs other than the New Mexico Institute of Mining and Technology in the numerical analyses.

These data did help to refine the preparation techniques so that the samples analyzed at the New Mexico Institute of Mining and Technology were of good quality. The ^{18}O and deuterium data reported from analyses performed at the New Mexico Institute of Mining and Technology were run on a Finnegan-MAT Delta E mass spectrometer. Finnegan-MAT reports the analytical precision of the Delta E as $\pm$ 0.1 °/$_{oo}$ (permil) for CO_2 and $\pm$ 0.5 °/$_{oo}$ for hydrogen.

4.1.6 Thermal Properties of Soil. The analysis of unsaturated moisture flow under non-isothermal conditions, both in the liquid and vapor phases, should take thermal effects into account. An approximation of temperature within the soil is required to estimate the heat-flow contribution to soil-water movement. A model describing the periodic temperature variation in soil due to diurnal and seasonal fluctuations is presented in the next section. In estimating the heat flow due to conduction, two independent thermal parameters are required: thermal conductivity, λ, and volumetric heat capacity, C.

Both the thermal conductivity and volumetric heat capacity may be estimated by experimental or theoretical techniques. Thermal conductivity as a function of volumetric moisture content can be estimated in the field or laboratory with a line-source thermal conductivity probe (DeVries and Peck, 1958a,b). DeVries (1963) developed a theoretical technique to estimate the thermal conductivity function. In the same work, he also formulated a theoretical method to estimate the volumetric heat capacity as a function of moisture content. The volumetric heat capacity is determined experimentally by calorimetry.

The line-source thermal conductivity probe consists of a thin diameter probe, 0.1 cm O.D., approximately 19 cm long, containing a heating element and a copper-constantin thermocouple. The probe is inserted into the soil, typically in a horizontal direction, and a constant current supplied to the heating element for a short period of time, approximately 120 seconds. The heating time is kept short to minimize thermally-induced fluid flow during the test. The temperature is measured periodically with the thermocouple during heating, and subsequently during cooling. The temperature rise during heating, and fall during cooling, depends upon the rate at which heat is conducted from the probe by the porous media, and therefore is dependent on the thermal conductivity of that soil.

Following Horton and Wierenga (1984), the general heat-flow equation is given as:

$$\frac{\lambda}{r}\frac{\partial}{\partial r}\left(r\frac{\partial T}{\partial r}\right) = C\frac{\partial T}{\partial t} \qquad (1)$$

where λ is the thermal conductivity (cal cm^{-1} s^{-1} C^{-1}), r is the radial distance (cm), T is the temperature (C), C is the volumetric heat capacity (cal cm^{-3} C^{-1}), and t is time (s). Solving this equation for the conditions applying to the line-source probe allows for the estimation of the thermal conductivity.

The boundary conditions for both heating and cooling are:

$$q = -\lim_{r \to 0}\left(2\pi\lambda r\frac{\partial T}{\partial r}\right) \qquad 0 \le t \le t_1 \qquad (2)$$

$$q = 0 \qquad t > t_1 \qquad (3)$$

where q is the constant line heat source (cal cm^{-1} s^{-1}), also $T = T_o$ at $t = 0$, and $r = \infty$, t is finite, and t_1 is the time at which heating was discontinued. Subject to these conditions, the solution to equation 1 is (DeVries and Peck, 1958a):

$$T - T_o = (q/4\pi\lambda)(-Ei(-r^2/4\alpha t) + Ei(-r^2/4\alpha(t-t_1))) \quad (4)$$

where E_i is the exponential integral, α is the thermal diffusivity, such that $\alpha = \lambda/C$ (cm^2 s^{-1}). Neglecting very early times, the heating time solution can be reduced to:

$$T - T_o = (q/4\pi\lambda)(\ln(t/t_o)) \quad (5)$$

The variable t_o respresents the time at which the current was discontinued and heating of the probe ceased. Knowing the uniform current applied to the probe, I (cal s^{-1}), and the resistance of the probe, R (ohms cm^{-1}), the heat source is estimated to be $q=I^2R$. A plot of $T-T_o$ versus $\ln(t/t_o)$ for various times yields a slope equal to $(q/4\pi\lambda)$. The thermal conductivity can then be solved for directly.

For the cooling case, the following condition must be met:

$$(r^2/4\alpha(t-t_1)) \ll 1 \quad (6)$$

and the solution becomes:

$$T - T_o = (q/4\pi\lambda)(\ln(t/(t-t_1))) \quad (7)$$

For this case, plotting $T-T_o$ versus $\ln(t/(t-t_1))$ for various times yields a slope equal to $(q/4\pi\lambda)$, where q was the heating current that was discontinued at time t_1. The accuracy of this method was estimated by DeVries and Peck (1958a) to be 5%.

The annular gap between the probe and the soil is an important consideration in evaluating the results of a line-source thermal conductivity analysis. The gap should be small in comparison to the probe and the soil

particle size. DeVries and Peck (1958a) suggest plotting $T-T_o$ versus t, from which an extrapolated intercept, t_c, with the horizontal axis (at $[T-T_o]=0$) is:

$$t_c = (r^2/4\alpha)e^{\gamma-2\eta} \tag{8}$$

where r is the radius of the probe (cm), γ is Euler's constant, 0.5772, and η is a dimensionless contact resistance. The following equation can then be solved to estimate the annular gap thickness, r (i.e., 'skin effect'):

$$\eta = (\lambda/\lambda_{air})\ \ln(r+r)/r \tag{9}$$

The theoretical estimation of the thermal properties of soil presented by DeVries (1963) is based upon the sizes, shapes, and arrangements of the various constituents making up the porous media. For the thermal conductivity approximation, a weighted average is used:

$$\lambda = \sum_{i=0}^{n} (k_i\ x_i\ \lambda_i) \ /\ \sum_{i=0}^{n} (k_i\ x_i) \tag{10}$$

where x_i is the volume fraction of each soil constituent (e.g., quartz grains, organic matter, soil water, and air), λ_i is the thermal conductivity of each constituent, n is the number of soil constituents, and k_i is the weighting factor. The weighting factor is dependent upon the shape and orientation of the soil granules, and calculated by:

$$k_i = (1/3) \sum_{j=1}^{3} (1 + [(\lambda_i/\lambda_o) - 1]\ g_j)^{-1} \tag{11}$$

where λ_o refers to the conductivity of the continuous medium, e.g. air for dry soil and water for moist soil. k_o is equal to 1. According to DeVries (1963), the

shape factor, g_j, depends on the shape of the ith particles, and typically: $g_1 + g_2 + g_3 = 1$.

Values of λ_i for quartz grains, water, and air at 20 °C are given by DeVries (1963) as 20.4, 1.42, and 0.0615 mcal cm^{-1} s^{-1} C^{-1}, respectively. Values of g_j for all solid particles are given as 0.144 for g_1 and g_2, and 0.712 for g_3. For air, g_1 and g_2 vary linearly from 0.33 at saturation to 0.134 at "field capacity" (~ 0.07 cc/cc). From field capacity to oven dryness, g_1 and g_2 vary linearly down to 0.013. DeVries (1963) estimates the accuracy of calculating thermal conductivity with this method to be 5 to 10%.

DeVries and Philip (1986) have suggested a combination approach to estimating thermal conductivity over the entire range of moisture content in the soil. They recommend the experimental determination of several thermal conductivity values, and a subsequent fitting of the theoretical model of DeVries (1963) to the measured data. The shape factor terms are used as fitting parameters, inasmuch as they are the least accurate parameters of estimate.

The volumetric heat capacity can be calculated theoretically with the following equation (DeVries, 1963):

$$C = 0.46\ x_m + 0.60\ x_o + x_w \qquad (12)$$

where x_m is the volume fraction of soil minerals, x_o is the fraction of organic matter, and x_w the volumetric water content (cc/cc).

4.2 Mathematical Modeling Methods

The main purpose of this study was to investigate the processes related to soil-water movement in natural desert soils. One important objective was to estimate the relative contribution of the water vapor flux to soil-water movement. Phillips et al. (1988) have shown that bomb-pulse ^{36}Cl and ^{3}H have markedly different travel path/time characteristics. They attributed the discrepancy in peak depths for these two tracers to enhanced vapor-phase movement of the tritium. Therefore, a technique for quantifying the vapor flux was needed in order to evaluate their hypothesis and understand better the processes involved in soil-water movement in natural desert soils.

A theoretical model for predicting the vapor flux of water during steady evaporation from a water table was developed by Barnes and Allison (1984), hereafter referred to as the 'non-isothermal evaporation model', or 'NIE' model. Their model also predicts the shape of the $H_2{}^{18}O$ and H^2HO (or HDO) profiles under non-isothermal conditions. With some modifications to the Barnes and Allison (1984) theory, a formulation can be derived to relate downward vapor and liquid fluxes to total recharge.

Prior to developing a model, some basic assumptions must be made to characterize the system to be modeled. First, the movement of water is occurring in both the liquid and vapor phases in response to thermal and moisture gradients. Formulations describing heat and moisture flow have previously been presented by Philip and DeVries (1957) and Taylor and Carey

(1964). The main problem in applying these two theories is in estimating the various diffusivities. This is not as difficult however, if one is modeling the relative fluxes of the isotopic species in the water molecule, rather than the bulk fluid movement. The diffusivities of the isotope species vary little with changes in moisture content, unlike the liquid moisture diffusivity which can vary over orders of magnitude. The system under consideration is described as follows: quasi-steady, one-dimensional vertical flow of water vapor from a plane of zero flux at the evaporation front down toward the water table, and a downward advective liquid flux. These conditions occur at the Sevilleta research site during the summer months when the vapor flux is probably greatest.

The various fluxes need to be separated into liquid- and vapor-phase components. Within the liquid phase, an advective-diffusive process is assumed. However, in the vapor phase only a diffusive component is assumed applicable, which can be modeled according to Fick's law. The net effect of barometric pressure influences is assumed to be negligible with regard to advective vapor-phase movement. Further investigation beyond the scope of this work would be required to investigate fully the possible potential for advective vapor-phase movement.

In addition, Knudsen vapor transport phenomenon are considered negligible for the conditions under investigation. Thorstenson and Pollock (1989) have stated that "... pure Knudsen diffusion is equivalent to stating that all of the "resistance" to diffusion occurs through collisions with walls and there is no resistance to diffusion arising as a result of intermolecular collisions." Knudsen

diffusivities therefore relate the viscous and diffusive vapor-flux components. Thorstenson and Pollock note that natural soils are hardly ever fine grained enough for Knudsen transport to be a dominant transport mechanism. It is possible, however, that Knudsen transport is important under the conditions of interest in this study, and therefore is recommended for further investigation.

Other factors related to isotopic behavior must also be addressed. Isotopic fractionation occurs when the water changes state between a liquid and vapor phase. This is due to differences in chemical potentials between the isotopic species. The heavier isotopes tend to fractionate into the liquid phase relative to the isotopically lighter vapor phase. The result is a concentration gradient in the isotopic species. Differences in the isotopic diffusivities will also enhance the concentration gradient. Temperature effects on the model parameters can be accounted for by making these parameters functions of temperature.

Development of a model to describe the isotope profile and quantify the vapor flux is based on the works of Philip and de Vries (1957) and Barnes and Allison (1984). Assuming one-dimensional vertical flow, the equation for the liquid flux is given by Darcy's law, where:

$$q^l/\rho = - Ki = - K \frac{d\Phi}{dz} = - K \frac{d(-z+\psi)}{dz} \qquad (13)$$

The symbols are defined in table 1. For the minor isotopes of hydrogen and oxygen in water, given a symbol i, there is both an advective and diffusive flux, such that:

TABLE 1 - LIST OF SYMBOLS

Symbol	Description
D^*, D	(effective=*) self-diffusion coefficient of water [m^2/s]
D^*_i, D_i	(effective=*) diffusion coefficient of isotopic species i in liquid phase [m^2/s]
D^{v*}, D^v	(effective=*) diffusivity of water vapor in air [m^2/s]
D_i^{v*}, D^v_i	(effective=*) vapor diffusivity of isotopic species i in air [m^2/s]
h	relative humidity
i	subscript to denote isotopic species, either ^{18}O or ^{2}H
K	unsaturated hydraulic conductivity [m/s]
l	sub- or super-script to denote liquid phase
N^{sat}	saturated water vapor density in air [kg m^{-3}]
q^l, q^v, q^v_i, q^l_i	mass flux of water or isotopes [kg m^{-2} s^{-1}]
p	porosity
$R^v_i, R_i, R_i^{rec}, R^s_i$	isotope ratio (s superscript denotes standard ratio, and rec superscript denotes recharge water ratio)
v	sub- or super-script to denote vapor phase
W	recharge rate [m/s]
z	depth below land surface [m]
z_l, z_v	characteristic length factor [m]
α_i	equilibrium fractionation factor
$\gamma^v, \gamma^v_i, \gamma_i, \gamma$	pore geometry factor
k	mass flow constant
δ_i, δ_i^{rec}	delta value, or standardized isotope ratio
ϵ_i	equilibrium enrichment factor
η_i	diffusion ratio excess
θ	volumetric water content
ν, ν_i	mass flow factor
ρ	density of liquid water [kg m^{-3}]
σ_i, σ_i^v	diffusion ratio factor
Φ	total potential [m]
ψ	hydraulic or pressure head [m]
p_v, p_A	vapor pressure and atmospheric pressure, respectively

$$q_i^l = q^l R_i - \rho D_i^* \frac{dR_i}{dz} \tag{14}$$

The effective diffusivity of species i in the liquid water is determined by:

$$D_i^* = \gamma_i D_i \tag{15}$$

where D_i is the molecular diffusion coefficient of species i in liquid water. The temperature dependence of D (assumed to be equal to D_i) is given by Mills (1973). The pore geometry factor, γ_i, accounts for the effect of tortuosity and changing water content. γ_i is estimated as follows:

$$\gamma_i = \tau^l \theta \tag{16}$$

τ^l is the liquid tortuosity factor, and θ is volumetric water content.

For the water vapor movement, Fick's law of diffusion is applicable, where:

$$q^v = -D^{v*} \frac{d(hN^{sat})}{dz} \tag{17}$$

Refer to table 1 for parameter definitions. Both the effective diffusivity of water vapor, D^{v*}, and the saturated vapor density, N^{sat}, are dependent on temperature. Under non-isothermal conditions (i.e., where temperature changes with depth) these parameters will change with depth. The effective diffusivity of water vapor can be defined as follows:

$$D^{v*} = \gamma^v \nu D^v \tag{18}$$

The molecular diffusivity of water vapor in air, D^v, as a function of temperature, was given by Jaynes and Rogowski (1983). The pore geometry factor for the vapor phase is given as:

$$\gamma^v = \tau^v (p - \theta) \tag{19}$$

where τ^v is the vapor-phase tortuosity factor, and p is porosity. The mass flow factor, ν, accounts for the simultaneous movement of water vapor and air. Barnes and Allison (1984) suggest the following relationship:

$$\nu = 1 + k \left(p_v / (P_A - p_v) \right) \tag{20}$$

where p_v is the water vapor pressure, and P_A is the atmospheric pressure. The mass flow constant, k, is a constant which depends upon the effective diffusivity, permeability and viscosity of water vapor and air in the soil. Philip and DeVries (1957) have suggested that ν should be of the same order of magnitude as $P_A/(P_A-p_v)$. Therefore, k should be on the order of 1.

For the minor isotopes of hydrogen and oxygen in water, the following vapor flux equation holds:

$$q_i^v = - D_i^{v*} \frac{d(R_i^v \, h \, N^{sat})}{dz} \tag{21}$$

Equation 18 can be adjusted for the isotope species to determine D_i^{v*}.

The following equation relates the liquid to vapor isotope ratio:

$$R_i^v = \alpha_i \, R_i \tag{22}$$

The temperature dependence of the equilibrium fractionation factor, α_i, is given by Majoube (1971) for deuterium and oxygen-18. The equilibrium enrichment factor, ϵ_i, can be expressed as follows:

$$\epsilon_i = 1 - \alpha_i \tag{23}$$

The diffusivity of water vapor in air is related to the isotopic vapor diffusivity by the diffusion ratio factor, σ_i^v, where:

$$\sigma_i^v = D^{v*}/D_i^{v*} = (\gamma^v \, D^v) \; / \; (\gamma_i^v \, D_i^v) \tag{24}$$

The diffusion ratio excess, η_i, relates the relative difference in abilities of species i molecules to escape from the surface compared to pure water molecules. η_i represents the 'kinetic effect', and is related to σ_i by:

$$\sigma_i = 1 + \eta_i \tag{25}$$

η_i is generally considered to be independent of temperature. A vapor-length factor is given by:

$$z_v = (N^{sat} D^{v*})/(W\rho) \tag{26}$$

where N^{sat} is the saturated vapor density, which is dependent upon temperature, and W is the recharge rate. The corresponding liquid-length factor is given as:

$$z_l = D^*/ W \tag{27}$$

The isotope ratio is related to a standard, SMOW (Standard Mean Ocean Water), and expressed as:

$$\delta_i = (R_i/R_i^s) - 1 \tag{28}$$

Again, consult table 1 for definitions of these parameters.

The recharge rate, W, is equivalent to the deep flux of water below the root zone which eventually recharges the underlying ground water. The total recharge flux, q, can be represented as:

$$q = -W\rho = q^l + q^v \tag{29}$$

and for the isotope species the analogous expression is:

$$q_i = -W\rho\ R_i^{Rec} = q_i^l + q_i^v \tag{30}$$

where R_i^{Rec} represents the isotopic composition of the soil water at depth. Some mathematical relationships useful in manipulating these equations for this derivation are:

$$\frac{d(\ln A)}{dz} = \frac{1}{A}\frac{d(A)}{dz} \tag{31}$$

$$\ln (A\ B) = \ln A + \ln B \tag{32}$$

$$\frac{d(A + B)}{dz} = \frac{dA}{dz} + \frac{dB}{dz} \tag{33}$$

Using the relationships defined by equations 26 and 31, equation 17 can be rewritten as:

$$q^v/(W\rho) = - h\ z_v \frac{d[\ln(h\ N^{sat})]}{dz} \tag{34}$$

from equation 21, and the expressions in equations 22, 24, and 26:

$$q_i^v/(W\rho) = - (h\ z_v\ R_i\ \alpha_i\ /\sigma_i^v) \frac{d[\ln(\alpha_i\ R_i\ h\ N^{sat})]}{dz} \tag{35}$$

from equation 14, and the relations in equations 24 and 27 we obtain:

$$q_i^l/(W\rho) = (q^l\ R_i)/(W\rho) - (z_l\ R_i\ /\sigma_i) \frac{d[\ln(R_i)]}{dz} \tag{36}$$

Combining equations 29, 30, and 34 through 36 to eliminate the flux terms will yield an expression describing the profile shape. To begin this manipulation of the equations, substitute equation 34 into 29, and rearrange to solve for q^l, to obtain:

$$q^l = -W\rho + (h\ z_v\ W\rho) \frac{d[\ln(h\ N^{sat})]}{dz} \tag{37}$$

Substituting equation 35 into 30 yields:

$$q_i^l - (h\ z_v\ W\rho\ R_i\ \alpha_i\ /\sigma_i^v)\ \frac{d[\ln(\alpha_i\ R_i\ h\ N^{sat})]}{dz} = -W\rho\ R_i^{Rec} \qquad (38)$$

Substituting equation 36 into 38 gives:

$$q^l\ R_i - (z_l\ R_i\ W\rho/\sigma_i)\ \frac{d[\ln(R_i)]}{dz} -$$

$$(h\ z_v\ W\rho\ R_i\ \alpha_i\ /\sigma_i^v)\ \frac{d[\ln(\alpha_i\ R_i\ h\ N^{sat})]}{dz} = -W\rho\ R_i^{Rec} \qquad (39)$$

Substituting equation 37 into 39 produces:

$$-W\rho\ R_i - (z_l\ R_i\ W\rho/\sigma_i)\ \frac{d[\ln(R_i)]}{dz} + (h\ z_v\ R_i\ W\rho)\ \frac{d[\ln(h\ N^{sat})]}{dz} -$$

$$(h\ z_v\ W\rho\ R_i\ \alpha_i\ /\sigma_i^v)\ \frac{d[\ln(\alpha_i\ R_i\ h\ N^{sat})]}{dz} = -W\rho\ R_i^{Rec} \qquad (40)$$

Dividing both sides of equation 40 by $W\rho$, and rearranging:

$$(h\ z_v\ R_i)\left(\frac{d[\ln(h\ N^{sat})]}{dz} - (\alpha_i\ /\sigma_i^v)\ \frac{d[\ln(\alpha_i\ R_i\ h\ N^{sat})]}{dz}\right) -$$

$$(z_l\ R_i\ /\sigma_i)\ \frac{d[\ln(R_i)]}{dz} = R_i - R_i^{Rec} \qquad (41)$$

Utilizing the mathematical expressions from equations 31 through 33, and rearranging equation 41 yields:

$$(h\ z_v\ R_i)\ \left[(1-(\alpha_i\ /\sigma_i^v))\ \frac{d[\ln(h\ N^{sat})]}{dz}\ -\ (\alpha_i\ /\sigma_i^v)\ \frac{d[\ln(\alpha_i\ R_i)]}{dz}\ \right] =$$

$$R_i\ -\ R_i^{Rec}\ +\ (z_l\ /\sigma_i)\ \frac{d(R_i)}{dz} \qquad (42)$$

Substituting equation 28 into 42 gives:

$$(h\ z_v\ R_i^s\ (1+\delta_i))\ \left[(1-(\alpha_i\ /\sigma_i^v))\ \frac{d[\ln(h\ N^{sat})]}{dz}\ -\right.$$

$$\left.(\alpha_i\ /\sigma_i^v)\ \frac{d[\ln(\alpha_i\ (1+\delta_i))]}{dz}\right]\ =\ R_i^s\ \left[\ \delta_i\ -\right.$$

$$\left.\delta_i^{Rec}\ +\ (z_l\ /\sigma_i)\ \frac{d(\delta_i)}{dz}\ \right] \qquad (43)$$

Dividing by R_i^s and applying equation 23 to 43 produces:

$$(h\ z_v\ (1+\delta_i))\ \left[(1\ -\ ((1-\epsilon_i)/\sigma_i^v))\ \frac{d[\ln(h\ N^{sat})]}{dz}\ -\right.$$

$$\left.((1-\epsilon_i)/\sigma_i^v)\ \frac{d[\ln((1-\epsilon_i)(1+\delta_i))]}{dz}\ \right]\ =\ \left[\ \delta_i\ -\right.$$

$$\left.\delta_i^{Rec}\ +\ (z_l\ /\sigma_i)\ \frac{d(\delta_i)}{dz}\ \right] \qquad (44)$$

Assuming $\sigma_i \approx \sigma_i^v$, and substituting equation 25 into 44 gives:

$$(h\ z_v)\ [(1+\delta_i)\ ((\epsilon_i+\eta_i)/(1+\eta_i))\ \frac{d[\ln(h\ N^{sat})]}{dz} -$$

$$((1-\epsilon_i+\delta_i-\epsilon_i\delta_i)/(1+\eta_i))\ \frac{d[\ln(1-\epsilon_i+\delta_i-\epsilon_i\delta_i)]}{dz}\ ] = [\ \delta_i -$$

$$\delta_i^{Rec} + (z_l\ /(1+\eta_i)\ \frac{d(\delta_i)}{dz}\ ] \qquad (45)$$

Several simplifying assumptions can be made to reduce equation 45 to a more manageable form: $((1+\delta_i)/(1+\eta_i)) \approx 1$; $\epsilon_i\delta_i \approx 0$; and $(1/(1+\eta_i)) \approx 1$. The result is:

$$(h\ z_v)\ [\ (\epsilon_i+\eta_i)\ \frac{d[\ln(h\ N^{sat})]}{dz} - \frac{d(\delta_i-\epsilon_i)}{dz}\ ] =$$

$$[\ \delta_i - \delta_i^{Rec} + (z_l)\ \frac{d(\delta_i)}{dz}\ ] \qquad (46)$$

Rearranging equation 46 to the form:

$$(h\ z_v)(\epsilon_i+\eta_i)\ \frac{d[\ln(h\ N^{sat})]}{dz} + (h\ z_v)\ \frac{d(\epsilon_i)}{dz} =$$

$$\delta_i - \delta_i^{Rec} + (z_l + (h\ z_v))\ \frac{d(\delta_i)}{dz} \qquad (47)$$

The second term in equation 47 can be manipulated utilizing equations 31 to 33, and noting that η_i is assumed to be constant, so that:

$$\frac{d(\epsilon_i)}{dz} = \frac{d(\epsilon_i+\eta_i)}{dz} = \frac{(\epsilon_i+\eta_i)}{(\epsilon_i+\eta_i)} \frac{d(\epsilon_i+\eta_i)}{dz} =$$

$$(\epsilon_i+\eta_i) \frac{d[\ln(\epsilon_i+\eta_i)]}{dz} \tag{48}$$

Substituting equation 48 into 47 gives:

$$(h\ z_v)(\epsilon_i+\eta_i) \left[\frac{d[\ln(h\ N^{sat})]}{dz} + \frac{d[\ln(\epsilon_i+\eta_i)]}{dz} \right] =$$

$$\delta_i - \delta_i^{Rec} + (z_l + (h\ z_v)) \frac{d(\delta_i)}{dz} \tag{49}$$

Utilizing equations 32 and 33, and rearranging equation 49, yields:

$$(h\ z_v)(\epsilon_i+\eta_i) \left[\frac{d[\ln(h\ N^{sat}\ (\epsilon_i+\eta_i)]}{dz} \right] =$$

$$\delta_i - \delta_i^{Rec} + (z_l + (h\ z_v)) \frac{d(\delta_i)}{dz} \tag{50}$$

Equation 50 is useful in determining the shape of the profile for a given isotopic species of hydrogen or oxygen in water, preferably deuterium. This equation can be solved numerically, taking into account the temperature dependence of the various parameters.

By multiplying both sides of equation 50 by the recharge rate, W, and rearranging, the following expression is obtained:

$$W\ (\ \delta_i - \delta_i^{Rec}\ ) =$$

$$((h\ N^{sat}\ D^{v^*})/\rho)(\epsilon_i+\eta_i)\ \left[\ \frac{d[\ln(h\ N^{sat}\ (\epsilon_i+\eta_i)]}{dz}\ \right]\ -$$

$$(D^*\ +\ ((h\ N^{sat}\ D^{v^*})/\rho))\ \frac{d(\delta_i)}{dz} \qquad (51)$$

Equation 51 has a form which allows for the evaluation of the various physical processes that this model accounts for. Namely, the recharge rate (or total soil-water movement) is a function of both a temperature gradient and a concentration gradient in the liquid and vapor phases. The first term on the right side of equation 51 represents the effect of the temperature gradient on the vapor-phase component of soil-water movement. The second (or final) term on the right side of equation 51 represents the effect of the isotopic concentration gradient in both the liquid and vapor phases.

Equations 29, 30, and 34 through 36 may also be combined in a similar fashion to obtain the ratio of the total vapor flux to the total recharge flux. The resultant equation has the form:

$$-q^v/(W\rho) = (\epsilon_i + \eta_i)^{-1}\ \left[\ \delta_i - \delta_i^{Rec} + (z_v + z_l)\ \frac{d\delta_i}{dz} - z_v\ \frac{d\epsilon_i}{dz}\ \right] \qquad (52)$$

A numerical model has been written to solve equations 50 and 52. Appendix C contains a source listing of this code. In solving equation 50, a

non-linear least-squares optimization approach has been used to fit the model to an observed set of data. A Marquardt solution was used for the least-squares approach. Certain parameters may be specified as fitted variables: vapor tortuosity factor (τ^v), liquid tortuosity factor (τ^l), isotopic composition of the recharge water (δ_i^{Rec}), and the recharge rate (W). Limits may be placed on the bounds of each fitted variable, or the variables may be held constant at the user's discretion. This numerical approach is henceforth referred to as the 'non-isothermal recharge' model, or 'NIR' model.

If the recharge flux is estimated by an independent method (e.g., tritium mass balance method, or chloride mass balance method), then the quantification of the vapor and liquid fluxes can be made quite readily. Otherwise, the NIR model will solve for the recharge rate. In fact, the NIR model may be used specifically as a technique for estimating the recharge rate. A comparison of NIR model predicted recharge rates and the results from other techniques is presented below in chapter 6.

The NIR model was developed to evaluate the vapor- and liquid-phase movement of soil water under non-isothermal conditions. It follows that a key input parameter to the model must be temperature. Temperature versus depth data was collected at the time of sampling the SSIP cores. This data does not necessarily represent the effective temperature regime under which the isotopic composition of the soil water came into equilibrium. To evaluate the effect of temperature on the NIR model results, an independent means of approximating

temperature with depth was desired. A heat-flow modeling technique has been employed.

Soil temperature varies in response to changing meteorological conditions at the soil surface. From a simplistic viewpoint, the temperature variation may be considered sinusoidal for both the diurnal and yearly cycles. This is not strictly true, when one considers changing weather conditions, and a soil-water and thermal regime which varies in response to wetting and drying of the profile. Under spring and summer conditions at the research site, the soil-water regime was gradually drying. Assuming this to represent quasi-steady conditions, the application of a heat-flow model to predict the temperature distribution with time in the soil should be warranted.

Assuming that the average temperature in the soil is the same for all depths, the following expression accounts for the combined effects of diurnal and annual temperature variations (VanWijk and DeVries, 1963):

$$T(z,t) = T_y + A_y \left(e^{-z/d_y}\right) \left[\sin(\omega_y t + \varphi_y - z/d_y) \right] + A_d \left(e^{-z/d_d}\right) \left[\sin(\omega_d t + \varphi_d - z/d_d) \right] \quad (53)$$

where T is the temperature (C) at some depth z (cm) and time t (sec); T_y is the annual mean temperature (C); A_y is the amplitude of the annual sinusoidal temperature variation at the land surface (C); A_d is the amplitude of the daily sinusoidal temperature variation at the land surface (C); ω_y is the annual radial frequency, or $\omega_y = 2\pi/(31{,}536{,}000) = 1.99\text{x}10^{-7}$ sec^{-1}; ω_d is the daily radial

frequency, or $\omega_d = 2\pi/(86{,}400) = 7.27\text{x}10^{-5}$ sec^{-1}; φ_y is the annual phase constant, or $\varphi_y = -\omega_y t_o$, with t_o = starting time (sec); φ_d is the daily phase constant, or $\varphi_d = -\omega_d t_o$; d_y is a characteristic depth, the annual damping depth (cm); d_d is a characteristic depth, the daily damping depth (cm).

The damping depth may be calculated with the following relation:

$$d_j = (2\lambda/C\omega_j)^{\frac{1}{2}} = (2\alpha/\omega_j)^{\frac{1}{2}} \qquad (54)$$

where λ is thermal conductivity (cal cm^{-1} s^{-1} C^{-1}); C is volumetric heat capacity (cal cm^{-3} C^{-1}); α is thermal diffusivity (cm^2 s^{-1}); and the subscript j denotes either daily or annual. The damping depth represents the depth at which the temperature amplitude has decreased to 0.37 (i.e., 1/e) of the surface amplitude, A_d or A_y. Therefore, the amplitude at some depth z for the daily or annual cycle would be: $A_z = A_j(\exp(-z/d_j))$. This expression also imparts a phase shift, or a time delay, to the temperature peak with depth, which is equal to $-z/d_j$. In combination then, there is an increase in phase lag and decrease in amplitude of the temperature wave as it propagates into the soil at depth. The reason for this phenomenon is that heat can be either absorbed or released from the soil as the soil temperature increases or decreases.

Calibration of the heat-flow model to existing temperature data from the site would add more credibility to the model results. Temperature data has been collected previously at the study site by Stephens et al. (1985) in their soil-physics based work. Specifically, temperature was measured at various depths on a weekly or bi-weekly schedule from December 1982 through May 1985. The data appears to be sinusoidal in nature, thus lending some qualitative assurance that

the analytical heat-flow model should be appropriate. A more detailed discussion of the data and model is presented in chapter 6. Therefore the application of this heat-flow modeling technique should provide a reasonable estimate of the temperature distribution for use in the NIR model.

The use of the NIR model is limited to quasi-steady conditions, and therefore not applicable during all times of the year. As will be shown below, considerable seasonal variation in isotope and water content profiles has been observed at the research site. These variations are in response to wetting, drying and redistribution of soil water in the profile. In order to explain the observed changes in isotope and water content profiles, a one-dimensional mass balance/mixing model is proposed. Hereafter this model is referred to as the MBM model. The MBM model is intended for use in demonstrating that mass balance/mixing phenomena are a potential means of explaining the observed water content and isotope changes with time. Corroboration of the model results with the observed data does not imply that the MBM model conditions are indeed true and accurate, because there may be other phenomena occurring which have not been accounted for. Therefore the MBM model only demonstrates that a mass balance/mixing scenario may be feasible.

For any discretized depth interval the following mass balance equation applies:

$$M_i - M_f = \Delta M = M_o - M_e \tag{55}$$

where M_i is the initial mass of water in the depth interval; M_f is the final mass of water; ΔM represents the change in mass; M_o is the mass of water leaving, or

outflow from, the depth interval; and M_e is the mass of water entering into the depth interval. With multiple depth intervals, M_o from one interval will be M_e for the next adjacent interval. By specifying M_e at one boundary, and having measured M_i and M_f, the equation may be solved for M_o at each successive depth interval, the direction depending on whether drying or wetting is occurring. One may decide to increment the ΔM term to effectively temporalize the solution. In other words, by incrementing ΔM a stepwise iterative procedure results. Therefore this stepwise iterative procedure resembles (to a degree) the actual transient nature of the redistribution process.

For the mixing process, assume an instantaneous blending of water initially in a given depth interval with that which enters. Subsequently, the isotopic composition of the resultant mixture equals the final and outflow compositions. The mixing equation to be solved simultaneously with the mass balance solution becomes:

$$M_i\delta_i + M_e\delta_e = M_o\delta_o + M_f\delta_f = (M_o + M_f)\,\delta_{fo} \qquad (56)$$

where δ_{fo} is the final and outflow isotopic composition of the mixture.

Various techniques have been outlined above for quantifying soil-water movement rates (e.g., soil-physics, chloride mass balance, bomb-pulse ^{3}H and ^{36}Cl), in addition to the NIR model just presented. Another independent technique exists which is worthy of comparison to those just mentioned. Allison et al. (1984) presented a method for calculating the recharge flux from stable-isotope-profile data. The system under consideration is one in which piston displacement and mixing are the primary mechanisms causing the recharge flux. Their technique will henceforth be referred to as the 'piston

displacement/mixing' model, or 'PD/M' model. The PD/M model assumes that a series of precipitation events, all with the same isotopic composition, infiltrate episodically into the soil. Between rainfall events the soil water has a chance to evaporate, and hence become more enriched isotopically. The next precipitation occurrence displaces this heavier water downward in the profile, and the waters mix. If this cycle happens with some degree of regularity, the composition of the soil water on average should be displaced relative to the meteoric water line, but still maintain the meteoric water line slope. The meteoric water line is representative of the isotopic compostion of precipitation in the area. Therefore, a plot of D versus ^{18}O should contain a linear array of data that is some distance to the right of the meteoric water line, and parallel to it. The difference in deuterium excess values for this data versus the meteoric water line can then be used to estimate recharge.

Allison et al.(1984) have plotted the displacement of δD from the meteoric water line against the inverse of the square root of recharge. Their recharge estimates for calibrating this model are from tritium and chloride mass balance techniques. The lower the recharge rate, according to this model, the greater the relative deuterium displacement. Conversely, the higher the recharge rate the closer the isotope values will lie to the meteoric water line. For recharge rates greater than 1 cm/yr, the deuterium displacement becomes so small that the technique loses its sensitivity.

5. A QUANTITATIVE EVALUATION OF A VACUUM DISTILLATION TECHNIQUE TO EXTRACT SOIL WATER FOR STABLE-ISOTOPE ANALYSES

This chapter is a manuscript written for submittal to Chemical Geology, Isotope Geoscience Section, for publication in the Isotope Geoscience journal. The authors are: Robert G. Knowlton, Jr., Andrew R. Campbell, Tim C. Hobbs, and Fred M. Phillips. All the authors are affiliated with the Geoscience Department, New Mexico Institute of Mining and Technology, Socorro, New Mexico.

5.0 ABSTRACT

The study of the stable isotopes of hydrogen and oxygen in soil water requires the extraction of the water from the soil prior to preparation and analysis. We present a detailed methodology for a new vacuum distillation technique. This vacuum distillation technique consists of three steps: 1. freezing the soil water into the soil; 2. evacuation of the distillation apparatus to remove atmosphere; 3. heating of the soil sample to distill the water to a collection flask. The technique was tested to determine optimum freezing times, and heating times as a function of the volume of water in the sample. The accuracy and reproducibility of the distillation procedure was evaluated using a hierarchical analysis of variance (a components-of-variance model). The hierarchical statistics provided estimates of the variance attributed to each level of sample preparation (i.e. distillation method, gas preparation technique, and mass spectrometer analyses). The overall standard deviation associated with preparation and analysis of a soil-water sample is $\pm$ 0.15 $^{\circ}/_{oo}$ for $\delta^{18}O$ and $\pm$ 1.2 $^{\circ}/_{oo}$ for δD. The distillation procedure adds only 0.077 $^{\circ}/_{oo}$ to the uncertainty of $\delta^{18}O$ and 0.45 $^{\circ}/_{oo}$ to the δD. The proposed distillation method is therefore satisfactorily reproducible.

5.1 INTRODUCTION

The systematics of the stable isotopes of hydrogen and oxygen in the water cycle have been understood since the paper by Craig (1961).

Subsequently, numerous studies have focused on investigating stable isotopes in soil water. The behavior of hydrogen and oxygen isotopes in soil water under saturated conditions was first studied by Zimmerman et al. (1967). Allison and co-workers (e.g. Allison 1982; Allison et al. 1985) have investigated stable isotopes in unsaturated soils for estimating evaporation rates. Knowlton et al. (1989) have used the stable isotopes of hydrogen and oxygen in the unsaturated zone to quantify the liquid and vapor components of soil-water movement.

Employing stable-isotope techniques to study soil-water movement in both saturated and unsaturated porous media (as in the studies mentioned above) requires the extraction of water from the soil without isotopic fractionation. Several distillation techniques have been used for accomplishing this task. The procedures for these techniques are outlined below, including a new method developed in the present study.

The results of distillation testing cannot be evaluated directly. Water that is extracted from a soil sample must be subjected to a gas preparation technique prior to analysis of its hydrogen or oxygen isotope ratio on a ratio mass spectrometer. There is a potential error inherent in each step of the process of measuring the isotopic composition of a soil-water sample. A hierarchical analysis of variance, or components-of-variance analysis, was used to estimate the variance of each preparation and analysis step in the above-mentioned procedures. In other words, the analytical error associated with each procedure (i.e. the distillation, hydrogen reduction, CO_2 /H_2O equilibration, and mass

spectrometry procedures) is quantified as a separate component in this statistical analysis.

5.2 DISTILLATION TECHNIQUES

Two techniques are commonly used for extracting soil water from a soil sample without appreciable isotopic fractionation; azeotropic toluene distillation and vacuum distillation. The first technique was discussed briefly by Allison et al. (1985) and the second by Saxena and Dressie (1983). In this paper, we present a vacuum distillation technique, which is significantly different from the Saxena and Dressie (1983) method. The azeotropic toluene and vacuum distillation techniques have been applied in order to provide water samples for analysis of the stable isotopes of hydrogen and oxygen, and also tritium, a radioactive isotope of hydrogen.

5.2.1 Azeotropic Distillation. The azeotropic distillation method relies upon the formation, and subsequent boiling, of an azeotrope to extract water from soil with negligible fractionation. An azeotrope is formed by mixing certain hydrocarbons (e.g. toluene) with water. An azeotrope has the property that its boiling point is different than either of its constituents. For the case of a toluene/water azeotrope, the boiling point is 84 °C (Kirk-Othmer, 1983), significantly lower than the boiling point of water (100 °C) and toluene (110 °C). The boiling of a high weight azeotrope should result in minimal isotopic fractionation (Kirk-Othmer, 1983). Hence, it follows that the distillation of water from a soil sample by azeotropic distillation does not require the complete extraction of the water.

Before beginning an azeotropic distillation, the soil sample must be split, one subsample being used for distilling the soil water, and the other for determining gravimetric water content. The distillation apparatus consists of a soil flask connected to a condensing column, and a heating mantle (Allison et al., 1985). The soil sample is placed in the boiling flask and toluene is added until it just covers the top of the soil. The heating element is set under the flask and the soil/toluene mixture is distilled at a temperature between 84 and 100 °C. When the water/toluene mixture is condensed in the sidearm of the apparatus, the two constituents separate, but some residual dissolved toluene is left in the water.

The water obtained from each sample is purified of toluene contamination by introducing paraffin wax into the sample and heating. The paraffin is intended to absorb the dissolved toluene from the water. Through repeated experimentation, we have found that the effectiveness of the paraffin in purging the sample of toluene is sometimes inadequate. The residual toluene contamination carries through the gas preparation techniques, causing contamination in the mass spectrometer. The accuracy and reproducibility of the azeotropic toluene distillation procedure has not been evaluated in the published literature.

5.2.2 Vacuum Distillation. The first vacuum distillation procedure to be discussed was presented by Saxena and Dressie (1983) (hereafter referred to as the S&D method). The technique requires the use of a desiccation chamber, heating element, vacuum line including two vapor traps, cooling chamber, and a vacuum pump.

The setup of the distillation line includes the connection of the desiccation chamber to the two vapor traps, in series. A valve is placed between the chamber and the traps. The other side of the vapor trap assembly is connected to a valve, which in turn is connected to a vacuum pump. The heating element is placed in the desiccation chamber, with the soil container on the heating element. The vapor traps are cooled to -60 °C with an alcohol-filled chamber and a compressor.

To begin an extraction, the valve to the desiccation chamber is closed, the valve to the vacuum pump opened, and the line is evacuated. The traps are cooled for about 20 minutes. The desiccation chamber valve is slowly opened and the heating element turned on. Approximately 5 hours is required for complete distillation of the soil water. Saxena and Dressie (1983) stated that during standardization of the technique "... the recovery of moisture is almost 100% and practically no fractionation in ^{18}O occurs during storage and extraction". No statistical evaluation was presented in their work.

The second vacuum distillation method for extracting soil water is our new procedure, which is significantly different from the S&D method. The technique employs the use of a distillation line, liquid nitrogen, gaseous nitrogen, a heating element, and a vacuum pump. Figure 5 illustrates the distillation line setup schematically.

This vacuum distillation procedure consists of three steps. First, the soil water is frozen. Next, a vacuum is applied to the distillation line. Finally, the soil sample is heated and the soil water distilled over to a collection flask cooled

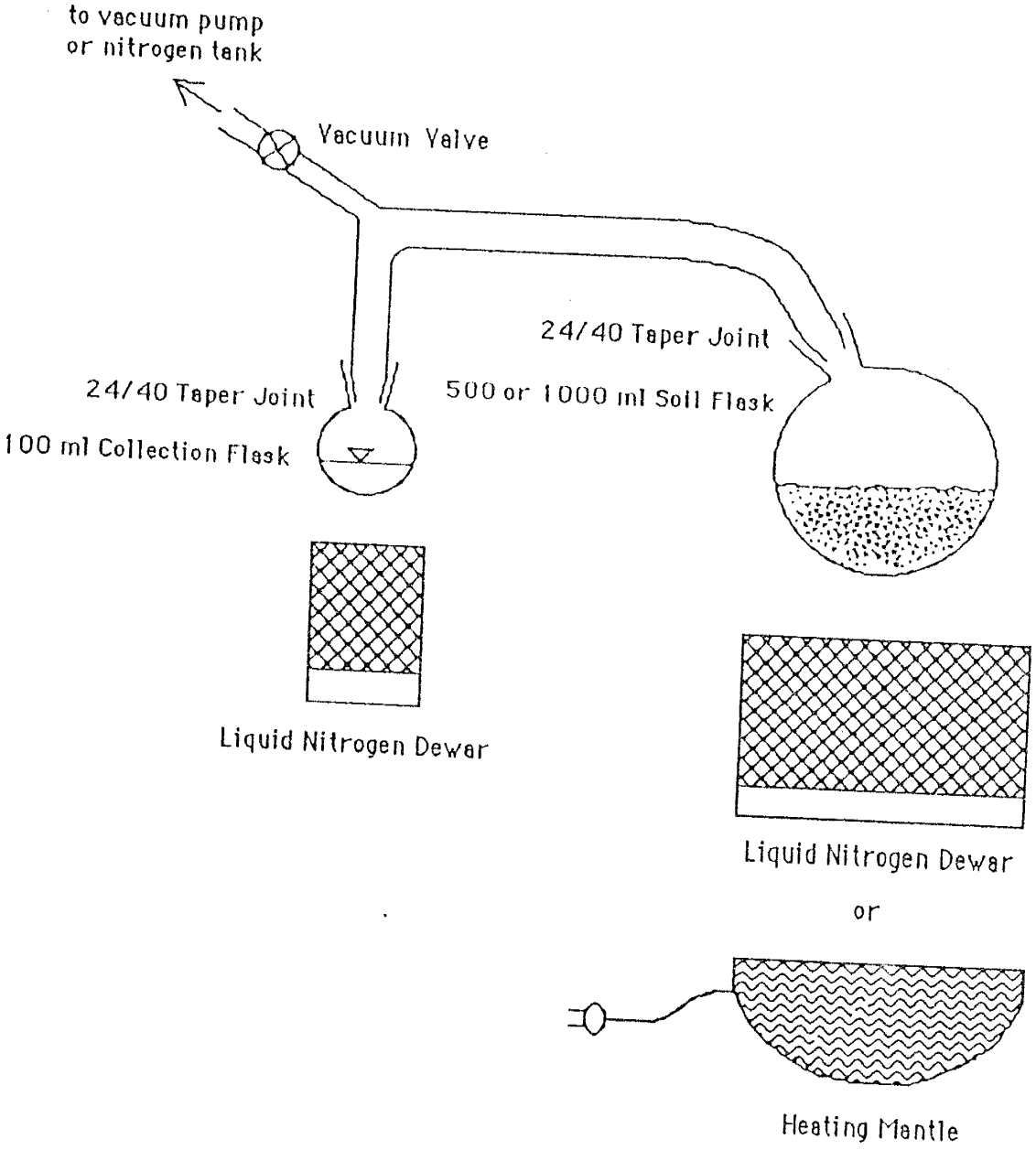

Figure 5 - Schematic diagram of vacuum distillation line setup

with liquid nitrogen. The distillation continues until all the water is extracted from the soil. A more detailed discussion of the procedures involved in this vacuum distillation technique follows.

In the first step, the glass flasks and the distillation line are flooded with gaseous nitrogen from a compressed gas cylinder, which displaces atmospheric gases and water vapor. A soil sample is placed in the boiling/freezing flask and the distillation line is assembled. With the distillation line completely sealed, a liquid nitrogen bath is placed around the soil flask. The soil water is frozen for a period of approximately 10 minutes.

Next, a vacuum pump is attached to the vacuum valve and the atmosphere in the distillation line is evacuated. The pressure is decreased to a vacuum pressure of 100-200 millitorr (approximately 5 minutes of pumping time) which speeds the distillation process. The vacuum valve is closed, the liquid nitrogen taken away, and a heating element placed under the soil flask. A liquid nitrogen filled dewar is placed around the capture vessel.

The distillation of soil water from the soil flask to the capture vessel proceeds under a vapor pressure gradient (which may impart an advective flow component if the diffusion gradient is great enough). This procedure may take several hours depending on the amount of soil water in the sample, and the soil texture. When all the soil water has been condensed into the capture flask, as evidenced by the cessation of condensation, the distillation line is flooded with gaseous nitrogen again. This step minimizes atmospheric contamination, and pressurizes the line for subsequent dismantling. The capture flask is removed

and immediately capped. If moisture content data is desired, the weighing of flasks before and after distillation enables that calculation, inasmuch as all the water is distilled from the soil. The sample does not need to be split to determine water content, as in the azeotropic distillation procedure. After the frozen water in the collection flask has thawed it is transferred to a storage bottle. It is imperative that the soil water be stored in sealed sample bottles, with an additional paraffin seal around the top, to prevent any evaporation or contamination.

5.3 EVALUATION

5.3.1 Vacuum Distillation Testing

Various aspects of our vacuum distillation technique have been tested to assure that adequate extractions can be performed. The lengths of time for freezing and heating the soil water are two of the most important factors in the distillation procedure. Without adequate freezing and heating times there is a greater fractionation potential, because of incomplete yield. Also, the volume of soil water to be distilled is a major factor in determining the time required for freezing and heating.

Before discussing the issue of adequate freezing and heating times, the potential for fractionation due to incomplete yield will be addressed. The change in isotopic composition versus residual fraction of water in the distillation process is quantitatively evaluated through a Rayleigh distillation/mass balance approach.

The estimation of the isotopic composition of the water not yet distilled, or the residual fraction, is modeled as a simple Rayleigh distillation process:

$$\delta_r = \delta_i + \epsilon \ln f \tag{57}$$

where,

δ_r = isotopic composition of residual water

δ_i = isotopic composition of initial water

ϵ = isotopic enrichment factor

f = mass fraction of residual water in the soil

The water retrieved in the cold trap, the distillate, is related to the initial and residual isotopic compositions as:

$$\delta_i = \delta_r f + \delta_d (1-f) \tag{56}$$

where δ_d is the isotopic composition of the distillate. Therefore, for a given residual fraction of water left in the soil, f, the difference in isotopic composition between the distillate water and the initial water is:

$$\delta_d - \delta_i = [\ (\delta_i - (\delta_r f))/(1-f)\ ] - \delta_i \tag{59}$$

Rearranging equation 59 yields:

$$\delta_d - \delta_i = ((\delta_i - \delta_r)\ f)/(1-f) \tag{60}$$

Substituting equation 57 into equation 60 gives:

$$\delta_d - \delta_i = ((-\epsilon \ln f)\ f)/(1-f) \tag{61}$$

The isotopic enrichment factor, ϵ, is related to the equilibrium fractionation factor, α, by:

$$\epsilon = 1 - \alpha \tag{62}$$

The equilibrium fractionation factors for ^{2}H and ^{18}O are temperature dependent. From Majoube (1971), the formulation of α for deuterium is:

$$10^3 \ln\alpha = 24.844(10^6/T^2) - 76.248(10^3/T) + 52.612 \quad (63)$$

and for oxygen-18:

$$10^3 \ln\alpha = 1.137(10^6/T^2) - 0.4156(10^3/T) - 2.0667 \quad (64)$$

where T is temperature in Kelvin.

The effect of incomplete yield is therefore evaluated by applying equations 61 through 64 to relate the residual fraction of water remaining in the soil to the deviation in isotopic composition between the distillate and the initial water. Figure 6 illustrates the relationship between the change in isotopic composition of δD and the residual fraction of water distilled, for several distillation temperatures. A similar set of data are presented in figure 7 for the change in δ^{18}O with residual fraction. From these graphs, we can infer that the soil water yield has to be greater than 99.75 percent of the total water in the soil sample, or the isotopic composition of the water will change by almost 1 $^{\circ}/_{oo}$ for δD and 0.1 $^{\circ}/_{oo}$ for δ^{18}O. The results of this analysis illustrate the importance of acquiring as complete a yield of soil water from the sample as possible in the distillation process. Unfortunately the analytical precision associated with weighing the sample is inadequate to evaluate a $\geq$ 99.75% yield.

An adequate freezing time is important to assure that all the soil water remains in the soil when the vacuum is applied to the distillation line. There is a potential for fractionation if water is lost from the system. Figure 8 shows a plot of δ^{18}O versus freezing time for a fine-grained sand with volumetric water content of 0.115 cc/cc, and a total volume of water equal to 15 ml. Water of a known isotopic composition was used for each test. The mean value of the

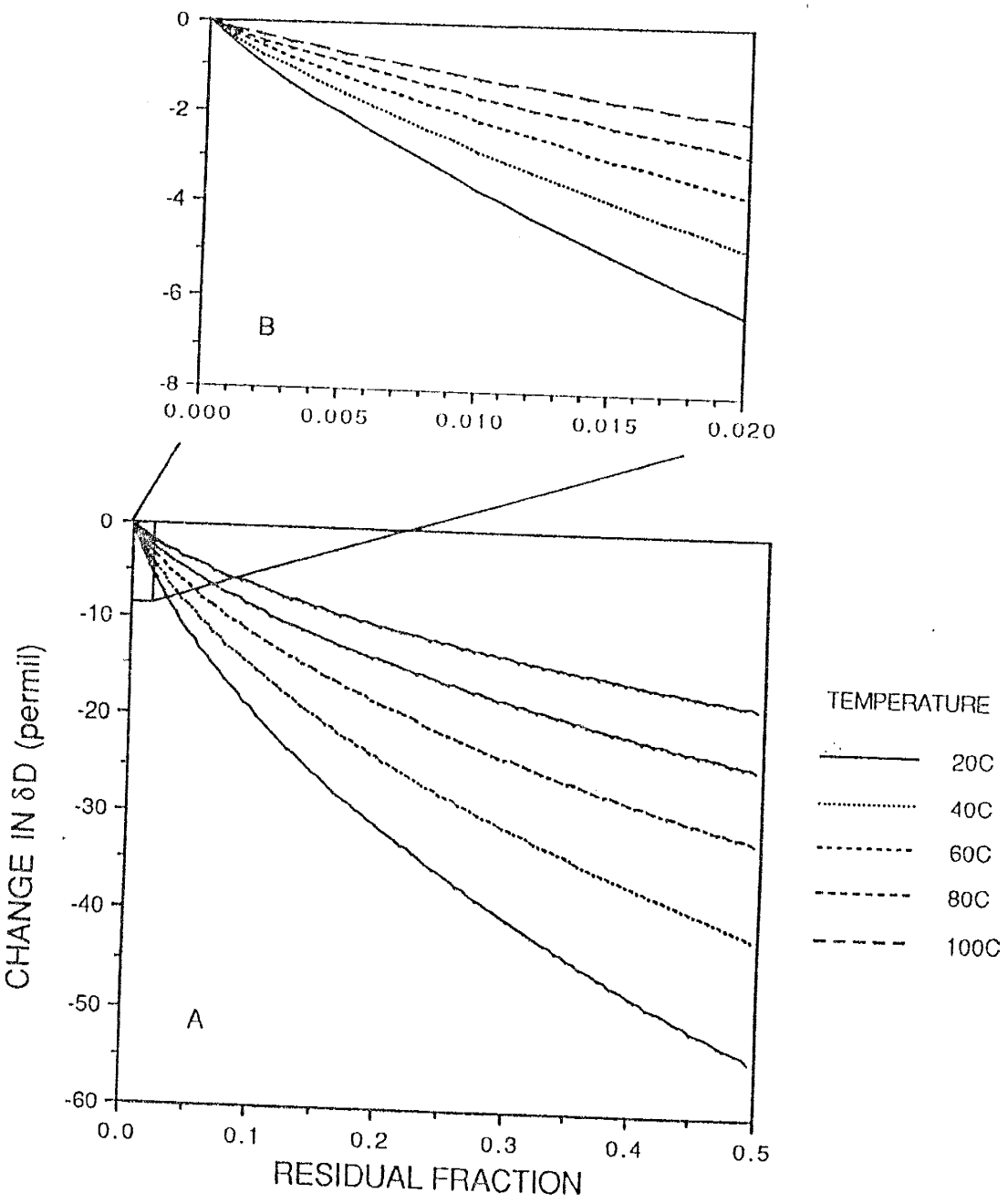

Figure 6 - Change in δD versus residual fraction of water remaining during the distillation process. Figure 6B is a subset of 6A

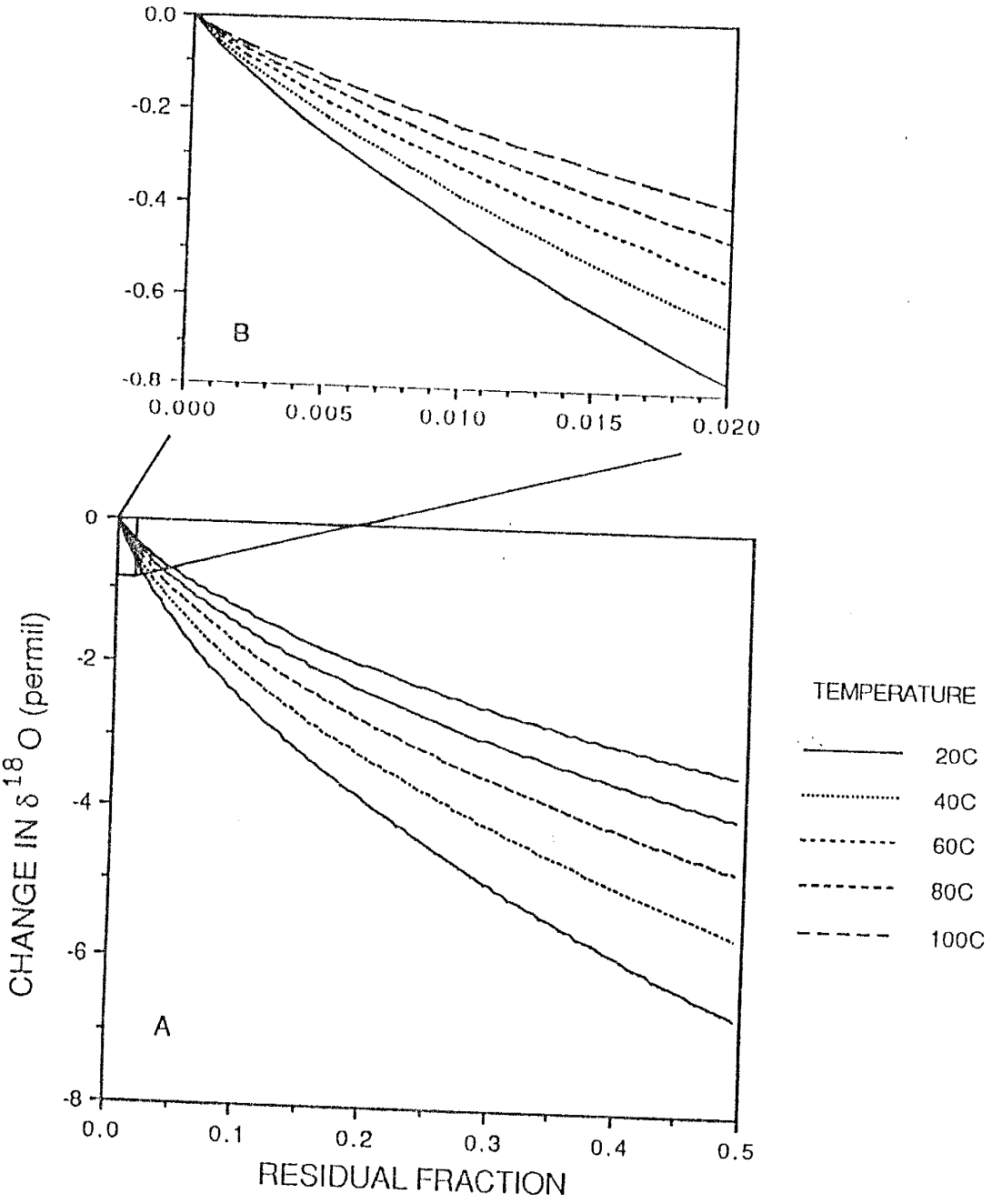

Figure 7 - Change in $\delta^{18}O$ versus residual fraction of water remaining during the distillation process. Figure 7B is a subset of 7A

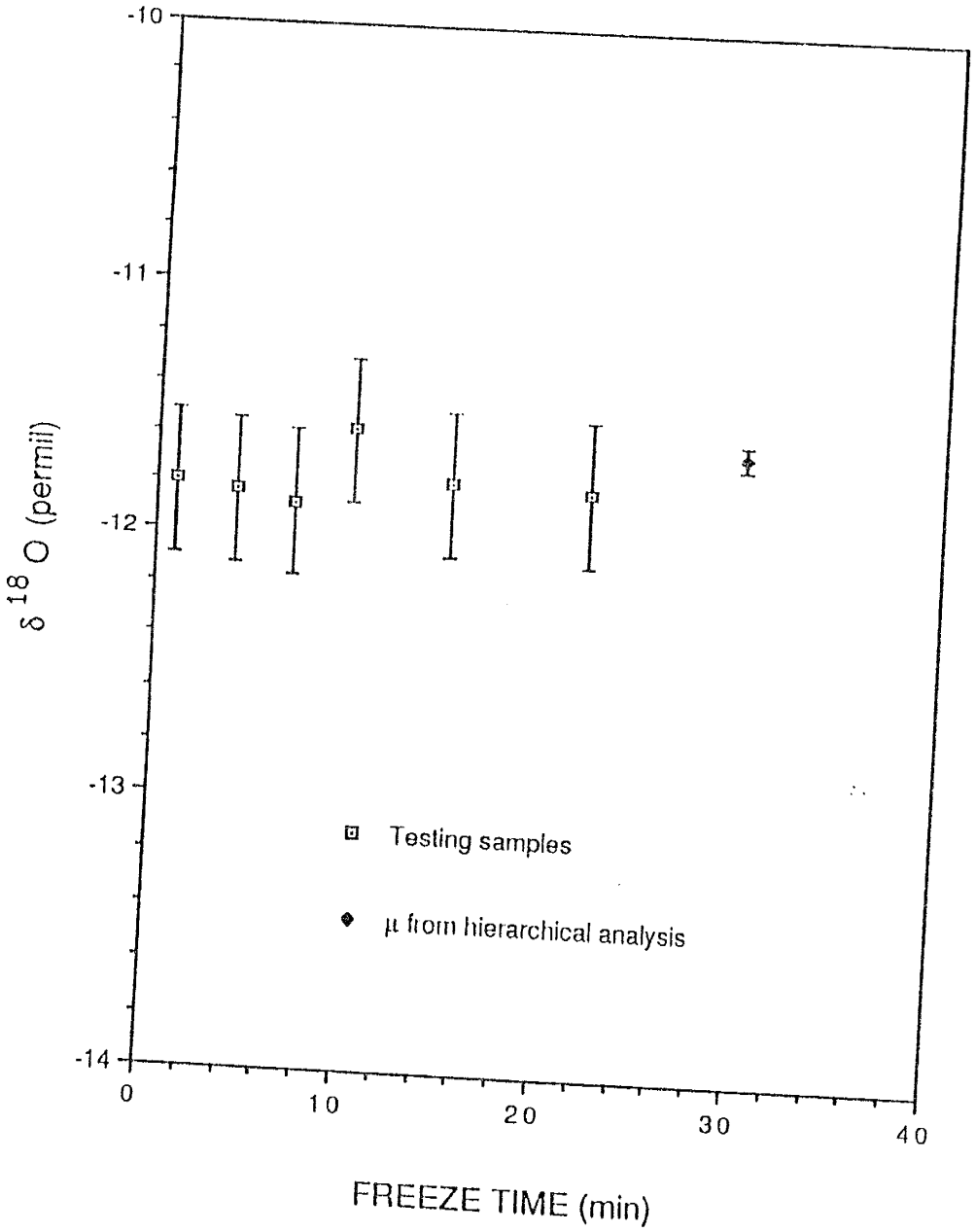

Figure 8 - $\delta^{18}O$ versus freezing time for a sand with 15 ml of water, and volumetric water content of 0.115 cc/cc. The mean and 95% confidence intervals are calculated from the hierarchical statistical analysis

isotopic composition of this water was determined through the hierarchical statistical analysis, discussed below. The analytical error bars shown on the plot are also defined in the next section. The minimum freezing time for this sample type is about 10 minutes. The heating time for each sample was 3 hours. For soils of differing texture, and/or volume of water, the minimum freezing time may vary slightly.

The time of heating is important to assure adequate distillation results. Figure 9 depicts the $\delta^{18}O$ ratio versus time of heating for the same soil and water used in the freeze-time testing. For each sample shown in figure 9, a 30 minute freezing time was employed. The heating time is considered to commence as soon as the liquid-nitrogen bath is removed from the frozen soil flask and the heater applied. Hence, several minutes may elapse before the soil water begins to melt and distill over. The total heating time for this soil and water should be about 2.5 hours, based upon the data in figure 9.

The heating time required varies for soil samples of different water contents, and is most strongly dependent upon the volume of water in the soil, not strictly the water content. Textural differences (i.e. sand, silt, or clay) may also influence the heating time required for an adequate distillation.

An empirical estimation of heating time versus volume of water distilled can be made from data obtained by Knowlton et al. (1989). In their study, several unsaturated soil cores were collected and the isotopic composition of the soil water analyzed. The samples from each soil core were relatively homoge-

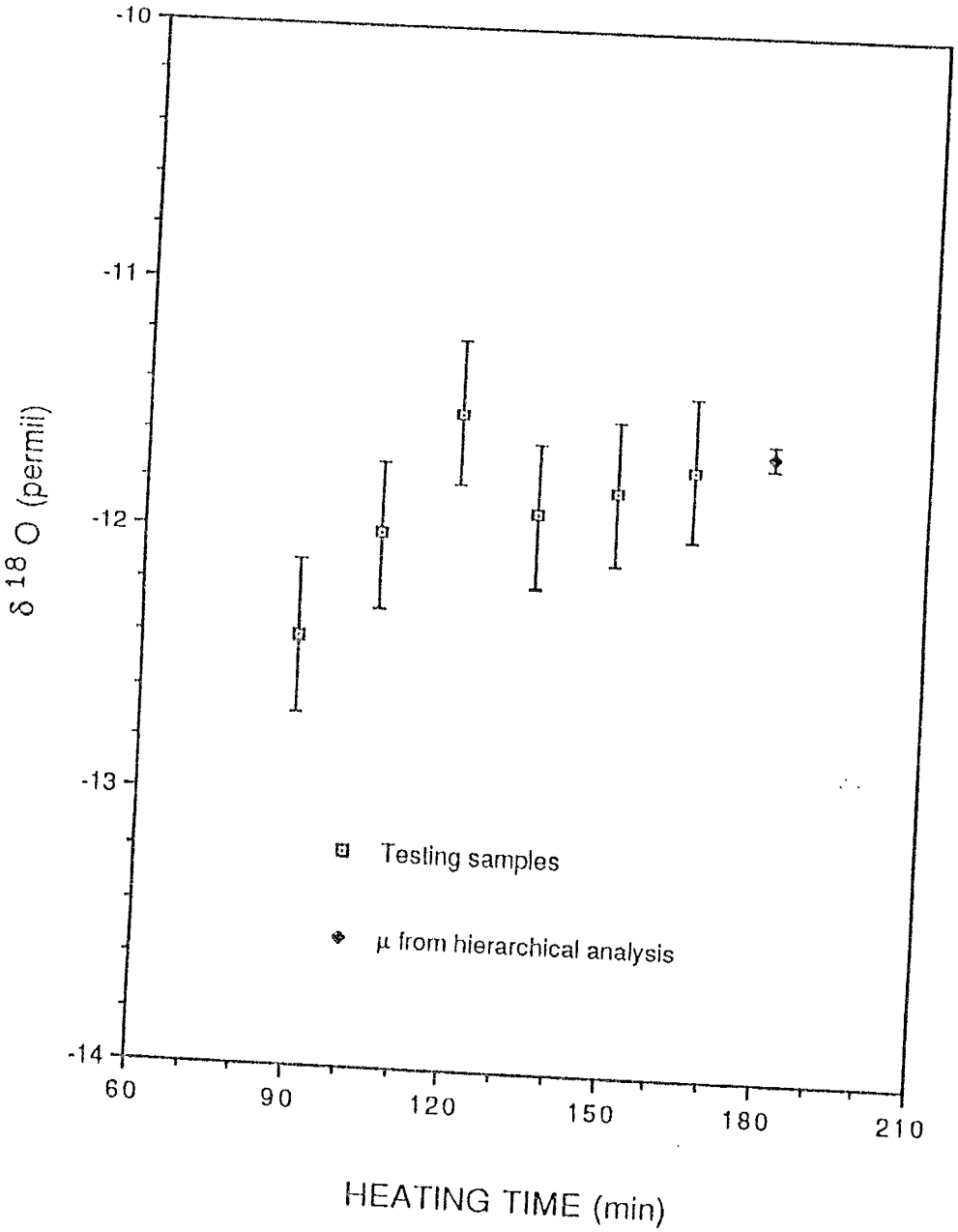

Figure 9 - $\delta^{18}O$ versus heating time for a sand with 15 ml of water, and volumetric water content of 0.115 cc/cc. The mean and 95% confidence intervals are calculated from the hierarchical statistical analysis

neous in texture (fine-grained sand), but did vary somewhat in terms of water content and sample size.

The heating time for each sample distilled by Knowlton et al. (1989) was determined subjectively, by the lab technician deciding when the distillation was complete. The heating process was augmented periodically by utilizing a heat gun to vaporize any condensed water in the line so it can condense into the collection flask. The cessation of any condensation of water at the top of the collection flask indicated a probable end to the distillation. An additional 15 to 20 minutes of heating time was then allowed as a factor of safety. Figure 10 shows a plot of heating time versus volume of water distilled. A linear regression on this data yields the following result:

$$t = 91.1 + 6.13(V) \tag{65}$$

where t = heating time (min), V = volume of soil water distilled (ml), and R^2 = 0.87. This is an empirical result, and as such, may not apply to other soils.

5.3.2 Analysis of Variance

A hierarchical analysis of variance, or components- of-variance model, is frequently used to compare sources of variability when factors are 'nested' within other factors. The model has been presented in Snedecor and Cochran (1973) and Graybill (1961). This technique allows for the estimation of the variance in the final result attributed to each level of the sample preparation procedures. Therefore, an estimate of variance is made for each of the following: distillation

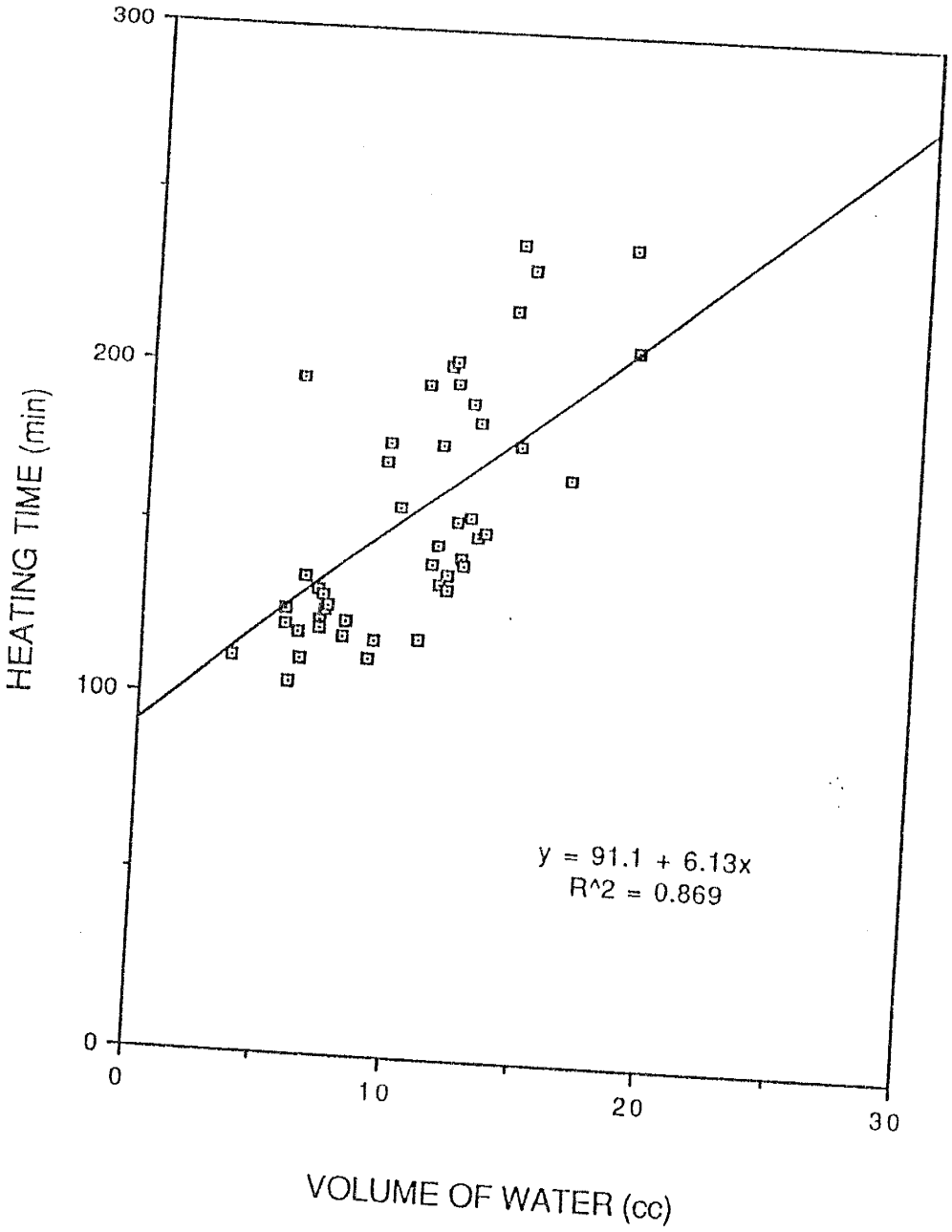

Figure 10 - Heating time versus volume of soil water distilled from field samples collected by Knowlton et al. (1989)

method, hydrogen reduction technique, CO_2 /H_2O equilibration procedure, and mass spectrometry measurements.

The soil-water extraction method employed in this testing was the new vacuum distillation technique presented above. The soil and water used are the same as those described in the previous section. A 'zinc' hydrogen reduction method (Kendall and Coplen, 1985; Coleman et al., 1982) was employed as the gas preparation technique for deuterium. For the ^{18}O gas preparation, we used the CO_2 /H_2O equilibration procedure that has been outlined by Epstein and Mayeda (1953) and Roether (1970). The isotope ratio measurements for δD and $\delta^{18}O$ (relative to SMOW) were performed on a Finnegan-MAT Delta E ratio mass spectrometer at the New Mexico Institute of Mining and Technology in Socorro, NM. The manufacturer's quoted precision on $\delta^{18}O$ measurements is $\pm$ 0.05 °/$_{oo}$ (permil), and on δD is $\pm$ 0.5 °/$_{oo}$.

The measured isotope ratio value of a given test sample is represented as Y_{ijk}, where:

$$Y_{ijk} = \mu + D_i + G_{ij} + M_{ijk} \qquad (66)$$

with:

$$i = 1,2,...,I; \quad j = 1,2,...,J; \quad k = 1,2,...,K$$

where:

$\mu = E(Y_{ijk})$ = overall mean

E() = expected or average value

D_i = a random variable, representing the effect of distillation i

G_{ij} = a random variable, representing the effect of gas preparation j, from distillation i

M_{ijk} = a random variable, representing the effect of mass spectrometry result k, from gas preparation j, which is from distillation i

D_i, G_{ij}, and M_{ijk} are all assumed to be statistically independent of each other. The expected values of the uncertainties are assumed to equal zero:

$$E(D_i) = E(G_{ij}) = E(M_{ijk}) = 0$$

The variances of the uncertainties are represented as:

$$var(D_i) = \sigma_D^2 \; ; \; var(G_{ij}) = \sigma_G^2 \; ; \; var(M_{ijk}) = \sigma_M^2$$

The total number of distillations performed is I, the number of gas preparations performed on each distillation (i) is J, and the number of mass spectrometry analyses done on each gas preparation (j) is K. For the case where all K's are equal for each j, and all J's are equal for each i, the model is considered balanced.

For each level, or factor, in the analysis (i.e. distillation = factor 1, gas prep = factor 2, mass spectrometry = factor 3) the sum of the squares must be calculated. Snedecor and Cochran (1973) give formulas for calculating the sum of the squares for each factor (i.e. SS1, SS2, and SS3). The mean square estimate of each factor is obtained by dividing the sum of the squares term by the degrees of freedom, such that:

$$MS1 = SS1/(I-1) \tag{67}$$

$$MS2 = SS2/(I(J-1)) \tag{68}$$

$$MS3 = SS3/(IJ(K-1)) \tag{69}$$

The expected value of the mean square estimates is then given as:

$$E(MS1) = \sigma_D^2 + K\sigma_G^2 + JK\sigma_M^2 \tag{70}$$

$$E(MS2) = \sigma_D^2 + K\sigma_G^2 \tag{71}$$

$$E(MS3) = \sigma_D^2 \tag{72}$$

Estimates of the variance at each level are made by:

$$\hat{\sigma}_M^2 \approx MS3 \tag{73}$$

$$\hat{\sigma}_G^2 \approx (MS2\text{-}MS3)/K \tag{74}$$

$$\hat{\sigma}_D^2 \approx (MS1\text{-}MS2)/JK \tag{75}$$

An analysis of variance (ANOVA) table is constructed as in table 2 to facilitate the calculation of the formulas presented above.

A hierarchical analysis of variance was performed on two sets of experiments, for deuterium and oxygen-18. Four distillations were performed, such that I=4. For the oxygen-18 experiments, three CO_2 /H_2O equilibrations were done on each distilled water sample, for J=3. Three hydrogen reductions were also performed on each distilled sample, so that J=3. Three mass spectrometric analyses were performed on each gas sample prepared, for K=3, on both the hydrogen and oxygen gases.

The results of these analyses are presented in the ANOVA tables 3a and 3b. The overall variance estimate for a given sample is equal to the sum of the variances at each level, or:

$$\hat{\sigma}_T^2 \approx \hat{\sigma}_M^2 + \hat{\sigma}_G^2 + \hat{\sigma}_D^2 \tag{76}$$

Table 2 - Analysis of Variance (ANOVA) table setup

Source	SS	d.f.	MS	E(MS)
Factor 1	SS1	I-1	MS1	$\sigma_M^2 + K\sigma_G^2 + JK\sigma_D^2$
Factor 2	SS2	I(J-1)	MS2	$\sigma_M^2 + K\sigma_G^2$
Factor 3	SS3	IJ(K-1)	MS1	σ_M^2

Note: SS = sum of the squares; d.f = degrees of freedom; MS = mean square estimate; E(MS) = expected value of the mean square estimate.

Table 3a - ANOVA table for $\delta^{18}O$ testing

Source	SS	d.f.	MS	E(MS)
Distillation	0.50	3	0.168	(0.00047)+(3)(0.0049)+(3)(3)(0.017)
CO2/H2O Equil.	0.12	8	0.015	(0.00047)+(3)(0.0049)
Mass Spec.	0.01	24	0.0005	(0.00047)

Table 3b - ANOVA table for δD testing

Source	SS	d.f.	MS	E(MS)
Distillation	30.1	3	10.04	(0.021)+(3)(0.54)+(3)(3)(0.97)
H2 Reduction	13.2	8	1.65	(0.021)+(3)(0.54)
Mass Spec.	0.50	24	0.021	(0.021)

The square root of the variance estimate is equal to the standard deviation. Table 4 summarizes the variance and standard deviation estimates for each level of analysis, including the overall statistics.

The estimates of variance made for each of these preparation and analysis procedures are indicative of the variability in our methods and equipment. Other laboratories may have slightly different analytical errors associated with their techniques. If other gas preparation techniques are used, such as uranium reduction in place of zinc reduction, then the variance estimate at this level may not be applicable, and other tests should be performed to quantify the variability.

5.4 CONCLUSIONS

The accuracy of measuring the stable-isotopic composition of soil water depends upon the analytical uncertainty of the various preparation and analysis techniques. Through a hierarchical analysis of variance technique, estimates of the variance at each level of sample preparation are made (i.e. distillation method, gas preparation technique, and mass spectrometry).

For the hierarchical analysis performed to evaluate the variability in each step with regard to $\delta^{18}O$, the following results apply: the variance of the distillation method is 0.017, with $\sigma = 0.13\ ^{\circ}/_{oo}$; the variance of the CO_2 /H_2O equilibration technique is 0.0049, with $\sigma = 0.07\ ^{\circ}/_{oo}$; the variance of the mass spectrometry analyses is 0.00047, with $\sigma = 0.022\ ^{\circ}/_{oo}$; and an overall variance of 0.022, with $\sigma = 0.15\ ^{\circ}/_{oo}$.

Table 4 - Variance and standard deviation estimates

Source	$\delta^{18}O$		δD	
	variance	σ	variance	σ
Distillation	0.017	0.13	0.93	0.97
Gas Prep.	0.0049	0.070	0.54	0.74
Mass Spec.	0.00047	0.022	0.021	0.14
Total	0.022	0.15	1.5	1.2

The same type of analysis performed for δD yields the following: the variance of the distillation method is 0.93, with $\sigma = 0.97\ ^{\circ}/_{oo}$; the variance of the zinc hydrogen reduction technique is 0.54, with $\sigma = 0.74\ ^{\circ}/_{oo}$; the variance of the mass spectrometry analyses is 0.021, with $\sigma = 0.14\ ^{\circ}/_{oo}$; and an overall variance of 1.5, with $\sigma = 1.2\ ^{\circ}/_{oo}$.

Our distillation procedure adds only $0.077\ ^{\circ}/_{oo}$ to the uncertainty of ^{18}O and $0.45\ ^{\circ}/_{oo}$ to the uncertainty of D. The reproducibility of our proposed distillation technique is therefore satisfactory for isotopic investigations of soil water.

6. RESULTS AND DISCUSSION

6.1 Field Sampling and Analytical Results

In order to use the theory presented in chapter 4, a number of soil cores were obtained throughout the term of the project. The eight cores, or profiles sampled, cannot all be used in evaluating the processes that contribute to soil-water movement, inasmuch as some of the earlier data were needed to refine preparation and analytical techniques. Data obtained in the sampling of these profiles, both isotopic and soil moisture related, are presented in appendix B. All profiles were collected at the Sevilleta National Wildlife Refuge research site. More specifically, the cores were taken near the same locale that Phillips et al. (1988) sampled for bomb-pulse ^{36}Cl and ^{3}H, and adjacent to the site investigated by Stephens and Knowlton (1986) (see figure 4).

The first core was taken during the fall of 1986. The Sevilleta Stable Isotope Profile 1, SSIP1, was sampled from land surface to a depth of 5.0 meters with the NMEID auger rig. The soil water was distilled from each subsample with the azeotropic toluene distillation technique, described above. The CO_2/H_2O equilibration technique was used to obtain CO_2 gas to analyze at Yale University. These samples contained enough toluene contamination so as to interfere with the mass spectrometric analyses. Owing to the relatively small water volumes obtained from these subsamples, additional isotopic work could not be performed on this core.

The second core from the site, SSIP2, was also obtained with the aid of the EID drill rig. This core was drilled to a depth of 5.0 meters in September 1987. Again, azeotropic toluene distillations were performed to extract the soil water from the subsamples. Special precautions were taken in purifying the soil water of dissolved toluene. This involved the repeated application of a paraffin absorbent. Oxygen analyses were performed at the University of New Mexico. Despite the added precautions, these samples also proved to be contaminated with toluene. The azeotropic toluene distillation procedure was then considered inadequate for consistent reproducibility. At this point a new vacuum distillation procedure was developed and tested, as discussed in chapter 5.

The third core, SSIP3, was hand augered on April 20, 1988 to a depth of 4.40 meters. The new vacuum distillation technique was used to obtain the soil-water samples. The oxygen-18 data were analyzed at two different laboratories, the University of Missouri laboratory at St. Louis, MO, and the U.S. Geological Survey (USGS) laboratory in Reston, VA. The depth versus $^{18}O/^{16}O$ ratio for this core is shown in figure 11. The hydrogen was obtained from these samples using the zinc reduction technique, discussed above. The $^{2}H/H$ ratios were obtained at the University of New Mexico. Figure 12 shows the depth versus $^{2}H/H$ ratios for SSIP3. Appendix B contains the isotopic, water content, and temperature data versus depth for this core.

Data from SSIP3 were not of sufficiently high quality to use for the determination of soil-water movement, for several reasons. First, considerable scatter in the isotope ratios with depth is apparent from figures 11 and 12. This

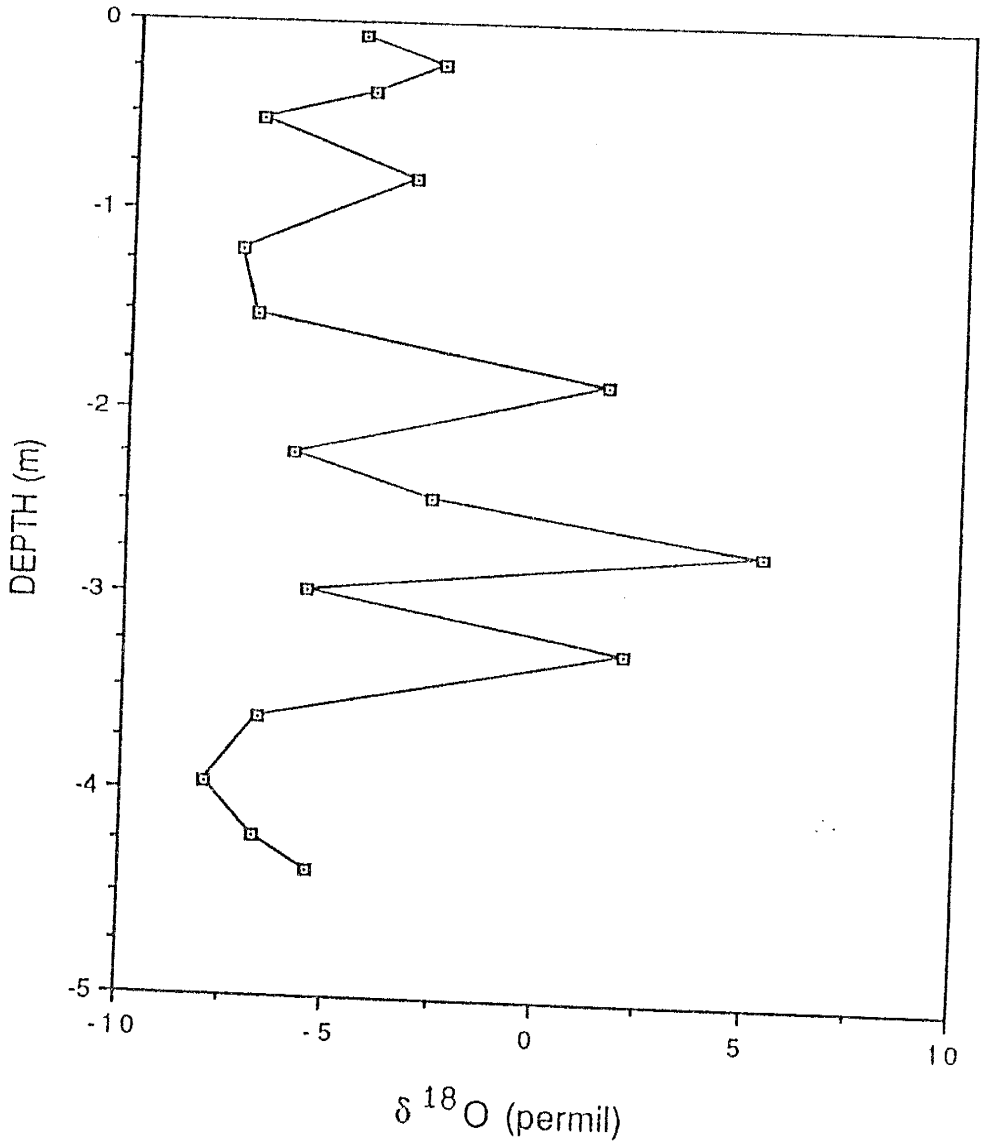

Figure 11 - Depth versus $\delta^{18}O$ for SSIP3 core

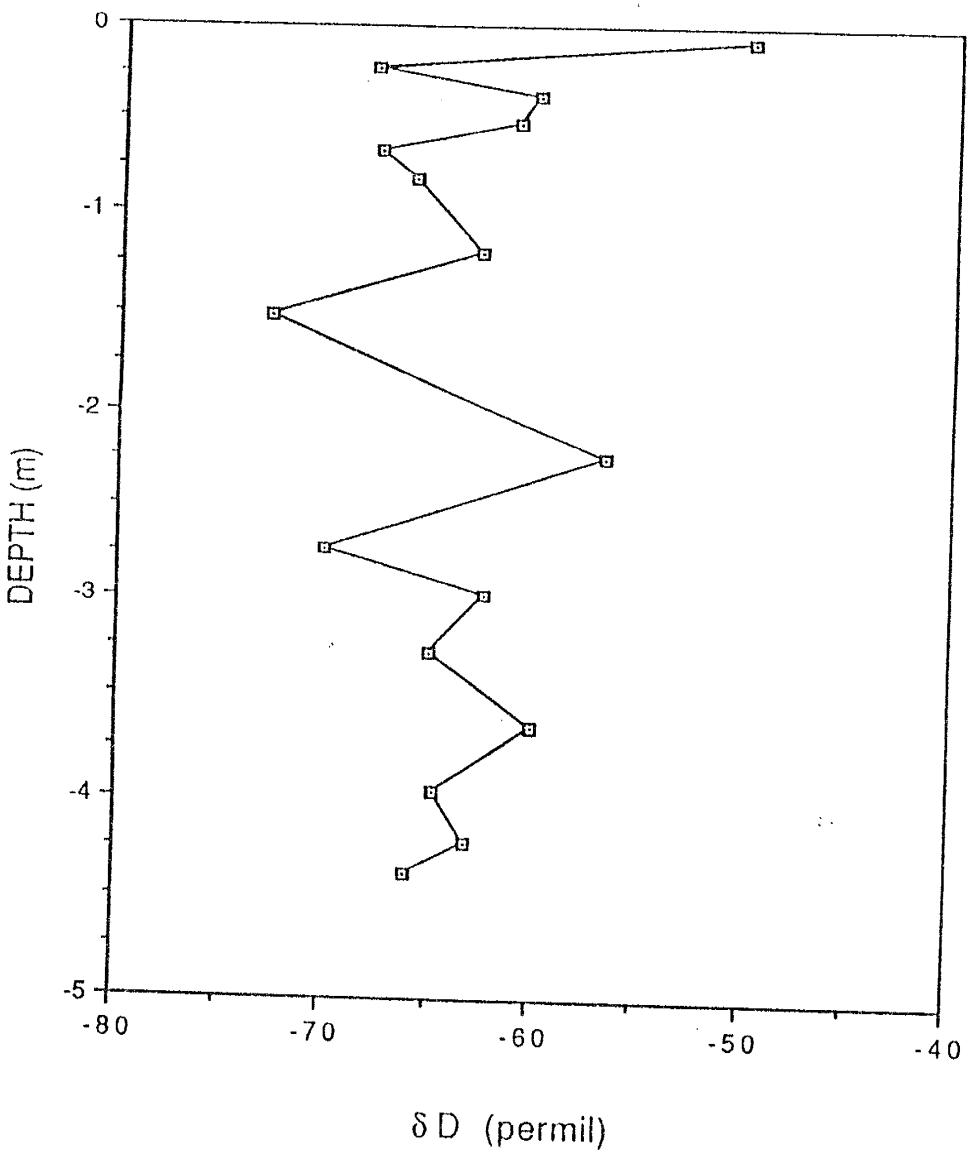

Figure 12 - Depth versus δD for SSIP3 core

scatter is probably due to the inadequacies of the distillation technique at the time. Refinements in the distillation procedure were made to correct for this problem, as discussed in the distillation section above.

In addition, the data obtained from the University of Missouri were potentially in error due to a machine malfunction. Unfortunately, the mass spectrometer at Missouri had developed a leak in the inlet system, causing fractionation of the standard gas, and consequently erroneous results. Correction factors were formulated and applied to the ratio data. These data, in conjunction with the data obtained from the USGS lab, make a very irregular plot of depth versus oxygen-18. Also, several duplicate samples were sent to both labs, with markedly different results. The Missouri data are considered most suspect, owing to the machine breakdown. However, the number of oxygen-18 data from the USGS analyses is insufficient to adequately define the profile.

The hydrogen data from SSIP3 also exhibit considerable scatter with depth, even though all isotopic analyses were performed at UNM. Again, this is probably due to developmental problems with the distillation procedure at the time. In addition, the profile does not have an adequate depth discretization within the top 30 cm or so to define the characteristic shape of the profile. Therefore, this core was considered a test case for defining better sampling and preparation techniques for the next profile.

The fourth soil profile collected, SSIP4, was sampled to a depth of 5.0 meters by hand augering on May 17, 1988. This profile was sampled a few days

after a precipitation event (Stein, T., personal communication, May 17, 1988). Figure 13 shows the monthly precipitation versus time at the Sevilleta site over a one year period from January 1988 through December 1988. Refinements in the vacuum distillation technique were applied during preparation of these samples. The oxygen-18 and deuterium analyses were performed at the New Mexico Institute of Mining and Technology. Figures 14 and 15 show the depth versus $\delta^{18}O$ and depth versus δD, respectively, for SSIP4.

The data presented in figures 14 and 15 show some scatter, in comparison to the relatively smooth profiles reported previously in the literature (e.g. Allison et al., 1984). Sources of error probably include insufficient distillation times and/or improper sealing of the soil-water storage bottles. These problems have been addressed in the methods section above.

On August 4, 1988, two soil cores were obtained at the Sevilleta research site, SSIP5 and SSIP6. The two borings were made approximately 70 cm apart. The reason for obtaining duplicate cores was to assure reproducibility in the sampling and processing of soil cores. The concern over reproducibility stems from the variability in isotopic compositions with depth observed in the SSIP4 profile. The SSIP5 and SSIP6 cores were hand-augered to depths of 4.55 and 3.40 meters, respectively.

The vertical discretization of sampling within the SSIP5 core was increased, relative to the other profiles collected at the site, to define better the characteristic shape of the isotope profiles. Figures 16 and 17 show the depth versus $\delta^{18}O$ and depth versus δD profiles, respectively, for the SSIP5 core. The

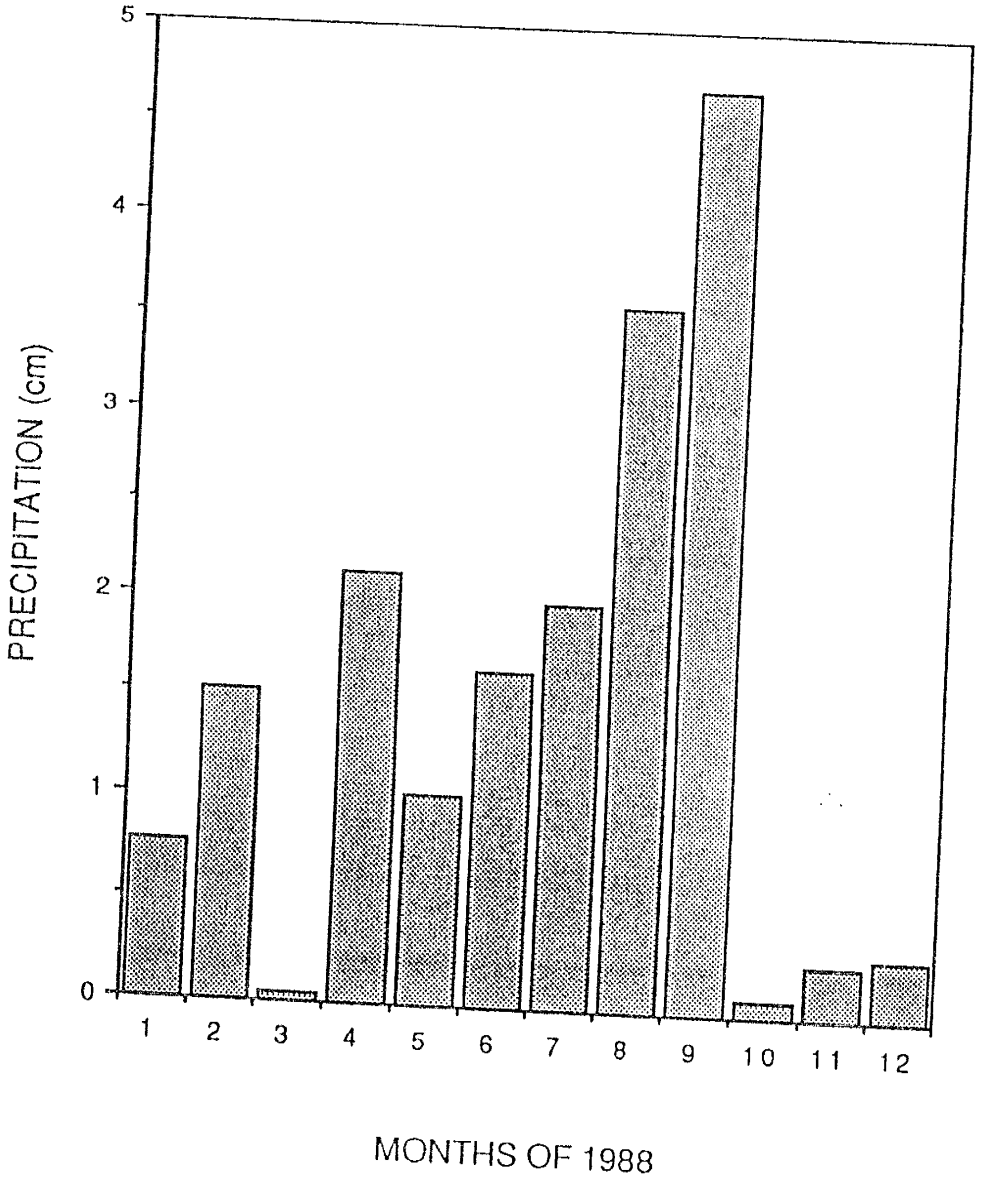

Figure 13 - Time versus precipitation (Stein,T., written communication, May 1989)

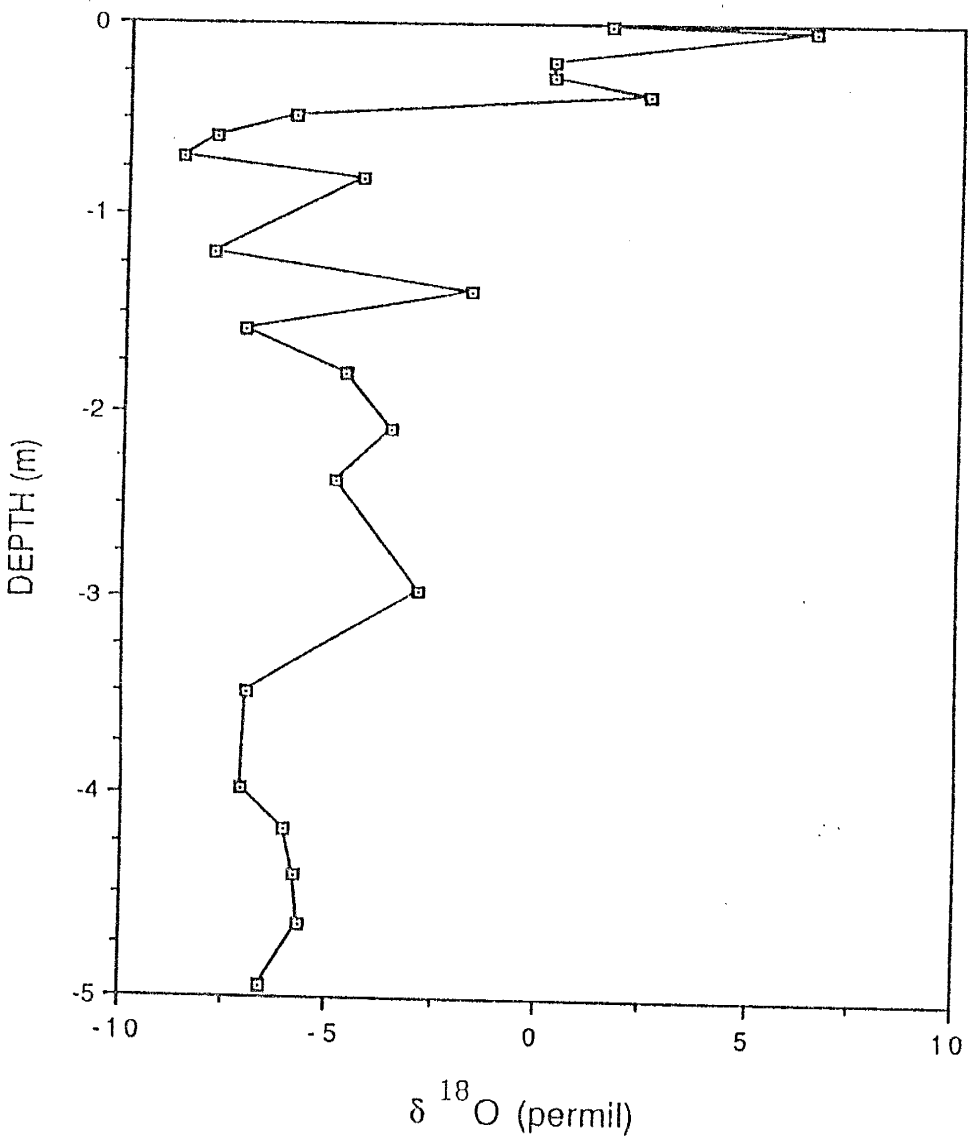

Figure 14 - Depth versus $\delta^{18}O$ for SSIP4 core

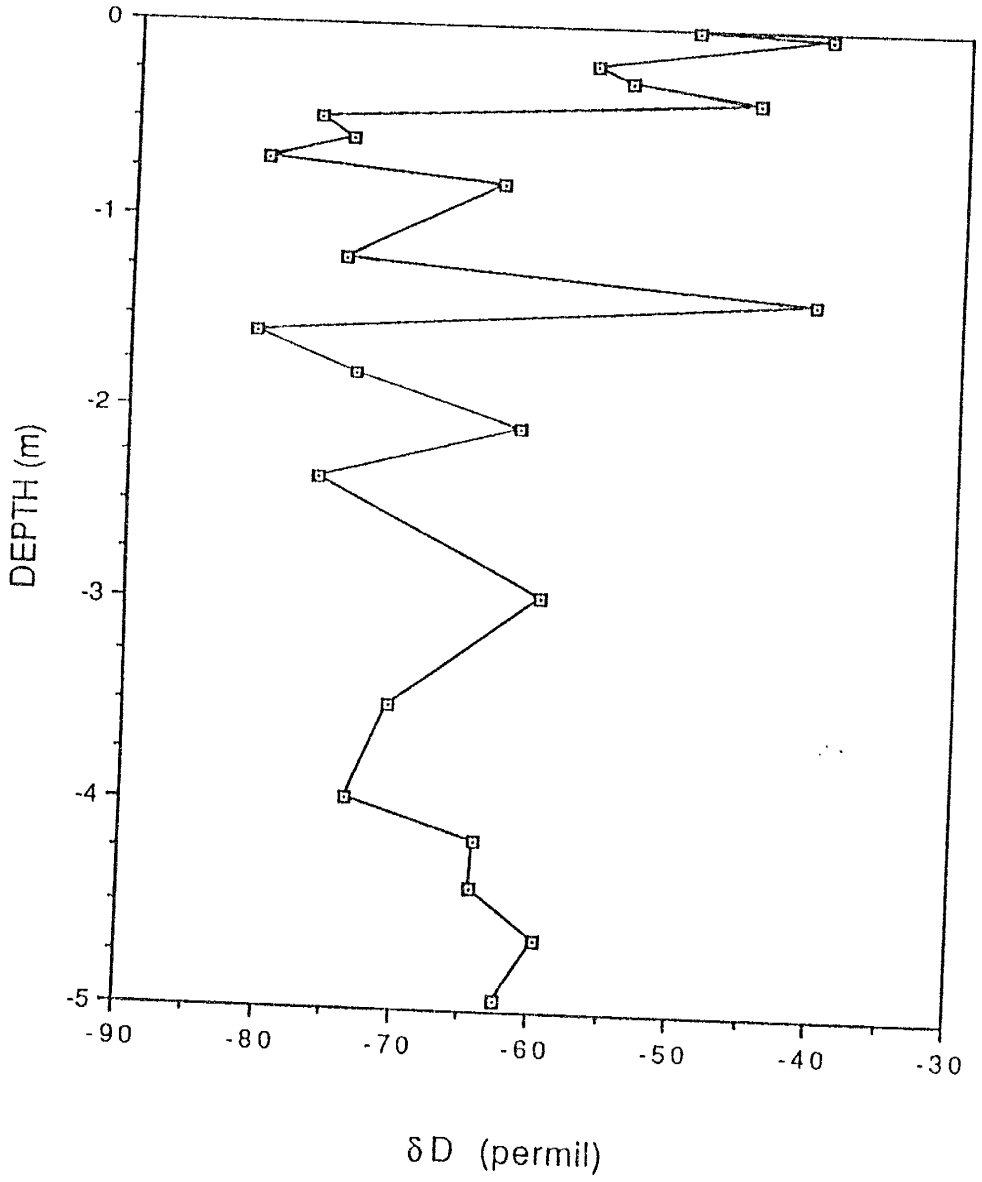

Figure 15 - Depth versus δD for SSIP4 core

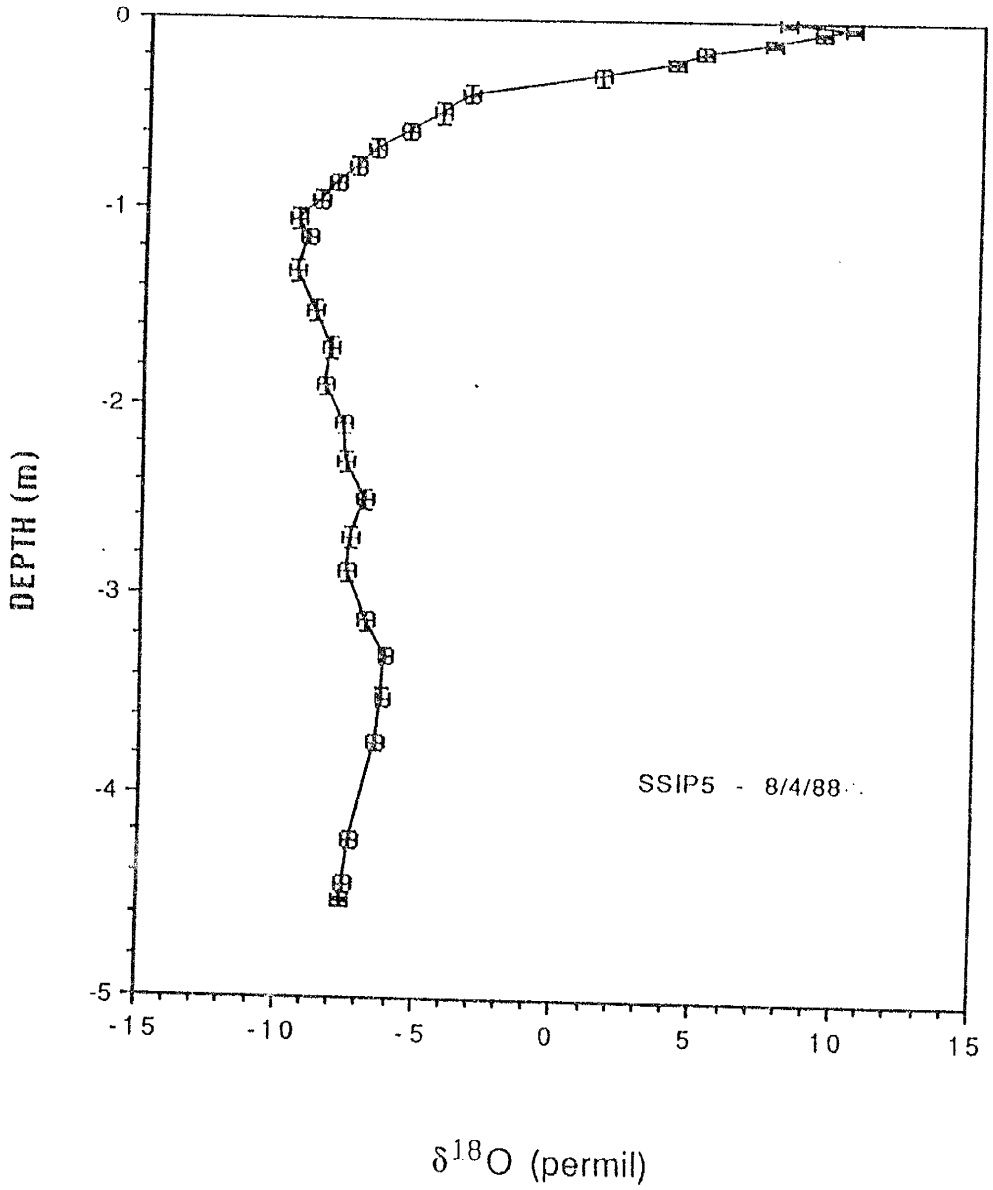

Figure 16 - Depth versus $\delta^{18}O$ for SSIP5 core, Y error bars indicate sampling interval, X error bars indicate 95% confidence interval

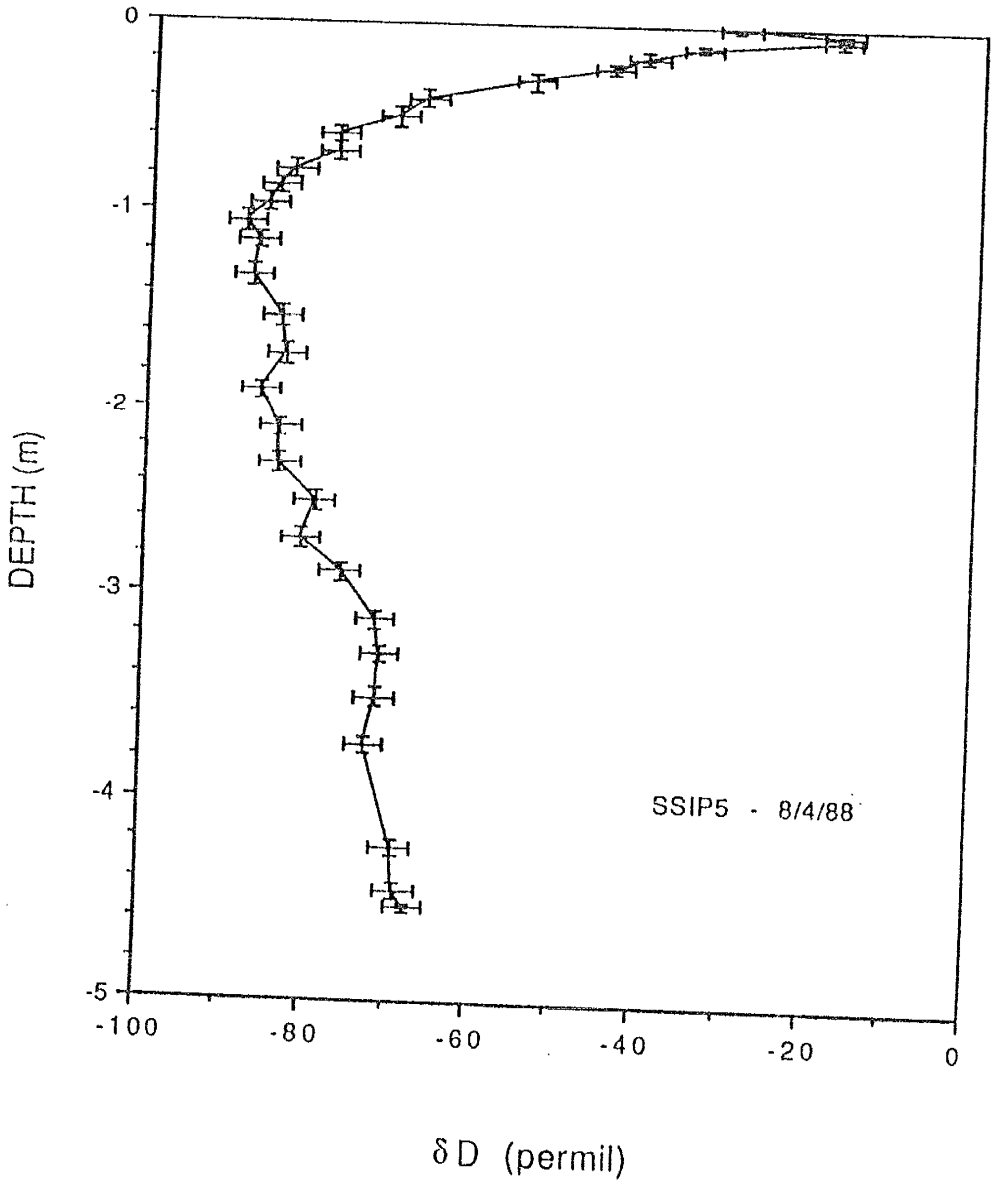

Figure 17 - Depth versus δD for SSIP5 core, Y error bars indicate sampling interval, X error bars indicate 95% confidence interval

variability within these profiles is relatively small. Figure 18 depicts both the $\delta^{18}O$ and δD against depth, showing the relative differences in behavior for both isotopic species within the profile. Figure 19 is a plot of δD versus $\delta^{18}O$, with the corresponding meteoric water line (MWL) for this area (Vuataz and Goff, 1986). The meteoric water line is indicative of precipitation for this area. Also included in Figure 19 are the isotopic compositions of two precipitation events that occurred in Socorro, NM (collected on 8/23/88 and 1/27/89), and of a ground-water sample from monitor well 5 near the isotope sampling site (collected on 2/15/89).

Data from the SSIP6 profile corroborate the SSIP5 profile. Figure 20 depicts the depth versus water content for both the SSIP5 and SSIP6 cores. There is considerable variability in moisture content between the two cores, despite their close proximity to each other. These differences in moisture are attributed to spatial variability in soil texture. Figure 21 shows a plot of depth versus δD for both the SSIP5 and SSIP6 cores. The two profiles are markedly similar, despite the observed variability in water content. All the data obtained from these cores are presented in Appendix B.

On October 27, 1988 a seventh core, SSIP7, was taken at the Sevilleta site. Figure 22 shows the depth versus δD data for the SSIP7 core. During the 'rainy season', August through September, 1988, there was an appreciable amount of precipitation occurring at the site. Figure 13 depicts the monthly precipitation amounts for the year 1988 at the research site. Figure 23 shows a plot of depth versus water content for both the SSIP5 and SSIP7 cores. The SSIP7 profile exhibits a pronounced elevation in moisture content above a 1

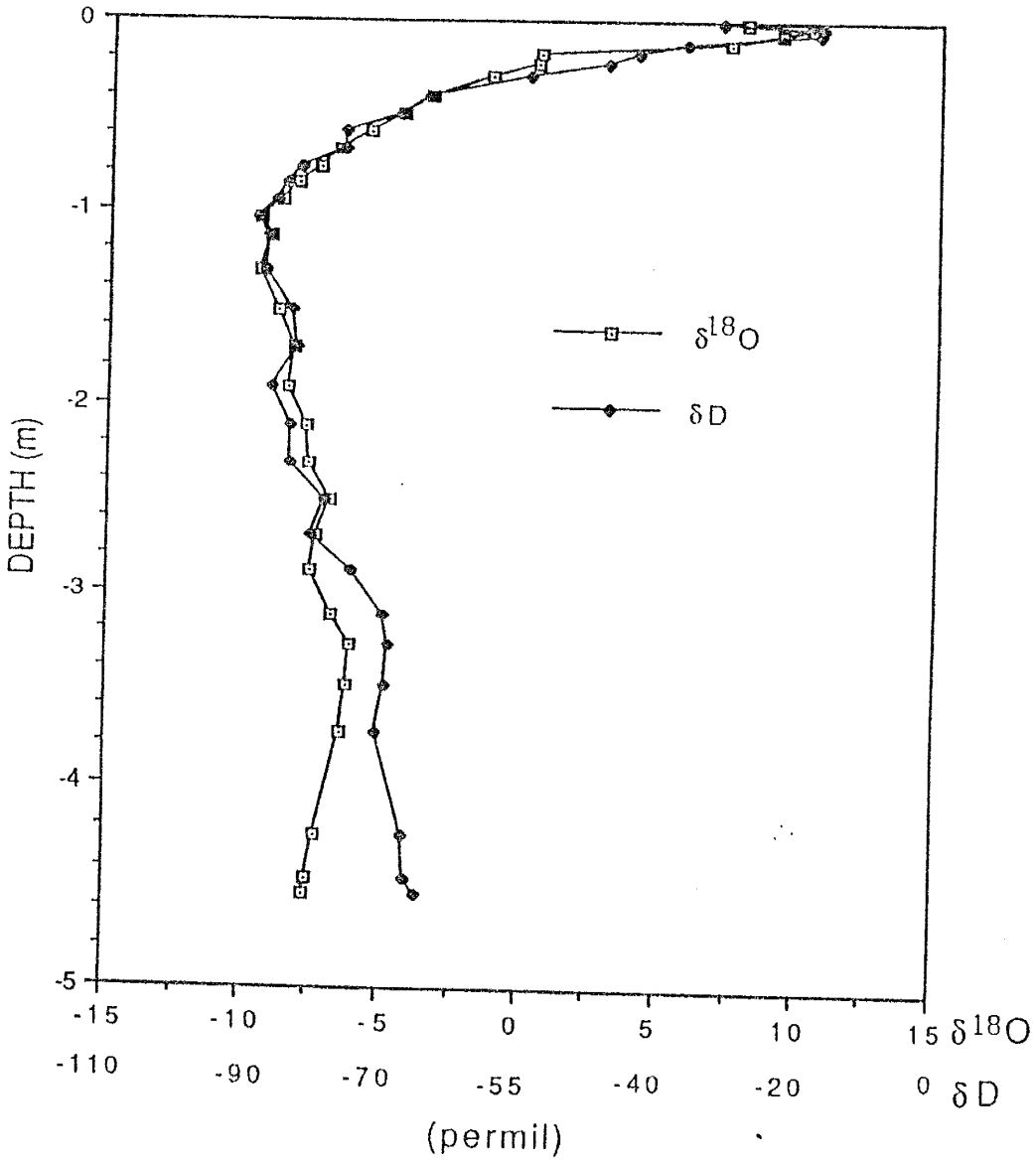

Figure 18 - Depth versus δD and $\delta^{18}O$ for SSIP5 core

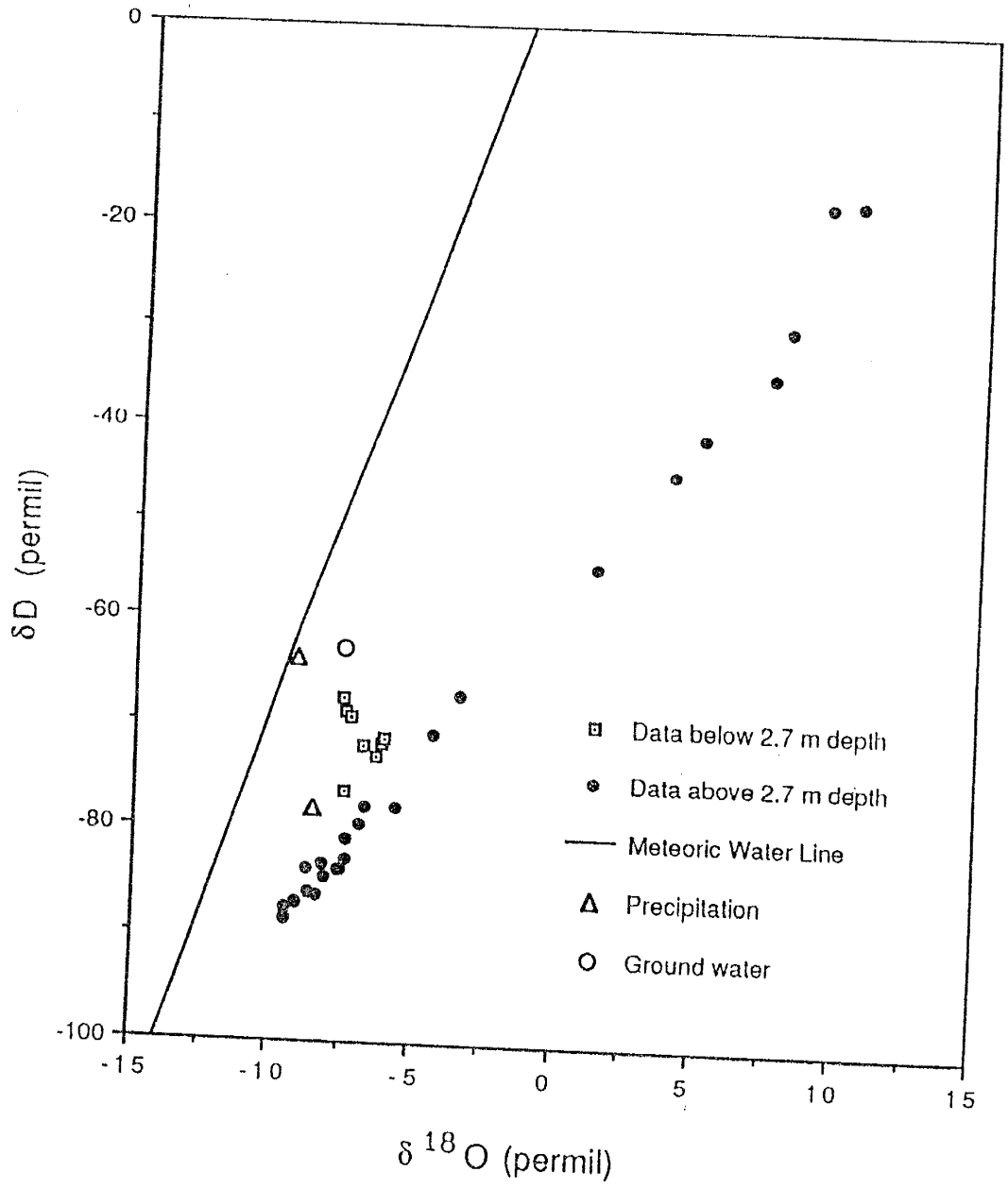

Figure 19 - δD versus $\delta^{18}O$ for SSIP5 core

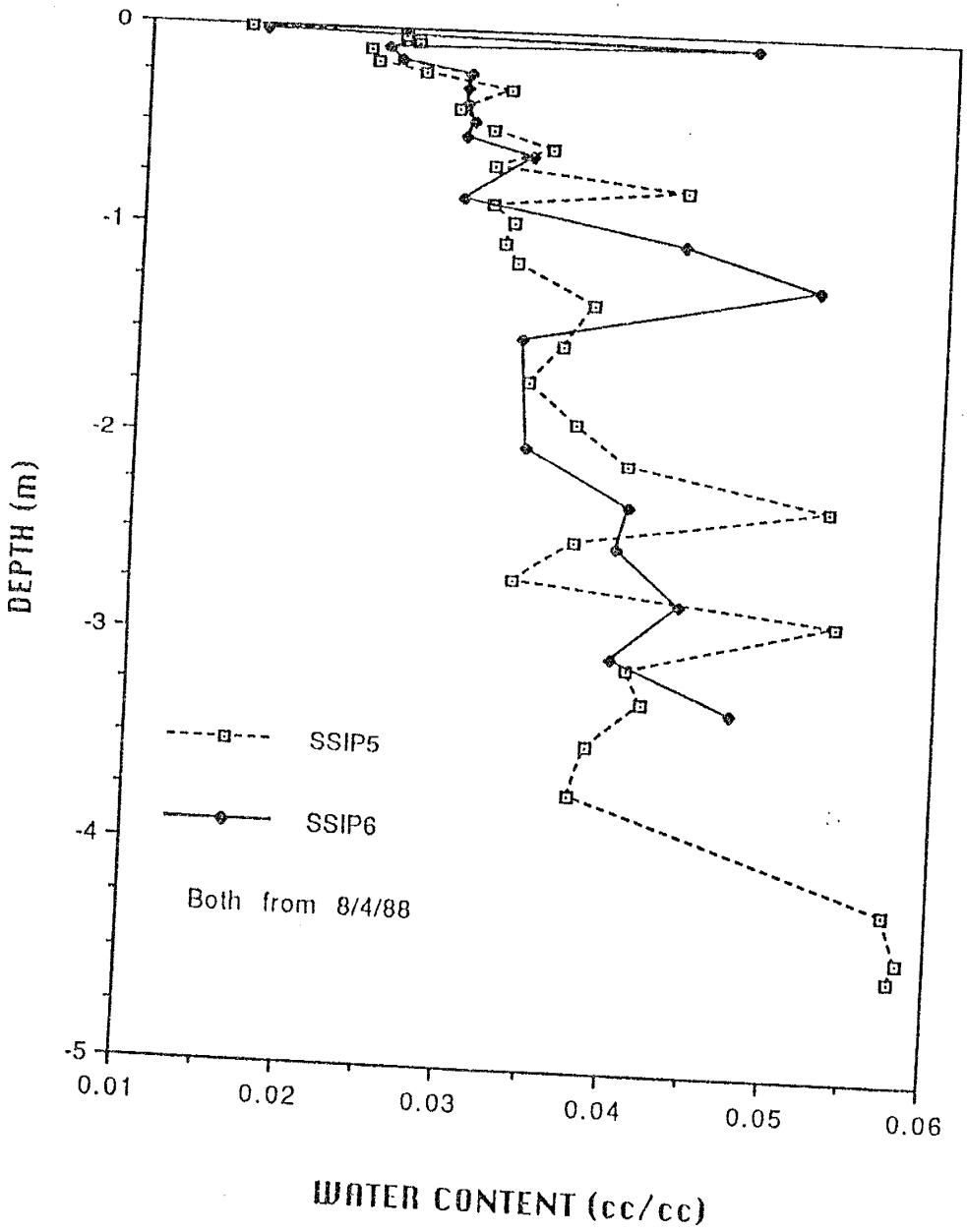

Figure 20 - Depth versus water content for SSIP5 and SSIP6 cores

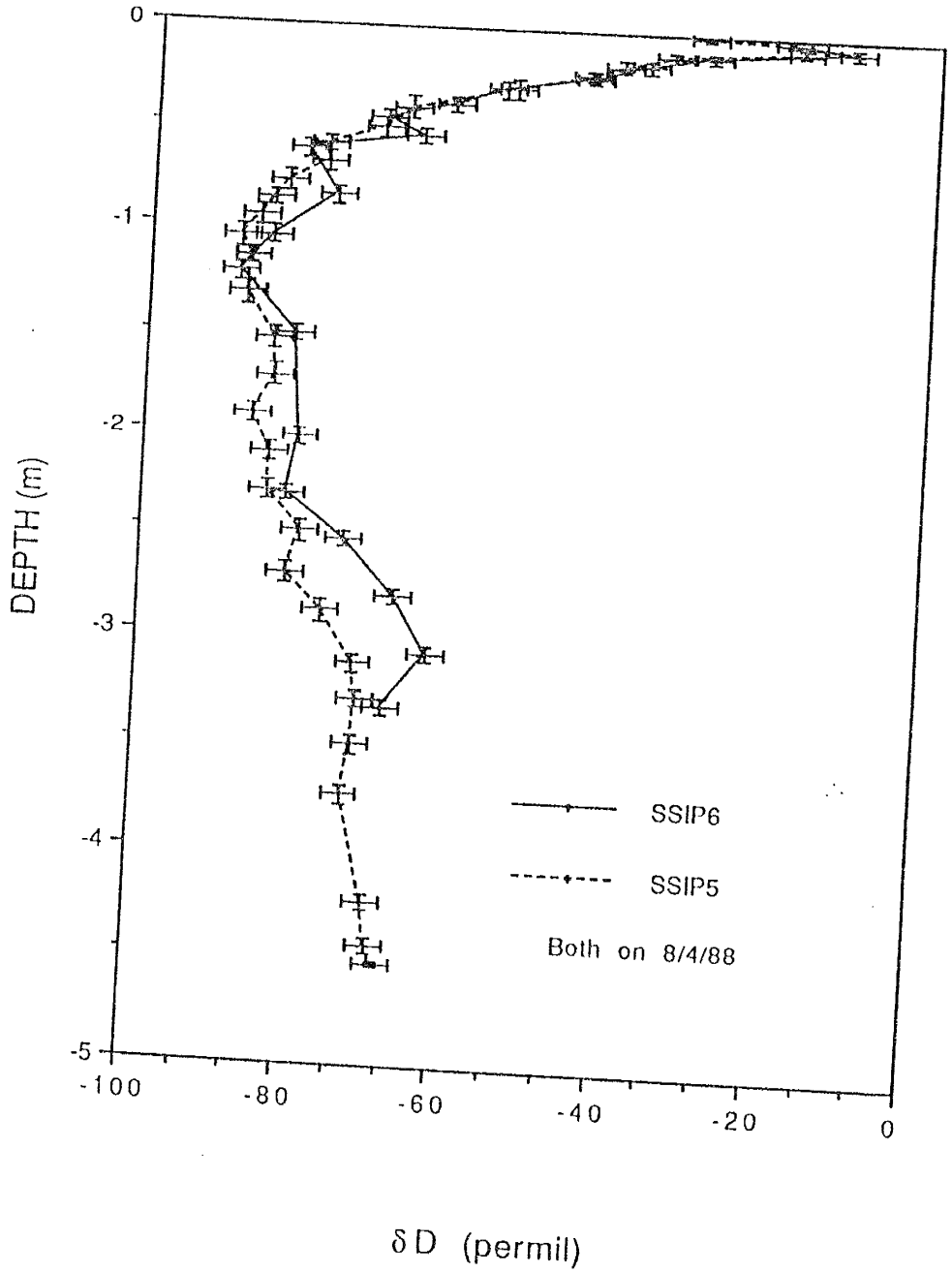

Figure 21 - Depth versus δD for SSIP5 and SSIP6 cores, Y error bars indicate sampling interval, X error bars indicate 95% confidence interval

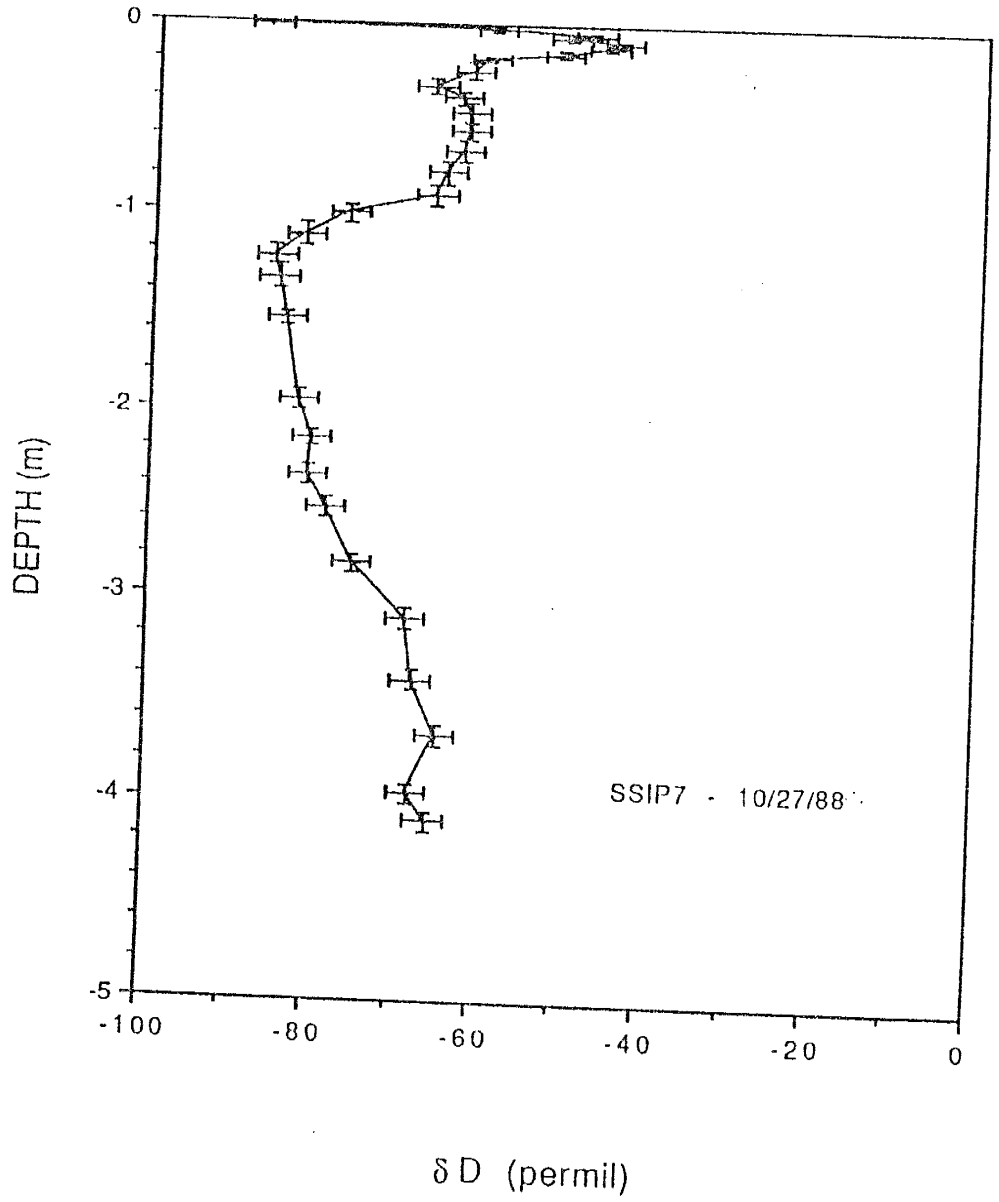

Figure 22 - Depth versus δD for SSIP7 core, Y error bars indicate sampling interval, X error bars indicate 95% confidence interval

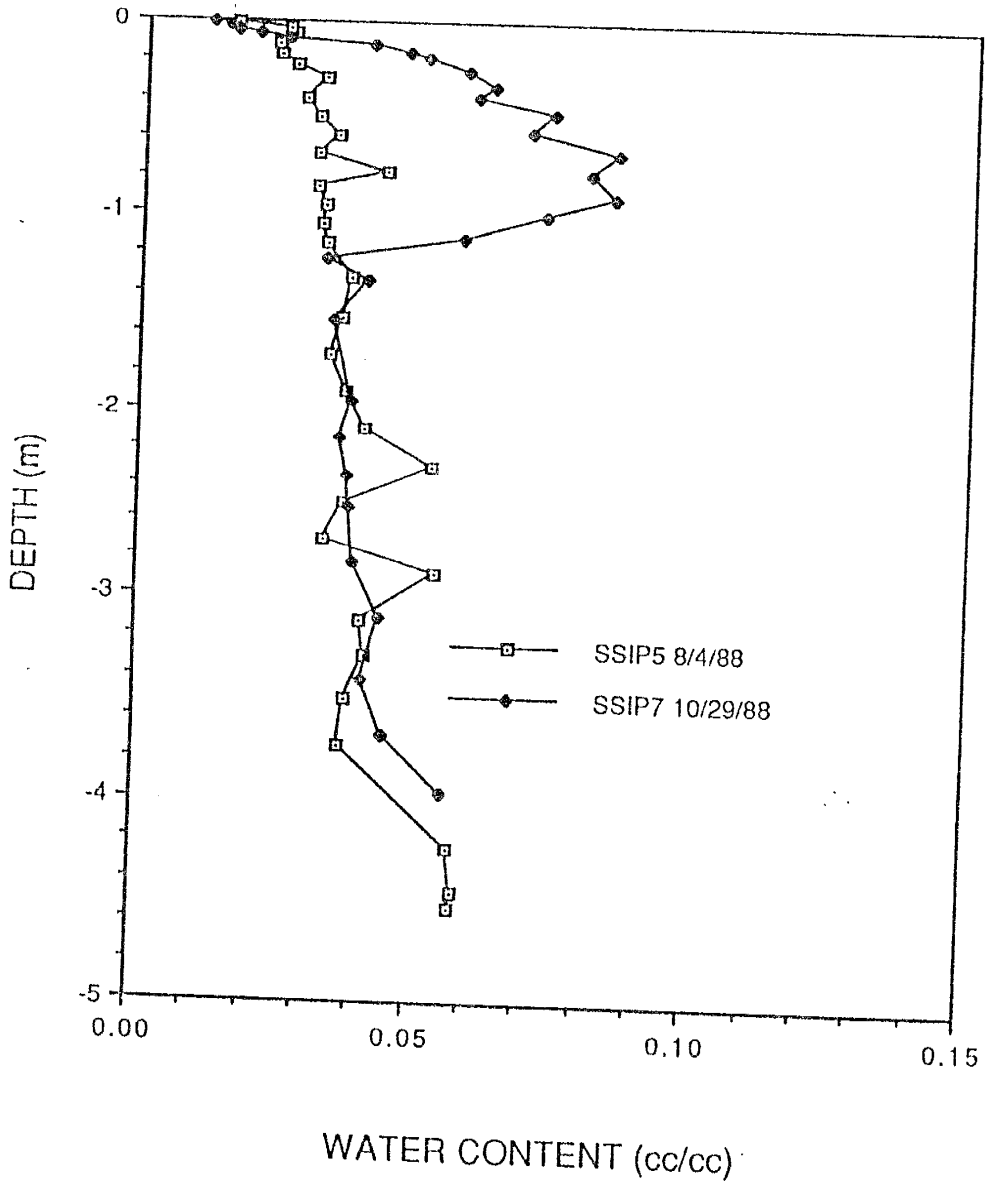

Figure 23 - Depth versus water content for SSIP5 and SSIP7 cores

meter depth, relative to the SSIP5 profile. This increase in moisture is indicative of infiltration of precipitation between August 4 and October 27. The difference in soil-moisture storage between the SSIP5 and SSIP7 profiles is approximately 3.7 cm of water. Nearly 8.5 cm of precipitation occurred at the site during this time interval (Stein, T., written communication, March 1989). Therefore approximately 43% of the precipitation which occurred between August 4 and October 27, 1988 was accounted for as increased soil-moisture storage as of the latter date. Figure 24 is a plot of depth versus δD for the SSIP5 and SSIP7. The differences in isotopic composition between the two profiles in the upper meter is indicative of infiltration (and mixing), the implications of which will be discussed below.

The eighth core, SSIP8, was collected on January 24, 1989. Figures 25 and 26 exhibit the depth versus δ^{18}O and depth versus δD data, respectively, for SSIP8. Figure 27 depicts the depth versus δD data for both the SSIP5 and SSIP8 cores. Figure 28 gives the depth versus δD data for the SSIP7 and SSIP8 cores. Therefore, figures 24, 27, and 28 depict a time history of isotopic changes in the soil at the site over three seasons of the year. Figure 29 shows a plot of depth versus water content for the SSIP5 and SSIP8 profiles. Figure 30 is a plot of depth versus water content for the SSIP7 and SSIP8 cores. Figures 23, 29, and 30 show the seasonal changes in moisture distribution at the site.

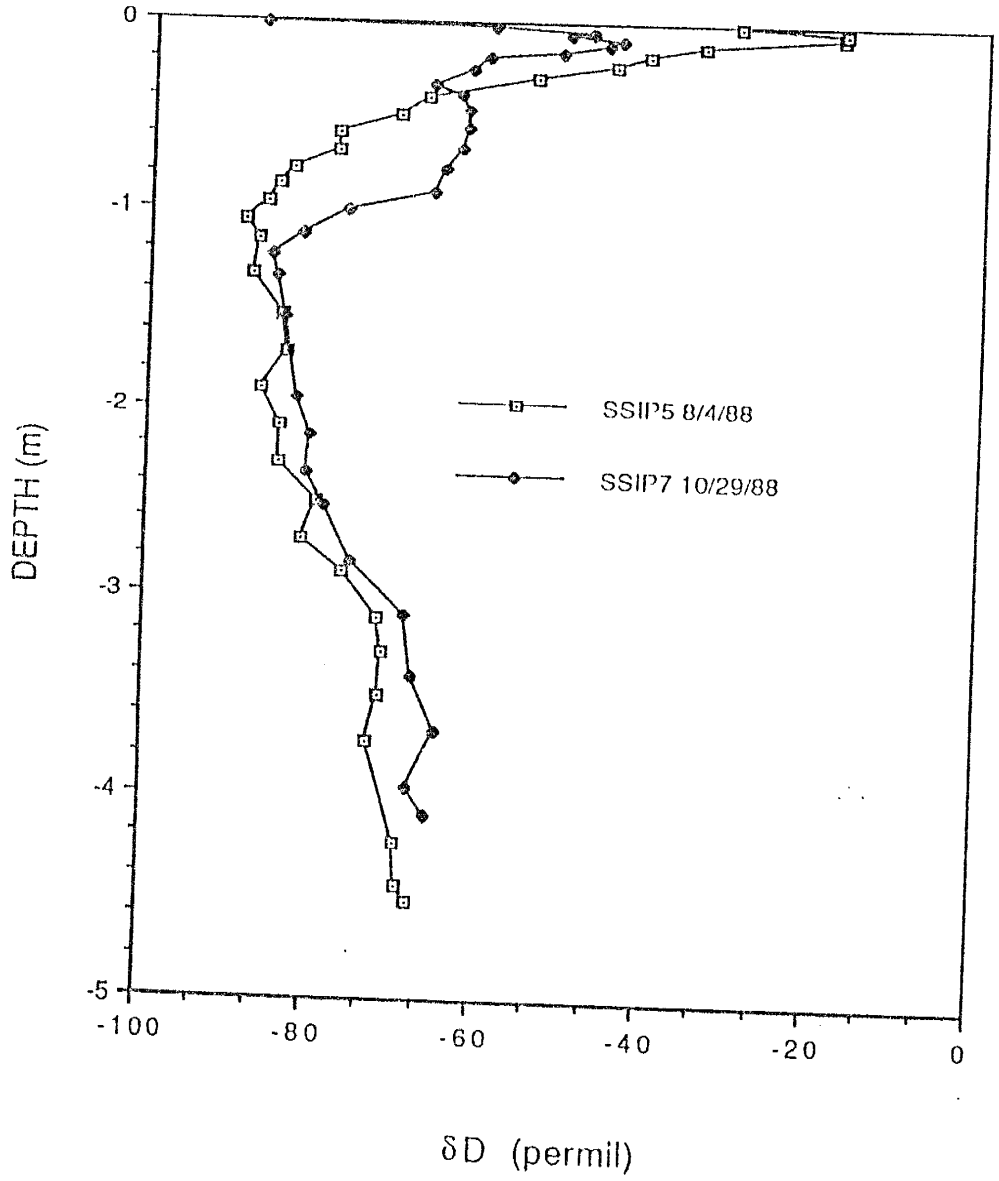

Figure 24 - Depth versus δD for SSIP5 and SSIP7 cores

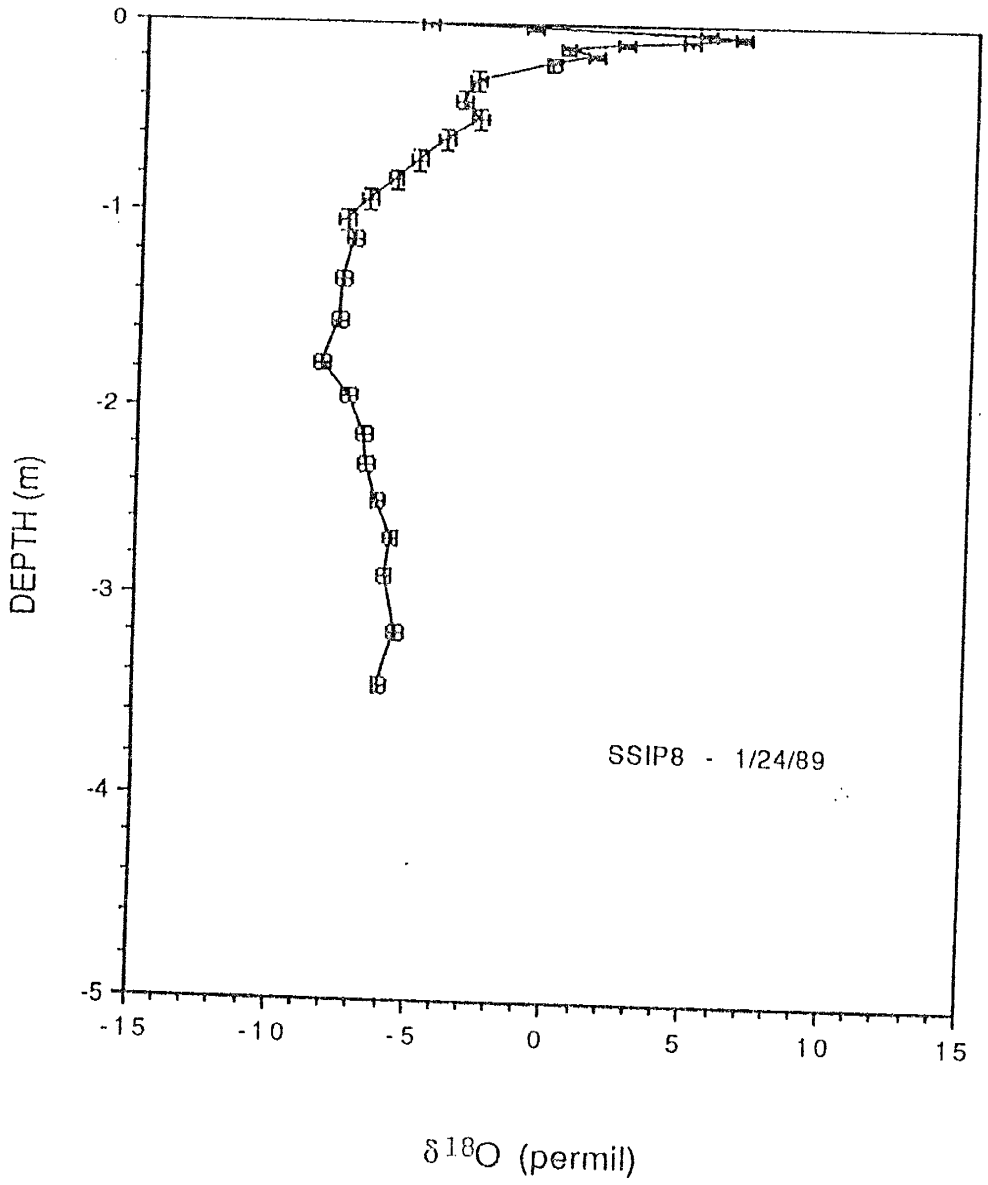

Figure 25 - Depth versus $\delta^{18}O$ for SSIP8 core, Y error bars indicate sampling interval, X error bars indicate 95% confidence interval

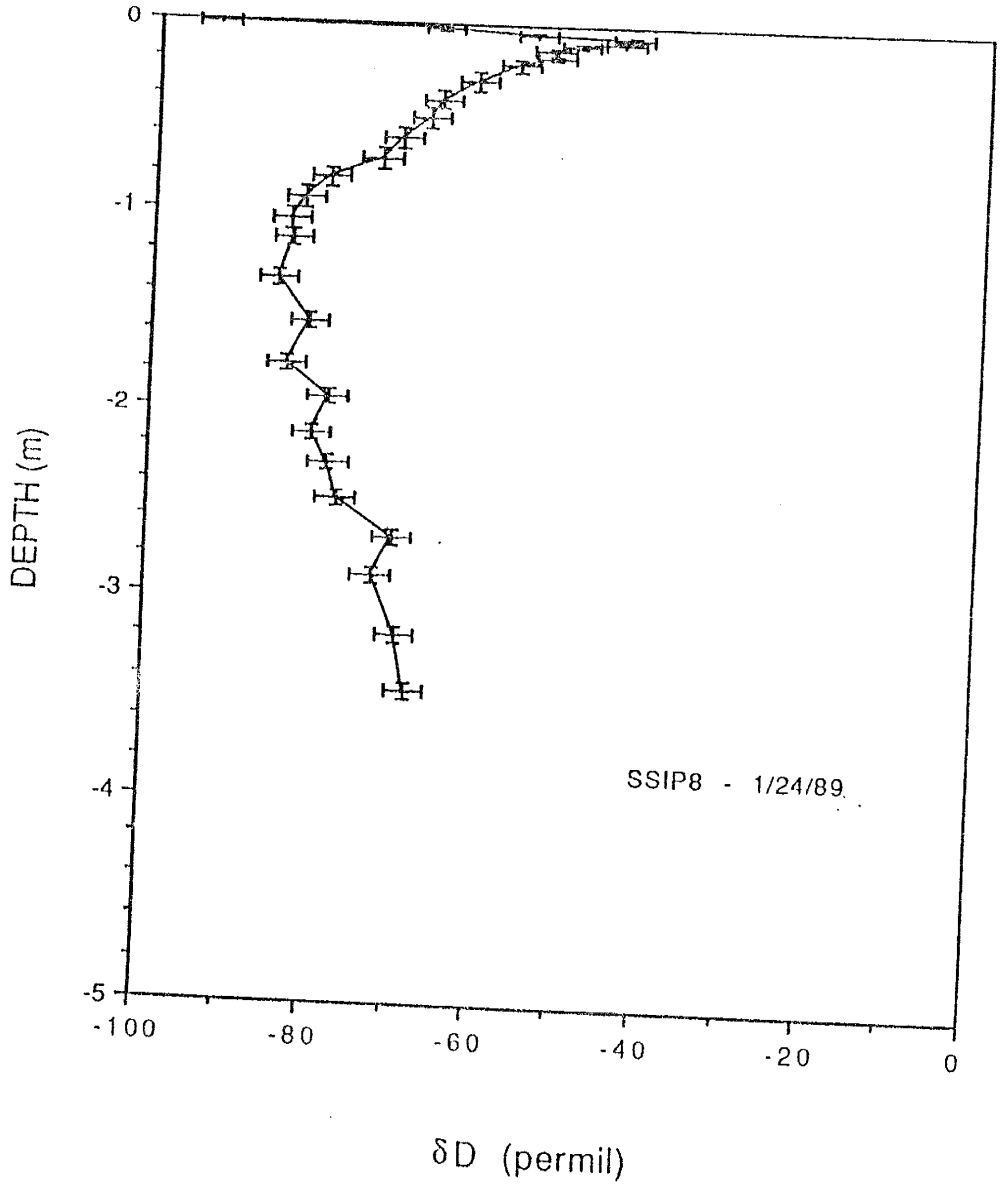

Figure 26 - Depth versus δD for SSIP8 core, Y error bars indicate sampling interval, X error bars indicate 95% confidence interval

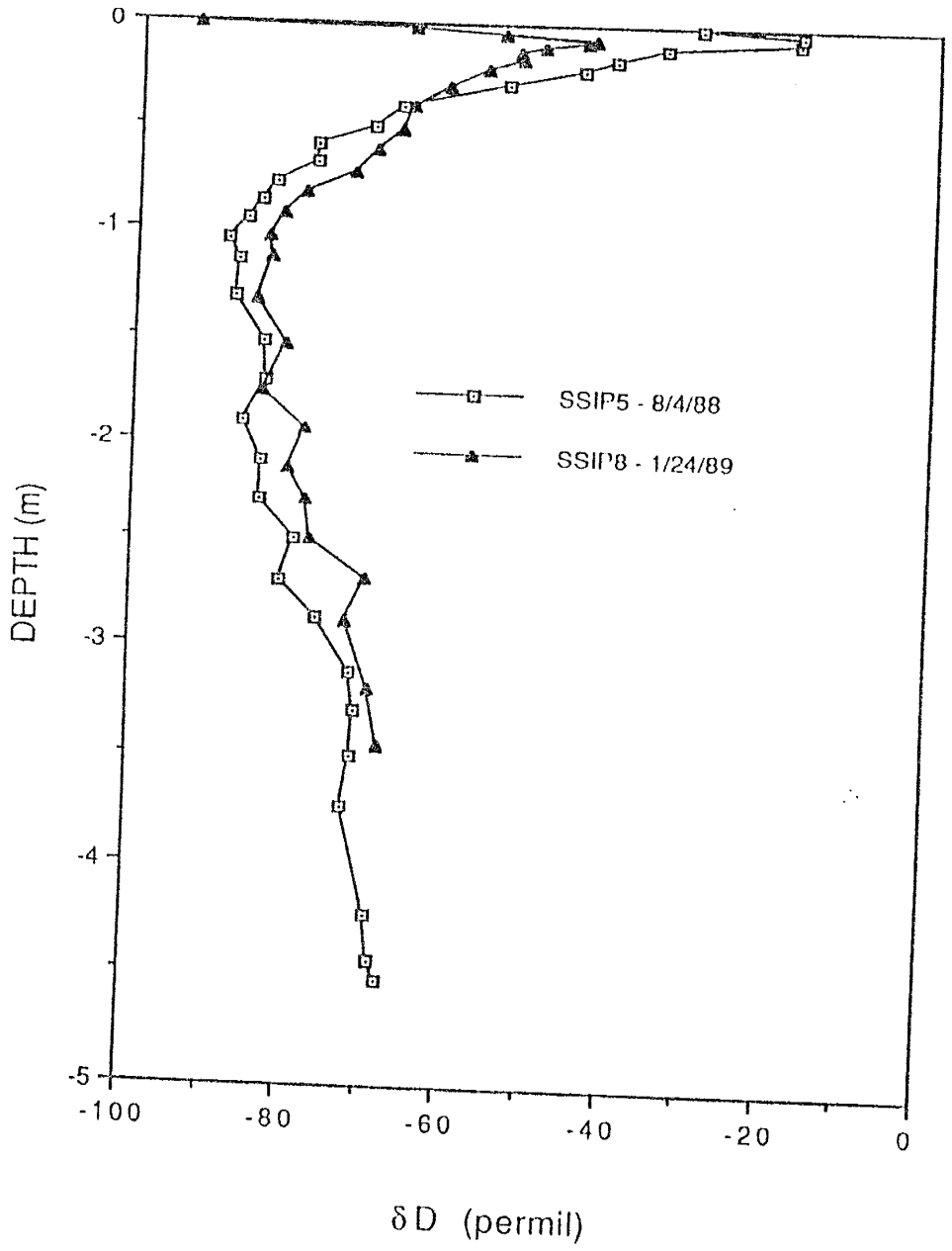

Figure 27 - Depth versus δD for SSIP5 and SSIP8 cores

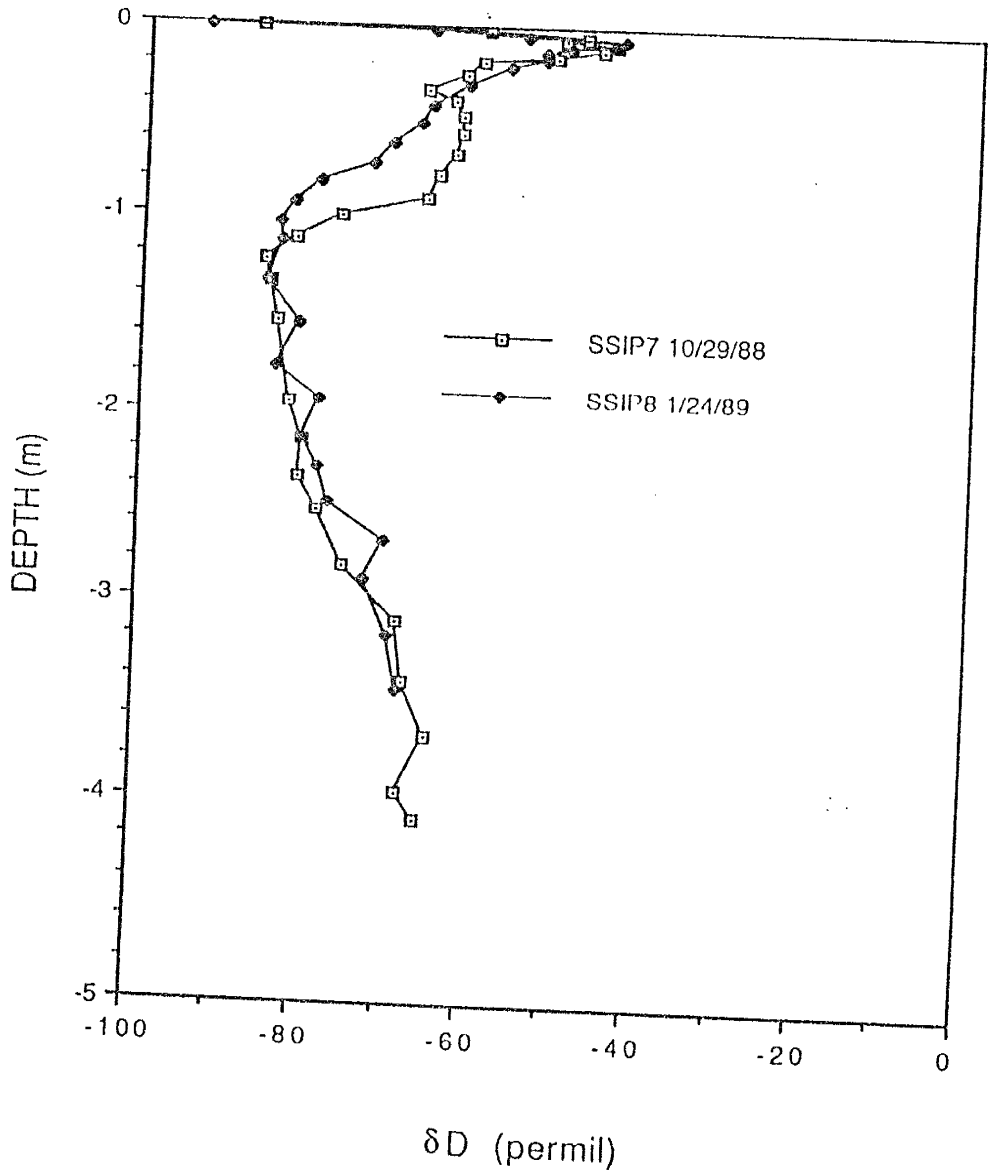

Figure 28 - Depth versus δD for SSIP7 and SSIP8 cores

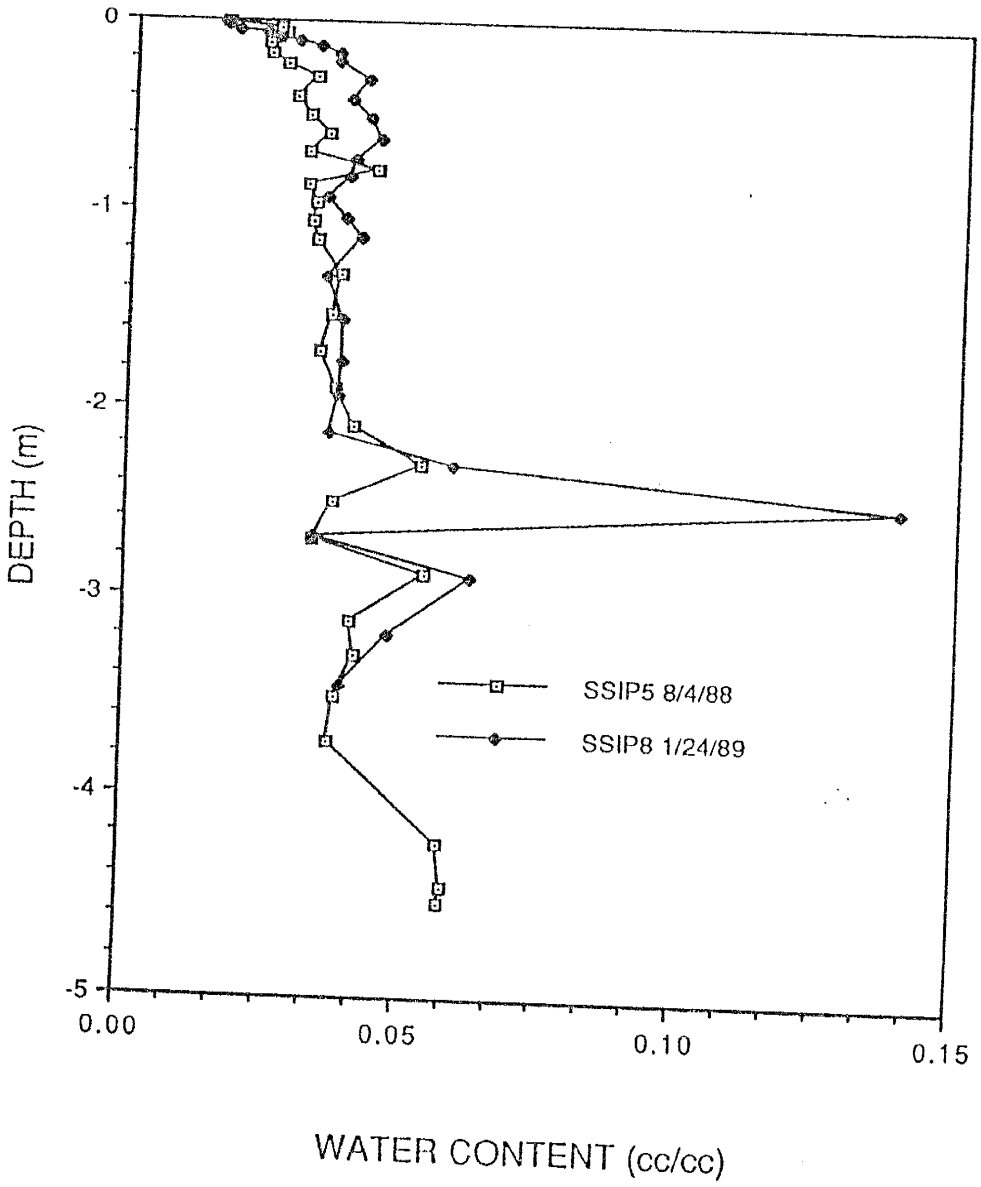

Figure 29 - Depth versus water content for SSIP5 and SSIP8 cores

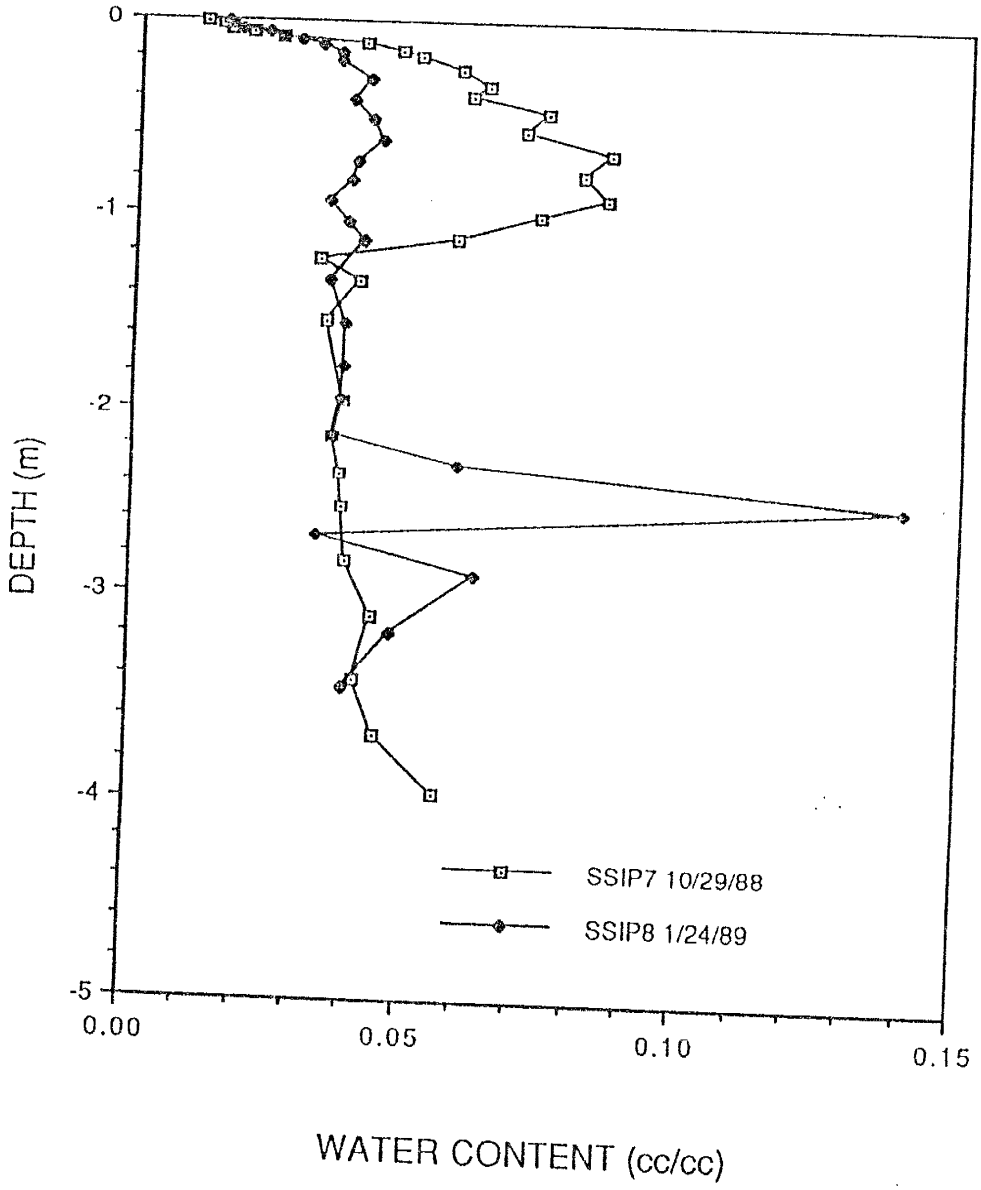

Figure 30 - Depth versus water content for SSIP7 and SSIP8 cores

6.2 Modeling Results

The numerical modeling techniques outlined in chapter 4 were developed or presented to better understand soil-water movement in natural desert soils. Previous work by Phillips et al. (1988) utilizing bomb-pulse ^{3}H and ^{36}Cl as tracers led to a hypothesis that the vapor-phase movement of soil water may be appreciable. Their hypothesis would help explain the differences in the observed distribution of the two isotopic species in the profile. The models presented in chapter 4 are therefore intended to help address the concerns of Phillips et al. directly, and to aid in our overall understanding of soil-water movement.

The first model presented in chapter 4 above was a non-isothermal recharge (NIR) model. The NIR model was developed to estimate the vapor and liquid flux contributions of the soil-water movement that leads to recharge. The NIR model is also capable of estimating the recharge rate. The quantitative numerical analysis presented above for the NIR model contains several assumptions worth discussing. First, the model assumes a one-dimensional vertical flow. The vapor flux is assumed to be downward in response to temperature-induced vapor-pressure gradients. The liquid flux contains both an advective and diffusive component. The advective liquid flux (below the zone of evaporation) is assumed to be vertically downward. If the vapor and/or liquid flux is opposite to the assumed direction of flow, then the model results will indicate that condition by assigning a negative value to the predicted flux.

As stated, the NIR model is limited to quasi-steady state conditions. A soil-moisture regime which is slowly varying in time would be indicative of quasi-steady state conditions. In an an effort to evaluate the existing stable-isotope data for potential use in the NIR model, the results of additional monitoring at the site are useful. Figures 31, 32, and 33 present depth versus water content data from May 1988 to January 1989 (Stein,T., written communication, March 1989) for a neutron probe at the Stephens, Hicks, and Stein research site at the Sevilleta (see figure 4 for proximity to the SSIP site). It should be noted that in figures 31, 32, and 33 the water content data changes markedly below a depth of 3.5 meters. These changes are most likely due to a rising and falling water table (and capillary fringe). The neutron logging shows that for several months prior to sampling the SSIP5 and SSIP6 cores the profile was slowly drying within the upper meter of the profile. Figure 32 indicates active wetting and drying phases (i.e., a wetting front pulse) in the top meter of the profile during the late summer and autumn months, which are not indicative of quasi-steady conditions. Figure 33 shows that slowly drying conditions occurred from late autumn into winter. Therefore, only the SSIP5, SSIP6, and SSIP8 profiles satisfy the quasi-steady state criteria. In other words, the water content profiles indicate that conditions were slowly varying with time prior to sampling SSIP5, SSIP6, and SSIP8. Between the SSIP5 and SSIP6 profiles, both of which were collected on the same day, the SSIP5 core was discretized into finer sampling intervals and consequently has more data associated with it. The SSIP5 core was therefore preferred for analysis over the SSIP6 core. The SSIP7 core was collected at a

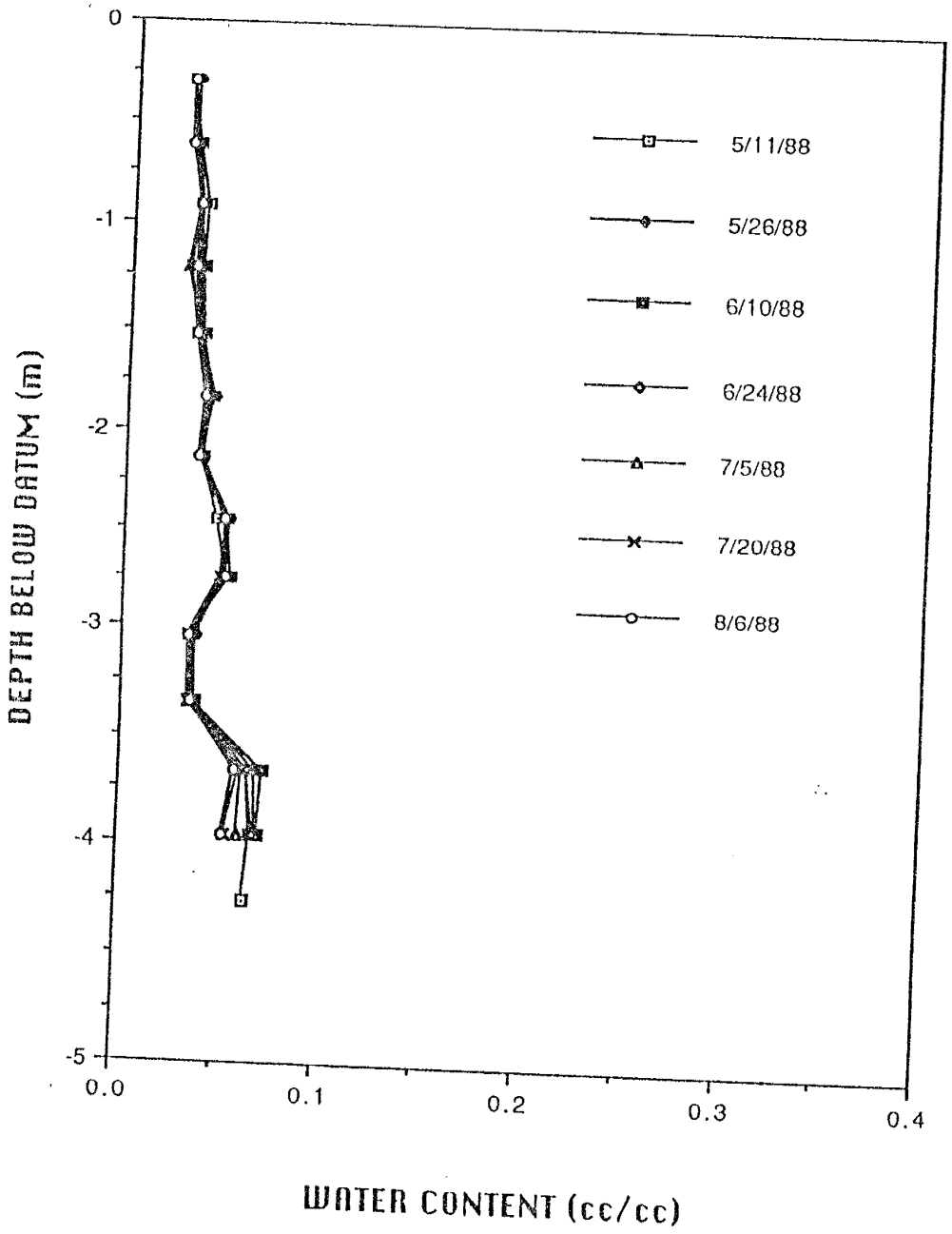

Figure 31 - Depth versus water content data from neutron logging for various times at the Stephens, Hicks, and Stein site (Stein,T. written communication, March 1989)

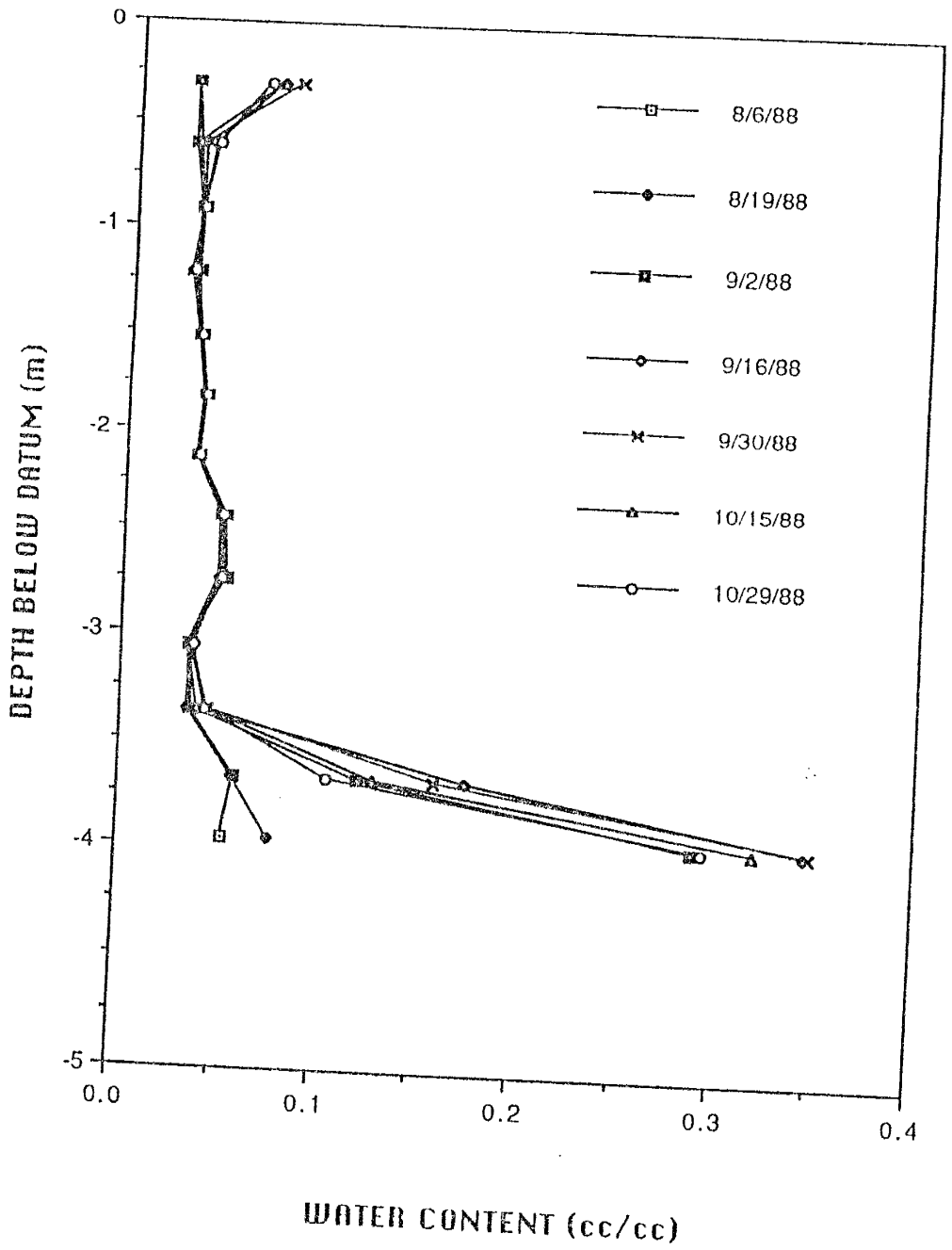

Figure 32 - Depth versus water content data from neutron logging for various times at the Stephens, Hicks, and Stein site (Stein,T. written communication, March 1989)

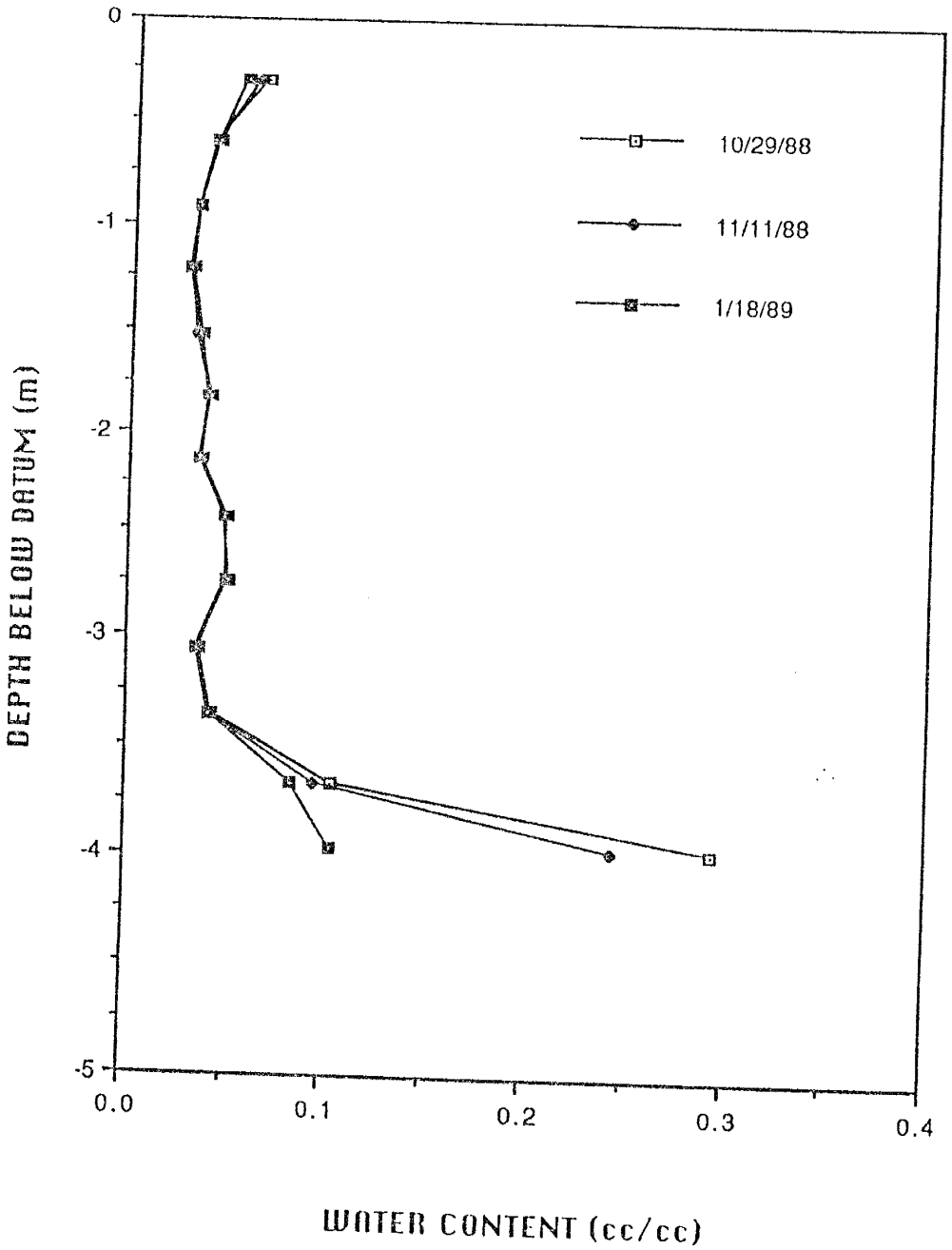

Figure 33 - Depth versus water content data from neutron logging for various times at the Stephens, Hicks, and Stein site (Stein,T. written communication, March 1989)

time when the soil-water movement was presumed to be under transient conditions, following wetting of the profile after the 'rainy season'. Therefore, SSIP7 is not suitable for analysis with the NIR model.

The first step in the NIR modeling procedure is a determination of input parameters to equation 50. Equation 50 describes the shape of the isotope profile. Figures 17 and 26 show the results of sampling for depth versus δD from the SSIP5 and SSIP8 cores, respectively. Barnes and Allison (1984) prefer deuterium over oxygen-18 in their non-isothermal evaporation (NIE) model. Their conclusion was based on the fact that the kinetic fractionation is relatively insensitive to temperature, and ^{18}O is much less sensitive than deuterium. Therefore, the effect of temperature on the isotope profiles is relatively greater for deuterium than ^{18}O. Matching the observed deuterium data with the theoretical model should provide a qualitative estimate of the reliability of the input parameters to the model. For this analysis, the curve-matching technique was performed over the 0.1 to 2.70 meter depth interval. This zone corresponds to the liquid- and vapor-phase flow region below the evaporation front, but above the zone in which the water table influences the stable-isotopic composition in the profile.

Many of the parameters required for the numerical solution to equation 50 can be expressed as functional relationships of temperature or depth. Parameters such as ϵ_D, N^{sat}, p_v, D^v, and D^l are given in the literature as functions of temperature (from Majoube, 1971; Weast, 1975; Weast, 1975; Jaynes and Rogowski, 1983; and Mills, 1973; respectively). The water content versus depth

relationship determined from field sampling may be regressed and expressed mathematically. The diffusion ratio excess, η_D, is taken from Merlivat (1979). The parameter estimations with the least degree of confidence are probably the tortuosity terms. The recharge rate, W, could be assumed equivalent to the specific flux determined from the movement of bomb tritium over the past 20 years, 0.84 cm/yr (Phillips et al., 1988), or fitted by the model.

A non-linear least-squares optimization approach was taken to evaluate the goodness of fit between equation 50 and the observed deuterium data. The fitted variables in this model were: the isotopic composition of the recharge water (δ_D^{Rec}), the recharge rate (W), the liquid tortuosity factor (τ^l), and the vapor tortuosity factor (τ^v).

An earlier version of the NIR model was utilized by Knowlton et al. (1989) to estimate the vapor flux with the SSIP5 data. Two realizations of the temperature profile were utilized by Knowlton et al. to investigate the effect of temperature on the curve-fitting procedure and the vapor flux determinations. These temperature profiles were obtained from curve-fitting to the temperature data (i.e., thermistor data) collected during the SSIP5 field sampling activities. A subsequent comparison of this temperature data to long term monitoring by Stephens et al. (1985) at an adjacent site several years prior to sampling SSIP5 resulted in an interesting observation. It appears that the temperature data collected in the open hole during the SSIP5 sampling activities were markedly higher than those reported by Stephens et al. at similar depths. The SSIP5 temperature data is also erratic, which one would not expect under equilibrium

conditions. Consequently, the temperature data collected during the isotope sampling activities for all profiles was considered suspect. Therefore an alternative approach was required. Heat-flow modeling has been used, in conjunction with the temperature data of Stephens et al., to obtain more realistic representations of the diurnal and annual fluctuations in temperature with depth at the study site.

In order to perform the heat-flow modeling, the thermal properties of the soil must be characterized. In chapter 4.1.6 above, experimental and theoretical techniques were outlined to estimate the thermal conductivity, λ, as a function of water content, θ. Also, a theoretical method to predict the volumetric heat capacity, C, as a function of water content was presented.

Five experimental values of thermal conductivity were determined in situ with the line-source thermal conductivity probe. The tests were performed as outlined in section 4.1.6. A computer program was written to calculate λ from each of the data sets, for both heating and cooling. A simple logarithmic regression was used to calculate the required slope parameters. The code also calculated the effective annular gap between the probe and soil. Table 5 presents a summary of the results.

In addition to the experimental results, the thermal conductivity function was calculated with DeVries' (1963) theoretical model. As mentioned above in section 4.1.6, DeVries and Philip (1986) recommend fitting experimental data to DeVries theoretical model for a more accurate fit. They suggested using the shape factor as a fitting parameter. With this in mind, the thermal conductivity of the continuous medium, λ_o, (used in equation 11 in determining the shape

Table 5 - Summary of λ Results From Line-source Thermal Conductivity Probe Experiments

Sample Number	λ^1 from Heating	λ^1 from Cooling	λ^1 avg[2]	θ (cc/cc)	Annular Gap (cm)
TC-A	0.000553	0.000512	0.000533	0.012	0.010
TC-B	0.000824	0.000847	0.000836	0.021	0.008
TC-C	0.00115	0.00121	0.00118	0.042	0.006
TC-D	0.00170	0.00160	0.00165	0.054	0.003
TC-E	0.00196	0.00207	0.00202	0.063	0.004

1 units: cal cm^{-1} s^{-1} C^{-1}

2 average of heating and cooling data

factor) was used as the fitting parameter. The other parameters used in this model have been defined previously in section 4.1.6. A computer code was written to match the experimental data to DeVries' model. A source listing of this code is provided in appendix C. The computed $\lambda(\Theta)$ function is plotted against the experimental data in figure 34.

The $\lambda(\Theta)$ function shown in figure 34 was used in the heat-flow model presented in section 4.2. The theoretical DeVries (1963) model to estimate the volumetric heat capacity, $C(\Theta)$, presented in section 4.1.6, was used in the heat-flow model. These thermal characteristics were then utilized in conjunction with the observed water content data from the SSIP5 core and the temperature data of Stephens et al. (1985) to manually calibrate the other coefficients needed in the heat-flow model of equation 53.

In order to calibrate the heat-flow model to representative field conditions temperature data from Stephens et al. (1985) were employed. Figure 35 presents the observed temperature data from Stephens et al. for seven depths for the period December 1982 through May 1984. This temperature data is assumed to be representative of present day conditions, even though the data was collected several years prior to sampling of the isotope profiles. The temperature data in figure 35 appear to exhibit a sinusoidal seasonal variation, which is consistent with the assumptions in the analytical heat-flow model. In addition, it is evident from figure 35 that the amplitude of the temperature wave is damped and lagged with increasing depth, which again is consistent with the analytical heat-flow model. Assuming that the estimated thermal conductivity and calculated specific heat capacity relationships presented above apply, and that the media is

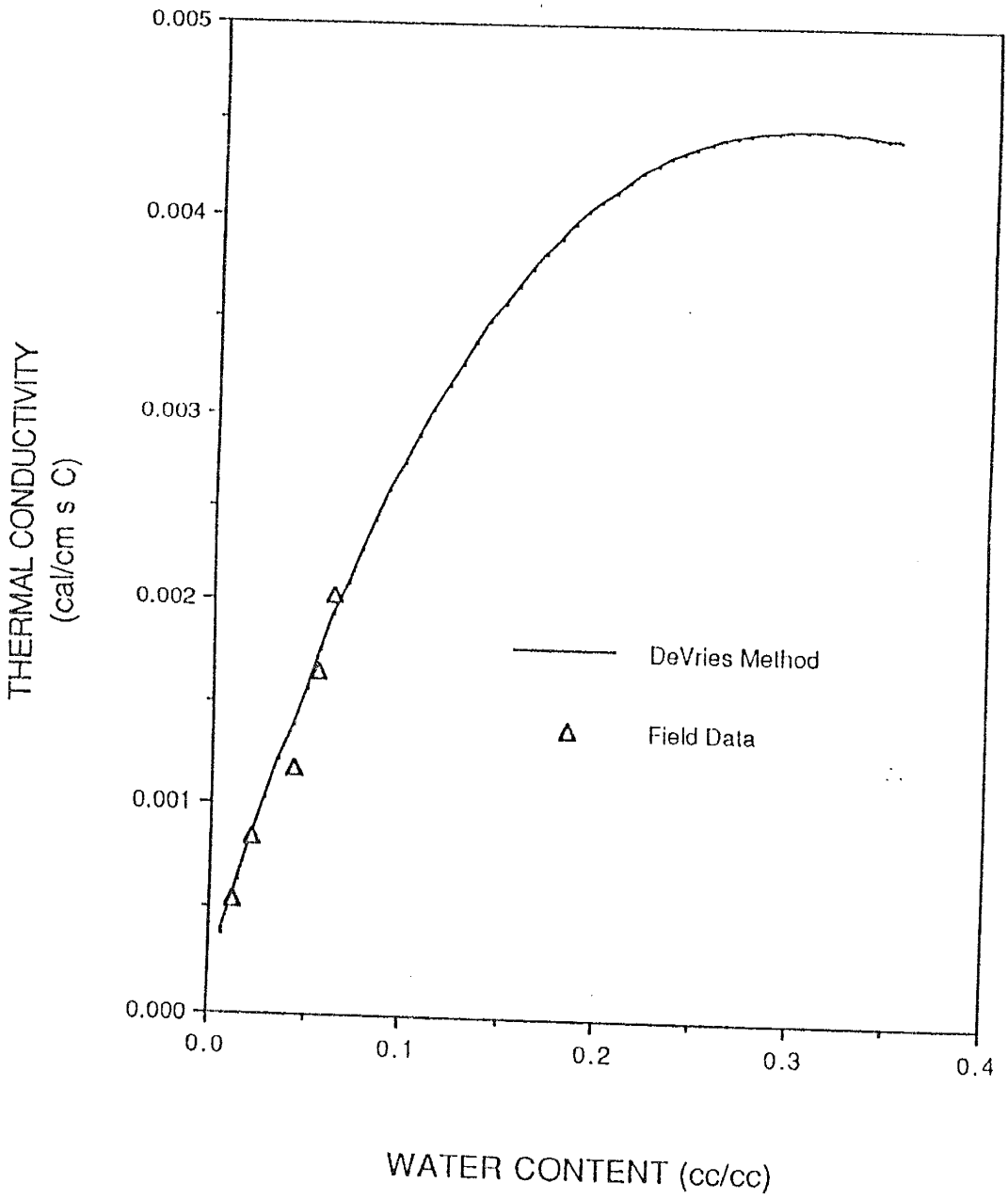

Figure 34 - Thermal conductivity versus water content data, data points from in-situ experimental results, calculated functional relationship from DeVries (1963) method

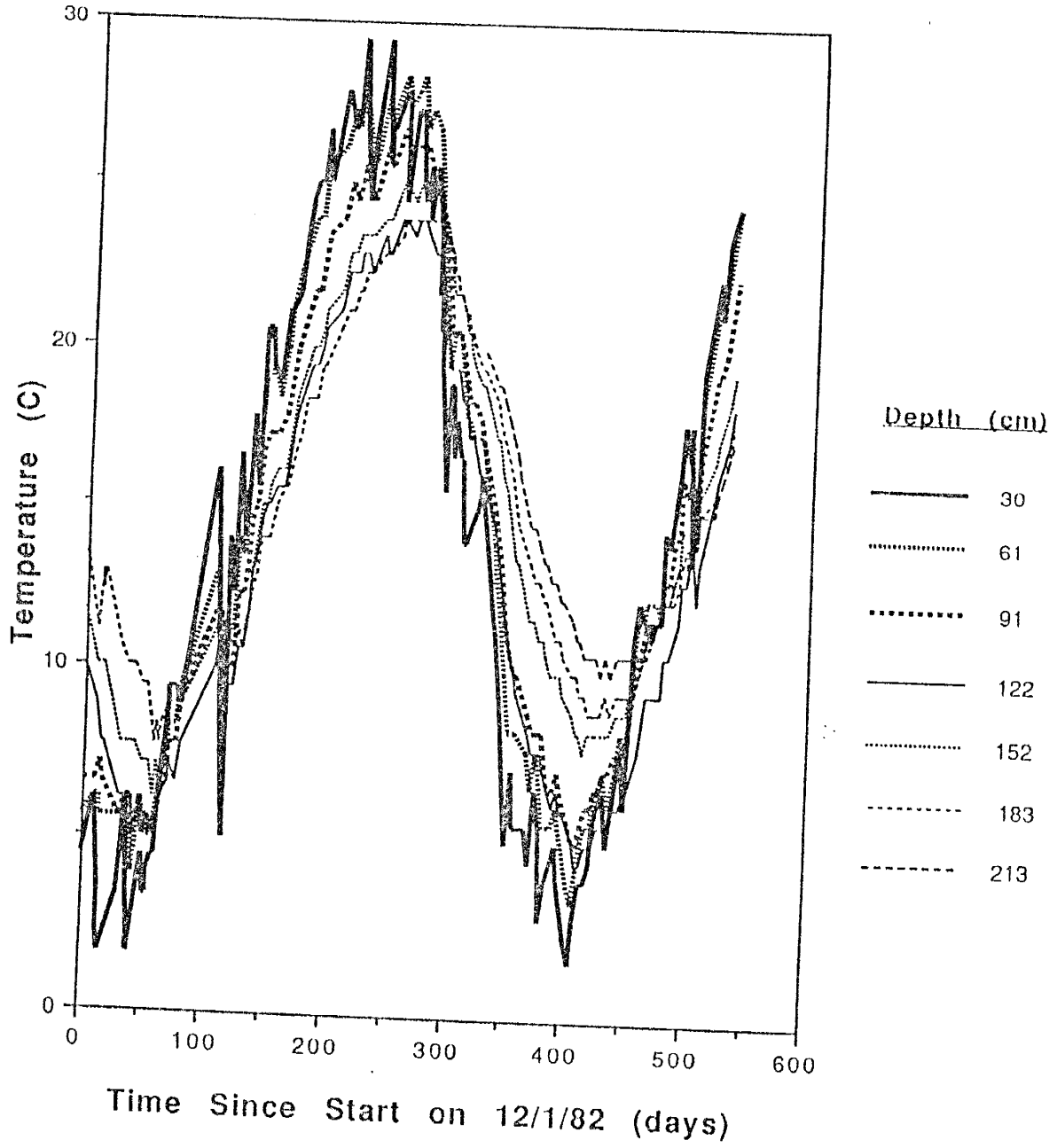

Figure 35 - Observed temperature versus time for seven depths between 30 and 210 cm, starting 12/1/82 (from Stephens et al., 1985)

homogeneous and isotropic, then the heat-flow model may be calibrated to the observed data by optimizing the parameters T_y (average annual temperature), A_y (amplitude of the annual temperature cycle at the land surface), and possibly A_d (amplitude of the daily temperature cycle at the land surface).

In order to calibrate the model to the observed data a water content versus depth profile must be supplied. It is realized that the soil-moisture profile changes with time in response to infiltration, evapotranspiration, and redistribution phenomena. Incorporating the moisture and temperature history into a model is quite rigorous, and would involve the application of a numerical heat and moisture flow model. This is beyond the scope of work for this analysis. An analytical heat-flow model has been presented above which requires a steady-state moisture regime. In view of the fact that the heat-flow model was intended primarily for predicting the temperature profile during the summer months, the moisture content profile observed from the SSIP5 profile was used as the steady-state input data to the heat-flow model.

As just mentioned, the analytical heat-flow model does not take into account changing soil moisture conditions, which undoubtedly occur in the near surface following precipitation events. With an increase in soil moisture comes an increase in the volumetric heat capacity, or rather the soil water becomes capable of storing more heat. Also, an increase in water content causes the effective thermal conductivity of the medium to rise. This results in an increased potential for heat to be transferred deeper into the profile. The opposite is also true: with a decrease in soil moisture comes a decrease in λ and C. Therefore,

with wetting and drying of the soil, heat has the potential to be absorbed or released from the porous media. Also, the wetting/drying history affects the transport of heat to depth in the profile. In addition, the heat-flow model does not adequately account for the transfer of latent heat, or the movement of heat in the vapor phase. Consequently, the actual temperature profile may be different than the one simulated by this heat-flow model.

The results of calibrating the heat-flow model to the observed temperature data are shown in figures 36, 37, 38, and 39. The fitted parameter values are: T_y = 16.2 °C and A_y = 15 °C. The resultant fits appear to be quite adequate. Only the temperature data fit from the 1.2 meter depth appears to be questionable. Several possible explanations may be posed: the calibration of the temperature thermistor at that depth was suspect; the porous media is not truely homogeneous, and therefore the uniform thermal characteristics used in the model are not indicative of actual conditions; or that the transient behavior of the soil-moisture regime has a larger influence on the temperature history than expected (as discussed in the previous paragraph).

The average annual air temperature in Socorro, approximately 24 km south of the research site, is approximately 15 °C, according to National Oceanic and Atmospheric Administration (NOAA) records. Considering that the optimized parameter T_y is an effective annual temperature at the land surface, and that air temperature just above land surface would be expected to be greater than that measured one or two meters above land surface, then the average annual air temperature is in good agreement with the model calibrated value.

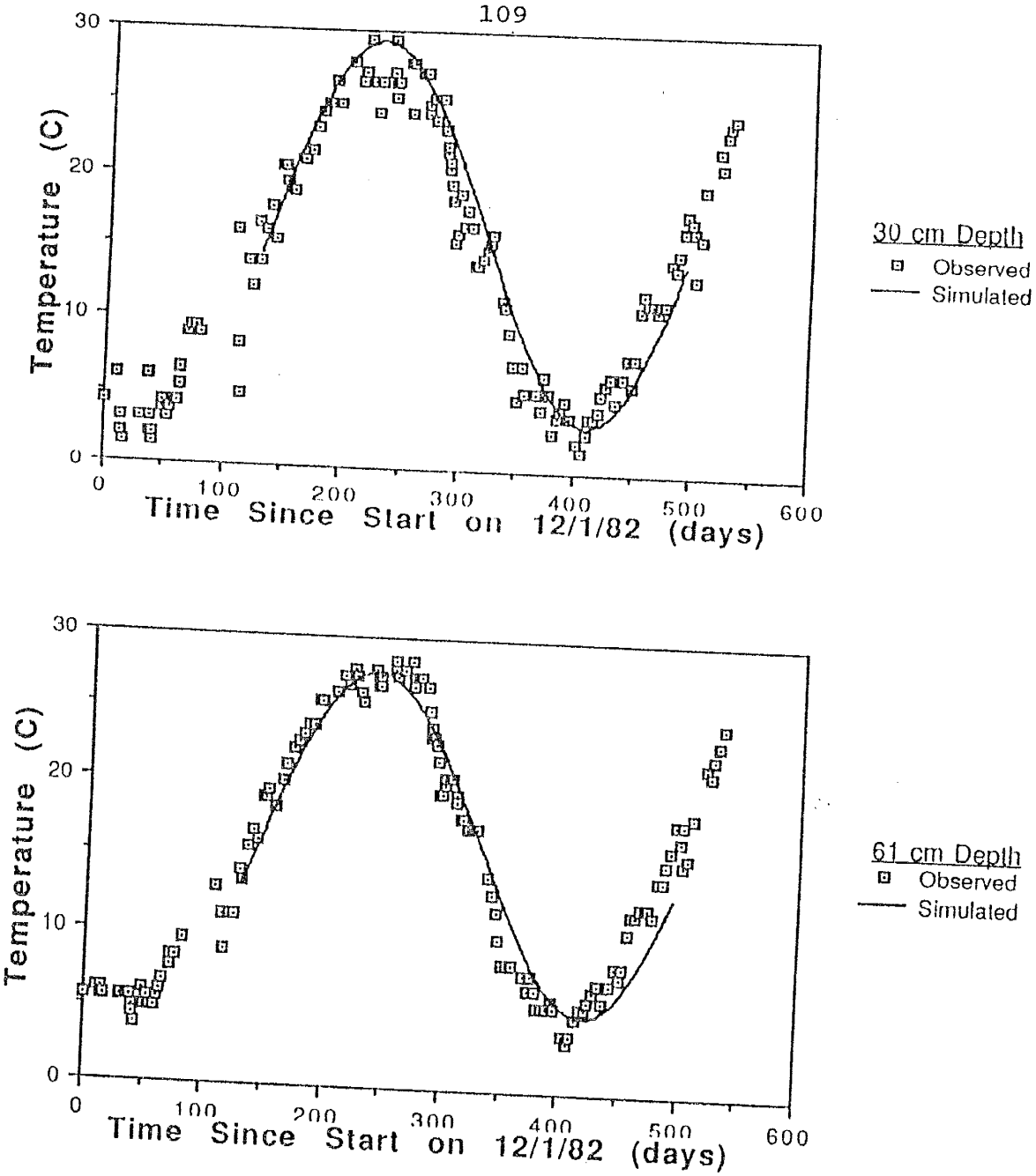

Figure 36 - Results of the analytical heat-flow modeling versus observed temperature data

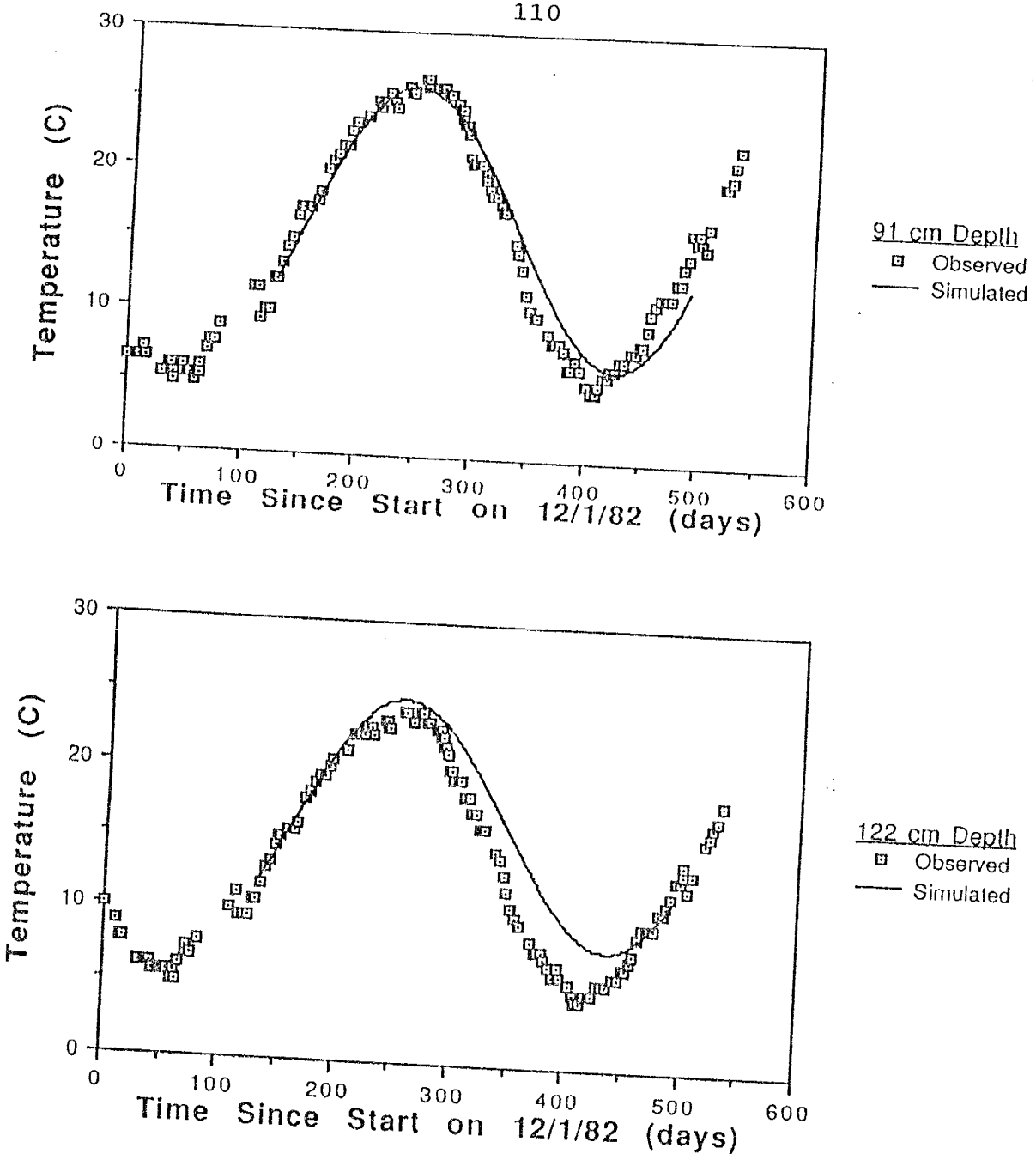

Figure 37 - Results of the analytical heat-flow modeling versus observed temperature data

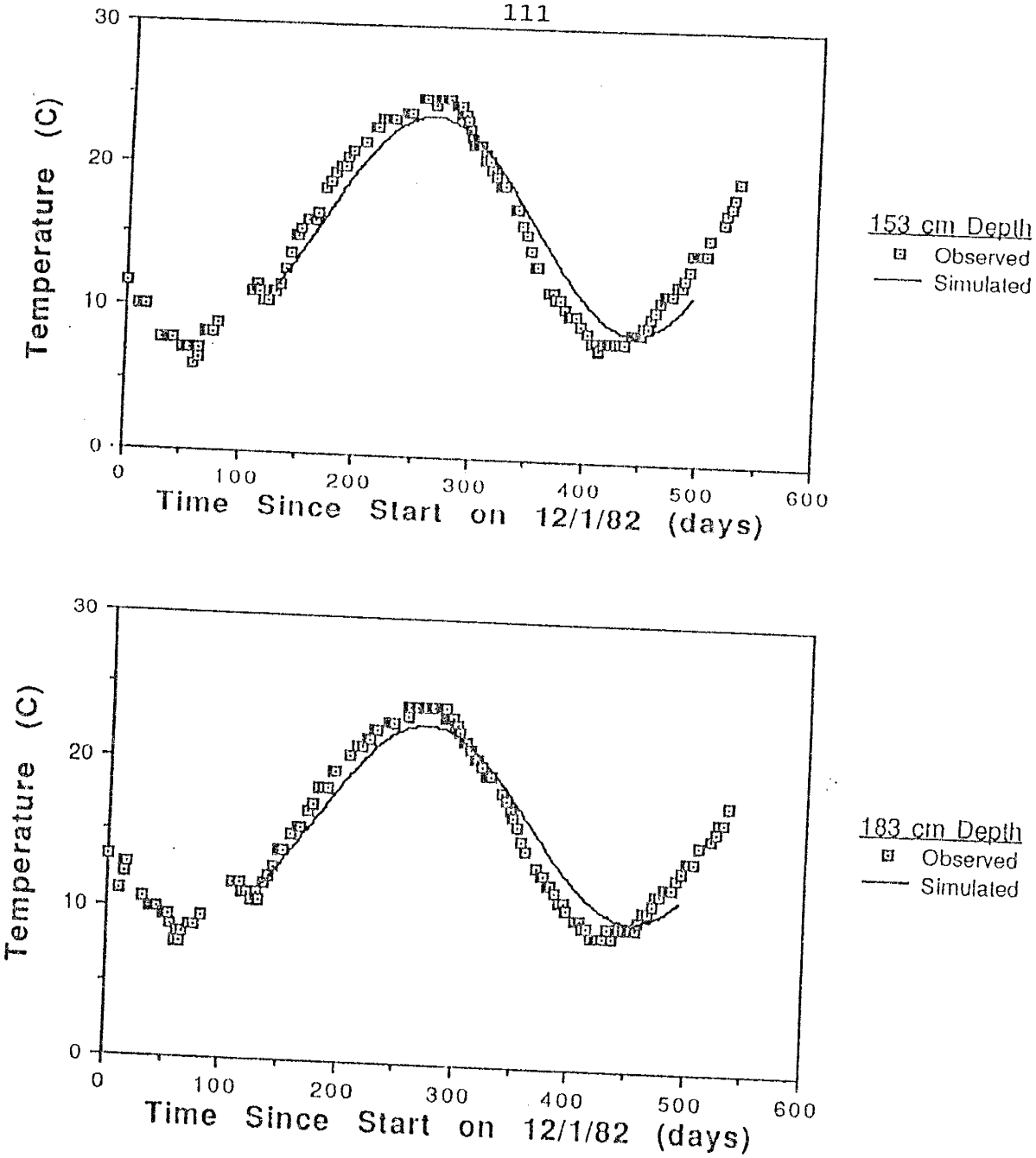

Figure 38 - Results of the analytical heat-flow modeling versus observed temperature data

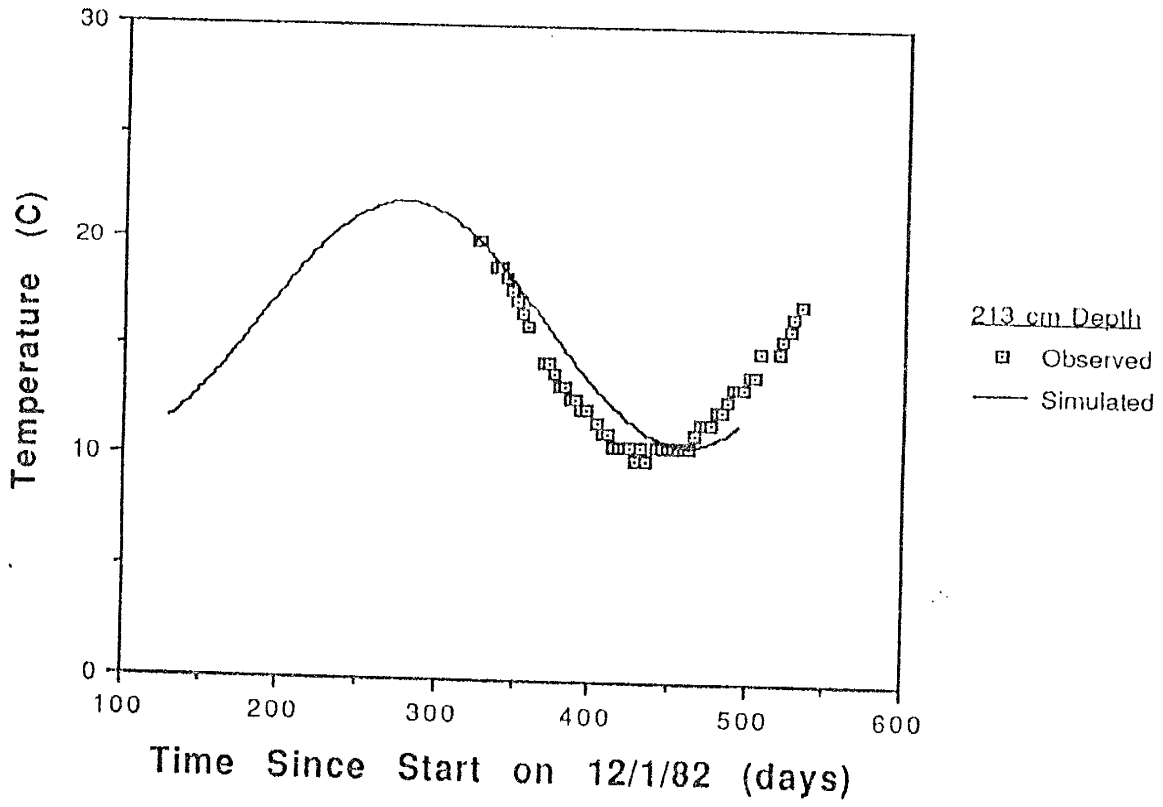

Figure 39 - Results of the analytical heat-flow modeling versus observed temperature data

The amplitude of the daily surface temperature cycle, A_d, was not approximated in the calibration of the heat-flow model. The shallowest observed temperature data was collected at a depth of about 30 cm. No hourly temperature data was available from this depth. Even if it were, it would be of limited use, inasmuch as the calculated daily damping depth, d_d, is on the order of 10 cm. Therefore the observed data cannot be used to calibrate the A_d term. A range of A_d values has therefore been used to generate potential temperature profiles for input to the NIR stable-isotope model, namely 0 °C, 5 °C and 10 °C. With these A_d values, the daily damping depth was calculated in the range of 8 to 11 cm, and the annual damping depth was 150 to 220 cm.

The effective temperature profile which resulted in the observed stable-isotopic compositions of δD and $\delta^{18}O$ at the time of sampling is not truely known. It is presumed that some prior thermal history had a more pronounced influence on the isotopic compositions than did the temperature at the time of sampling. This assumption is based on the fact that isotopic equilibrium takes time. The actual time for equilibration in a transient system is not known. Therefore the NIR model was run for a suite of calculated temperature profiles stepping back in time from the day of sampling. It is assumed that the better the fit of the observed to calculated isotope data, the more closely the calculated temperature profile resembles the effective temperature profile which affected the observed isotopic compositions.

Several simulated temperature realizations have been computed with the heat-flow model for input to the NIR model to match the observed stable-

isotope compositions from the SSIP5 core. Figure 40 shows the simulated temperature versus depth profiles from 5/26 to 8/4, in weekly increments. These data were used in the NIR model to fit to the observed stable-isotope data. Four parameters were optimized during each trial run: the isotopic composition of the recharge water (δ_D^{Rec}), the recharge rate (W), the liquid tortuosity factor (τ^l), and the vapor tortuosity factor (τ^v).

Tables 6 and 7 show the results of the model fitting to the observed SSIP5 isotopic data for A_d values of 5 °C and 10 °C, respectively. The vapor tortuosity factor was given an upper limit of 1.0. The liquid tortuosity factor was given a lower limit of 0.03, based upon calculations by Phillips et al. (1988). Barnes and Allison (1984) have suggested that both the vapor and liquid tortuosity factors should be on the order of 0.667. It is obvious from tables 6 and 7 that the model results for temperature profiles prior to about 6/17 are suspect. The calculated vapor tortuosity factors prior to this date were markedly greater than 0.667. The temperature profiles prior to 6/17 are probably not indicative of the effective temperature profile which influenced the stable-isotopic compositions observed from SSIP5, which was collected on 8/4/88. This is not surprising, inasmuch as the time span between 6/17 and 8/4 is about 7 weeks. Therefore the temperature data for times within 6 weeks of the sampling are considered more appropriate. It is probably not necessary to choose one temperature profile as that which affected the isotopic composition most, because the maximum difference in the optimized parameter values over the six week period from 6/24 to 8/4 is on the order of 20%. The sensitivity of the

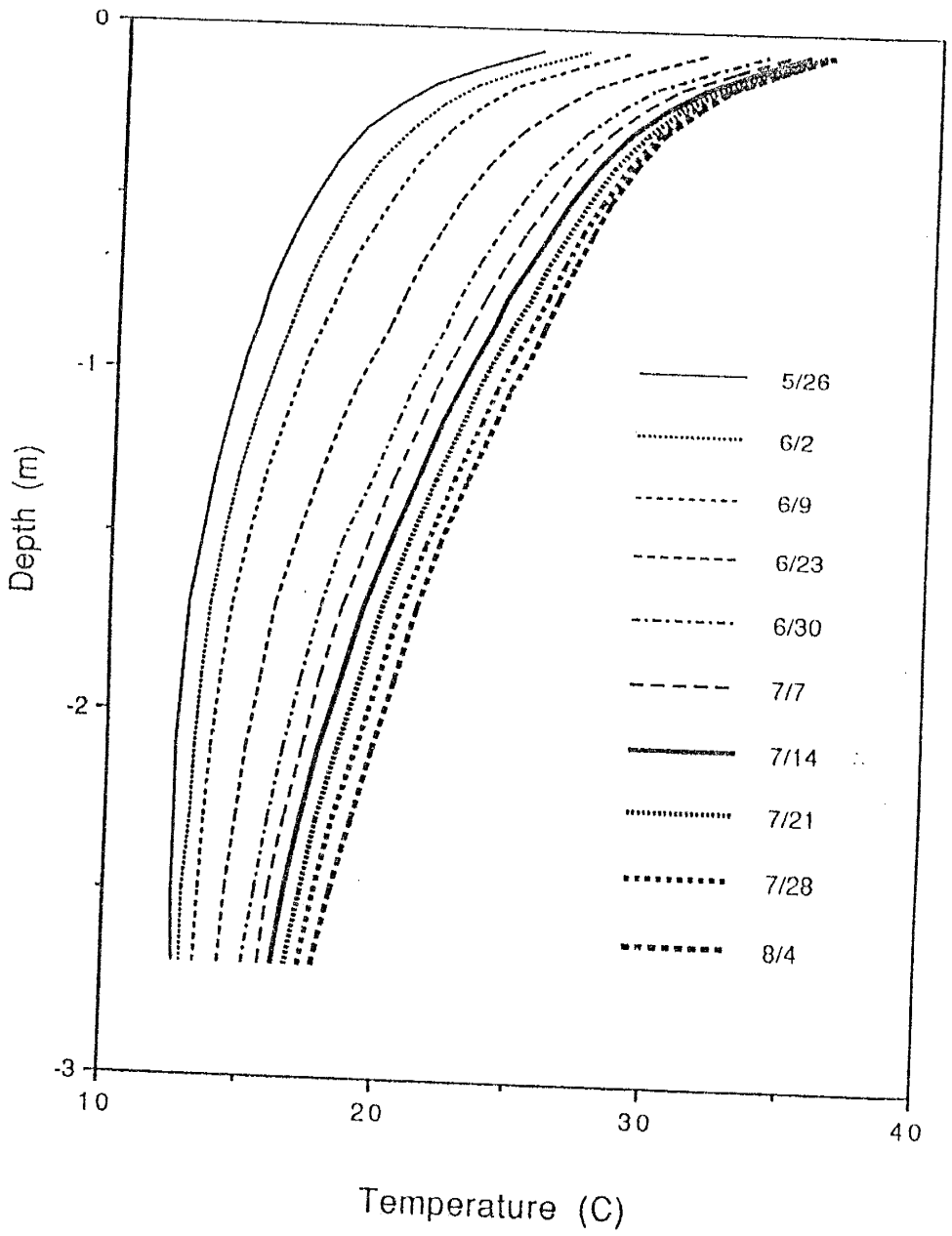

Figure 40 - Simulated temperature versus depth profiles from 5/26 to 8/4

Table 6 - Results of Profile Fitting and Vapor Flux Calculations at Various Times During the Spring and Summer From SSIP5 Data[1]

Date	Vapor Tortuosity Factor	Liquid Tortuosity Factor	Recharge Rate (cm/yr)	δD Recharge (permil)	SSQR[2]	Maximum Vapor/Total Flux Ratio
5/21	0.996	0.030	0.98	-82.3	101.	0.80
5/28	0.994	0.030	1.08	-81.6	98.4	0.82
6/03	0.998	0.030	1.19	-81.1	96.4	0.84
6/10	0.754	0.030	1.10	-80.4	95.4	0.84
6/17	0.564	0.030	0.91	-80.2	96.0	0.82
6/24	0.465	0.030	0.83	-80.1	96.7	0.79
7/01	0.423	0.030	0.82	-80.1	97.9	0.77
7/08	0.348	0.030	0.73	-80.2	99.9	0.73
7/15	0.331	0.030	0.75	-80.4	103.	0.69
7/22	0.323	0.030	0.76	-80.5	107.	0.67
7/29	0.312	0.030	0.79	-80.8	112.	0.61
8/04	0.306	0.030	0.80	-81.0	119.	0.56

[1] - Maximized diurnal fluctuation, where A_d = 5 C

[2] - Sum of the squares of the residuals

Table 7 - Results of Profile Fitting and Vapor Flux Calculations at Various Times During the Spring and Summer From SSIP5 Data[1]

Date	Vapor Tortuosity Factor	Liquid Tortuosity Factor	Recharge Rate (cm/yr)	δD Recharge (permil)	SSQR[2]	Maximum Vapor/Total Flux Ratio
5/21	0.982	0.030	0.58	-80.9	132	2.58
5/28	0.974	0.030	0.63	-79.8	124	2.64
6/03	0.968	0.030	0.69	-78.9	117	2.66
6/10	0.465	0.030	0.43	-78.2	110	2.50
6/17	0.808	0.030	0.81	-77.8	109	2.48
6/24	0.608	0.030	0.68	-77.8	109	2.38
7/01	0.509	0.030	0.64	-77.9	111	2.24
7/08	0.427	0.030	0.60	-78.1	115	2.10
7/15	0.355	0.030	0.55	-78.5	121	1.95
7/22	0.343	0.030	0.57	-78.8	128	1.81
7/29	0.367	0.030	0.66	-79.2	139	1.68
8/04	0.354	0.030	0.67	-79.6	152	1.54

[1] - Maximized diurnal fluctuation, where A_d = 10 C

[2] - Sum of the squares of the residuals

model fit to different values of A_d in the temperature realizations is also on the order of 20%. The choice of an appropriate value for A_d in the heat-flow modeling appears to be more important in estimating the vapor flux, as discussed below. Figure 41 shows a plot of NIR model results versus the observed δD profiles for three of the simulated temperature realizations. Each of the profiles plotted in figure 41 appear to be good curve-fits to the observed data, including an adequate representation of the minimum in the isotope profile at about one meter in depth.

It is interesting to note that the earlier NIR model results presented by Knowlton et al. (1989) did not achieve as accurate a curve-fit as the current work does, for the same stable-isotope data but different temperature realizations. The sum of the squares of the residuals in the current work is on the order of 100, whereas in Knowlton et al. it is around 300 or so. The discrepancy in the two curve-fitting procedures (i.e., Knowlton et al. versus the current work) appears to be rooted in the temperature realization. In the Knowlton et al. work the temperature realization was based upon the observed temperature profile at the time of sampling. As mentioned above, the thermistor used for the temperature measurement may not have been in true equilibrium with the surrounding soil at any given sampling depth. The temperature profiles used in the Knowlton et al. simulations were markedly higher than those used in the current work. As a consequence, Knowlton et al.'s simulated minimum in the isotope profile was substantially deeper in depth than the observed minimum (i.e., about 1.3 meters in depth versus 1 meter). The current heat-flow modeling

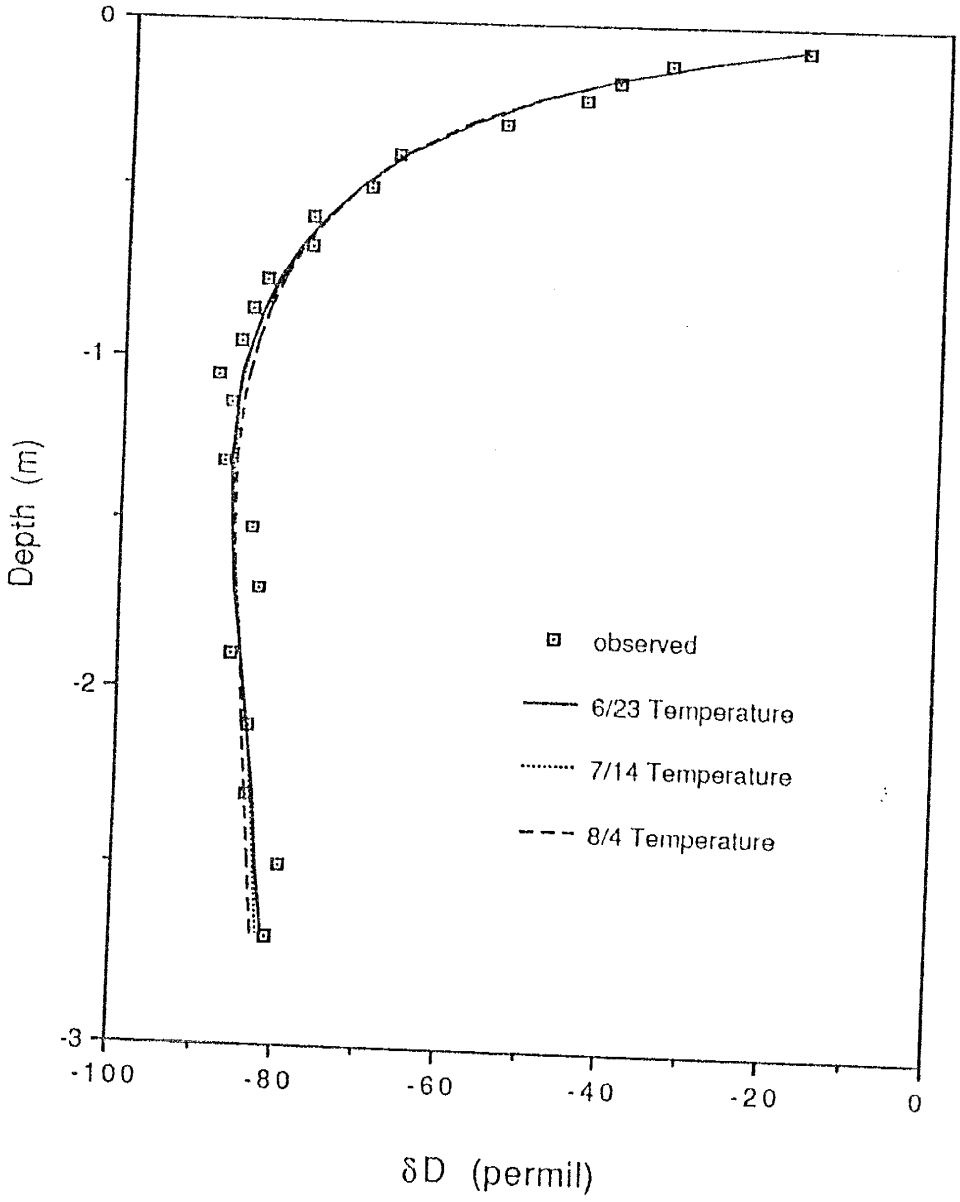

Figure 41 - NIR model calculated versus observed SSIP5 δD profile for three simulated temperature realizations

results are calibrated to observed data from the site and therefore considered more representative of actual conditions. Therefore the use of thermistors in obtaining quick temperature data when sampling an isotope profile is not recommended, at least in terms of the methodology used by Knowlton et al. (1989).

Having achieved an approximate fit between the model and observed data in the current work, the next step was to estimate the relative contribution of the vapor flux to the recharge process. Equation 52 was solved numerically using the input and fitted parameters mentioned above for the various temperature realizations. The liquid flux was computed using equation 29. For presentation purposes, the liquid and vapor fluxes are computed as fractions of the deep flux of soil water, or recharge. Tables 6 and 7 contained a column displaying the maximum vapor flux for each of the temperature realizations. There appears to be a marked difference in predicted vapor flux depending upon the value of A_d chosen. Figure 42 shows the results of these analyses for three of the temperature realizations presented above, when A_d is equal to 0, 5, and 10 °C. As expected, the larger the value of A_d (the amplitude of the daily surface temperature variation) the greater the vapor flux.

Figure 43 shows a plot of the NIR model calculated vapor and liquid flux profiles for the case when A_d = 10 °C. The negative values of the liquid/deep flux fraction are indicative of upward soil-moisture movement. The point at which the liquid and vapor flux curves cross indicates the change from a vapor to liquid dominated flow field. As mentioned above, these results are for a profile

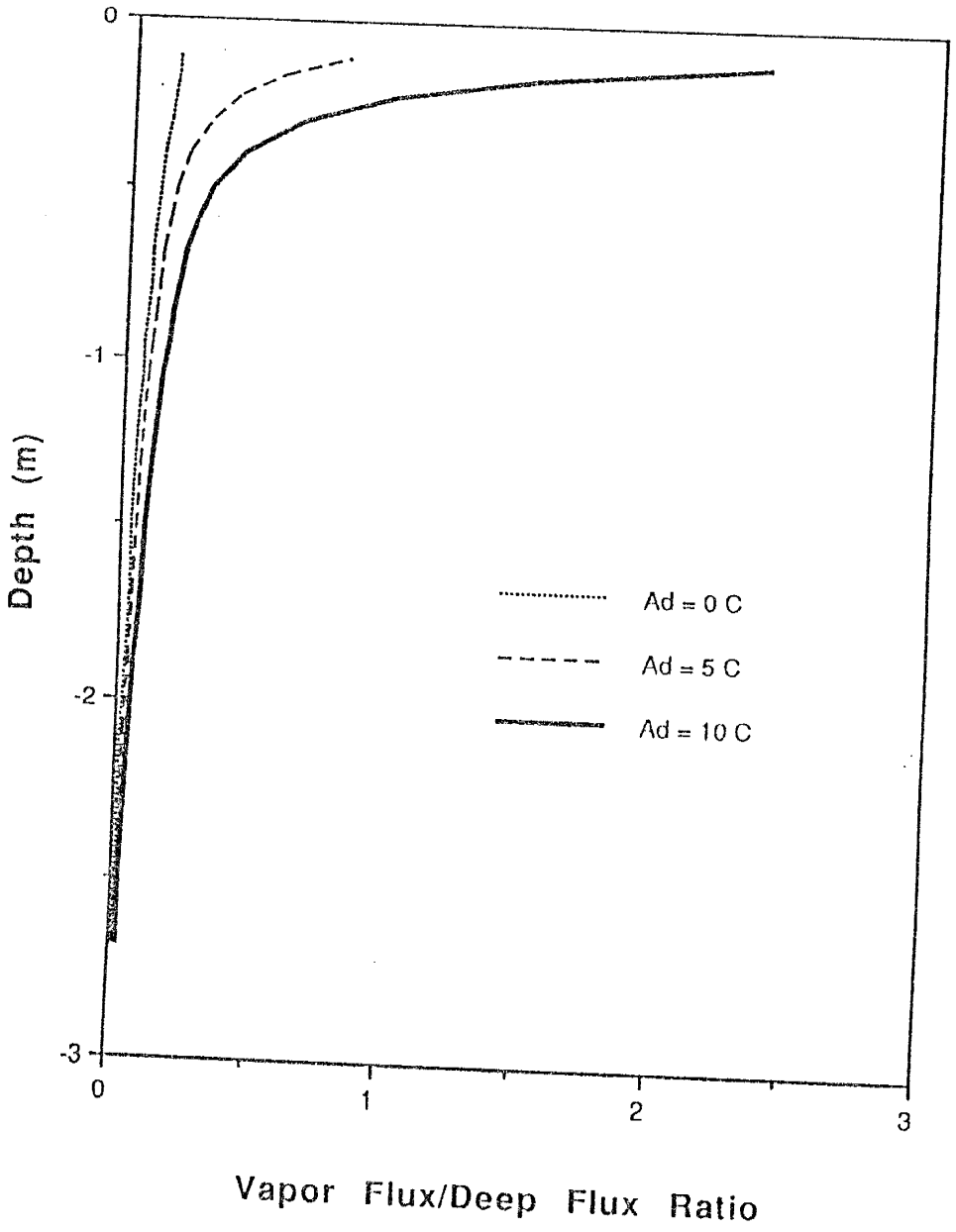

Figure 42 - Simulated vapor flux versus depth for three temperature realizations from SSIP5 data, where A_δ = 0, 5, and 10°C

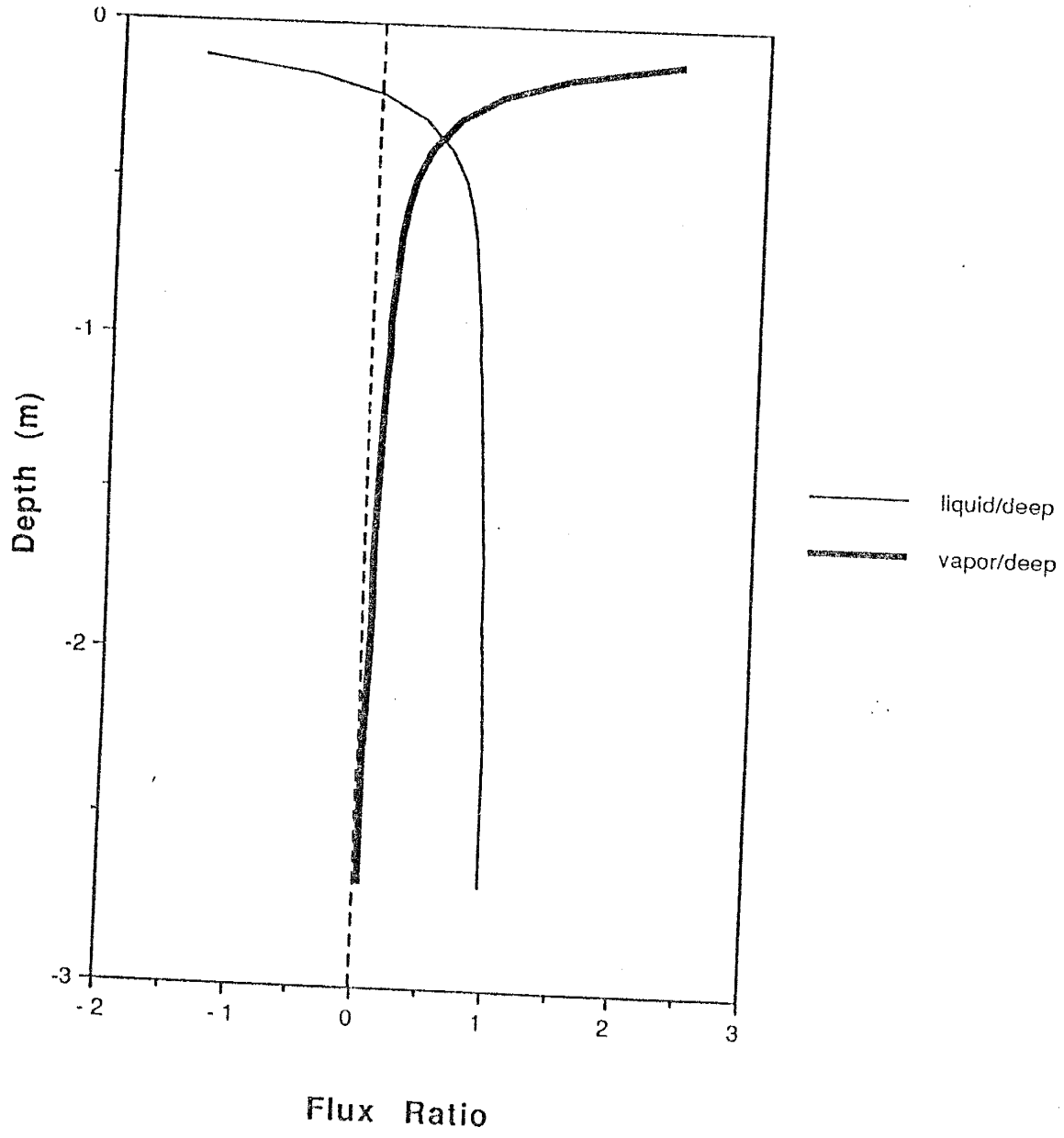

Figure 43 - NIR model simulated liquid and vapor-flux profiles for A_δ = 10°C

sampled at only a single time, and not necessarily indicative of the long-term average flux at the site.

The point at which the liquid/deep flux ratio equals zero is indicative of a divergence of flow, a null point or point of zero flux. In other words, the liquid flux above this null point was upward, and below it the flow was downward. The upward liquid flow was presumably a result of capillary pressure gradients developed from evaporation, and the drying of the soil, at the land surface. For the case shown in figure 43, the liquid flux null point was estimated at 0.20 meters in depth. The vapor-flux null point was at the evaporation front, approximately 7 cm below land surface. Therefore, the vapor flux was downward, while simultaneously the liquid flux was upward. For this realization, the zone in which the liquid and vapor flow were simultaneously in opposite directions for this realization was between 7 and 20 cm.

The NIR model has been formulated for flow conditions below the plane of divergence of the vapor flux. The model predicts a large vapor flux just below the plane of divergence, due to the finite-differencing scheme used in the calculations. Figure 44 depicts a conceptualization of the liquid and vapor fluxes from about one meter in depth up to the land surface. The vapor flux at the null point, by definition, must be zero. Above the null point the vapor flux is upward, due to vapor-pressure gradients brought about by the evaporative demand at the land surface. The relative humidity is decreasing within this zone, with a value close to unity near the evaporation front (i.e., null point) and a value approaching that of the overlying air at the land surface. This zone above

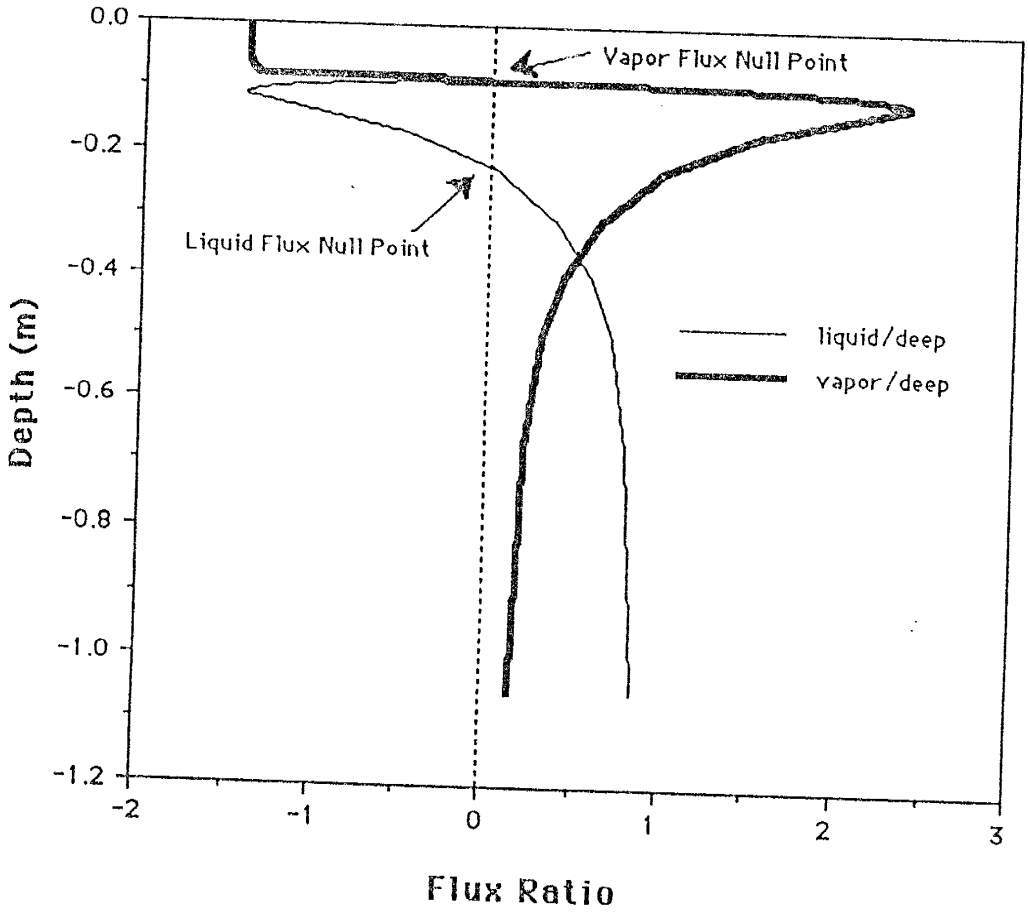

Figure 44 - Conceptual depiction of the liquid and vapor-flux distributions from land surface to approximately one meter in depth

the vapor-flux null point is quite dry if no recent infiltration events have occurred. The soil is dry enough within this zone that it probably does not yield much water to the evaporation flux. The liquid flux of water in this region is probably negligible. Therefore the vapor flux within this region will be relatively uniform with depth. The soil water that changes from a liquid to a vapor phase in response to the evaporative demand is probably emanating from a small zone right around the vapor-flux null point. As time procedes the vapor-flux null point progresses deeper into the profile as the soil water vaporizes and is given up to the evaporative demand and the downward vapor flux. As the evaporation front gets deeper, the vapor-pressure gradient above the null point decreases, and hence the evaporation rate decreases. This scenario procedes until an infiltration event occurs. Subsequently, the evaporation front starts at the land surface and moves down into the profile in the same manner as just described, creating a cycle. Therefore, the soil water which becomes the downward vapor flux emanating from the vapor-flux null point maintains the upper boundary flux condition for the NIR model.

The analyses just presented allow us to draw some conclusions with regard to the relative importance of the vapor-flux contribution to soil-water movement. During summer months in arid soils, the downward soil-water movement in the top meter of the profile is predominantly in the vapor phase. The liquid flux is upward above a null point, some 0.20 meters below the land surface, in response to capillary pressure gradients brought about by the evaporative demand. Therefore, in the upper portion of the profile, water may

be simultaneously moving downward during summer months (in the vapor phase), while solutes are moving upward (in the liquid phase). This phenomenon has been investigated previously by Rose (1968) through conventional modeling techniques. Jackson et al. (1973) performed a detailed field experiment in which their results suggest a divergence in the liquid and vapor-flux directions. They also mapped out the transient nature of the liquid-flux null point in response to diurnal temperature effects on the soil moisture regime. From these observations a separation in volatile versus conservative solute tracer movement would be expected. The radioisotope tracer results of Phillips et al. (1988) support this assumption, based upon the distribution of bomb-pulse ^{36}Cl and ^{3}H in the soil profile. A conceptual model of soil-water movement, as influenced under prevailing summer conditions, is presented in figure 45.

The conclusions just drawn with regard to the relative importance of vapor-phase soil-water movement were based upon data collected during the summer only. The question of whether there is a net downward vapor flux over an annual time frame needs to be addressed. In an attempt to evaluate the net effect of non-isothermal conditions at the research site, the NIR model has been applied to the data collected from the SSIP8 core, which was sampled on January 24, 1989. By coincidence, the SSIP5 core (sampled on August 4, 1988) was obtained during that time of the year when the temperature gradient was greatest in a downward direction, and the SSIP8 data was collected at a time when the temperature gradient was greatest in an upward direction. This

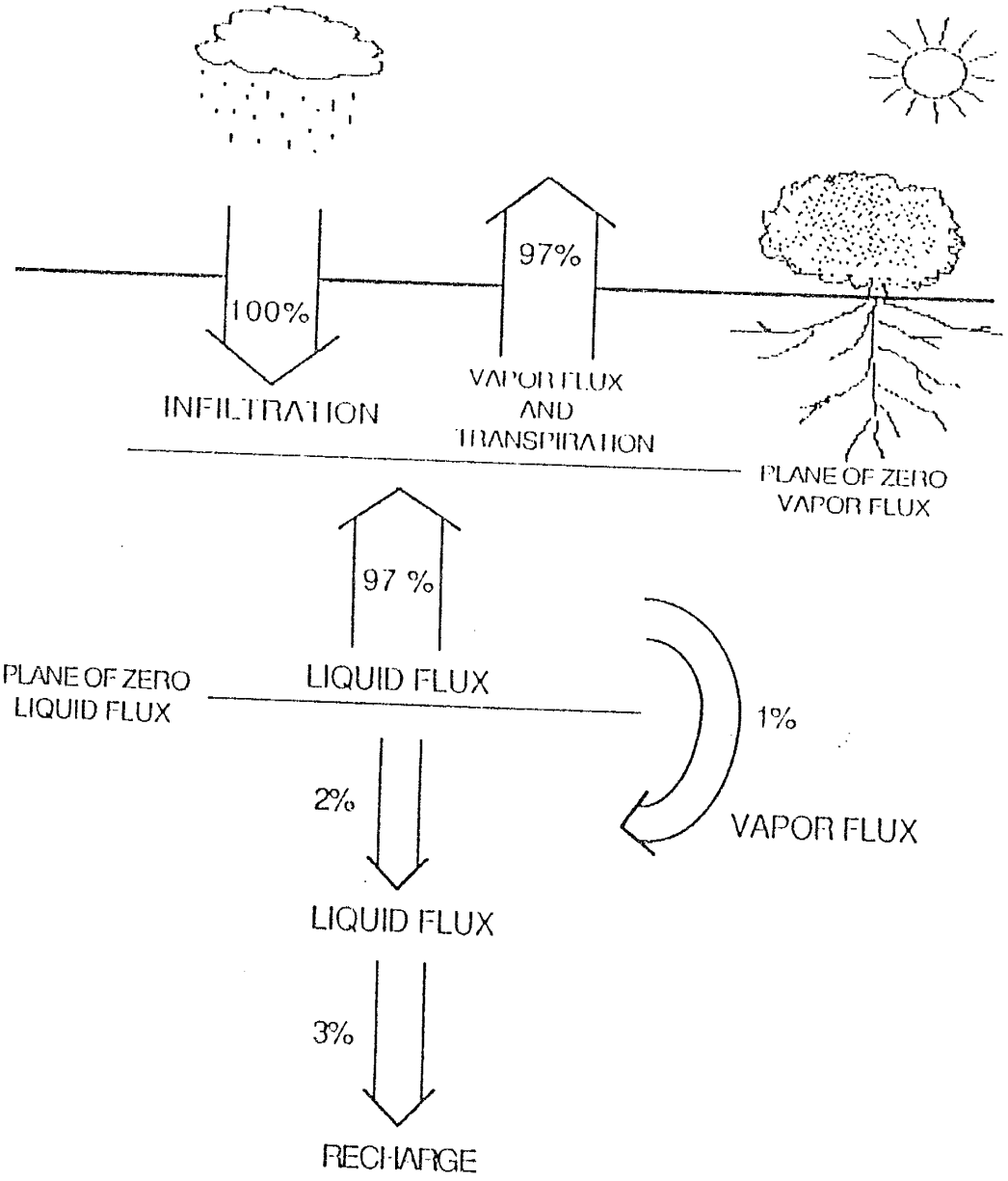

Figure 45 - Conceptual depiction of soil-moisture movement under summer conditions. The plane of zero vapor flux occurs approximately 0.07 m below land surface, and the plane of zero liquid flux at 0.35 m.

observation was made with the aid of the temperature data collected by Stephens et al. (1985) a few years prior to sampling the SSIP5 and SSIP8 cores.

Assuming that the SSIP5 and SSIP8 cores were indeed collected at times of the year when the temperature gradients were in relative extremes (i.e., downward and upward maximum temperature gradients, respectively), then a comparison of the predicted vapor flux from both sets of data should yield a simplified qualitative estimate of the net vapor-phase movement of soil water. The calibrated heat-flow model was used to predict temperature profiles for input to the NIR model to analyze the SSIP8 data. As was done for the analysis of the SSIP5 profile, several temperature realizations were used in the analysis of the SSIP8 profile. Again, the daily amplitude of temperature variation at the land surface, A_d, is not known. Therefore several values of A_d were used in the heat-flow modeling to investigate the range of responses to this parameter. Tables 8 and 9 show the results of the NIR modeling of the SSIP8 data for A_d values of 5 °C and 10 °C, respectively. Figure 46 shows the NIR model curve-fitting results to the observed stable-isotope data from the SSIP8 profile for several of the temperature realizations. Figure 47 shows the results of the vapor-flux estimates for the various values of A_d used in generating the temperature realizations.

The NIR model curve-fit to the observed data from the SSIP8 data shown in figure 46 did not match as well as that obtained from the SSIP5 data shown in figure 41. From figure 46 it is evident that in the 0.5 to 1 meter depth interval the isotopic composition of the soil water was still under the influence of the

Table 8 - Results of Profile Fitting and Vapor Flux Calculations at Various Times During the Winter From SSIP8 Data[1]

Date	Vapor Tortuosity Factor	Liquid Tortuosity Factor	Recharge Rate (cm/yr)	δD Recharge (permil)	SSQR[2]	Maximum Vapor/Total Flux Ratio
11/30	0.030	0.667	0.43	-81.0	329	-0.028
12/07	0.030	0.667	0.42	-81.2	330	-0.026
12/14	0.030	0.667	0.40	-81.3	330	-0.025
12/21	0.030	0.667	0.39	-81.3	330	-0.024
12/28	0.030	0.667	0.38	-81.4	329	-0.023
1/03	0.030	0.667	0.37	-81.4	328	-0.022
1/10	0.030	0.667	0.36	-81.4	326	-0.021
1/17	0.030	0.667	0.35	-81.4	324	-0.020
1/24	0.030	0.667	0.35	-81.4	321	-0.020

[1] - Minimized diurnal fluctuation, where A_d = 5 C

[2] - Sum of the squares of the residuals

Table 9 - Results of Profile Fitting and Vapor Flux Calculations at Various Times During the Winter From SSIP8 Data[1]

Date	Vapor Tortuosity Factor	Liquid Tortuosity Factor	Recharge Rate (cm/yr)	δD Recharge (permil)	SSQR[2]	Maximum Vapor/Total Flux Ratio
11/30	0.030	0.667	0.43	-81.1	328	-0.040
12/07	0.030	0.667	0.41	-81.1	330	-0.038
12/14	0.030	0.667	0.40	-81.2	330	-0.032
12/21	0.030	0.667	0.38	-81.3	330	-0.035
12/28	0.030	0.667	0.38	-81.4	329	-0.033
1/03	0.030	0.667	0.36	-81.4	327	-0.032
1/10	0.030	0.667	0.36	-81.4	323	-0.031
1/17	0.030	0.667	0.35	-81.4	323	-0.031
1/24	0.030	0.667	0.34	-81.5	320	-0.031

[1] - Minimized diurnal fluctuation, where A_d = 10 C

[2] - Sum of the squares of the residuals

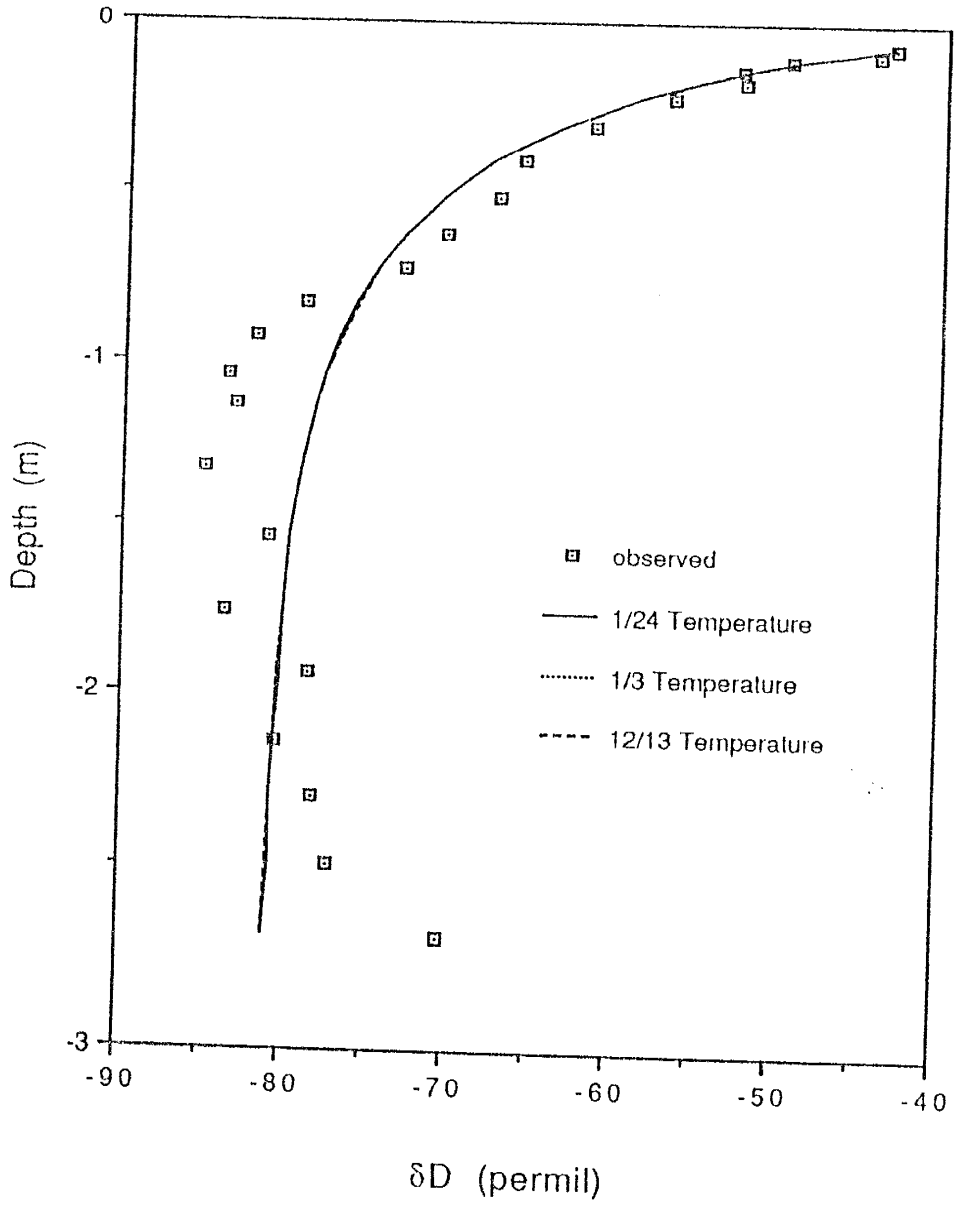

Figure 46 - NIR model calculated versus observed SSIP8 δD profile for three simulated temperature realizations

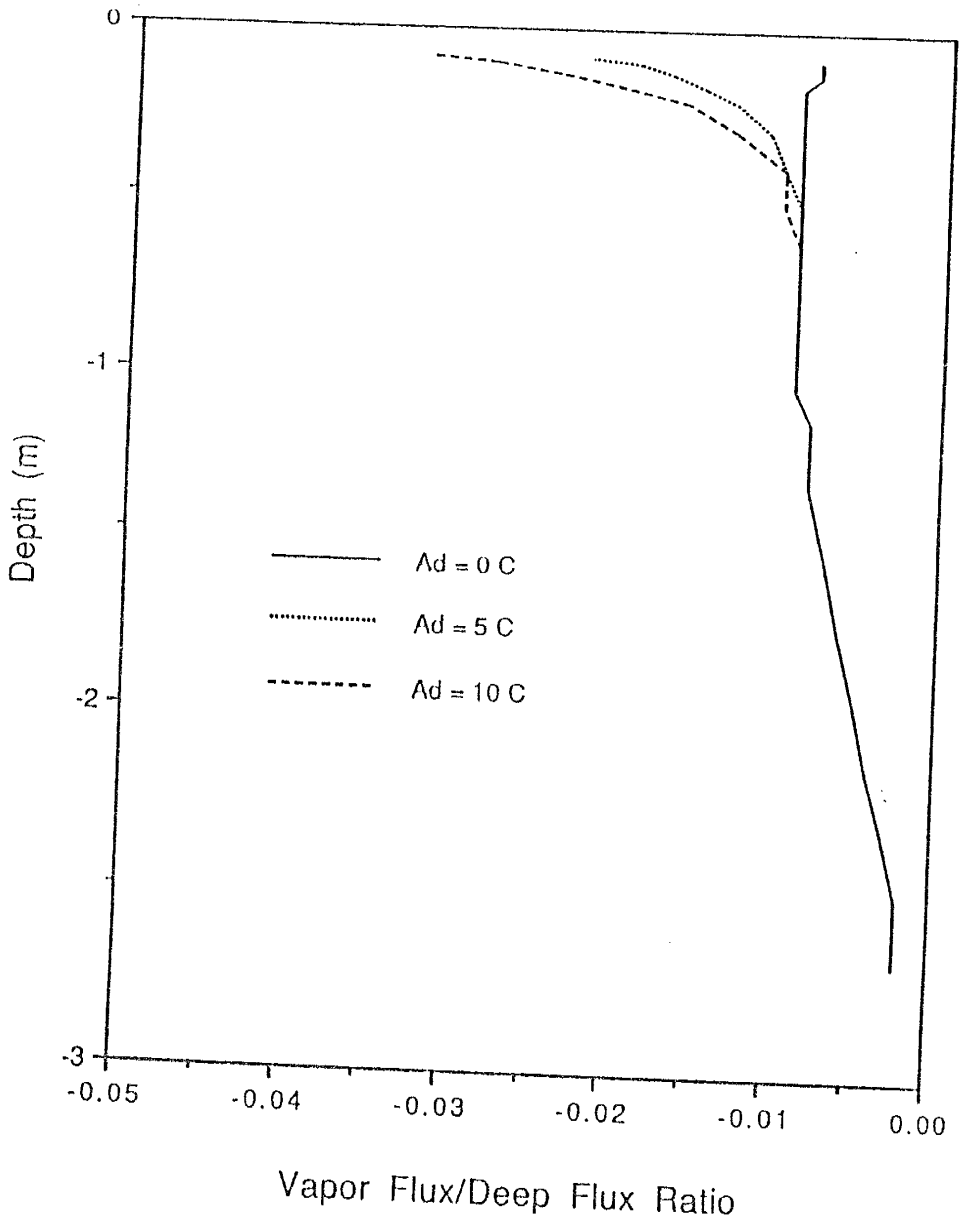

Figure 47 - Simulated vapor flux versus depth for three temperature realizations from SSIP8 data, where A_δ = 0, 5, and 10°C

autumn drying and redistribution period. An inspection of figures 27 and 28 supports this conclusion. Below one meter in depth, the persistence of the summer isotopic distribution is noticeable. Again, figures 27 and 28 bear out this observation. However, the NIR model does successfully match the observed conditions in the upper 0.5 meters of the profile that formed during the winter months. The isotopic compositon of the soil water below 0.5 meters is indicative of a slow response to environmental forcing.

It is evident from comparing the results of the vapor-flux calculations of the SSIP5 profile (seen in figure 42) and those of the SSIP8 profile (in figure 47) that the downward vapor flux during the summer months is much greater in magnitude than the upward vapor flux during the winter months. Assuming that the SSIP5 and SSIP8 cores are indicative of the two extreme temperature gradient conditions, then the net effect of annual temperature variations is a net downward vapor flux. This conclusion is consistent with the hypothesis by Phillips et al. (1988) in which they assumed that a net downward vapor flux was responsible for the observed differences in the transport characteristics of bomb-pulse ^{3}H and ^{36}Cl at the same locale currently under investigation.

As mentioned above, the temperature data collected by Stephens et al. (1985) are not sufficient enough to allow the determination of the A_d parameter in the calibration of the heat-flow model, hence several values of the parameter were utilized. An indirect means of evaluating the relative magnitude of this parameter would entail a comparison of a soil-physics based determination of the liquid flux versus the NIR model results for the assumed values of A_d. In other

words, calculate the liquid-flux distribution with a Darcy's law based analysis using the observed moisture content conditions from the SSIP5 data, evaluate the depth of the liquid-flux null point (i.e., point of divergence between upward and downward flow), and compare to the NIR model results.

The Darcy's law approach to estimating the liquid flux of soil water is a routine soil-physics technique. Stephens and Knowlton (1986) and Stephens et al. (1985) outlined the application of the technique to the research site currently under investigation. Data needs (e.g., $K(\Theta)$ functional relationship) were presented by these authors. Equation 13 in chapter 4 shows the mathematical expression representing Darcy's law. For the analysis at hand, the hydraulic gradient was estimated from the moisture content data through the use of the soil-moisture characteristic curve. The unsaturated hydraulic conductivity was estimated from the $K(\Theta)$ relationship developed from an in-situ instantaneous rofile test. Results of this analysis are presented graphically in figure 48. The recharge rate for this analysis was taken as that which was calculated at the base of the profile, and equal to 0.28 cm/yr. The null point in the liquid-flux profile is approximately 25 cm in depth. Recall that the NIR model results presented above yielded a liquid flux null point at approximately 20 cm in depth for an assumed A_d value of 10 °C. Considering the uncertainty related to soil-physics based methods, a closer agreement between the two approaches would not be expected. In addition, it should be noted that the Darcy's law approach used here assumes isothermal conditions, and therefore temperature effects have not been taken into account.

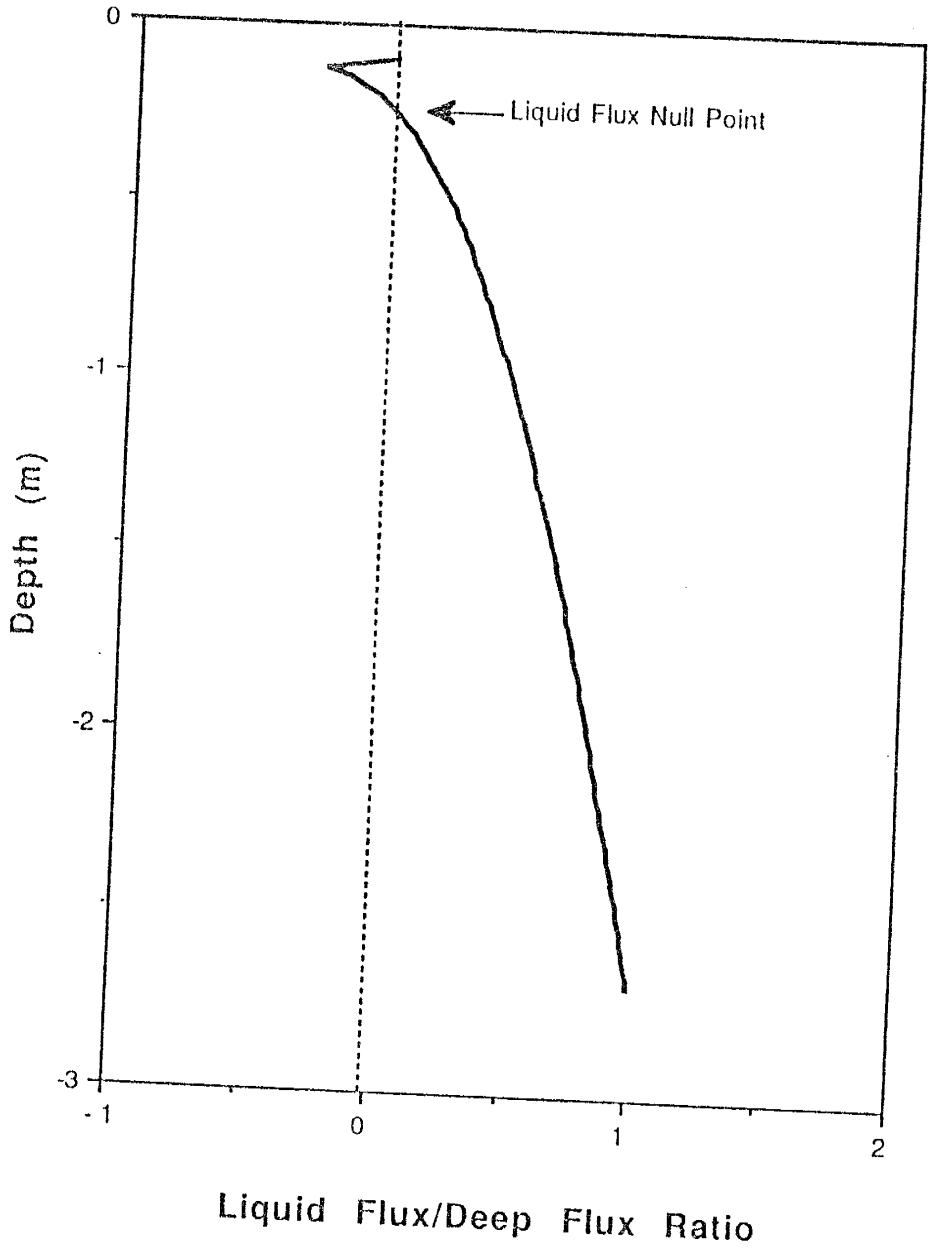

Figure 48 - Results of a Darcy's law based analysis of the liquid flux distribution from SSIP5 data

The sensitivity of the NIR model to changes in the input or fitted parameters is important in trying to evaluate the uniqueness of the results. The results of the NIR model for a number of temperature realizations has just been presented in tables 6 through 9.

The relative sensitivity of the model predictions of vapor flux to the fitted parameters can be estimated by perturbing the parameters by some specified percentage. By evaluating equation 52, all of the fitted parameters are linearly related to q^v. This implies that for a given percent change in any one of the fitted parameters, q^v should also change by a percentage of the same order or less. To evaluate this effect quantitatively, each fitted parameter was perturbed $\pm$ 10% from the values obtained in one of the temperature realizations presented above for the SSIP5 profile. The resultant curve-matching criteria (i.e. sum of the squares of the residuals) and maximum predicted vapor flux/deep flux ratio are summarized in table 10.

In addition to its ability to predict the liquid- and vapor-phase flux of soil water in the subsurface, the NIR model may also be used quite effectively in approximating the recharge rate. The recharge rate is one of four parameters which may be optimized in the NIR model to obtain a fit to the observed stable-isotope data. In all the analyses presented above, the temperature profiles that were input to the NIR model were generated with the heat-flow model. Calibration of a heat-flow model, or the observation of temperature data in the subsurface, are not always convenient or practical. Therefore, in order to evaluate the usefulness of the NIR model as a tool in estimating the recharge

Table 10 - Sensitivity of NIR Model Results to Changes in Fitted Parameters

Parameter Perturbed	Percent Change in Parameter[1]	SSQR[2]	$q_v/\rho W^3$	Percent Change in $q_v/\rho W^3$
τ_v	-10%	116.	2.14	-10%
τ_v	+10%	116.	2.62	+10%
τ_l	-10%	109.	2.38	0%
τ_l	+10%	109.	2.38	0%
W	-10%	119.	2.65	+11%
W	+10%	115.	2.16	-9%
δ_D^{Rec}	-10%	823.	2.38	0%
δ_D^{Rec}	+10%	818.	2.38	0%
Base Case	-	109	2.38	-

1 % change from base case, where: τ_v=0.608, τ_l=0.030, δ_D^{Rec}=-77.8°/$_{oo}$, W=0.68 cm/yr

2 SSQR = sum of the squares of the residuals between observed and predicted data

3 maximum predicted vapor flux/deep flux ratio

rate, an isothermal temperature profile has been utilized. The constant temperature selected was that of the average annual air temperature, 15 °C. This value of the isothermal temperature was chosen because it was easily obtained from NOAA records, and corresponds with the estimated average annual air temperature used in the heat-flow modeling, 16.2 °C (as discussed above).

In order to evaluate the ability of the NIR model to adequately predict the recharge rate under isothermal conditions, the data from both the SSIP5 and SSIP8 profiles were used. Figures 49 and 50 show the results of the NIR model curve fitting to the observed data for the SSIP5 and SSIP8 profiles, respectively. The fitted values of the recharge rate for the two analyses were 0.90 and 0.44 cm/yr, respectively. The recharge rate corresponding to the SSIP5 curve fit is approximately twice that of the SSIP8 recharge rate. The apparent reason for the discrepancy in the predicted recharge rates between the summer and winter data appears to be related to the overall concentration gradient of the isotopic species for the two profiles. Figures 49 and 50 show that the observed isotopic data from the summer profile (i.e., SSIP5) exhibit a larger concentration gradient than that during the winter (i.e., SSIP8). The NIR model has been formulated to predict the transport of the isotopic species (e.g., deuterium) and equate the flux of the isotopic species to the overall flux of soil water. Upon examination of equation 51, the recharge rate multiplier on the left side (i.e., the term in parentheses) and the last term on the right side of the equation will be directly linked to the isotopic-concentration gradient. With a smaller gradient during

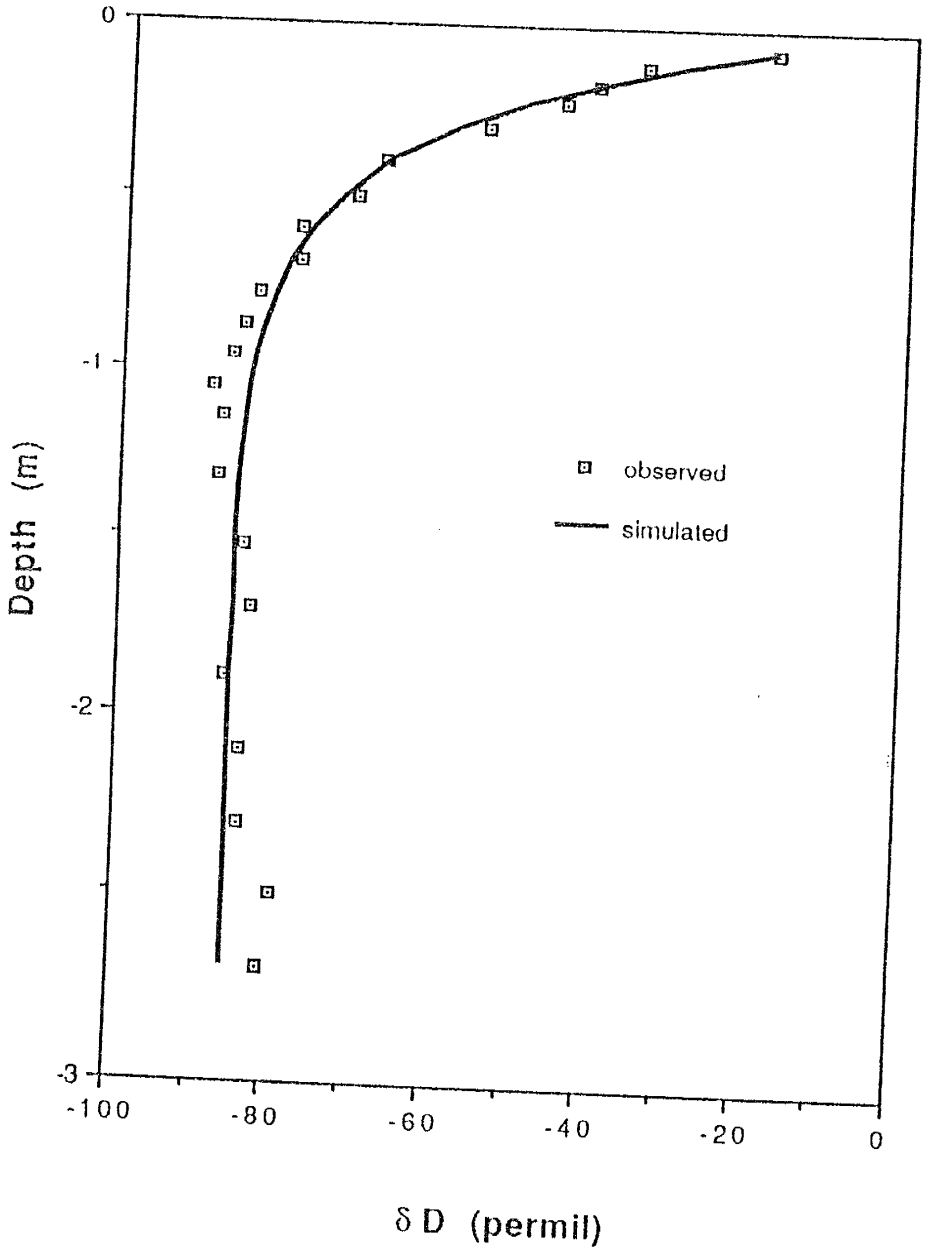

Figure 49 - NIR model calculated versus observed SSIP5 δD profile for an isothermal temperature realization

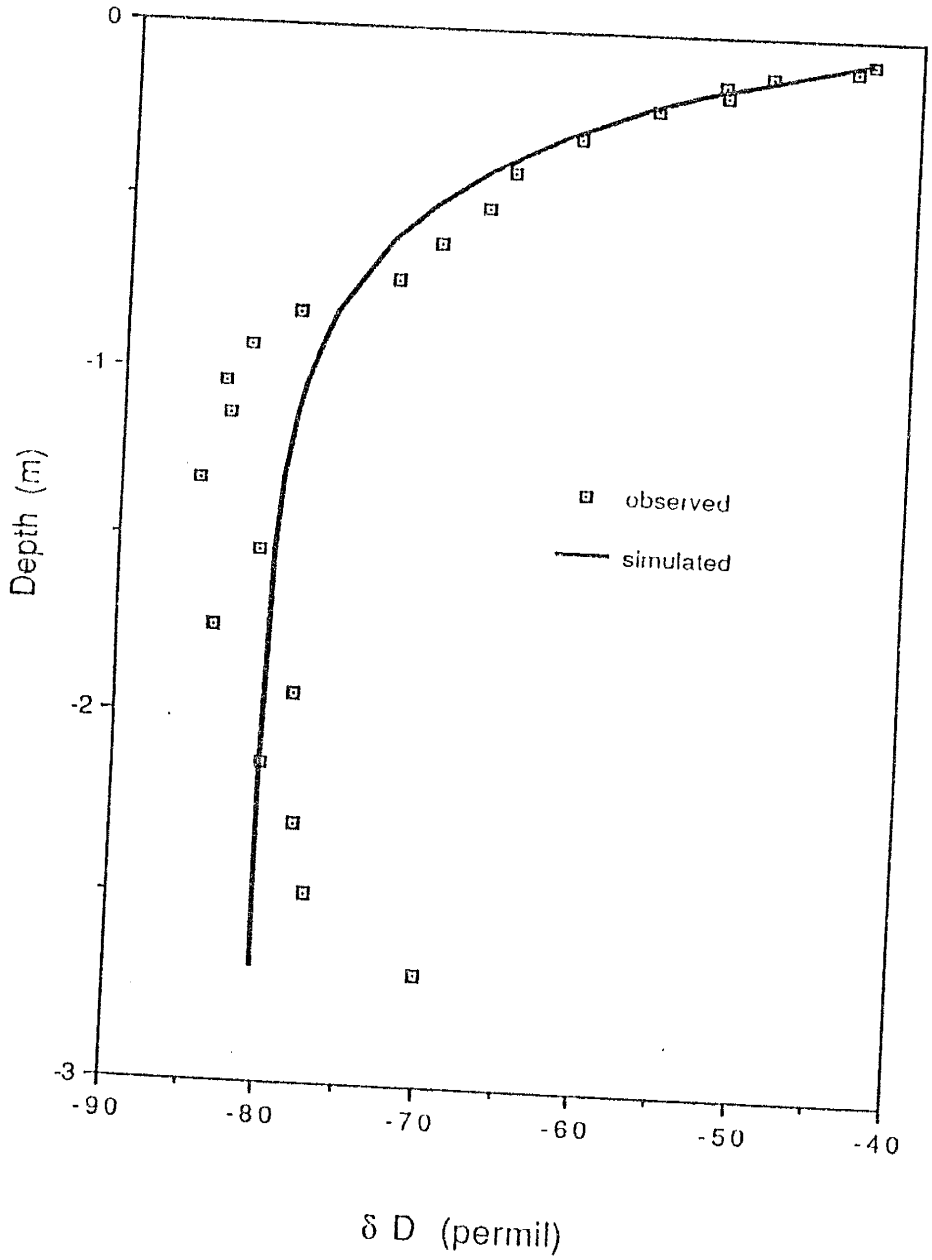

Figure 50 - NIR model calculated versus observed SSIP8 δD profile for an isothermal temperature realization

winter conditions than summer, the recharge rate should be correspondingly smaller. Therefore it appears that the recharge rate may not be constant throughout the year, but may undergo seasonal variations in response to changing heat and moisture flow conditions. It is anticipated that at some depth below the land surface, probably below the effect of annual temperature variation, that the soil-water movement rate will stabilize. It is interesting to note that the vapor-pressure gradient term in equation 51 is zero for the isothermal case, thereby forcing the model to neglect any possible vapor-flux contribution.

Other possibilities exist to explain the differences in calculated recharge rates for the summer versus winter results. The first possible explanation relates to the relative transient nature of the soil-water flux during the winter months. The profile may still be undergoing redistribution following the late summer to early autumn infiltration events. If soil water is moving vertically upward in response to an evapotranspirative demand, then the recharge rate calculated by the NIR model might be less than that which would occur during strictly downward soil-water movement. Therefore it might be more appropriate to estimate the recharge rate from a profile collected during the summer months, or following a relatively long period when no net infiltration has taken place. Another possible scenario to explain the differences in calculated recharge rates, which should always be considered when evaluating destructively sampled profiles, is spatial variability.

The subject of spatial variability at the research site can be addressed with the existing data. Figure 20 depicted the moisture content distribution for the SSIP5 and SSIP6 cores, collected 70 cm apart on the same day. There is considerable variation with depth between these two profiles. This implies that there are textural differences between the two sampling sites. The isotopic data presented in figure 21 for the same two cores are lacking in any appreciable variation, however. The uniformity in the isotope profiles implies that the slight textural differences have little to do with isotopic changes. Allison and Hughes (1983) discuss the issue of replication, and conclude that errors associated with limited tracer data may not be as serious as expected. In addition, Foster and Smith-Carrington (1980) sampled six tritium profiles over a sizeable area and found very good lateral uniformity. Therefore we assume that these profiles, although collected at only two points, are representative of soil moisture movement over a larger area.

The recharge rates calculated with the NIR model under isothermal conditions compare quite favorably with results from other techniques used at the research site to estimate soil-water movement rates. Table 11 shows the results of work by Stephens and Knowlton (1986), Phillips et al. (1988), and the present work, all of which were conducted in close proximity to each other. Stephens and Knowlton estimated the recharge rate through the use of soil-physics techniques (i.e., Darcy's law approach). Phillips et al. estimated the recharge rate with several techniques: bomb-pulse ^{3}H and ^{36}Cl tracer methods, and the chloride mass balance method. The total range of recharge estimates

Table 11 - Summary of Results for Various Methods of Estimating the Recharge Rate at the SNWR Research Site

Method	Recharge Specific Flux (cm/yr)
NIR Stable-isotope Model	0.90 (0.44)[A]
Darcy's Law, with harmonic mean K averaging	0.70
Tritium Peak Method	0.84
Tritium Mass Balance Method	0.64
^{36}Cl Peak Method	0.80 (0.30)[B]
Chloride Mass Balance Method	0.25

[A] - calculated from isothermal summer and winter data, respectively

[B] - calculated from overall depth of ^{36}Cl penetration, and from maximum observed peak, respectively

with these techniques is 0.25 to 0.9 cm/yr. The mean recharge rate for these eight estimates combined is 0.61 cm/yr. This recharge rate represents approximately 3 percent of the average annual precipitation (Stephens et al., 1985).

It is interesting to note some of the limitations involved in these various techniques for estimating soil-water movement rates. In the case of the soil-physics techniques, the unsaturated hydraulic conductivity function (e.g., $K(\Theta)$) must be estimated. As discussed above, the uncertainty associated with estimating $K(\Theta)$ is quite large, approaching an order of magnitude. For the radioisotope and stable-isotope techniques, the limitation lies mostly in the number of sample profiles collected. Generally with destructive sampling techniques such as these, one profile is collected. Spatial variability and the transient behavior of the soil-water movement are generally not accounted for. However, these isotope techniques generally yield results that are applicable over longer time frames than the soil-physics techniques. The chloride mass balance method also suffers from the same limitations as the isotope techniques, inasmuch as it too involves destructive sampling. It suffers from one additional qualification, and that is piston displacement is assumed. Piston displacement is probably not the major mechanism controlling soil-water movement in the upper meter of the profile, as will be discussed below. Additional qualifications could be stated for each of these techniques, but the main points have been covered. Therefore it is most interesting to note that these various techniques, with some

uncertainty associated with each, yield results that are markedly similar for the research site under investigation.

Stable-isotope and water content data have been presented for several seasons of the year at the research site. It is evident from the data that a fair amount of seasonal changes occur in the profile with regard to stable-isotope and soil-moisture conditions. Figures 24, 27, and 28 showed the relationship between δD profiles for this seasonal data. Figures 23, 29, and 30 presented the water content data from the same cores. These seasonal changes in isotopic composition and soil-moisture conditions may have an effect on the observed distribution of the bomb-pulse ^{3}H and ^{36}Cl radioisotopes. As mentioned above, the NIR model developed in this research effort is only applicable under quasi-steady state conditions. Under seasonally varying conditions a different approach must be taken to understand the changes that are occurring, and the impacts on solute distributions and soil-water movement.

From figure 23, it is evident that a significant amount of water (approximately 3.7 cm of water, or 43% of the precipitation which occurred) infiltrated into the soil to a depth slightly exceeding one meter between the August and October samplings. Figure 13 shows the monthly precipitation at the site (Stein,T., written communication, May 1989). The months of August and September are considered the 'rainy season'. During this period, the predominant precipitation form was thunderstorm activity. A sample of water from one precipitation event in Socorro was analyzed during this period, on August 23, 1988. The δD isotopic composition was -78 $^{\circ}/_{oo}$. Figure 24 presented

the δD profiles for the summer and fall sampling times. The isotopic composition of the soil water within the zone of wetting has been markedly altered during this time frame. The infiltrated precipitation has presumably mixed with the water initially in the profile, resulting in the observed October data. To evaluate this hypothesis, the mass balance/mixing (MBM) model described in section 4.2 was employed.

The MBM model was intended as a tool to investigate the possibility that a mass balance/mixing phenomena may be responsible for the observed changes in the isotopic and soil-water distributions. Other mechanisms may also be occurring, but further investigation is considered beyond the scope of this work. Certainly a heat and moisture flow model would be appropriate to simulate these changing conditions, but would undoubtedly be costly, time consuming, and yield a fair degree of uncertainty in the results. Considering the amount of data that has been compiled from this site (e.g., hydraulic characteristics; thermal characteristics; time history of soil moisture, pressure head, temperature, and meteorological data; and the geochemical/isotopic results) it would be advantageous to utilize a heat and moisture flow model for future work at the site.

A computer code was written to perform the necessary MBM model calculations. The code was designed to evaluate wetting conditions, and to optimize for a value of the effective δD of the infiltrating precipitation. The initial conditions were taken as the August SSIP5 core data. The final conditions were assumed to be represented by the October SSIP7 core data. The total

difference in volume of water between these two end points was assumed to be the amount of water infiltrating into the top of the profile. The top of the profile, for the MBM model, was taken to be 0.20 meters, which is below the zone of isotopic enrichment due to the evaporation process. The sampling intervals for the SSIP5 and SSIP7 cores were not equivalent, and therefore an averaging procedure was required. The isotopic and water content data from both the SSIP5 and SSIP7 cores were depth averaged over seven discrete intervals. The results of the MBM model for this wetting period are presented in figure 51, and provide satisfactory agreement to the observed data. The calculated effective isotopic composition of the infiltrate was -60 $^{\circ}/_{oo}$.

The calculated value of the infiltrate coincides fairly well with that measured from precipitation in Socorro on August 23, 1988, or -78 $^{\circ}/_{oo}$. The model predicted value is enriched in comparison, possibly due to evaporation, or the highly variable nature of the isotopic composition of precipitation. Spatial variability in precipitation is also a consideration. The model predicts the infiltrate isotopic composition at the upper boundary of the modeled zone (i.e., 20 cm). Precipitation infiltrating from land surface to the 20 cm depth has to pass through the zone enriched significantly by the evaporation process in the upper 10 cm of the profile. The precipitation is relatively isotopically light compared to the model predicted infiltrate, but the peak enrichment due to the evaporation process is markedly heavier. Therefore the resultant mixing of the infiltrating water with the enriched water in the zone of evaporation might well have an isotopic composition equivalent to that which was calculated by the

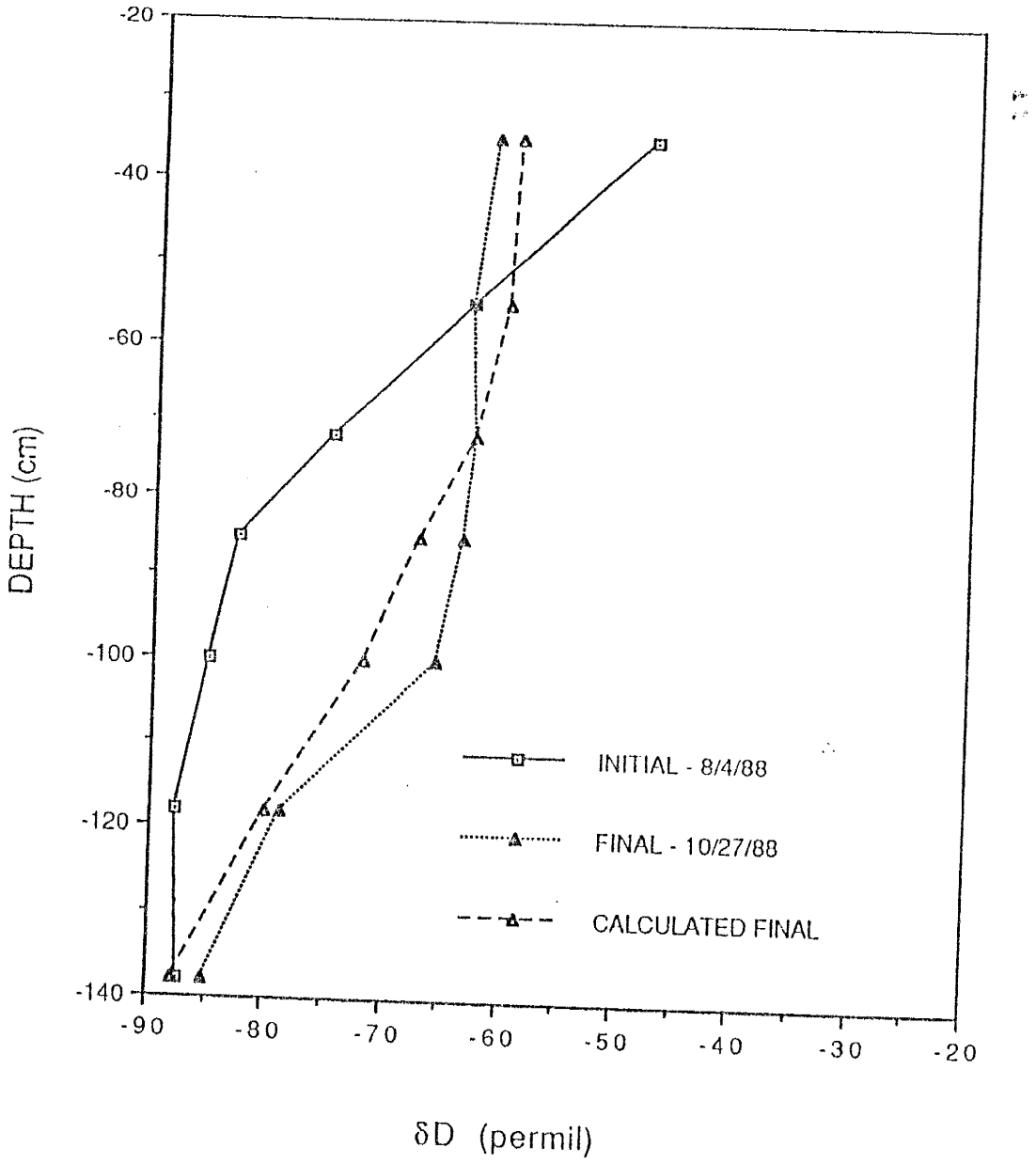

Figure 51 - Depth versus δD for observed data (depth-averaged into seven discrete intervals) and MBM wetting model calculated results

MBM model. The MBM model satisfactorily predicts the final isotopic composition of the soil water, as evidenced by figure 51.

The MBM model does not perfectly predict the isotopic composition change from August to October. There are several factors that may lead to slight discrepancies in the predicted versus observed isotopic compositions. The first factor deals with spatial variability. Although it was shown above that the isotopic composition of the soil water does not change significantly in space, the water content distribution does, owing to textural variability. Therefore, the mass balance calculations are affected by the initial water content distribution used, which may not have been the initial condition at the site where the final profile was collected, and vice versa. In addition, if the October sampling was not on a wetting trend, but rather already drying and/or redistributing, then the assumption of pure mixing during wetting has been violated. Considering the satisfactory fit between observed and calculated final isotopic compositions, the profile has probably not undergone much redistribution/drying. Also, the discretization of the profile in the model may also affect the model results.

Transpiration may also influence the distribution of soil water, and also the isotopic composition. It has been shown that plants do not fractionate soil water directly (Allison and Hughes, 1983). Allison and Hughes (1983) have presented evidence to suggest that if water transfer to plant roots occurs by vapor diffusion across gaps between plant roots and the soil, then the water in the soil will become fractionated.

The interval between the October and January sampling was presumably a time in which the soil-water in the profile was redistributing. The soil water during this period was both moving upward in response to capillary pressure gradients caused by evaporation at the land surface, taken from the soil by transpiration, and moving downward due to gravity drainage. It is assumed that the net increase in the gravity-drainage component of the soil-water redistribution was negligible, because no net transfer of water was observed deep in the profile after the October sampling. In support of this assumption, consider the neutron logging data of figure 33. The water content data in figure 33 show that the upper portion of the profile was drying between October and January. Gravity drainage has to be occurring in order to maintain recharge through the profile, but it does not appear that it was enhanced due to the infiltration event. Below the zone of wetting the moisture content did not increase during the redistribution phase, or in other words, there was no net transfer of water to depth. Assuming that all the water in the profile above 140 cm between the October and January sampling has moved upward and through the 20 cm depth horizon due to an evapotranspirative demand, then a mass/balance mixing model should adequately predict the final isotopic composition of the soil water.

A computer code was written to evaluate the MBM model for these drying conditions. A source listing of the code is contained in appendix C. The initial condition was represented by the October SSIP7 data, and the final condition the SSIP8 data. The observed data was depth averaged into seven

distinct zones. The soil-water movement was assumed to have been upward and out at the top of the modeled profile. The total amount of water moving out of the model was equal to the difference in water volumes between the initial and final profiles. To begin, an incremental decrease in volume of water was assigned to the uppermost depth interval, which was the amount of water leaving the modeled zone. If the next successive depth interval contained a higher water content, then an increment of water was transferred from this horizon to the one above. This procedure proceeded iteratively with depth until all the excess water in the profile was transferred out. For each increment of soil-water movement, the isotopic composition of the soil-water was assumed to be instantaneously mixed. The increment of volumetric water content depletion was arbitrarily assumed to be 0.005. Figure 52 represents the results of this modeling effort. The MBM model satisfactorily approximates the observed data.

Some of the reasons for possible discrepancies between the predicted and observed data were discussed above for the MBM wetting model (i.e. effects of spatial variability and transpiration). Also, if additional wetting of the profile occurred during this time frame the drying MBM model assumptions would be violated. However, the neutron logging data suggests that no wetting of the profile occurred.

These results imply that during seasons of the year other than summer, different mechanisms may be important in the transport of soil water other than vapor-phase movement. There appears to be a strong potential for 'cycling' of water movement in the upper meter of the profile on a seasonal basis. During

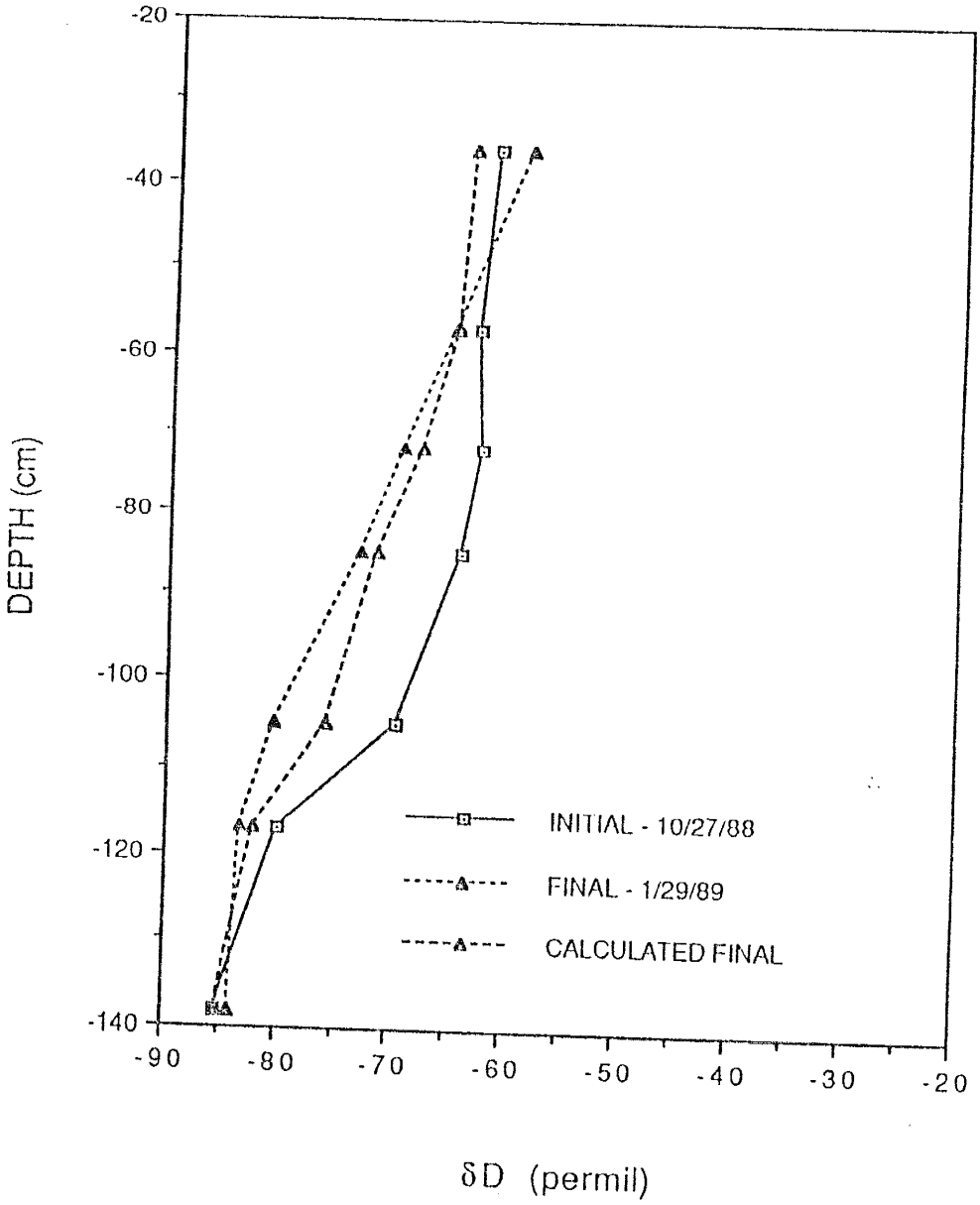

Figure 52 - Depth versus δD for observed data (depth-averaged into seven discrete intervals) and MBM drying model calculated results

the 'rainy season', water and solutes infiltrate to depth, in this case about one meter. Following the rainy season, there is a drying of the profile, probably due to capillary-pressure gradients induced by evaporation at the land surface, and transpirative uptake. The net result of the drying process is the transport of water and solutes back up toward the land surface. The combined effect resulting a cycling phenomenon.

The ^{36}Cl profile presented in figure 1 has a distribution which is worthy of discussion. At the land surface, the $^{36}Cl/Cl$ ratio was at a maximum. Just above a 1 meter depth there is an elevated ratio, or peak. The data below this lower peak exhibit a relatively uniform decrease down to a depth of 3.5 meters. The distribution of ^{36}Cl is therefore markedly different than the tritium distribution, with its broad peak between 2 and 3 meters depth. A similar distribution of both ^{36}Cl and ^{3}H was presented by Phillips et al. (1988) for a site in southern New Mexico, near Las Cruces. In addition, figure 53 presents plots of depth versus $^{36}Cl/Cl$ for a site near Artesia, New Mexico (F.M. Phillips, written communication, January 1989), the Las Cruces data, and the Sevilleta National Wildlife Refuge data. The same characteristic profile is exhibited in each of the plots. Namely, there is a maximum ratio at the top of the profile, and an elevated ratio at around one meter in depth. All three sites are located in arid environments. It is possible that the cycling phenomenon discussed above may have some influence on the observed distribution of the conservative tracer, bomb-pulse ^{36}Cl. This distribution of ^{36}Cl with depth implies that there is a very complicated history of soil-water movement natural desert soils.

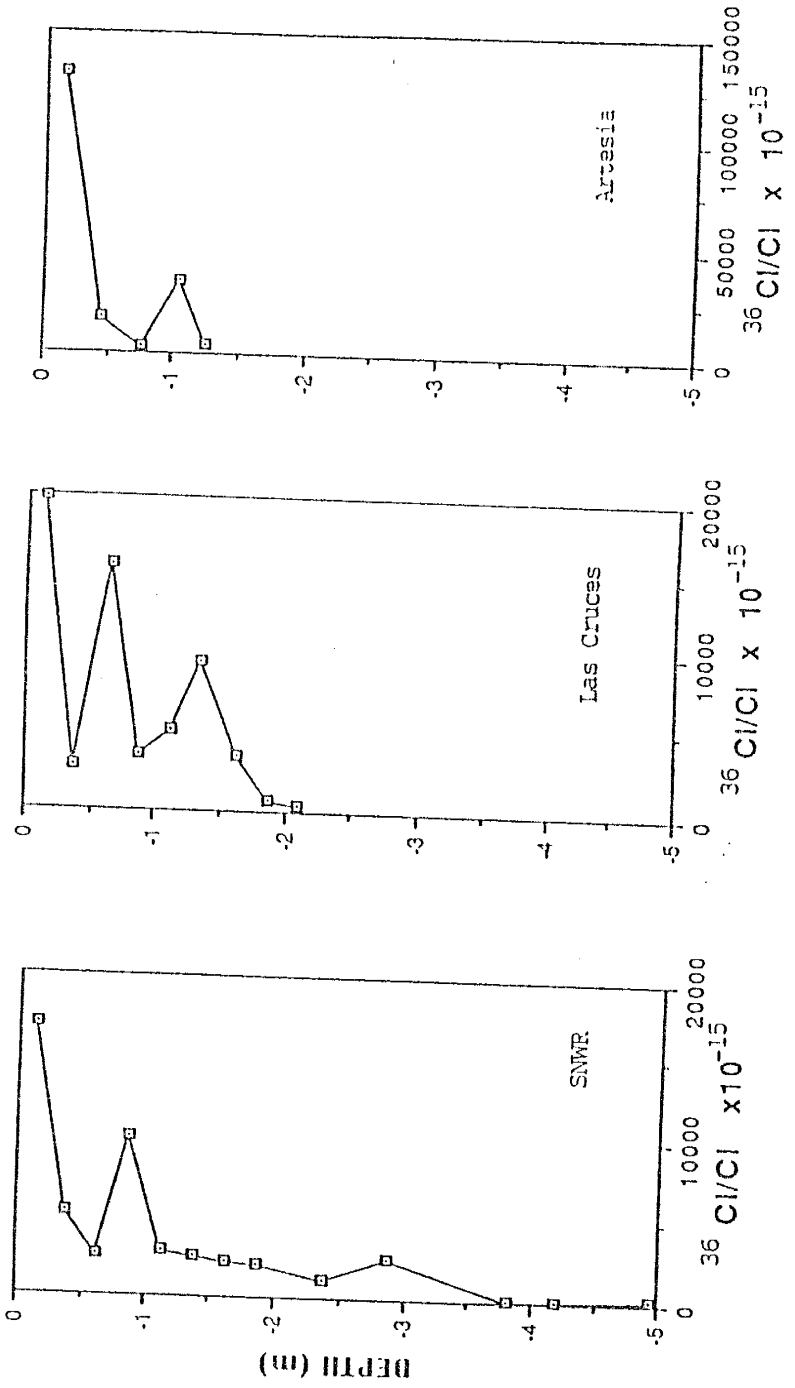

Figure 53 - Depth versus $^{36}Cl/Cl$ for three sites in New Mexico: near Artesia, near Las Cruces, and the SNWR research site

The chlorine-36 distribution at depth is also worth discussing. The $^{36}Cl/Cl$ ratios within the 1 to 3.5 meter depth interval are lower than the peak value, but are still representative of bomb-pulse levels. Chlorine-36 is assumed to have traveled to depth in the profile, below the zone of cycling in the upper meter, due to episodic, larger-scale infiltration events. When a large enough infiltration event (or series of events) occurs, soil water may move significantly below the zone dominated by evapotranspiration processes. Therefore solutes (such as ^{36}Cl) moving below the zone of cycling will continue to move to depth at the prevailing recharge rate. Diffusion of the isotope species may also occur due to a concentration gradient. This type of deep wetting due to larger scale infiltration events was observed in neutron logging by Stephens et al. (1985) in their work at the SNWR research site.

The compilation of data just presented leads to some interesting conclusions. During periods of high precipitation enough water may infiltrate into the soil to significantly increase the soil-moisture storage in the top meter of the profile, and undoubtedly transport solutes to depth. Subsequent redistribution of soil water causes the solutes to move both upward and downward in the profile. A maximum $^{36}Cl/Cl$ is maintained at the soil surface, and an elevated level is observed at about one meter depth. During the spring and early summer months the precipitation is small compared with the evapotranspiration demand. The soil-water profile develops into a quasi-steady state condition by mid-summer. The downward vapor-flux movement of soil water in the top meter of the profile causes water to be transported to depth

while conservative solutes are moving upward toward the dry surface layer in response to capillary pressure gradients. The entire process is controlled by highly complicated and episodic (diurnal and longer) forcing. The vapor-flux portion of soil-water movement cannot be ignored in any rigorous treatment of unsaturated flow under natural arid conditions.

Another factor related to the shape of the isotope profiles in the SSIP5 core is the influence of the water table. In figure 18 it is evident that the ^{18}O and ^{2}H profiles deviate relative to each other between the 2.70 meter depth and the bottom of the profile. The bottom of the SSIP5 profile was very near the water table elevation. This displacement implies that the ^{18}O-^{2}H relationship is changing due to factors different from those influencing the upper portion of the profile. Figure 19 depicts the δD versus $\delta^{18}O$ relationship. The data from above 2.7 meters in depth plot on a straight line with a slope of 3.3, indicative of evaporation through an unsaturated soil profile. The data for the deeper depths are shown as deviating from this trend toward the isotopic composition of the ground water beneath the site and the meteoric water line. This deviation is attributed to a mixing of isotopic compositions between the areal recharge water infiltrating through the profile from the land surface and the water table at depth. The water-table elevation at the site varies in response to stream-induced recharge along the reach of the Rio Salado. Therefore the isotopic composition of the ground water influences the composition within the unsaturated portion of the profile just above the existing water table. This water-table influence is also shown in figure 1 for the tritium data. Bomb-pulse levels of tritium occur below

a depth of 3.5 meters. Just above the 3.5 meter depth, tritium is at background levels. The elevated levels of tritium at depth are an artifact of the changing water table and capillary fringe elevations (Phillips et al., 1988).

The shapes of the SSIP5 profiles in figures 16 through 18 imply certain qualitative information about the distribution of liquid and vapor fluxes. The maximum enriched value of the isotopic species in the upper 12 cm of the profile is indicative of the evaporation front. The depth of this evaporation front corresponds to a plane of zero flux for water vapor movement at the time this profile was sampled. The flux of water above this depth is predominantly in the vapor phase, i.e., the liquid flux is essentially negligible. This portion of the profile is generally very dry (very low liquid moisture content). The unsaturated hydraulic conductivity of the porous media at these low water contents is very small, and hence negligible when there are long time intervals between precipitation events. The vapor flux in this upper region is upward in response to the lower atmospheric humidity.

Below the plane of zero vapor flux the vapor movement is downward. Several factors contribute to this downward vapor transport process. Two of these mechanisms are a concentration gradient of the isotopic species, and a temperature gradient, which in turn influences the vapor pressure gradient. Under quasi-steady state conditions with no appreciable temperature influence, an exponentially decaying isotopic profile would develop due to concentration driven diffusion (Allison et al., 1984). If, however, a strong temperature gradient exists, there should be a minimum in the profile. Figure 21 shows the depth

versus deuterium profiles for the SSIP5 and SSIP6 cores. The minimum in the SSIP5 and SSIP6 isotope profiles is indicative of a strong downward vapor flux within the zone of 0.12 to 1.25 meters depth. The lighter isotopes of water, ^{16}O and ^{1}H, are condensing out at the deeper portion of this zone, and therefore decreasing the ratios of $^{18}O/^{16}O$ and $^{2}H/H$. A minimum in the isotope profile is a result of a strong temperature gradient (and therefore vapor pressure gradient) which enhances the effect of the concentration-driven diffusive process mentioned previously.

A determination of the slope of the isotope data in figure 19 can indicate a relative evaporation effect. Performing a linear regression on these data yields the following relationship: $\delta D = 3.30(\delta^{18}O) - 54.5$; where $R^2 = 0.95$. A δD versus $\delta^{18}O$ slope of 5.0 would be representative of evaporation from a free water surface. A slope of 2.0 or less would be observed if there were a very thick laminar layer associated with the vapor-flux region of evaporation. The data for SSIP5 fall in between these two extremes, as expected. Several techniques (Barnes and Allison, 1983) can be used to quantify the evaporation rate from stable-isotope profile data.

The final technique discussed in chapter 4 on the numerical modeling methods involves the calculation of the recharge flux by the piston displacement/mixing (PD/M) model of Allison et al. (1984). In this model the recharge flux is assumed to be the result of episodic infiltration events which occur as piston displacement. Some mixing is assumed to occur after the major piston displacement events have taken place. Evaporative enrichment also takes

place in the upper portion of the profile between infiltration events. The isotopic composition of the soil water is therefore displaced relative to the meteoric water line (which characterizes the isotopic composition of precipitation).

Figure 54 shows the δD versus $\delta^{18}O$ data from the SSIP5 core plotted with the meteoric water line (MWL). A line has been drawn through the lightest portion of this data, parallel to the meteoric water line (a slope of 8), to define the deuterium displacement. The deuterium displacement is estimated at 22 $^{\circ}/_{oo}$. The corresponding recharge flux, from the graph in Allison et al. (1984), is estimated at 0.083 cm/yr. This estimate is almost one order of magnitude smaller than the estimates of recharge made at the site with other methods (and summarized in table 11).

The difference in the predicted recharge rates is attributed to a violation of the governing assumptions in the PD/M technique. The main assumption in the PD/M model is that the recharge flux occurs due to piston displacement of infiltrating soil water. If different mechanisms control the recharge flux, then this technique would be invalid. Because the recharge rate is considered to be on the order of 0.8 cm/yr, but the deuterium displacement is large enough to be indicative of a low recharge rate, then piston displacement is probably not the main mechanism affecting recharge. This conclusion implies that the net downward vapor-flux component of soil-water movement and/or the cycling phenomenon observed in the upper meter of the profile may be important enough to invalidate the PD/M model for calculating recharge at this site.

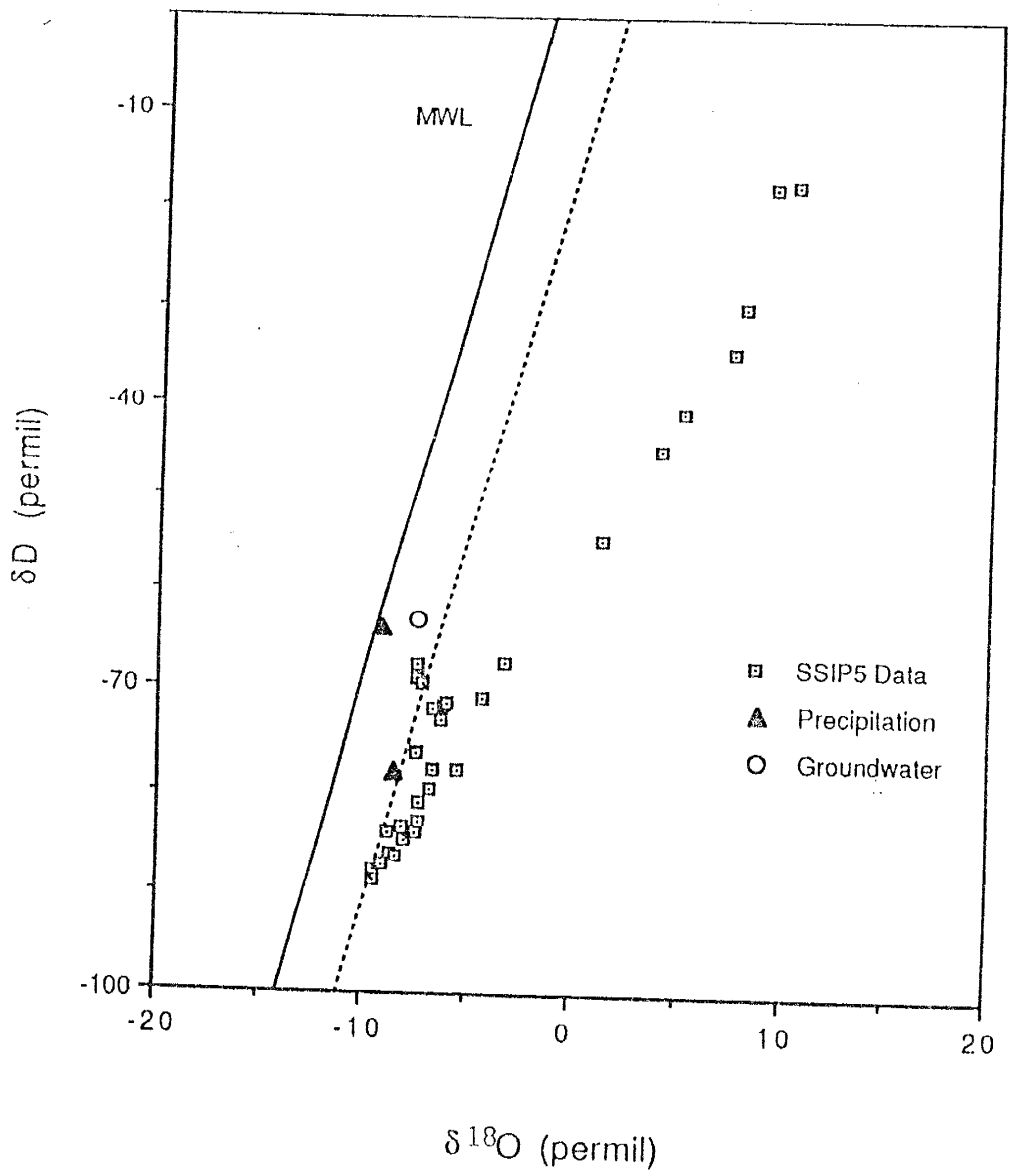

Figure 54 - δD versus δ^{18}O for the SSIP5 core, with the MWL, and a line drawn parallel to the MWL at the intersection of the SSIP5 data to determine the deuterium excess for the PD/M recharge model

Therefore the techniques summarized in table 11 for estimating the recharge rate in natural desert systems are considered most applicable for this research site.

7. PRINCIPAL FINDINGS, CONCLUSIONS, AND RECOMMENDATIONS

The stable-isotope data obtained in this study have been used to quantitatively model the vapor- and liquid-phase transport of soil moisture in natural desert soils. Qualitatively, the isotope information has also been used to draw conclusions about the relative importance of the downward vapor flux.

A model was presented which predicts the shape of the stable-isotope profiles of ^{2}H or ^{18}O, and the liquid- and vapor-flux portions of soil-water movement that lead to recharge under quasi-steady one-dimensional non-isothermal flow conditions. An equation describing the relative shape of the stable-isotope profile was used to fit parameters to a known isotope profile by means of a non-linear least-squares analysis. The parameters determined from this fitting procedure were then used in the model to quantify the liquid- and vapor-flux portions of soil-water movement. This non-isothermal recharge (NIR) model may be used under isothermal or non-isothermal conditions to estimate the recharge rate. The estimates of recharge rate with the NIR model compare quite favorably with other methods used at the research site under investigation (e.g., soil-physics approach, radioisotope tracer techniques, and the chloride mass balance method). It is interesting to note that the stable-isotope method of calculating recharge by Allison et al. (1984) does not yield results which are consistent with the other techniques used at the site.

Results of this study have shown that during the summer months there was a potential for solutes to travel upward with the liquid water, in the top meter of the profile, due to capillary pressure gradients resulting from evaporation at the land surface. However, water movement was also downward, due to a strong vapor flux in response to downward vapor-pressure gradients. This leads to a potential separation of volatile versus conservative solute tracer movement. This idea is consistent with the conclusions drawn by Phillips et al. (1988) in their work with radioisotopes at this same site. The magnitude of the vapor flux is such that it plays a major role in solute transport in the system. The vapor flux is of a sufficient size to influence the total recharge flux. Comparing summer and winter NIR model results suggests that there is a net annual downward vapor flux of soil water at the site under study. Therefore, it may be advantageous to account for the vapor-phase flux when determining recharge rates in water resources planning or hazardous waste siting analyses. The vapor-flux portion of soil-water movement is most important in the summer months, but during other seasons of the year liquid-phase infiltration, evapotranspiration, and redistribution are probably the dominant processes.

The seasonal behavior of the isotopic and soil-water distributions was also investigated. It appears that a significant amount of water may infiltrate into the profile during the 'rainy' season, from late summer through early autumn. Subsequently, soil-water redistribution occurs in response to upward capillary-pressure gradients induced by evapotranspirative demands. The net result of this infiltration/evapotranspiration/redistribution process is a 'cycling' phenomenon,

whereby conservative solutes are transported upward and downward in the upper meter of the profile in a cyclic fashion. This phenomenon also helps explain the observed radioisotope distributions presented by Phillips et al. (1988).

Qualitatively, the stable-isotope profiles support the conclusion that the vapor flux is appreciable (but the liquid flux dominates) in the recharge process. The presence of the minimum in the isotope profiles from SSIP5 is the basis for making this statement. There is a strong diffusive transport of lighter isotopes downward below the evaporation front, where the lighter isotopes are condensed out to form the minimum in the profile around one meter in depth (figure 16).

In addition to the vapor-flux estimates, a new laboratory distillation technique has been developed during the course of this study. This new vacuum distillation technique offers a reliable alternative to other extraction techniques for isotopic studies of soil water.

The work presented here should prove very useful to scientists, engineers, and water resource planners. The role of vapor-phase water movement in the recharge process appears to be important. It is important from both a water resources planning perspective, and a solute transport perspective. For the water resource planner, the amount of recharge calculated for a given area may be larger when taking into account the vapor-flux component. The model is well suited to estimating the recharge rate, under isothermal and non-isothermal conditions. Also, the transport of volatile contaminants in the vadose zone may be greatly enhanced due to vapor-phase flow, whereas non-volatile constituents

only travel within the liquid phase at a potentially slower rate. This could be very important in hazardous waste siting.

Additional work on this topic might include the following: a more rigorous treatment of the numerical modeling approach, from both a theoretical and practical viewpoint; a transient numerical analysis of the isotope profiles, including evaporation, and maybe even transpiration, effects in arid environments; a transient analysis of the diurnal and seasonal temperature effects on the isotope behavior; further study into the effects of tortuosity on the liquid and vapor-flux components of soil-water movement; a complete heat and moisture flow simulation utilizing all the hydraulic, thermal, geochemical, and isotopic data available at the site; application of the NIR model to other sites to validate its range of use; a more rigorous treatment of the effect of the diurnal temperature and/or barometric pressure variations on soil-water movement, especially as related to the NIR model; an evaluation of the relative importance of Knudsen transport mechanisms as related to the NIR model; a multi-dimensional analysis to evaluate the effects of spatial variability and the potential for preferential flow paths; and an extension of the model to deep vadose zone environments to predict the long-term recharge history for paleoclimatic purposes.

8. SUMMARY

A model is presented which can predict the shape of the stable-isotope profiles in the vadose zone, and also quantify the liquid- and vapor-flux portions of soil-water movement that leads to recharge. Through a non-linear least-squares approach, the model is matched to an observed stable-isotope profile (^{2}H or ^{18}O) by optimizing the values of specified variables. The fitted parameters are then used to solve numerically for the liquid and vapor fluxes as a function of depth. This technique of modeling the isotope species transport is much more robust than conventional heat and moisture flow modeling techniques. This conclusion stems from the fact that the effective diffusivities vary little with water content in the former analysis as compared with the latter. Also, a technique such as this, which estimates flux terms directly, should be very useful in conjunction with other modeling efforts to calibrate unsaturated flow codes.

A comparison of summer and winter modeling results suggests that there is a net annual downward vapor flux of soil water within the top meter of the profile. The vapor flux is sufficient to strongly influence the solute transport characteristics of the system. The liquid-flux component of recharge is, however, the dominant transport mechanism. This result is consistent with conclusions

made by Phillips et al. (1988) in explaining the differences in bomb-pulse ^{36}Cl and ^{3}H distributions.

A qualitative analysis of the isotope profiles also confirms the conclusion that the vapor flux is significant in influencing soil-water movement. The development of an isotope minimum at depth in the profile is indicative of a strong downward vapor flux. This minimum in the profile is a result of the condensation of the lighter isotope species.

A seasonal analysis of the changes in isotopic and soil-moisture distributions suggests that a 'cycling' phenomenon is occurring. It appears that a significant amount of water may infiltrate into the profile during the 'rainy' season, from late summer through early autumn. Subsequently, soil-water redistribution occurs in response to upward capillary-pressure gradients induced by evapotranspirative demands. The net result of this infiltration/evapotranspiration/redistribution process is a 'cycling' phenomenon, whereby conservative solutes are transported upward and downward in the upper meter of the profile in a cyclic fashion. This phenomenon also helps explain the observed radioisotope distributions presented by Phillips et al. (1988).

A new vacuum distillation technique was developed during this project. A statistical analysis has shown that the reproducibility of this distillation method is satisfactory for isotopic studies of soil water.

APPENDIX A

Laboratory Procedures

A.1 Manometer Calibration

In the course of preparing gases for analysis on a mass spectrometer, the amount of gas needs to be measured. Gases such as CO_2 and SO_2 are prepared via extraction techniques on a vacuum line system (figure A1). The vacuum line setup generally contains a mercury manometer for measuring the number of moles of a condensible gas. In order to determine the number of moles of gas versus the change in mercury height, one must calibrate the manometer.

Before beginning the calibration process, a sample bottle (figure A2) with a known volume must be obtained. The volume of an existing sample bottle can be determined using mercury. Remove the stopcock from the sample bottle and clean it. Grease the stopcock sparingly, because the opening to the bottle neck must be clear. Weigh the bottle and stopcock assembly. Pour mercury into the bottle till it is just full, with a rounded portion of mercury protruding just above the stopcock barrel. Close the stopcock, and pour out any excess mercury from the stem of the bottle. Make sure that the bottle is completely full of mercury. Weigh the bottle again. The difference between the two weighings represents the mass of mercury in the bottle. Divide this number by the unit weight of mercury, 13.55 g/cc. The result is the volume of the sample bottle with the stopcock closed.

The manometer calibration technique involves several iterative steps, and some calculations using the ideal gas law. The ideal gas law is represented

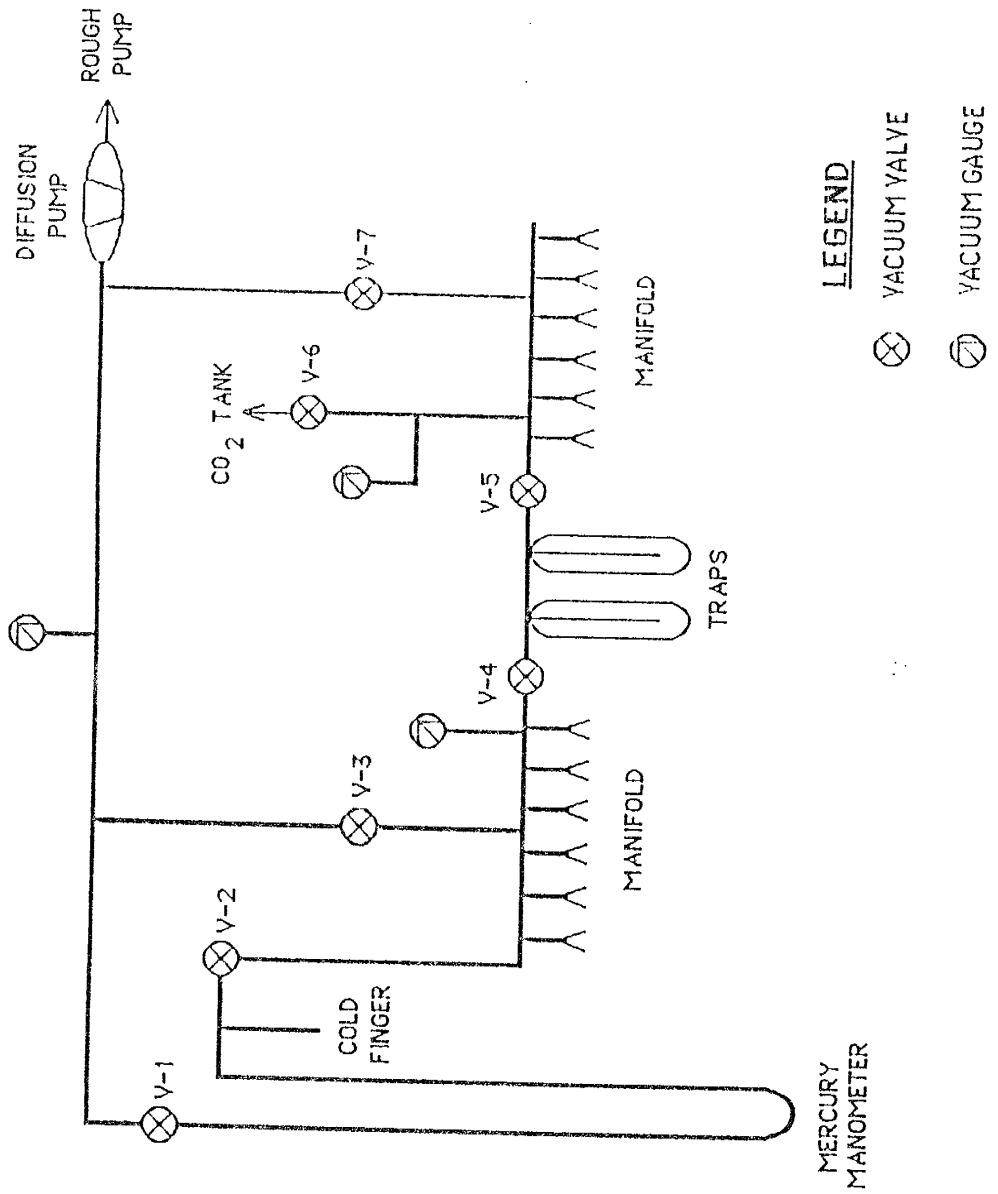

Figure A1 - Schematic of a vacuum line system

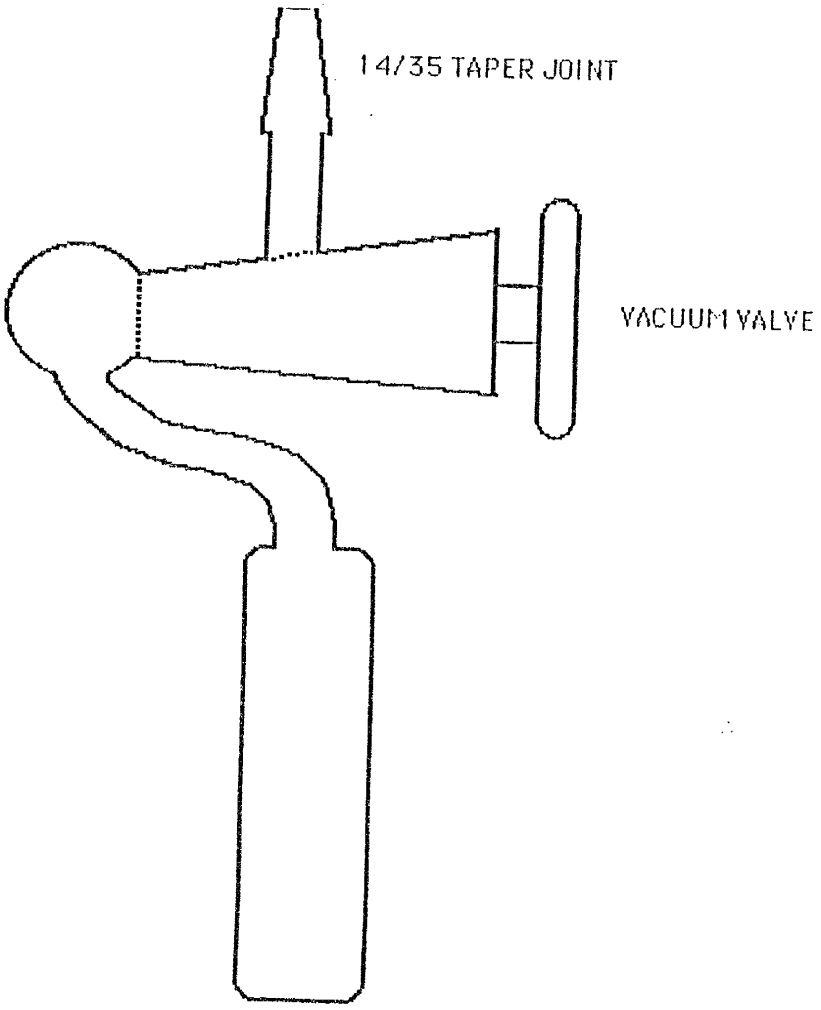

Figure A2 - Schematic of a gas sample bottle

mathematically by the following equation:

$$PV = nRT \qquad (A.1)$$

where:

P = pressure, in atmospheres
V = volume, in liters
n = moles of gas
R = ideal gas constant (0.08206 liter atm/mole °K)
T = temperature, in degrees Kelvin

Van der Waal's equation for real gases could be used as an alternative to the ideal gas law, but the resultant difference in calculated moles of gas is negligible. Therefore, for calibration of the manometer with a gas such as CO_2, the ideal gas law is adequate.

The iterative procedure mentioned above involves the repeated expansion and condensation of various amounts of CO_2 on the vacuum line. A source of CO_2 is required. Attaching a cylinder of compressed tank CO_2 to the vacuum line is probably the easiest method of generating the gas. The gas should be put through a water trap before utilizing it in the calibration procedure (a 'pea soup' mixture of 2-butoxyethanol and solid CO_2 (dry ice chips) in a dewar). Referring to figure A.1, it is recommended that the CO_2 be introduced into the manifold on the right side of the vacuum line. The water trap mixture should be placed on one of the in-line traps between the two manifolds. The freezing and thawing procedures can then be carried out on the left side of the line in conjunction with the mercury manometer.

Before beginning the procedure, a few details must be attended to. Have sample bottles or blanks attached to all joints of the manifolds. One of these

sample bottles on the left side manifold should be the bottle with the known volume. Make sure that the line is pumped down to a good vacuum, utilizing both the rough pump and the diffusion pump. Included in the pump down phase is the evacuation of the known volume sample bottle (hereafter simply referred to as the sample bottle, inasmuch as it is the only bottle to be used in this procedure). All other sample bottles should have closed stopcocks. In the course of outlining the procedures, the valve numbers in figure A1 will be referred to. The line connecting valve V-6 to the CO_2 tank should be evacuated as well as possible. Close valves V-4 and V-7. Put the water trap dewar on one of the traps. Slowly turn up the pressure regulator on the CO_2 tank to admit a slight positive pressure of gas into the right side manifold. The iterative calibration procedure is now ready to begin.

The first step of the calibration method involves the introduction of CO_2 gas into the sample bottle at a known pressure. To do this, is to open valve V-2, close V-3, and open the sample bottle stopcock. Slowly open V-4 until a slight change in mercury level is present on the manometer. Close V-4 and record the change in mercury level. This height difference, in centimeters of mercury, can be divided by 76 cm of Hg/atm to obtain a pressure estimate, P. This calculated pressure represents the pressure of CO_2 gas throughout the manifold, manometer, and sample bottle. Close the sample bottle stopcock, and open V-3 to pump away all the residual CO_2 in the left side manifold and manometer.

The second step of this calibration procedure involves the transfer of the CO_2 in the sample bottle to the manometer. After the manifold and manometer have been completed pumped out, close valve V-3. A dewar of liquid nitrogen is then

placed around the cold finger in the manometer section of the line. The stopcock on the sample bottle is then opened and all the CO_2 transferred to the cold finger under a diffusion gradient. When all the CO_2 has been frozen over, V-3 is opened momentarily to pump away any residual non-condensible gases that might be present. After a short wait valve V-2 is closed and the liquid nitrogen dewar is removed. Heat the cold finger briefly with a heat gun to expand the CO_2 sample within the manometer. Record the difference in mercury height. Record the room temperature, also. Open V-2, V-3, and the sample bottle to pump away all residuals before the next run.

The calculation of moles of gas using equation B.1 is relatively simple. The sample bottle volume, V, was determined by weighing with mercury, and remains a constant throughout these procedures. The pressure, P, in the bottle was calculated from the difference in mercury heights upon initial filling of the manifold with CO_2. The temperature is also known. Therefore, equation B.1 can be solved readily for n, the number of moles of CO_2 that were in the sample bottle. This is also the number of moles of CO_2 that was transferred into the manometer in the second step of the procedure. Therefore, the difference in mercury height obtained in step two (delHg), paired with the calculated number of moles of gas (n), is one set of data for the calibration curve of the manometer (delHg versus n).

The iterative nature of this calibration process is necessary to obtain enough points on a curve to define the calibration curve. Steps one and two should be repeated for differing amounts of CO_2 until adequate definition of the curve is obtained. The range of values should start from several micromoles of gas up to a

high relative to the largest samples used in analyses on a mass spectrometer (probably several hundred micromoles). A plot of delHg versus n can then be developed.

A.2 CO_2/H_2O Equilibration Technique

An equilibration procedure between CO_2 gas and water is necessary to obtain $^{18}O/^{16}O$ ratio values of the water. Water samples generally cannot be injected directly into a mass spectrometer as CO_2 can to determine $^{18}O/^{16}O$ ratios. Therefore CO_2 gas is equilibrated with a water sample, and the resultant CO_2 composition analyzed to determine the original $^{18}O/^{16}O$ ratio of the water.

Certain equipment is necessary to carry out the equilibration procedure. A high vacuum line, such as a carbonate-CO_2 extraction vacuum line, is required. Figure A1 shows a schematic of the line used at the NMTech Stable Isotope Laboratory. The line has been modified to include an inlet valve to introduce tank CO_2 gas into the vacuum line. Special sample bottles must be constructed for the equilibration process.

The design of the equilibration vessels is modified after Roether (1970). Figure A3 shows a schematic of the reaction vessel design. The following procedures will outline a slightly different technique than Roether's for transferring the CO_2 gas to and from the vessels, because capillaries have not yet been installed in the NMTech bottles. If the capillary method were employed it would save considerable time in transferring the CO_2 gas. However, the capillary transfer technique is not without fault. The primary negative factor is that some water vapor is lost from the reaction vessels whenever pumping occurs on the bottle. With a slight loss of water vapor there is a potential for fractionation. Steps must be taken to ensure that this fractionation potential is minimized. Brenninkmeijer and

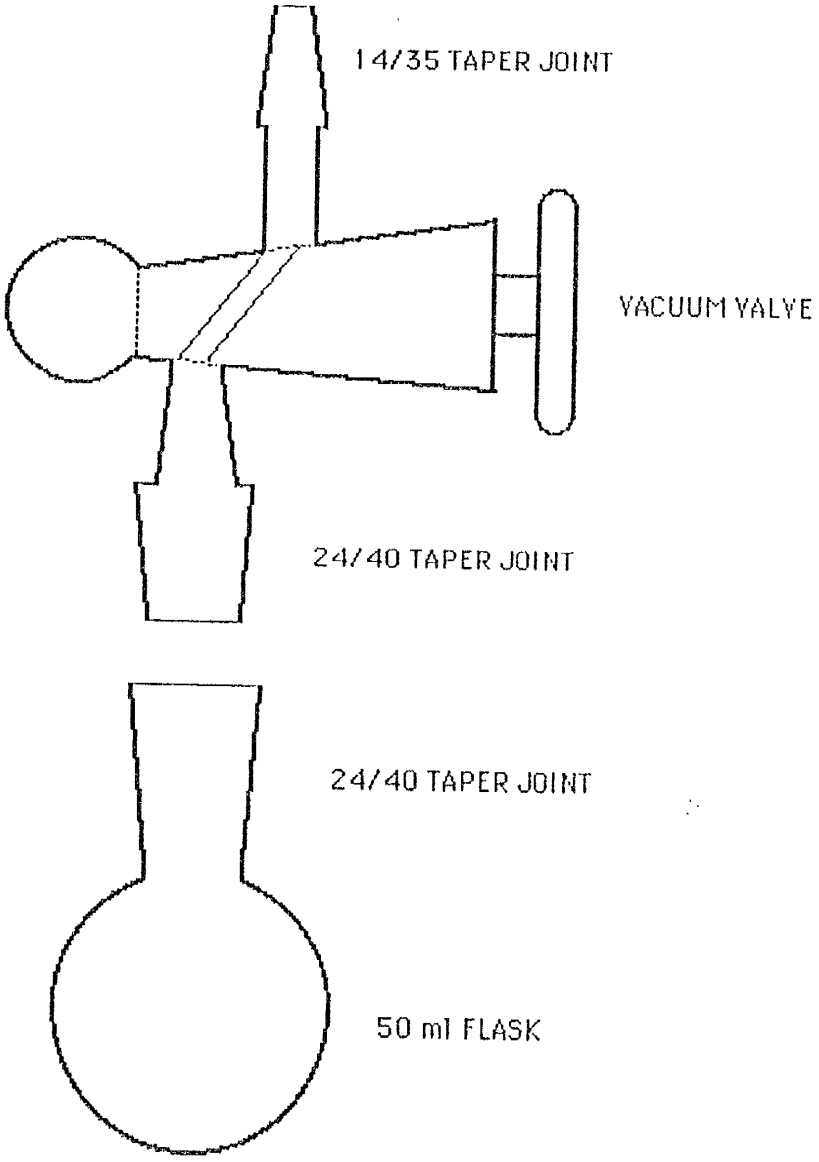

Figure A3 - Schematic of the CO_2/H_2O reaction vessel

Morrison (1987) have addressed this issue, so it will not be discussed here.

A slight variation in reaction vessel design may also be employed. A single piece vessel with a removeable vertical stopcock is sold by ACE Glass (catalog #7408-10). The advantage to this design over the former is that there is no greased joint within the flask portion of the vessel. The greased joint offers a potential leakage point in the bottles.

The first step in preparing for the equilibration of CO_2 and H_2O is measuring out the quantity of CO_2 gas to be used in each sample. Referring to figure A1, the sample bottles should be attached to the left side manifold of the vacuum line. The reaction vessels, minus their respective flasks, can be attached to the right side manifold. A water trap should be placed around one of the center traps. This water trap is made by mixing solid CO_2 (dry ice chips) with 2-butoxyethanol in a dewar until a 'pea soup' consistency is obtained. The vacuum line and sample bottles are pumped down with the diffusion pump. The sample bottles should all be left open. Referring again to figure A1, valves V-3, V-4, V-6, and V-7 are closed. The CO_2 gas is pressurized slightly into the line behind valve V-6. Valve V-6 is then opened to allow entry of CO_2 into the right side of the line. Make sure valve V-2 is open. Slowly open valve V-4 to allow CO_2 into the left side manifold. For the specific line used at NMTech, enough gas is allowed in such that the U-tube mercury manometer deflects approximately 7 to 8 cm. This allows approximately 150 to 175 micromoles of CO_2 to enter each of the sample bottles. Close V-4 and wait a minute or so to allow the CO_2 to mix. All sample bottles are then closed and the residual gas in the upper portion of the manometer is pumped

away. A sample of this initial CO_2 should be run on the mass spectrometer each time the sample bottles are filled. There is a potential for fractionation of the CO_2 gas as it is being bled into the left side manifold. If, however, this blank yields a constant $^{18}O/^{16}O$ ratio over multiple trials, then the initial CO_2 ratios should be checked only periodically.

The quantity of CO_2 in each of the sample bottles must then be measured. Valves V-3 and V-4 are closed, and V-2 is opened. A sample bottle stopcock is opened and a dewar of liquid nitrogen is placed around the cold finger in the manometer section of the line. Sufficient time is allowed to freeze the CO_2 into the cold finger. V-3 is then opened momentarily to pump away any residual non-condensible gases. V-2 is closed and the liquid nitrogen dewar removed. The cold finger is heated briefly to expand the CO_2 within the manometer. The deflection of mercury is noted, and referred to on a calibration curve to obtain the number of moles of CO_2 present. V-3 is closed and then V-2 opened. The liquid nitrogen dewar is placed on the sample bottle to freeze the CO_2 back. The sample bottle stopcock is closed when all the gas is frozen over. This process of measuring gas yields is repeated for each sample bottle.

The second step involves preparation of the water sample. The quantity of water used in this type of equilibration is preferably around 10 milliliters. Many times however, yields of distilled water from soil samples are much less, and a sample size of 1 ml is used, which is sufficient. Referring to figure A3, the reaction vessel flasks are 50 ml capacity. The water sample to be equilibrated is placed in the bottom of the flask using a pipette. An accurate measure of the quantity of

water used is important. The flask is then placed on the corresponding reaction vessel.

The third step of the procedure is a combination of evacuating the atmosphere from the reaction vessel and adding the known amount of CO_2 to the flask. A water trap is placed on one of the reaction vessels to freeze the water in the flask. When sufficient time has elapsed for complete freezing, the stopcock is opened and the atmosphere is pumped away. When the pressure has dropped sufficiently, the stopcock is closed and the water trap is replaced with a liquid nitrogen trap. Valves V-2, V-3, V-6, and V-7 are closed. Valves V-4 and V-5 are opened. The water trap dewar remains on one of the center traps. The stopcock is opened on the reaction vessel and the corresponding sample bottle of CO_2 gas. The liquid nitrogen dewar on the reaction vessel should freeze over all the CO_2 to the flask. When this is accomplished open V-7 momentarily to pump away any residual non-condensible gas that might be present. Close the stopcock on the reaction vessel. Repeat this procedure for all the water samples. The samples are now ready for equilibration.

The fourth step is the actual equilibration process. The reaction vessels are removed from the vacuum line and placed securely in a constant temperature water shaker bath. Make certain that the bath has been preheated to just above room temperature, around 20 to 25°C. Record the temperature before and after the equilibration. The speed of the shaker should be set at approximately 5.0 cycles/sec (300 cycles/min). The resonance frequency of water (3.7 cycles/sec) must be obtained in order for the reaction to take place rapidly (Roether 1970). The time

of equilibration should be approximately 2 hours.

The last step of the equilibration procedure is transferring the CO_2 from the reaction vessels back into the sample bottles. This step is somewhat time consuming if not using the capillaries in the reaction vessels. The reaction vessels are placed on the right side manifold again. The sample bottles and all the lines are pumped out. A liquid nitrogen dewar is placed on one of the reaction vessels to freeze out the CO_2 and water. Valves V-5 and V-7 are closed. The reaction vessel stopcock is opened and the pressure gauge is read. A qualitative determination of the amount of non-condensible gas in the sample bottle, if present, is made. If the pressure rise is deemed too great, it is indicative of a leak in the reaction vessel during shaking. If there was no appreciable contamination, then proceed to open V-7 to pump away the residuals. Close the stopcock on the reaction vessel. Warm up the sample with the heat gun to melt the water and expand the CO_2. Place a water trap dewar on the reaction vessel until the water is frozen. Make sure a water trap is still on one of the center traps. Open valves V-4, V-5, and the stopcock of the sample bottle that is receiving the equilibrated CO_2. Close valves V-2, V-3, and V-7. Place a liquid nitrogen dewar on the sample bottle. Open the stopcock of the reaction vessel with the water trap dewar on it. The CO_2 gas in the reaction vessel shoction vessels are removed from the vacuum line and placed securely in a constant temperature water shaker bath. Make certain that the bath has been preheated to just above room temperature, around 20 to 25°C. Record the temperature before and after the equilibration. The speed of the shaker should be set at approximately 5.0 cycles/sec (300 cycles/min). The resonance frequency

of water (3.7 cycles/sec) must be obtained in order for the reaction to take place rapidly (Roether 1970). The time of equilibration should be approximately 2 hours.

The last step of the equilibration procedure is transferring the CO_2 from the reaction vessels back into the sample bottles. This step is somewhat time consuming if not using the capillaries in the reaction vessels. The reaction vessels are placed on the right side manifold again. The sample bottles and all the lines are pumped out. A liquid nitrogen dewar is placed on one of the reaction vessels to freeze out the CO_2 and water. Valves V-5 and V-7 are closed. The reaction vessel stopcock is opened and the pressure gauge is read. A qualitative determination of the amount of non-condensible gas in the sample bottle, if present, is made. If the pressure rise is deemed too great, it is indicative of a leak in the reaction vessel during shaking. If there was no appreciable contamination, then proceed to open V-7 to pump away the residuals. Close the stopcock on the reaction vessel. Warm up the sample with the heat gun to melt the water and expand the CO_2. Place a water trap dewar on the reaction vessel until the water is frozen. Make sure a water trap is still on one of the center traps. Open valves V-4, V-5, and the stopcock of the sample bottle that is receiving the equilibrated CO_2. Close valves V-2, V-3, and V-7. Place a liquid nitrogen dewar on the sample bottle. Open the stopcock of the reaction vessel with the water trap dewar on it. The CO_2 gas in the reaction vessel should now freeze over to the sample bottle. When all the gas is frozen over, momentarily open V-3 and V-7 to pump away any residuals. Close the stopcocks on both the sample bottle and the reaction vessel. Repeat the procedure for all the samples. The final yields of CO_2 in each of the sample bottles could be

measured in the mercury manometer if desired. The sample bottles are now ready for analysis on a mass spectrometer.

The $^{18}O/^{16}O$ ratio of the original water for each sample must be calculated. The following equation is used:

$$\frac{X}{Y} = \frac{(\delta^{18}O[CO_2] - \delta^{18}O[CO_2])}{(\delta^{18}O[H_2O] - \delta^{18}O[H_2O])} \qquad (A.2)$$

where:

X = the number of moles of H_2O (5.556×10^4 micromoles/ml of H_2O)

Y = the number of moles of CO_2 gas

$\delta^{18}O[CO_2]$ = final $^{18}O/^{16}O$ permil value of CO_2

$\delta^{18}O[CO_2]$ = initial $^{18}O/^{16}O$ permil value of CO_2

$\delta^{18}O[H_2O]$ = initial $^{18}O/^{16}O$ permil value of H_2O

$\delta^{18}O[H_2O]$ = final $^{18}O/^{16}O$ permil value of H_2O

Also:

$$\alpha = \delta^{18}O[CO_2] / \delta^{18}O[H_2O] \qquad (A.3)$$

and,

$$1000\ln\alpha = -0.021(10^6/T^2) + 17.994(10^3/T) - 19.97 \qquad (A.4)$$

where T is the temperature of equilibration in degrees Kelvin.

Substituting and rearranging equations yields the following result for the initial $^{18}O/^{16}O$ permil value of the water:

$$\delta^{18}O[H_2O] = (Y/X)(\delta^{18}O[CO_2] - \delta^{18}O[CO_2]) + (\delta^{18}O[CO_2]/\alpha) \qquad (A.5)$$

A.3 Hydrogen Reduction Technique

These directions are specific to equipment used by New Mexico Tech's Geoscience Department, Stable Isotope Laboratory. The reaction vessels were constructed according to specifications by Coleman et al. (1982). The aluminum block heater was constructed and calibrated at NMTech. Therefore, rheostat heat settings given in these directions are specific to that unit. These procedures could be generalized without much difficulty.

Make sure reaction vessels have been cleaned properly. Hayes and Baker (Letter Report, February 1, 1986, Indiana University) recommend cleaning with "30% nitric acid, washed with soap and water, rinsed, and annealed for several hours at 400°C." The last step, annealing, can probably be modified to drying in an oven at 110°C for several hours. The annealing temperature of Pyrex glass is 565°C, therefore an oven temperature of 400°C should only benefit the drying of water from the glass.

No pre-treatment of the zinc is recommended unless there has been some trouble with reproducing blank values. That procedure, if necessary, is outlined in a memo by Hayes and Johnson (Letter Report, November 20, 1987, Indiana University). The zinc should be stored under vacuum in a vacuum dessicator to minimize any oxidation potential.

Weigh out approximately 50mg (0.05g) of zinc for every microliter of water sample to be analyzed. Hayes and Johnson recommend approximately 20mg (0.02g) per microliter of water, which has proven to be an insufficient quantity for complete reduction. Generally, 1 to 10 microliters of water is used in the reduction. Remove

the stopcock from the reaction vessel and place the zinc in the bottom of the vessel. Replace the stopcock and attach the vessel to a special adaptor on a vacuum line (see figure A4). The adaptor has a special septum injection port (Ace Glass) to facilitate the syringe injection of the water sample.

With the adaptor and reaction vessel stopcocks open, pump out the reaction vessel, taking care not to pump away any of the zinc shavings. Gently heat the tube of the reaction vessel with a heat gun to drive off any adventitious water. Allow the reaction vessel to cool. Close the valve on the adaptor. Place a liquid nitrogen dewar around the reaction vessel so that the zinc is just covered. With a syringe inject the water sample through the septum into the reaction vessel. Observe the transfer of water into the vessel. Under vacuum pressure the water will freeze upon entry into the vessel. If the water freezes at the syringe needle tip prior to injection of all the water, the syringe may become damaged if pressure is continued. Therefore, if freezing occurs make several injections.

After injection, use a heat gun to drive any water adhering to the walls of the reaction vessel down to the zinc. Allow approximately ten minutes to pass after the heat treatment to assure complete transfer of water to the zinc, topping off the liquid nitrogen level if necessary.

Open the adaptor stopcock and observe any abnormally high pressure rise that might occur. If the pressure rise is considered too high the septum may need replacing before the next sample is processed. Approximately 15 to 20 samples may typically be injected through one septum. Pump any residuals in the reaction vessel. Close the reaction vessel and adaptor stopcocks. Remove the liquid nitrogen dewar.

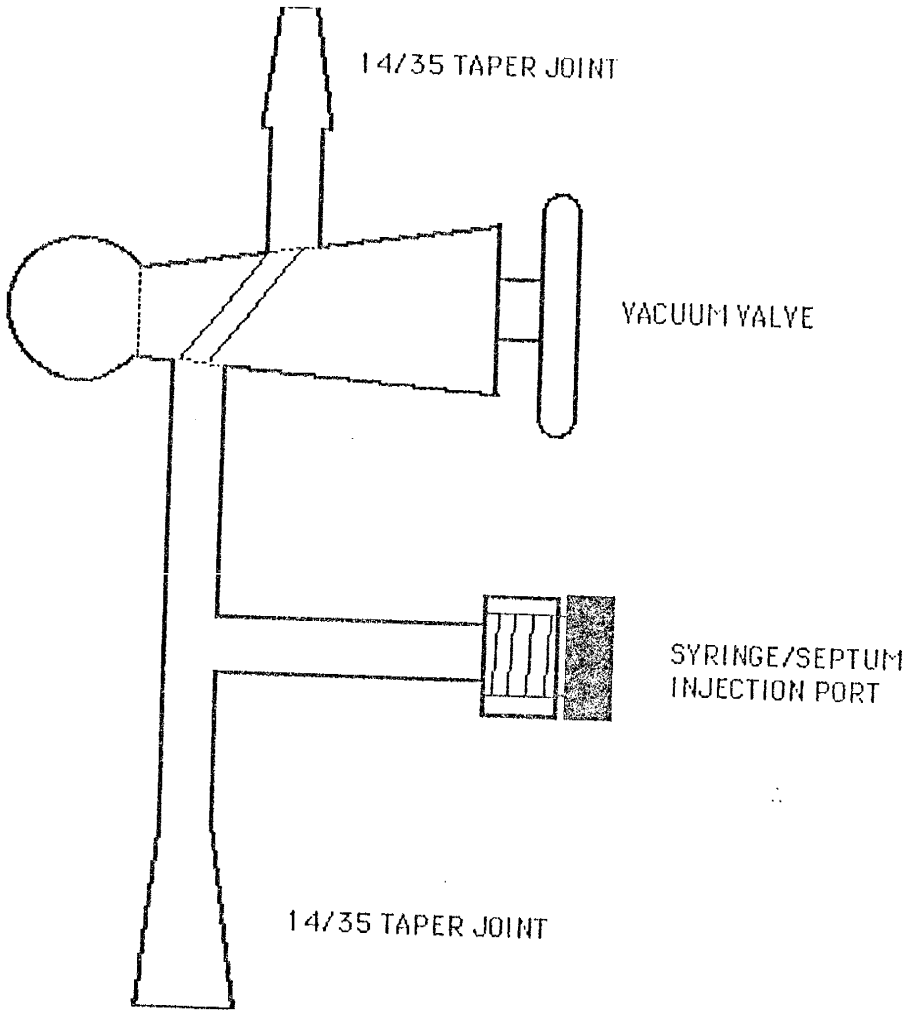

Figure A4 - Schematic of the H_2 reduction reaction vessel

Remove the reaction vessel from the adaptor and allow to warm to air temperature for several minutes. Wipe off any condensation on the outside of the reaction vessel.

Place the reaction vessel in the aluminum block heater. Heat the sample to 500°C (a rheostat setting of 110 for the NMTech heater). Allow the reaction to proceed for 30 minutes at the desired temperature. The sample is now ready for analysis.

APPENDIX B

Field and Laboratory Data

Field and Laboratory Data

Sevilleta Stable Isotope Profile 3

Depth (m)	δD (permil)	δ^{18}O (permil)	Water Content (cc/cc)	Temperature (°C)
-0.075	-50.0	-4.6	0.078	22.2
-0.225	-68.0	-2.7	0.087	19.6
-0.375	-60.1	-4.3	0.075	18.7
-0.525	-61.0	-7.0	0.059	18.4
-0.675	-67.7		0.043	18.2
-0.825	-66.0	-3.3	0.043	18.9
-1.200	-62.7	-7.4	0.034	19.4
-1.525	-72.8	-7.0	0.039	18.7
-1.840		1.5	0.035	18.1
-2.225	-56.6	-6.0	0.040	17.7
-2.465		-2.7	0.053	19.1
-2.735	-70.0	5.3	0.034	17.9
-2.970	-62.4	-5.6	0.053	17.9
-3.275	-65.0	2.0	0.039	18.5
-3.640	-60.0	-6.7	0.036	17.9
-3.970	-64.7	-8.0	0.336	18.8
-4.220	-63.1	-6.8	0.137	18.3
-4.375	-66.0	-5.5	0.055	19.0

Field and Laboratory Data

Sevilleta Stable Isotope Profile 4

Depth (m)	δD (permil)	δ^{18}O (permil)	Water Content (cc/cc)	Temperature (°C)
-0.013	-49.6	1.6	0.011	28.7
-0.043	-40.0	6.5	0.013	26.9
-0.205	-57.0	0.2	0.031	26.1
-0.285	-54.4	0.2	0.039	27.4
-0.380	-45.2	2.5	0.037	26.6
-0.480	-76.8	-6.0	0.039	26.8
-0.585	-74.4	-7.9	0.034	25.7
-0.695	-80.6	-8.7	0.037	25.5
-0.805	-63.5	-4.4	0.041	24.2
-1.200	-74.6	-7.9	0.030	22.4
-1.390	-40.6	-1.7	0.038	21.7
-1.585	-80.9	-7.1	0.033	22.3
-1.800	-73.6	-4.7	0.033	20.4
-2.085	-61.6	-3.6	0.041	22.9
-2.365	-76.3	-4.9	0.098	20.2
-2.955	-59.9	-2.9	0.054	22.3
-3.495	-70.8	-7.0	0.038	22.7
-3.980	-73.6	-7.1	0.254	20.1
-4.185	-64.2	-6.1	0.171	18.8
-4.405	-64.5	-5.8	0.071	22.8
-4.655	-59.8	-5.7	0.067	20.9
-4.945	-62.5	-6.6	0.077	20.5

Field and Laboratory Data

Sevilleta Stable Isotope Profile 5

Depth (m)	δD (permil)	$\delta^{18}O$ (permil)	Water Content (cc/cc)	Temperature (°C)
-0.013	-29.7	7.9	0.016	
-0.038	-17.2	10.3	0.026	
-0.070	-17.4	9.2	0.027	
-0.115	-34.2	7.4	0.024	
-0.170	-40.5	5.0	0.024	28.4
-0.225	-44.5	4.0	0.027	28.4
-0.300	-54.2	1.3	0.032	30.0
-0.400	-67.2	-3.4	0.029	30.1
-0.500	-70.6	-4.4	0.032	30.4
-0.590	-77.7	-5.6	0.035	30.5
-0.680	-77.7	-6.7	0.032	30.0
-0.775	-82.8	-7.4	0.044	30.8
-0.860	-84.6	-8.1	0.032	29.9
-0.950	-86.0	-8.7	0.033	30.0
-1.050	-88.6	-9.5	0.032	
-1.140	-87.0	-9.1	0.033	30.0
-1.320	-87.5	-9.5	0.038	28.5
-1.520	-83.9	-8.8	0.036	29.1
-1.705	-83.3	-8.2	0.034	27.9
-1.900	-86.2	-8.4	0.037	23.2
-2.100	-83.8	-7.7	0.041	
-2.300	-83.8	-7.6	0.053	28.0
-2.500	-79.5	-6.9	0.037	29.0
-2.700	-81.0	-7.4	0.034	25.8
-2.880	-76.2	-7.5	0.054	25.5
-3.125	-71.8	-6.8	0.041	
-3.290	-71.2	-6.1	0.042	25.6
-3.505	-71.6	-6.2	0.039	24.9
-3.740	-72.8	-6.4	0.038	24.3
-4.240	-69.3	-7.3	0.057	23.9
-4.450	-68.7	-7.5	0.058	23.6
-4.535	-67.5	-7.6	0.058	23.4

Field and Laboratory Data

Sevilleta Stable Isotope Profile 6

Depth (m)	δD (permil)	$\delta^{18}O$ (permil)	Water Content (cc/cc)	Temperature (°C)
-0.020	-19.1		0.017	
-0.060	-10.9		0.048	
-0.105	-29.0		0.025	
-0.165	-37.3		0.026	
-0.230	-44.2		0.030	
-0.300	-55.3		0.030	
-0.380	-61.7		0.030	
-0.460	-70.3		0.030	
-0.540	-65.5		0.030	
-0.620	-80.5		0.034	
-0.840	-76.3		0.030	
-1.040	-84.5		0.044	
-1.220	-88.4		0.052	
-1.500	-81.0		0.034	
-2.020	-79.9		0.034	
-2.310	-81.3		0.041	
-2.530	-73.8		0.040	
-2.800	-67.0		0.044	
-3.070	-62.4		0.040	
-3.330	-67.9		0.047	

Field and Laboratory Data

Sevilleta Stable Isotope Profile 7

Depth (m)	δD (permil)	$\delta^{18}O$ (permil)	Water Content (cc/cc)	Temperature (°C)
-0.010	-86.4		0.012	
-0.033	-59.3		0.015	
-0.053	-47.4		0.016	
-0.073	-50.3		0.020	
-0.098	-43.9		0.026	
-0.125	-45.7		0.041	
-0.155	-51.1		0.047	
-0.185	-60.1		0.051	
-0.250	-62.0		0.058	
-0.335	-66.4		0.063	
-0.395	-63.3		0.060	
-0.470	-62.3		0.074	
-0.570	-62.2		0.070	
-0.670	-63.0		0.086	
-0.785	-64.9		0.081	
-0.900	-66.1		0.085	
-1.000	-76.4		0.073	
-1.110	-81.7		0.058	
-1.220	-85.1		0.033	
-1.325	-84.7		0.041	
-1.535	-83.7		0.035	
-1.945	-81.9		0.038	
-2.150	-80.3		0.037	

Field and Laboratory Data

Sevilleta Stable Isotope Profile 8

Depth (m)	δD (permil)	$\delta^{18}O$ (permil)	Water Content (cc/cc)	Temperature (°C)
-0.010	-92.9	-4.8	0.016	
-0.030	-65.9	-1.0	0.016	
-0.050	-54.7	5.3	0.018	
-0.070	-43.1	6.5	0.023	
-0.090	-44.1	4.7	0.026	
-0.110	-49.6	2.3	0.029	
-0.140	-52.6	0.2	0.033	
-0.175	-52.4	1.2	0.036	
-0.220	-56.7	-0.3	0.037	
-0.305	-61.6	-3.0	0.042	
-0.410	-65.8	-3.5	0.039	
-0.515	-67.3	-2.9	0.042	
-0.620	-70.4	-4.1	0.044	
-0.725	-72.9	-5.1	0.040	
-0.825	-79.0	-5.9	0.039	
-0.925	-81.9	-6.8	0.035	
-1.035	-83.6	-7.6	0.039	
-1.130	-83.2	-7.3	0.041	
-1.330	-84.9	-7.7	0.035	
-1.540	-81.0	-7.8	0.038	
-1.760	-83.7	-8.4	0.038	
-1.940	-78.5	-7.4	0.038	
-2.140	-80.4	-6.8	0.036	
-2.300	-78.2	-6.7	0.059	
-2.490	-77.2	-6.3	0.140	
-2.690	-70.2	-5.8	0.034	
-2.890	-72.6	-6.0	0.063	
-3.190	-69.6	-5.6	0.048	
-3.450	-68.3	-6.1	0.039	

APPENDIX C

Computer Program Listings

C.1 CO_2/H_2O Equilibration Program

The following program listing of CO2H2O.FOR is intended for use in calculating the initial $\delta^{18}O$ ratio of water from a CO_2/H_2O equilibration. The program was written for use with the Microsoft Fortran package for IBM PC's or compatibles. The program is interactive to the user.

```
C
C PROGRAM CO2H2O.FOR
C
C A PROGRAM TO COMPUTE INITIAL ISOTOPE RATIOS FOR
C OXYGEN-18 OF WATER AFTER A CO2/H2O EQUILIBRATION
C
C       WRITTEN BY
C   ROBERT G. KNOWLTON, JR.
C
      CHARACTER*1 CH
      CHARACTER*10 SAMPNO
      CHARACTER*20 FILOUT
      DO 1 I=1,20
      Write(*,*)'  '
 1    CONTINUE
      Write(*,*)'                          CO2H2O PROGRAM'
      Write(*,*)'  A program written to correct Oxygen-18 values from'
      Write(*,*)'                CO2/H2O equilibration data'
      Write(*,*)'                       written by'
      Write(*,*)'                  Robert G. Knowlton, Jr.'
      Write(*,*)'                       Spring 1988'
      Write(*,*)'  '
      Write(*,*)'<Press RETURN to continue>'
      READ(*,2)CH
      Write(*,*)'  '
      Write(*,*)'Give the name of the output file: '
      Write(*,*)' '
      Read(*,21)FILOUT
      OPEN(UNIT=20,FILE=FILOUT)
 21   FORMAT(A20)
      Write(*,*)'  '
      Write(*,*)'The data that you will need to furnish for each'
      Write(*,*)'    sample is as follows:'
      Write(*,*)'  '
            Write(*,*)'Sample # - a sample number '
            Write(*,*)'Vwater - volume of water used in the equilibration'
            Write(*,*)'         process, in milliliters (ml)'
            Write(*,*)'Temp(C) - temperature of CO2/H2O equilibration (C)'
            Write(*,*)'n (CO2) - the number of micromoles of CO2 gas used'
            Write(*,*)'deltaCO2i - the permil value of Oxygen-18 for the'
            Write(*,*)'            initial CO2, prior to equilibration'
            Write(*,*)'deltaCO2f - the permil value of Oxygen-18 for the'
            Write(*,*)'            final CO2, after equilibration'
      Write(*,*)'<Press RETURN to continue>'
      Write(*,*)'  '
      READ(*,2)CH
 2    FORMAT(A1)
      WRITE(20,40)
C
C READ AND PROCESS INPUT DATA
C
 30   WRITE(*,*)'  '
```

```
      Write(*,*)'  '
      Write(*,*)'Give the sample number (max 10 characters):'
      Write(*,*)' '
      READ(*,20)SAMPNO
 20   FORMAT(A10)
      Write(*,*)'  '
      WRITE(*,*)'Give the following values:'
      WRITE(*,*)'Vwater, Temp(C), n(CO2), deltaCO2i, deltaCO2f'
      Write(*,*)' '
      READ(*,*)Vwater,Tempt,CO2n,delco2i,delco2f
C{correct final oxygen value to a real SMOW number}
C{    delCO2f[I]:=delCO2f[I]*1.01025+10.25;}
C{    delCO2i[I]:=delCO2i[I]*1.01025+10.25;}
      TK=Tempt+273.15
      VH2O=Vwater*55560.
      Dummy1=1./(TK*TK)
      BigDel=1000.*((17.994/TK)-(21.*Dummy1)-0.01997)
      Dummy2=delCO2f-BigDel
      Dummy3=(delCO2f-delCO2i)*CO2n
      del018=(Dummy3/VH2O)+Dummy2
      WRITE(*,*)'deltaO18 = ',del018
      WRITE(20,41)SAMPNO,Vwater,CO2n,delco2i,delco2f,del018
      Write(*,*)'  '
      Write(*,*)'  '
      Write(*,*)'Do you want to process another sample (Y/N)?  '
      Read(*,2)CH
      IF(CH.EQ.'Y')GOTO 30
      IF(CH.EQ.'y')GOTO 30
 40   FORMAT(//,20X,'CO2/H2O EQUILIBRATION RESULTS',
     1      //,25X,'CO2H2O.FOR PROGRAM',//,29X,'WRITTEN BY',
     2      /,23X,'ROBERT G. KNOWLTON, JR.',///,'SAMPLE',7X,
     3      'Vwater',5X,'n(CO2)',4X,'delCO2i',4X,'delCO2f',4X,
     4      'del018',/,2X,'No.',10X,'(ml)',4X,'(umoles)',3X,
     5      '(permil)',3X,'(permil)',3X,'(permil)',/)
 41   FORMAT(A10,5(F10.3,1X))
      CLOSE(20)
      end
```

C.2 Non-Isothermal Recharge Model

The following program listing of NIR.FOR is intended for use in optimizing a curve-fit to an observed δD profile, with subsequent calculation of the liquid and vapor phase components of soil-water movement, and the recharge rate. The program was written for use with the Microsoft Fortran package for IBM PC's or compatibles. The program is interactive to the user.

```
C
C                  PROGRAM NIR.FOR
C
C  TO APPROXIMATE THE SHAPE OF THE δD VERSUS DEPTH CURVE
C  UNDER NON-ISOTHERMAL CONDITIONS FROM OBSERVED δD DATA,
C  CALCULATES THE VAPOR AND LIQUID FLUXES AS A FUNCTION
C  OF DEPTH, ESTIMATES THE VAPOR AND LIQUID TORTUOSITY
C  TERMS, AND ESTIMATES THE RECHARGE RATE
C
C                      WRITTEN BY
C                 ROBERT G. KNOWLTON, JR.
C                       MAY 1990
C
C INPUT PARAMETERS:
C
C  Z = DEPTH OF STABLE ISOTOPE MEASUREMENT [cm]
C  DELD = STABLE ISOTOPIC COMPOSITION OF DEUTERIUM [permil]
C  TEMP = TEMPERATURE [C] (NOTE: THE USER HAS THE OPTION OF
C         SUPPLYING THIS PARAMETER DIRECTLY OR ALLOWING A
C         HEAT FLOW MODELING SUBROUTINE TO GENERATE THE
C         TEMPERATURE PROFILE REALIZATION)
C
C  INPUT PARAMETERS ARE FREE-FORMATTED
C
C  IN ADDITION, THE USER SHOULD SUPPLY A FUNCTIONAL RELATIONSHIP
C  FOR DEPTH VERSUS WATER CONTENT WITHIN THE SUBROUTINE WVSZ
C
C
C
      DIMENSION DELD(40),ZZ(40),TEMP(40),TH(40),
     1 DCALC(40),QR1(40),QR2(40),DELDV(40),AD(40)
      DIMENSION P(200),A(10,10),AC(10,10),X(40),BOINK(4)
      DIMENSION B(10),Z(40),Y(40),BV(10),BMIN(10),BMAX(10)
      COMMON X
      CHARACTER*20 FILIN,FILOUT,FILPLT
      CHARACTER*30 TITLE
      do 414 i=1,20
      write(*,*)' '
414   continue
      WRITE(*,205)
      WRITE(*,206)
      write(*,*)' '
      WRITE(*,*)' Give a title (Maximum 30 characters):'
      READ(*,109)TITLE
109   FORMAT(A30)
      write(*,*)' '
      WRITE(*,*)' Give the input file name:'
      READ(*,209)FILIN
209   FORMAT(A20)
      write(*,*)' '
      WRITE(*,*)' Give the output file name:'
      READ(*,209)FILOUT
```

```
      write(*,*)' '
      WRITE(*,*)' Give the plotting output file name:'
      READ(*,209)FILPLT
      OPEN(UNIT=20,FILE=FILIN,STATUS='OLD')
      OPEN(UNIT=22,FILE=FILOUT,STATUS='UNKNOWN')
      OPEN(UNIT=23,FILE=FILPLT,STATUS='UNKNOWN')
C
      WRITE(22,205)
      WRITE(22,206)
 205  FORMAT(/,72('*'),//,29X,'PROGRAM NIR.FOR',//,
     1 8X,'PROVIDES THE FOLLOWING CAPABILITIES:',//,5X,
     2 '1 - APPROXIMATES THE SHAPE OF THE δD',1X,
     2 'VERSUS DEPTH CURVE',/,9X,
     3 'UNDER NON-ISOTHERMAL QUASI-STEADY CONDITIONS',/,
     4 5X,'2 - CALCULATES THE LIQUID AND ',
     5 'VAPOR FLUXES AS A FUNCTION OF DEPTH')
 206  FORMAT(5X,'3 - ESTIMATES THE VAPOR AND LIQUID ',
     1 'TORTUOSITIES',/,5X,'4 - ESTIMATES THE RECHARGE ',
     2 'RATE',//,35X,'WRITTEN BY',/,28X,
     3 'ROBERT G. KNOWLTON, JR.',//)
      WRITE(22,207)TITLE
 207  FORMAT(2X,'PROBLEM TITLE: ',/,A30,//)
C READ IN INPUT DATA
      write(*,*)' '
      WRITE(*,*)' How many input points are there?'
      READ(*,*)NPTS
      write(*,*)' '
      write(*,*)' Choose the method by which the temperature'
      write(*,*)'    data is supplied:'
      write(*,*)' (1) manually supplied by the input file'
      write(*,*)' (2) calculated within the code using an'
      write(*,*)'     analytical heat flow routine'
      read(*,*)NTP
      IF(NTP.NE.1)THEN
      write(*,*)' '
      WRITE(*,*)' Give the time at which the analytical heat flow'
      WRITE(*,*)'    model will calculate temperature (days): '
      READ(*,*)TOUT
      CALL PARAM2(BOINK)
      ENDIF
      NN=NPTS
      KK=4
      IF(NTP.NE.1)THEN
      DO 33 I=1,NPTS
      READ(20,*)ZZ(I),DELD(I)
      DELD(I)=DELD(I)/1000
 33   CONTINUE
      ENDIF
      IF(NTP.EQ.1)THEN
      DO 34 I=1,NN
      READ(20,*)ZZ(I),DELD(I),TEMP(I)
      DELD(I)=DELD(I)/1000
```

```
 34     CONTINUE
        ENDIF
        DO 106 I=1,NPTS
C CONVERT DEPTH FROM cm TO meters
        ZZ(I)=ZZ(I)/100
        X(I)=ZZ(I)
        Y(I)=DELD(I)
 106    CONTINUE
        Y1=Y(1)
C
C FOUR UNKNOWNS, OR VARIABLES TO SOLVE FOR
C
C READ IN THE MAX-MIN AND INITIAL VALUES OF THE VARIABLES
        CALL PARAM(B,BMIN,BMAX)
C RECHARGE RATE, W
        W=EXP(B(4))
C δDrec VALUE
        DREC=B(3)
C VAPOR TORTUOSITY
        TORZV=B(1)
C LIQUID TORTUOSITY
        TORZL=B(2)
C OTHER CONSTANTS
        DN1=0.0243
        SIGD=1+DN1
        RHO=1000
C TEMPERATURE FUNCTION
        IF(NTP.NE.1)THEN
        CALL ANALTH(NN,TEMP,X,TOUT,BOINK)
        ENDIF
C
C MARQUARDT SOLUTION
C
C
        FNU=0.0
        FLA=0.0
        TAU=0.0
        EPS=0.0
        PHMIN=0.0
        I=0
        KD=KK
        FV=0.0
        DO 100 J=1,KK
        BV(J)=1
 100    CONTINUE
        ICON=KK
        ITER=0
        WRITE(22,15)
 15     FORMAT(//,10X,'BSOLVE REGRESSION ALGORITHM',//,
     1 ' ITERATION',4X,'ICON',8X,'PH',10X,'B(1)',8X,'B(2)',8X,
     2 'B(3)',8X,'B(4)',/,'   NUMBER',/)
C
```

```
 200  CALL BSOLVE(KK,B,NN,Z,Y,PH,FNU,FLA,TAU,EPS,PHMIN,I,ICON,
     1 BV,BMIN,BMAX,P,A,AC,GAMM,TEMP)
C
      IF(ITER.EQ.100)GOTO 886
      ITER=ITER+1
      WRITE(22,136)ITER,ICON,PH,B(1),B(2),B(3),B(4)
 136  FORMAT(3X,I3,10X,I3,1X,E14.4,1X,4(F10.4,1X))
      IF(ICON)10,300,200
 10   IF(ICON+1)20,60,200
 20   IF(ICON+2)30,70,200
 30   IF(ICON+3)40,80,200
 40   IF(ICON+4)50,90,200
 50   GO TO 95
 60   WRITE(22,4)
 4    FORMAT(//,2X,'NO FUNCTION IMPROVEMENT POSSIBLE')
      GO TO 300
 70   WRITE(22,5)
 5    FORMAT(//,2X,'MORE UNKNOWNS THAN FUNCTIONS')
      GO TO 300
 80   WRITE(22,6)
 6    FORMAT(//,2X,'TOTAL VARIABLES ARE ZERO')
      GO TO 300
 90   WRITE(22,7)
 7    FORMAT(//,2X,'CORRECTIONS SATISFY CONVERGENCE'
     1 1X,'REQUIREMENTS BUT LAMDA FACTOR (FLA) STILL LARGE')
      GO TO 300
 95   WRITE(22,8)
 8    FORMAT(//,2X,'THIS IS NOT POSSIBLE')
      GO TO 300
 886  WRITE(22,887)
 887  FORMAT(//,5X,'MAXIMUM NUMBER OF ITERATIONS ',
     1 '(100) REACHED',//)
 300  WRITE(22,2)
 2    FORMAT(//,2X,'SOLUTIONS OF THE EQUATIONS')
      DO 400 J=1,KK
      WRITE(22,3)J,B(J)
 3    FORMAT(/,2X,'B(',I2,') = ',E16.8)
 400  CONTINUE
      WRITE(22,23)
C CALCULATE THE FINAL FITTED DATA
      CALL EQN(B,NN,Z,Y1,TEMP)
      SUM=0
      W=EXP(B(4))
C CALCULATE THE SUM OF THE SQUARES OF THE RESIDUALS
      DO 350 I=1,NN
      DCALC(I)=Z(I)*1000
      DELD(I)=DELD(I)*1000
      DMIND=DELD(I)-DCALC(I)
      SUM=SUM+(DMIND**2)
      WRITE(22,25)ZZ(I),DELD(I),DCALC(I),DMIND
 350  CONTINUE
      TORZV=B(1)
```

```
      TORZL=B(2)
      DREC=B(3)
      DREC2=DREC*1000
      WREC=W*3.154E9
      WRITE(22,26)B(1),B(2),WREC,DREC2
      WRITE(22,27)SUM
 23   FORMAT(//,' RESULTS OF MODEL FIT FOR DEUTERIUM DATA',
     1 //,2X,'DEPTH',9X,'δD',8X,'δD (calc)',5X,'RESIDUAL',/,
     2 3X,'(m)',7X,'(permil)',5X,'(permil)',6X,'(permil)',/)
 25   FORMAT(F7.3,2X,F10.1,2X,F10.1,2X,F10.4)
 26   FORMAT(//,5X,'VAPOR TORTUOSITY FACTOR = ',F10.4,
     1 /,5X,'LIQUID TORTUOSITY FACTOR = ',F10.4,/,5X,
     2 'RECHARGE RATE = ',F10.3,' cm/yr'/,5X,
     3 'δD RECHARGE = ',F10.1,' permil')
 27   FORMAT(5X,'SUM OF THE SQUARES OF THE RESIDUALS = ',
     1 1P,E10.3,//)
 29   FORMAT(F7.1,1X,F7.1,1X,F6.3,1X,F6.1)
C
C COMPUTE THE VAPOR FLUX/RECHARGE RATIO USING THE FITTED
C VARIABLES
C
      WRITE(22,618)
 618  FORMAT(//,' RESULTS FROM LIQUID AND VAPOR FLUX ',
     1 'CALCULATIONS',//,2X,'DEPTH',4X,'TEMP',8X,'δD',6X,
     2 'δD(vapor)',6X,'q(l)/pW',3X,'q(v)/pW',/,3X,'(m)',
     3 5X,'(C)',6X,'(permil)',3X,'(permil)',/)
C CALCULATE THE VAPOR FLUX
      CALL VEQN(B,NN,QR2,DCALC,TEMP)
      WRITE(23,29)DCALC(1),DELD(1),-ZZ(1),TEMP(1)
      DO 620 I=2,NN
      Z3=X(I)
      T3=TEMP(I)
C EQUILIBRIUM FRACTIONATION FACTOR
      AD(I)=1-ETAD(T3)
C LIQUID FLUX/RECHARGE FLUX RATIO
      QR1(I)=1+QR2(I)
C VAPOR PHASE DELTA VALUE
      DELDV(I)=DELD(I)*AD(I)
      WRITE(22,625)ZZ(I),TEMP(I),DELD(I),DELDV(I),
     1 QR1(I),-QR2(I)
      WRITE(23,627)DCALC(I),DELD(I),-ZZ(I),TEMP(I),
     1 QR1(I),-QR2(I)
 620  CONTINUE
C COMPUTE THE MEAN FLUX RATIOS
      SUMMV=0
      SUMML=0
      DO 352 I=2,NN
      DELZ=X(I)-X(I-1)
      SUMMV=SUMMV-(DELZ*QR2(I))
      SUMML=SUMML+(DELZ*QR1(I))
 352  CONTINUE
      DELZ=X(NN)-X(1)
```

```
      SUMMV=SUMMV/DELZ
      SUMML=SUMML/DELZ
      WRITE(22,628)SUMML
      WRITE(22,629)SUMMV
625   FORMAT(F7.3,2X,F6.2,2X,F10.1,2X,F10.1,2X,F10.4,
     1 2X,F10.4)
627   FORMAT(F7.1,1X,F7.1,1X,F6.3,1X,F6.1,1X,F6.3,1X,F6.3)
628   FORMAT(//,'     MEAN LIQUID FLUX/RECHARGE RATIO = ',
     1 F6.3)
629   FORMAT(//,'     MEAN VAPOR FLUX/RECHARGE RATIO = ',
     1 F6.3)
      END
C
C SUBROUTINE PARAM - INTERACTIVELY SETS PARAMETER BOUNDS
C        AND INITIAL VALUES
C
      SUBROUTINE PARAM(B,BMIN,BMAX)
      DIMENSION B(10),BMIN(10),BMAX(10)
      CHARACTER*1 CH
C INITIAL VALUES
      B(1)=0.3
      B(2)=.03
      B(3)=-0.08
      B(4)=-22.07
      W=EXP(B(4))
      WREC=W*3.154E9
      DREC=B(3)*1000
5     WRITE(*,10)B(1),B(2),DREC,WREC
10    FORMAT(///,' THE FOLLOWING INITIAL VALUES HAVE BEEN',
     1 1X,'ASSIGNED TO THE VARIABLES:',//,' 1 - VAPOR TORTU',
     2 'OSITY FACTOR = ',F5.2,/,' 2 - LIQUID TORTUOSITY FACTOR',
     3 ' = ',F5.2,/,' 3 - δDrec = ',F6.1,/,' 4 - RECHARGE ',
     4'RATE = ',F6.2,' cm/yr',/,' 0 - NO FURTHER CHANGES ARE ',
     5'NECESSARY',//,' CHOOSE AN OPTION: ')
      READ(*,*)IPT
      IF(IPT.EQ.0)GOTO 20
      WRITE(*,*)'GIVE A NEW VALUE: '
      IF(IPT.EQ.1)READ(*,*)B(1)
      IF(IPT.EQ.2)READ(*,*)B(2)
      IF(IPT.EQ.3)READ(*,*)DREC
      IF(IPT.EQ.3)B(3)=DREC/1000
      IF(IPT.EQ.4)READ(*,*)WREC
      IF(IPT.EQ.4)B(4)=LOG(WREC/3.154E9)
      GO TO 5
20    BMIN(1)=0
      BMIN(2)=.03
      BMIN(3)=-.3
      BMIN(4)=-30
      WM=EXP(BMIN(4))
      WRECM=WM*3.154E9
      DRECM=BMIN(3)*1000
25    WRITE(*,12)BMIN(1),BMIN(2),DRECM,WRECM
```

```
 12    FORMAT(///,' THE FOLLOWING MINIMUM VALUES HAVE BEEN',
     1 1X,'ASSIGNED TO THE VARIABLES:',//,' 1 - VAPOR TORTU',
     2 'OSITY FACTOR = ',F5.2,/,' 2 - LIQUID TORTUOSITY FACTOR',
     3 ' = ',F5.2,/,' 3 - δDrec = ',F6.1,/,' 4 - RECHARGE ',
     4 'RATE = ',F6.2,' cm/yr',/,' 0 - NO FURTHER CHANGES ARE ',
     5 'NECESSARY',//,' CHOOSE AN OPTION: ')
       READ(*,*)IPT
       IF(IPT.EQ.0)GOTO 30
       WRITE(*,*)'GIVE A NEW VALUE: '
       IF(IPT.EQ.1)READ(*,*)BMIN(1)
       IF(IPT.EQ.2)READ(*,*)BMIN(2)
       IF(IPT.EQ.3)READ(*,*)DRECM
       IF(IPT.EQ.3)BMIN(3)=DRECM/1000
       IF(IPT.EQ.4)READ(*,*)WRECM
       IF(IPT.EQ.4)BMIN(4)=LOG(WRECM/3.154E9)
       GO TO 25
 30    BMAX(1)=1
       BMAX(2)=1
       BMAX(3)=.3
       BMAX(4)=-19.57
       WM=EXP(BMAX(4))
       WRECM=WM*3.154E9
       DRECM=BMAX(3)*1000
 35    WRITE(*,13)BMAX(1),BMAX(2),DRECM,WRECM
 13    FORMAT(///,' THE FOLLOWING MAXIMUM VALUES HAVE BEEN',
     1 1X,'ASSIGNED TO THE VARIABLES:',//,' 1 - VAPOR TORTU',
     2 'OSITY FACTOR = ',F5.2,/,' 2 - LIQUID TORTUOSITY FACTOR',
     3 ' = ',F5.2,/,' 3 - δDrec = ',F6.1,/,' 4 - RECHARGE ',
     4 'RATE = ',F6.2,' cm/yr',/,' 0 - NO FURTHER CHANGES ARE ',
     5 'NECESSARY',//,' CHOOSE AN OPTION: ')
       READ(*,*)IPT
       IF(IPT.EQ.0)GOTO 40
       WRITE(*,*)'GIVE A NEW VALUE: '
       IF(IPT.EQ.1)READ(*,*)BMAX(1)
       IF(IPT.EQ.2)READ(*,*)BMAX(2)
       IF(IPT.EQ.3)READ(*,*)DRECM
       IF(IPT.EQ.3)BMAX(3)=DRECM/1000
       IF(IPT.EQ.4)READ(*,*)WRECM
       IF(IPT.EQ.4)BMAX(4)=LOG(WRECM/3.154E9)
       GO TO 35
C
 40    RETURN
       END
C
C SUBROUTINE PARAM2
C
C TO INTERACTIVELY INPUT THE PARAMETERS FOR THE
C ANALYTICAL MODELING OF THE TEMPERATURE PROFILE
C
       SUBROUTINE PARAM(BOINK)
       DIMENSION BOINK(4)
       CHARACTER*1 CH
```

```
C INITIAL VALUES
      BOINK(1)=16.2
      BOINK(2)=0.0
      BOINK(3)=10.
      BOINK(4)=15.
 5    WRITE(*,10)(BOINK(J),J=1,4)
 10   FORMAT(///,' THE FOLLOWING INITIAL VALUES HAVE BEEN',
     1 1X,'ASSIGNED TO THE HEAT FLOW MODELING VARIABLES:',//,
     2 ' 1 - AVERAGE ANNUAL TEMPERATURE = ',F5.1,' C',/,
     3 ' 2 - ARBITRARY STARTING TIME = ',F5.1,' sec',/,
     4 ' 3 - Ad (DIURNAL AIR TEMPERATURE VARIATION) = ',F5.1,
     5 ' C',/,' 4 - Ay (ANNUAL AIR TEMPERATURE VARIATION) = ',
     6 F5.1,' C',/,' 0 - NO FURTHER CHANGES ARE ',
     7 'NECESSARY',//,' CHOOSE AN OPTION: ')
      READ(*,*)IPT
      IF(IPT.EQ.0)GOTO 20
      WRITE(*,*)'GIVE A NEW VALUE: '
      IF(IPT.EQ.1)READ(*,*)BOINK(1)
      IF(IPT.EQ.2)READ(*,*)BOINK(2)
      IF(IPT.EQ.3)READ(*,*)BOINK(3)
      IF(IPT.EQ.4)READ(*,*)BOINK(4)
      GO TO 5
 20   RETURN
      END
C
C FUNCTION ETAD - FRACTIONATION FACTOR
      FUNCTION ETAD(T)
      T1=T+273.2
      D1=1000000/(T1*T1)
      D2=1000/T1
      D3=24.844*D1-76.248*D2+52.612
      ALPHA=EXP(D3/1000)
      ETAD=1-(1/ALPHA)
      RETURN
      END
C
C FUNCTION VPVST - VAPOR PRESSURE VERSUS TEMPERATURE
C
      FUNCTION VPVST(T1)
      D1=6.87
      D2=0.342*T1
      D3=0.0397*(T1*T1)
      VPVST=D1-D2+D3
      RETURN
      END
C
C FUNCTION SATN - SATURATED VAPOR DENSITY
      FUNCTION SATN(T)
      D1=0.059
      SATN=0.00516*(EXP(D1*T))
      RETURN
      END
```

```
C
C FUNCTION DVVST - VAPOR DIFFUSIVITY
      FUNCTION DVVST(T)
      A1=-17.784
      B1=2.072
      T1=T+273.2
      D1=B1*LOG(T1)+A1
      D2=101
      DVVST=(EXP(D1))/D2
      RETURN
      END
C
C FUNCTION WVSZ - WATER CONTENT
      FUNCTION WVSZ(Z1)
      A1=.0345
      B1=.00393
      D1=LOG(Z1)
      WVSZ=A1+B1*(D1)
      RETURN
      END
C
C SUBROUTINE EQN
C
      SUBROUTINE EQN(B,NN,Z,Y1,TEMP)
      DIMENSION X(40),Z(40),B(10),SATND(40),ED(40),AD(40),
     1 TEMP(40),ZV(40),ZL(40),TH(40),DCALC(40)
      COMMON X
C
C
C ASSUME RELATIVE HUMIDITY EQUALS UNITY
      DREC=B(3)
      W=EXP(B(4))
      DN1=0.0243
      SIGD=1+DN1
      RHO=1000
      DO 15 I=1,NN
      Z3=X(I)
C CALCULATE WATER CONTENT
      TH(I)=WVSZ(Z3)
      T3=TEMP(I)
C CALCULATE VAPOR PRESSURE
      VPT(I)=VPVST(T3)
C CALCULATE FRACTIONATION FACTORS
      ED(I)=ETAD(T3)
      AD(I)=1-ED(I)
C CALCULATE SATURATED VAPOR DENSITY
      SATND(I)=SATN(T3)
 15   CONTINUE
      DO 14 I=1,NN
C CALCULATE VAPOR DIFFUSIVITY AND ZV
      D1=0.37-TH(I)
      T3=TEMP(I)
```

```
      D2=DVVST(T3)
C CALCULATE THE MASS FLOW FACTOR (FFT) CONTRIBUTION
      FFT=1.
      R4=1+FFT*(VPT(I)/(650-VPT(I)))
      DIFFV=D2*D1*B(1)*R4
      ZV(I)=(SATND(I)*DIFFV)/(RHO*W)
C CALCULATE LIQUID DIFFUSIVITY AND ZL
      A1=1.268E-9
      B1=0.0234
      T3=TEMP(I)
      DSD=A1*EXP(B1*T3)
      DS=DSD*TH(I)*B(2)
      ZL(I)=DS/W
 14   CONTINUE
C CALCULATE THE MODEL δD VALUES
      DCALC(1)=Y1
      DO 30 I=2,NN
      DELZ=X(I)-X(I-1)
      DELZ1=ZV(I)+ZL(I)+DELZ
      D1=SATND(I)*(ED(I)+DN1)
      D5=SATND(I-1)*(ED(I-1)+DN1)
      D2=ZV(I)*(ED(I)+DN1)
      DELED=LOG(D1/D5)
      D3=D2*DELED
      D4=DCALC(I-1)*(ZL(I)+ZV(I))
      D5=DREC*DELZ
      DCALC(I)=(D5+D4+D3)/DELZ1
 30   CONTINUE
      DO 100 JJ=1,NN
      Z(JJ)=DCALC(JJ)
 100  CONTINUE
C
      RETURN
      END
C
C SUBROUTINE VEQN
C
      SUBROUTINE VEQN(B,NN,QR2,DCALC,TEMP)
      DIMENSION X(40),B(10),SATND(40),ED(40),AD(40),
     1 TEMP(40),ZV(40),ZL(40),TH(40),DCALC(40),QR2(40)
      COMMON X
C
C
C ASSUME RELATIVE HUMIDITY EQUALS UNITY
      W=EXP(B(4))
      DREC=B(3)
      DN1=0.0243
      SIGD=1+DN1
      RHO=1000
      DO 15 I=1,NN
      Z3=X(I)
C CALCULATE WATER CONTENT
```

```
      TH(I)=WVSZ(Z3)
      T3=TEMP(I)
C CALCULATE VAPOR PRESSURE
      VPT(I)=VPVST(T3)
C CALCULATE FRACTIONATION FACTORS
      ED(I)=ETAD(T3)
      AD(I)=1-ED(I)
C CALCULATE SATURATED VAPOR DENSITY
      SATND(I)=SATN(T3)
 15   CONTINUE
      DO 14 I=1,NN
C CALCULATE VAPOR DIFFUSIVITY AND ZV
      D1=0.37-TH(I)
      T3=TEMP(I)
      D2=DVVST(T3)
C CALCULATE THE MASS FLOW FACTOR (FFT) CONTRIBUTION
      FFT=1.
      R4=1+FFT*(VPT(I)/(650-VPT(I)))
      DIFFV=D2*D1*B(1)*R4
      ZV(I)=(SATND(I)*DIFFV)/(RHO*W)
C CALCULATE LIQUID DIFFUSIVITY AND ZL
      A1=1.268E-9
      B1=0.0234
      T3=TEMP(I)
      DSD=A1*EXP(B1*T3)
      DS=DSD*TH(I)*B(2)
      ZL(I)=DS/W
 14   CONTINUE
C CALCULATE THE MODEL VAPOR FLUX/RECHARGE RATIO VALUES
      DO 203 I=1,NN
      DCALC(I)=DCALC(I)/1000
 203  CONTINUE
      DO 620 I=2,NN
      DELZ=X(I)-X(I-1)
      DELED=ED(I)-ED(I-1)
      DELDD=DCALC(I)-DCALC(I-1)
      D1=ZV(I)*(DELED/DELZ)
      D2=(ZV(I)+ZL(I))*(DELDD/DELZ)
      D3=1/(ED(I)+DN1)
      D4=DCALC(I)-DREC
      QR2(I)=D3*(D4+D2-D1)
 620  CONTINUE
      DO 204 I=1,NN
      DCALC(I)=DCALC(I)*1000
 204  CONTINUE
C
      RETURN
      END
C
C SUBROUTINE BSOLVE
C
      SUBROUTINE BSOLVE(KK,B,NN,Z,Y,PH,FNU,FLA,TAU,EPS,
```

```
     1 PHMIN,I,ICON,BV,BMIN,BMAX,P,A,AC,GAMM,TEMP)
       DIMENSION B(10),Z(40),Y(40),BV(10),BMIN(10),BMAX(10)
       DIMENSION P(200),A(10,10),AC(10,10),X(40),FV(10),DV(10)
C
       K=KK
       N=NN
       Y1=Y(1)
       KP1=K+1
       KP2=KP1+1
       KBI1=K*N
       KBI2=KBI1+K
       KZI=KBI2+K
       IF(FNU.LE.0.)FNU=10.0
       IF(FLA.LE.0.)FLA=0.01
       IF(TAU.LE.0.)TAU=0.001
       IF(EPS.LE.0.)EPS=0.00002
       IF(PHMIN.LE.0.)PHMIN=0.0
 120   KE=0
 130   DO 160 I1=1,K
 160   IF(BV(I1).NE.0.)KE=KE+1
       IF(KE.GT.0)GO TO 170
 162   ICON=-3
 163   GO TO 2120
 170   IF(N.GE.KE)GO TO 500
 180   ICON=-2
 190   GO TO 2120
 500   I1=1
 530   IF(I.GT.0)GO TO 1530
 550   DO 560 J1=1,K
       J2=KBI1+J1
       P(J2)=B(J1)
       J3=KBI2+J1
 560   P(J3)=ABS(B(J1))+1.0E-2
C 560  P(J3)=ABS(B(J1))+1.0E-4
       GO TO 1030
 590   IF(PHMIN.GT.PH.AND.I.GT.1)GO TO 625
       DO 620 J1=1,K
       N1=(J1-1)*N
       IF(BV(J1))601,620,605
C 601  CALL DERIV(K,B,N,Z,P(N1+1),FV,DV,J1,JTEST)
 601   WRITE(*,*)'NEED A DERIVATIVE FUNCTION!!!!'
       IF(JTEST.NE.(-1))GO TO 620
       BV(J1)=1.0
 605   DO 606 J2=1,K
       J3=KBI1+J2
 606   P(J3)=B(J2)
       J3=KBI1+J1
       J4=KBI2+J1
       DEN=0.001*AMAX1(P(J4),ABS(P(J3)))
       IF(P(J3)+DEN.LE.BMAX(J1))GO TO 55
       P(J3)=P(J3)-DEN
       DEN=-DEN
```

```
      GO TO 56
   55 P(J3)=P(J3)+DEN
   56 CALL EQN(P(KBI1+1),N,P(N1+1),Y1,TEMP)
      DO 610 J2=1,N
      JB=J2+N1
  610 P(JB)=(P(JB)-Z(J2))/DEN
  620 CONTINUE
C
C SET UP CORRECTION EQUATIONS
C
  625 DO 725 J1=1,K
      N1=(J1-1)*N
      A(J1,KP1)=0.
      IF(BV(J1))630,692,630
  630 DO 640 J2=1,N
      N2=N1+J2
  640 A(J1,KP1)=A(J1,KP1)+P(N2)*(Y(J2)-Z(J2))
  650 DO 680 J2=1,K
  660 A(J1,J2)=0.
  665 N2=(J2-1)*N
  670 DO 680 J3=1,N
  672 N3=N1+J3
  674 N4=N2+J3
  680 A(J1,J2)=A(J1,J2)+P(N3)*P(N4)
      IF(A(J1,J1).GT.1.E-20)GO TO 725
  692 DO 694 J2=1,KP1
  694 A(J1,J2)=0.
  695 A(J1,J1)=1.0
  725 CONTINUE
      GN=0.
      DO 729 J1=1,K
  729 GN=GN+A(J1,KP1)**2
C
C SCALE CORRECTION EQUATIONS
C
      DO 726 J1=1,K
  726 A(J1,KP2)=SQRT(A(J1,J1))
      DO 727 J1=1,K
      A(J1,KP1)=A(J1,KP1)/A(J1,KP2)
      DO 727 J2=1,K
  727 A(J1,J2)=A(J1,J2)/(A(J1,KP2)*A(J2,KP2))
  730 FL=FLA/FNU
      GOTO 810
  800 FL=FNU*FL
  810 DO 840 J1=1,K
  820 DO 830 J2=1,KP1
  830 AC(J1,J2)=A(J1,J2)
  840 AC(J1,J1)=AC(J1,J1)+FL
C
C SOLVE CORRECTION EQUATIONS
C
      DO 930 L1=1,K
```

```
      L2=L1+1
      DO 910 L3=L2,KP1
  910 AC(L1,L3)=AC(L1,L3)/AC(L1,L1)
      DO 930 L3=1,K
      IF(L1-L3)920,930,920
  920 DO 925 L4=L2,KP1
  925 AC(L3,L4)=AC(L3,L4)-AC(L1,L4)*AC(L3,L1)
  930 CONTINUE
C
      DN=0.
      DG=0.
      DO 1028 J1=1,K
      AC(J1,KP2)=AC(J1,KP1)/A(J1,KP2)
      J2=KBI1+J1
      P(J2)=AMAX1(BMIN(J1),AMIN1(BMAX(J1),B(J1)+AC(J1,KP2)))
      DG=DG+AC(J1,KP2)*A(J1,KP1)*A(J1,KP2)
      DN=DN+AC(J1,KP2)*AC(J1,KP2)
 1028 AC(J1,KP2)=P(J2)-B(J1)
      COSG=DG/SQRT(DN*GN)
      JGAM=0
      IF(COSG)1100,1110,1110
 1100 JGAM=2
      COSG=-COSG
 1110 CONTINUE
      COSG=AMIN1(COSG,1.0)
      GAMM=ARCOS(COSG)*180./(3.14159265)
      IF(JGAM.GT.0)GAMM=180.-GAMM
 1030 CALL EQN(P(KBI1+1),N,P(KZI+1),Y1,TEMP)
 1500 PHI=0.
      DO 1520 J1=1,N
      J2=KZI+J1
 1520 PHI=PHI+(P(J2)-Y(J1))**2
      IF(PHI.LT.1.E-10)GOTO 3000
      IF(I.GT.0)GOTO 1540
 1521 ICON=K
      GOTO 2110
 1540 IF(PHI.GE.PH)GOTO 1530
C
C EPSILON TEST
C
 1200 ICON=0
      DO 1220 J1=1,K
      J2=KBI1+J1
 1220 IF(ABS(AC(J1,KP2))/(TAU+ABS(P(J2))).GT.EPS)ICON=ICON+1
      IF(ICON.EQ.0)GOTO 1400
C
C GAMMA LAMBDA TEST
C
      IF(FL.GT.1.0.AND.GAMM.GT.90.0) ICON=-1
      GOTO 2105
C
C GAMMA EPSILON TEST
```

```
C
 1400  IF(FL.GT.1.0.AND.GAMM.LE.45.0) ICON=-4
       GOTO 2105
C
 1530  IF(I1-2)1531,1531,2310
 1531  I1=I1+1
       GOTO (530,590,800),I1
 2310  IF(FL.LT.1.0E+8)GOTO 800
 1320  ICON=-1
C
 2105  FLA=FL
       DO 2091 J2=1,K
       J3=KBI1+J2
 2091  B(J2)=P(J3)
 2110  DO 2050 J2=1,N
       J3=KZI+J2
 2050  Z(J2)=P(J3)
       PH=PHI
       I=I+1
 2120  RETURN
 3000  ICON=0
       GOTO 2105
C
       END
C
C
       FUNCTION ARCOS(Z)
C
       X=Z
       KEY=0
       IF(X.LT.(-1.))X=-1.
       IF(X.GT.1.)X=1.
       IF(X.GE.(-1.).AND.X.LT.0.)KEY=1
       IF(X.LT.0.)X=ABS(X)
       IF(X.EQ.0.)GOTO 10
       ARCOS=ATAN(SQRT(1.-X*X)/X)
       PIE=3.14159265
       D1=ARCOS
       IF(KEY.EQ.1)ARCOS=PIE-D1
       GOTO 999
 10    ARCOS=1.5707963
C
 999   RETURN
       END
C
C
C        PROGRAM ANALTH.FOR
C
C TO APPROXIMATE THE TEMPERATURE DISTRIBUTION USING
C AN ANALYTICAL SOLUTION TO THE FOURIER HEAT FLOW EQUATION
C
C            WRITTEN BY
```

```
C    ROBERT G. KNOWLTON, JR.
C
C MODIFIED FOR USE AS A SUBROUTINE
C        1/28/90
C
C KEY PARAMETERS DEFINED IN THE MAIN PROGRAM:
C
C TAVGY = AVERAGE YEARLY TEMPERATURE AT ALL DEPTHS (C)
C TZERO = ARBITRARY STARTING TIME (SEC)
C AOD = DAILY TEMPERATURE AMPLITUDE (C)
C AOY = YEARLY TEMPERATURE AMPLITUDE (C)
C TOUT = OUTPUT TIME TO CALCULATE TEMPERATURE PROFILE (DAYS)
C
      SUBROUTINE ANALTH(NN,TEMP,DEPTH,TOUT,BOINK)
      DIMENSION Z(80),X(80),WC(80),AY(80),AD(80),
     1 TEMP(80),DEPTH(80),ZTMP(80),BOINK(4)
C
      WRITE(22,205)
 205  FORMAT(//,72('*'),//,10X,'SUBROUTINE ANALTH.FOR',
     1 //,2X,'TO APPROXIMATE THE TEMPERATURE',1X,
     2 'DISTRIBUTION VERSUS DEPTH',//,2X,
     3 'Parameters utilized:',/)
      TAVGY=BOINK(1)
      TZERO=BOINK(2)
      AOD=BOINK(3)
      AOY=BOINK(4)
C CHANGE TOUT FROM DAYS TO SECONDS
      TOUT2=TOUT*86400
      NOUT=1
C CALCULATE PARAMETERS
      WD=0.0000727
      WY=0.000000199
      GAMD=WD*TZERO
      GAMY=WY*TZERO
C calculate the water content
      DO 20 I=1,NN
      D1=DEPTH(I)*100
      ZTMP(I)=D1
      if(d1.eq.0)d1=0.01
      WC(I)=WVSZ(D1)
 20   CONTINUE
C calculate the thermal conductivity
      CALL TC(WC,NN,Z)
      SUM=0
      DO 25 I=1,NN
      D3=Z(I)/(0.2868+WC(I))
      SUM=SUM+D3
 25   CONTINUE
      SUM=SUM/NN
      DD=SQRT(2*SUM/WD)
      DY=SQRT(2*SUM/WY)
      DO 30 I=1,NN
```

```
      AD(I)=AOD/EXP(ZTMP(I)/DD)
      AY(I)=AOY/EXP(ZTMP(I)/DY)
 30   CONTINUE
      WRITE(22,81)TAVGY,TZERO,AOD,AOY,DD,DY,TOUT
 81   FORMAT(/,'Average annual temperature = ',F8.2,' C',/,
     1 'Arbitrary starting time = ',1p,E10.2,' sec',/,
     2 'Daily surface temperature amplitude = ',0p,F8.2,
     3 ' C',/,'Yearly surface temperature amplitude = ',
     4 F8.2,' C',/,'Daily damping depth = ',F8.2,' cm',/,
     5 'Yearly damping depth = ',F8.2,' cm',/
     6 'Output time = ',F6.1,' days',//,72('*'),//)
C BEGIN CALCULATIONS
      DO 45 J=1,NN
      F1=SIN(WY*TOUT2+GAMY-ZTMP(J)/DY)
      TOUT3=TOUT2
C MAXIMIZE THE DAILY TEMPERATURE AMPLITUDE
      DO 40 K=1,24
      TOUT3=TOUT3+3600
      F2=SIN(WD*TOUT3+GAMD-ZTMP(J)/DY)
      F3=F2*AD(J)
      IF(K.EQ.1)F4=F3
      IF(F3.GT.F4)F4=F3
 40   CONTINUE
      TEMP(J)=TAVGY+(AY(J)*F1)+F4
 45   CONTINUE
C
      RETURN
      END
C
C SUBROUTINE TC
C
C TO CALCULATE THE THERMAL CONDUCTIVITY AT A GIVEN
C WATER CONTENT BY DEVRIES (1963) METHOD
C
C SEVERAL PARAMETERS HAVE BEEN ESTIMATED SPECIFICALLY
C FOR A FINE SANDY SOIL (KNOWLTON, R.G., JR., 1990, PhD
C DISSERTATION)
      SUBROUTINE TC(X,NN,Z)
      DIMENSION X(80),Z(80),B(10),DCALC(80),GA(3),GS(3)
C CALCULATE THE SHAPE FACTORS
C SOIL SHAPE FACTOR, ks, AND AIR SHAPE FACTOR, ka
      SK=0
      AK=0
      B(1)=0.1735
      B(2)=18.474
      GS(1)=0.144
      GS(2)=0.144
      GS(3)=0.712
      DO 30 I=1,NN
      IF(X(I).GE.0.12)GA(1)=0.0399+0.7840*X(I)
      IF(X(I).LT.0.12)GA(1)=0.013+1.0083*X(I)
      GA(2)=GA(1)
```

```
      GA(3)=1.-GA(2)-GA(2)
      TCV=0.0615+1.47*X(I)
      DO 10 K=1,3
      SK=SK+(1./(1.+((20.4/B(1))-1.)*GS(K)))
      AK=SK+(1./(1.+((TCV/B(2))-1.)*GA(K)))
 10   CONTINUE
      SK=SK/3
      AK=AK/3
      E1=(SK*20.4)+(X(I)*1.42)
      E2=AK*(0.37-X(I))*(0.0615+1.47*X(I))
      E3=X(I)+(SK*0.63)+(AK*(0.37-X(I)))
      DCALC(I)=(E1+E2)/E3
 30   CONTINUE
      DO 100 JJ=1,NN
      Z(JJ)=DCALC(JJ)/1000
 100  CONTINUE
C
      RETURN
      END
C
```

C.3 Mass Balance Program

The following program listing of SIMASS.FOR is intended for use as a mass balance model for the transient analysis of observed δD profiles. The program was written for use with the Microsoft Fortran package for IBM PC's or compatibles. The program is interactive to the user.

```
C
C                    PROGRAM SIMASSB.FOR
C
C  TO CALCULATE AN EFFECTIVE ISOTOPIC COMPOSITION OF INFILTRATION
C  WATER δD OR δ18O VALUE FROM CHANGING PROFILES BY A MASS
C  BALANCE TECHNIQUE
C
C                         WRITTEN BY
C                    ROBERT G. KNOWLTON, JR.
C
C
      DIMENSION DELD1(40),ZZ1(40),TH1(40),TH2(40),
     1      DELD2(40),ZZ2(40),DF(80),DI(80),THI(80),THF(80),
     2      VMI(80),VMF(80),VMP(80),XTP(80),DCALC(20),ZMB(20),
     3      DMBI(20),DMBP(20),DMBF(20),XMBI(20),XMBP(20),
     4      XMBF(20),THBI(20),THBP(20),THBF(20)
      DIMENSION P(200),A(10,10),AC(10,10),X(20)
      DIMENSION B(10),Z(20),Y(20),BV(10),BMIN(10),BMAX(10)
      COMMON /PAWG/X,XMBI,XMBP,XMBF,DMBI
      CHARACTER*20 FILIN1,FILIN2, FILOUT,FILPLT
      CHARACTER*30 TITLE
      WRITE(*,205)
      WRITE(*,206)
      WRITE(*,*)'GIVE A TITLE (MAX 30 CHARACTERS):'
      READ(*,109)TITLE
 109  FORMAT(A30)
      WRITE(*,*)'GIVE THE INPUT FILE NAME:'
      READ(*,209)FILIN1
 209  FORMAT(A20)
      WRITE(*,*)'GIVE THE OUTPUT FILE NAME:'
      READ(*,209)FILOUT
      WRITE(*,*)'GIVE THE PLOTTING OUTPUT FILE NAME:'
      READ(*,209)FILPLT
      OPEN(UNIT=20,FILE=FILIN1,STATUS='OLD')
      OPEN(UNIT=22,FILE=FILOUT,STATUS='UNKNOWN')
      OPEN(UNIT=23,FILE=FILPLT,STATUS='UNKNOWN')
C
      WRITE(22,205)
      WRITE(22,206)
 205  FORMAT(/,28X,'PROGRAM SIMASSB.FOR',//,12X,
     1      ' TO PERFORM MASS BALANCE CALCULATIONS',1X,
     2      'ON CHANGING ISOTOPE',/,24X,
     3      'PROFILES TO DETERMINE THE INPUT COMPOSITION',/)
 206  FORMAT(35X,'WRITTEN BY',/,28X,
     1      'ROBERT G. KNOWLTON, JR.',//)
      WRITE(22,109)TITLE
C READ IN INPUT DATA
      WRITE(*,*)'HOW MANY INPUT POINTS IN THE FIRST SET OF DATA?'
      READ(*,*)NPTS1
      WRITE(*,*)'HOW MANY INPUT POINTS IN THE SECOND SET OF DATA?'
      READ(*,*)NPTS2
      WRITE(*,*)'HOW MANY INPUT POINTS IN THE Z ARRAY?'
```

```
      READ(*,*)NXTP
      WRITE(*,*)'HOW MANY OUTPUT POINTS?'
      READ(*,*)NMB
      NN=NMB
      KK=1
      DO 106 I=1,NPTS1
      READ(20,*)ZZ1(I),DELD1(I),TH1(I)
      DELD1(I)=DELD1(I)*1000
 106  CONTINUE
      DO 107 I=1,NPTS2
      READ(20,*)ZZ2(I),DELD2(I),TH2(I)
      DELD2(I)=DELD2(I)*1000
 107  CONTINUE
      READ(20,*)(XTP(I),I=1,NXTP)
      READ(20,*)(ZMB(I),I=1,NMB+1)
C ASSUMING THAT Z(0)=0, LAND SURFACE, THEN ZZ1(1) OR ZZ2(1) IS
C THE BOTTOM OF THE FIRST DEPTH INTERVAL, WITHIN WHICH THE AVERAGE
C VALUES OF DELD1(1), DELD2(1), TH1(1), AND TH2(1) OCCUR
      XTP(0)=0
      DI(0)=DELD1(1)
      DF(0)=DELD2(1)
      DO 108 I=1,NXTP
      DI(I)=DI(I-1)
      DF(I)=DF(I-1)
      THI(I)=THI(I-1)
      THF(I)=THF(I-1)
      DO 113 J=1,NPTS1
      IF(ZZ1(J).LE.XTP(I).AND.ZZ1(J).GT.XTP(I-1))DI(I)=DELD1(J)
      IF(ZZ1(J).LE.XTP(I).AND.ZZ1(J).GT.XTP(I-1))THI(I)=TH1(J)
 113  CONTINUE
      DO 110 K=1,NPTS2
      IF(ZZ2(K).LE.XTP(I).AND.ZZ2(K).GT.XTP(I-1))DF(I)=DELD2(K)
      IF(ZZ2(K).LE.XTP(I).AND.ZZ2(K).GT.XTP(I-1))THF(I)=TH2(K)
 110  CONTINUE
 108  CONTINUE
      DO 111 I=1,NXTP
      VMI(I)=THI(I)*(XTP(I)-XTP(I-1))
      VMF(I)=THF(I)*(XTP(I)-XTP(I-1))
      VMP(I)=(THF(I)-THI(I))*(XTP(I)-XTP(I-1))
 111  CONTINUE
      DO 131 I=1,NMB
      DMBI(I)=0
      DMBF(I)=0
      XMBI(I)=0
      XMBP(I)=0
      XMBF(I)=0
      THBI(I)=0
      THBP(I)=0
      THBF(I)=0
      DO 114 J=1,NXTP
      IF(XTP(J).LE.ZMB(I+1).AND.XTP(J).GT.ZMB(I))XMBI(I)=
     1XMBI(I)+VMI(J)
```

```
      IF(XTP(J).LE.ZMB(I+1).AND.XTP(J).GT.ZMB(I))XMBF(I)=
     1XMBF(I)+VMF(J)
      IF(XTP(J).LE.ZMB(I+1).AND.XTP(J).GT.ZMB(I))DMBI(I)=
     1DMBI(I)+(DI(J)*(XTP(J)-XTP(J-1)))
      IF(XTP(J).LE.ZMB(I+1).AND.XTP(J).GT.ZMB(I))DMBF(I)=
     1DMBF(I)+(DF(J)*(XTP(J)-XTP(J-1)))
 114  CONTINUE
 131  CONTINUE
      TOTW=0
      DO 116 I=1,NMB
      TOTW=TOTW+(XMBF(I)-XMBI(I))
 116  CONTINUE
      XMBP(0)=TOTW
C STEP 1 - MASS BALANCE
      DO 184 I=1,NMB
      XMBO=XMBI(I)+XMBP(I-1)-XMBF(I)
      XMBP(I)=XMBO
C STEP 2 - MIXING
C     XMBV=XMBO+XMBF(I)
 184  CONTINUE
      DO 115 I=1,NMB
      THBI(I)=XMBI(I)/(ZMB(I+1)-ZMB(I))
      THBP(I)=XMBP(I)/(ZMB(I+1)-ZMB(I))
      THBF(I)=XMBF(I)/(ZMB(I+1)-ZMB(I))
      DMBI(I)=DMBI(I)/(ZMB(I+1)-ZMB(I))
      DMBF(I)=DMBF(I)/(ZMB(I+1)-ZMB(I))
      X(I)=DMBI(I)
      Y(I)=DMBF(I)
 115  CONTINUE
      BMIN(1)=-300.
      BMAX(1)=300.
      WRITE(*,*)'Give a value for δD of the percolate: '
      READ(*,*)BWAP
      B(1)=BWAP
C
C MARQUARDT SOLUTION
C
C
      FNU=0.0
      FLA=0.0
      TAU=0.0
      EPS=0.0
      PHMIN=0.0
      I=0
      KD=KK
      FV=0.0
      DO 100 J=1,KK
      BV(J)=1
 100  CONTINUE
      ICON=KK
      ITER=0
      WRITE(22,15)
```

```
 15   FORMAT(//,10X,'BSOLVE REGRESSION ALGORITHM',//,
     1       ' ITERATION',4X,'ICON',8X,'PH',10X,'B(1)',
     2       /,'   NUMBER',/)
 200  CALL BSOLVE(KK,B,NN,Z,Y,PH,FNU,FLA,TAU,EPS,PHMIN,I,ICON,FV,DV,
     1       BV,BMIN,BMAX,P,KD,A,AC,GAMM)
C
      ITER=ITER+1
      WRITE(22,136)ITER,ICON,PH,B(1)
 136  FORMAT(3X,I3,10X,I3,1X,E14.4,1X,F10.4)
      IF(ICON)10,300,200
 10   IF(ICON+1)20,60,200
 20   IF(ICON+2)30,70,200
 30   IF(ICON+3)40,80,200
 40   IF(ICON+4)50,90,200
 50   GO TO 95
 60   WRITE(22,4)
 4    FORMAT(//,2X,'NO FUNCTION IMPROVEMENT POSSIBLE')
      GO TO 300
 70   WRITE(22,5)
 5    FORMAT(//,2X,'MORE UNKNOWNS THAN FUNCTIONS')
      GO TO 300
 80   WRITE(22,6)
 6    FORMAT(//,2X,'TOTAL VARIABLES ARE ZERO')
      GO TO 300
 90   WRITE(22,7)
 7    FORMAT(//,2X,'CORRECTIONS SATISFY CONVERGENCE'
     1       1X,'REQUIREMENTS BUT LAMDA FACTOR (FLA) STILL LARGE')
      GO TO 300
 95   WRITE(22,8)
 8    FORMAT(//,2X,'THIS IS NOT POSSIBLE')
      GO TO 300
 300  WRITE(22,2)
 2    FORMAT(//,2X,'SOLUTIONS OF THE EQUATIONS')
      DO 400 J=1,KK
      WRITE(22,3)J,B(J)
 3    FORMAT(/,2X,'B(',I2,') = ',E16.8,//)
 400  CONTINUE
C PRINT OUT MASS BALANCE STUFF
      WRITE(22,*)'     MASS BALANCE CALCS'
      WRITE(22,*)'  '
      WRITE(22,*)' TOTAL MASS DIFFERENCE = ',TOTW
      WRITE(22,*)'  '
      WRITE(22,*)'  DEPTH (cm)       CHANGE IN MASS (g/cm^2)'
      WRITE(22,*)'  '
      DO 163 I=0,NMB
      XTR=XMBF(I)-XMBI(I)
      WRITE(22,*)ZMB(I),XTR
 163  CONTINUE
      WRITE(22,23)ZMB(1)
C CALCULATE THE FINAL FITTED DATA
      CALL EQN(KK,B,NN,Z,FV)
      SUM=0
```

```
C CALCULATE THE SUM OF THE SQUARES OF THE RESIDUALS
      DO 350 I=1,NN
      DCALC(I)=Z(I)
      DMIND=DMBF(I)-DCALC(I)
      SUM=SUM+(DMIND**2)
      WRITE(22,25)ZMB(I+1),DMBI(I),DMBF(I),DCALC(I),DMIND
      WRITE(23,25)ZMB(I+1),DMBI(I),DMBF(I),DCALC(I),DMIND
 350  CONTINUE
      WRITE(22,26)B(1)
      WRITE(22,27)SUM
 23   FORMAT(///,' RESULTS OF MODEL FIT FOR DEUTERIUM DATA',
     1      //,2X,'DEPTH',4X,'δD (initial)',4X,'δD (final)',
     2      4X,'δD (calc)',5X,'RESIDUAL',//,F7.3)
 25   FORMAT(F7.3,2X,F10.1,2X,F10.1,2X,F10.1,2X,F10.4)
 26   FORMAT(//,5X,'δD of infiltrating water = ',F10.4,/)
 27   FORMAT(5X,'SUM OF THE SQUARES OF THE RESIDUALS = ',
     1      1P,E10.3,//)
 29   FORMAT(F7.1,1X,F7.1,1X,F6.3)
C
      END
C
C SUBROUTINE EQN
C
      SUBROUTINE EQN(KK,B,NN,Z,FV)
      DIMENSION X(20),Z(20),B(10),XMBI(20),XMBP(20),
     1      XMBF(20),DMBI(20),DCALC(20),DMBP(20)
      COMMON /PAWG/X,XMBI,XMBP,XMBF,DMBI
C
C
C CALCULATE THE MODEL δD VALUES
C
      DMBP(0)=B(1)
      DO 30 I=1,NN
C STEP 1 - MASS BALANCE
      XMBO=XMBP(I-1)+XMBI(I)-XMBF(I)
C STEP 2 - MIXING
      XMBV=XMBO+XMBF(I)
      E1=DMBI(I)*XMBI(I)
      E2=DMBP(I-1)*XMBP(I-1)
      DCALC(I)=(E1+E2)/XMBV
      DMBP(I)=DCALC(I)
 30   CONTINUE
      DO 100 JJ=1,NN
      Z(JJ)=DCALC(JJ)
 100  CONTINUE
C
      RETURN
      END
C
C SUBROUTINE BSOLVE
C
      SUBROUTINE BSOLVE(KK,B,NN,Z,Y,PH,FNU,FLA,TAU,EPS,
```

```
     1       PHMIN,I,ICON,FV,DV,BV,BMIN,BMAX,P,KD,
     2       A,AC,GAMM)
      DIMENSION B(10),Z(20),Y(20),BV(10),BMIN(10),BMAX(10)
      DIMENSION P(200),A(10,10),AC(10,10),X(20),FV(10),DV(10)
C
      K=KK
      N=NN
      Y1=Y(1)
      KP1=K+1
      KP2=KP1+1
      KBI1=K*N
      KBI2=KBI1+K
      KZI=KBI2+K
      IF(FNU.LE.0.)FNU=10.0
      IF(FLA.LE.0.)FLA=0.01
      IF(TAU.LE.0.)TAU=0.001
      IF(EPS.LE.0.)EPS=0.00002
      IF(PHMIN.LE.0.)PHMIN=0.0
  120 KE=0
  130 DO 160 I1=1,K
  160 IF(BV(I1).NE.0.)KE=KE+1
      IF(KE.GT.0)GO TO 170
  162 ICON=-3
  163 GO TO 2120
  170 IF(N.GE.KE)GO TO 500
  180 ICON=-2
  190 GO TO 2120
  500 I1=1
  530 IF(I.GT.0)GO TO 1530
  550 DO 560 J1=1,K
      J2=KBI1+J1
      P(J2)=B(J1)
      J3=KBI2+J1
  560 P(J3)=ABS(B(J1))+1.0E-2
C 560 P(J3)=ABS(B(J1))+1.0E-4
      GO TO 1030
  590 IF(PHMIN.GT.PH.AND.I.GT.1)GO TO 625
      DO 620 J1=1,K
      N1=(J1-1)*N
      IF(BV(J1))601,620,605
C 601 CALL DERIV(K,B,N,Z,P(N1+1),FV,DV,J1,JTEST)
  601 WRITE(*,*)'NEED A DERIVATIVE FUNCTION!!!!'
      IF(JTEST.NE.(-1))GO TO 620
      BV(J1)=1.0
  605 DO 606 J2=1,K
      J3=KBI1+J2
  606 P(J3)=B(J2)
      J3=KBI1+J1
      J4=KBI2+J1
      DEN=0.001*AMAX1(P(J4),ABS(P(J3)))
      IF(P(J3)+DEN.LE.BMAX(J1))GO TO 55
      P(J3)=P(J3)-DEN
```

```
      DEN=-DEN
      GO TO 56
   55 P(J3)=P(J3)+DEN
   56 CALL EQN(K,P(KBI1+1),N,P(N1+1),FV)
      DO 610 J2=1,N
      JB=J2+N1
  610 P(JB)=(P(JB)-Z(J2))/DEN
  620 CONTINUE
C
C SET UP CORRECTION EQUATIONS
C
  625 DO 725 J1=1,K
      N1=(J1-1)*N
      A(J1,KP1)=0.
      IF(BV(J1))630,692,630
  630 DO 640 J2=1,N
      N2=N1+J2
  640 A(J1,KP1)=A(J1,KP1)+P(N2)*(Y(J2)-Z(J2))
  650 DO 680 J2=1,K
  660 A(J1,J2)=0.
  665 N2=(J2-1)*N
  670 DO 680 J3=1,N
  672 N3=N1+J3
  674 N4=N2+J3
  680 A(J1,J2)=A(J1,J2)+P(N3)*P(N4)
      IF(A(J1,J1).GT.1.E-20)GO TO 725
  692 DO 694 J2=1,KP1
  694 A(J1,J2)=0.
  695 A(J1,J1)=1.0
  725 CONTINUE
      GN=0.
      DO 729 J1=1,K
  729 GN=GN+A(J1,KP1)**2
C
C SCALE CORRECTION EQUATIONS
C
      DO 726 J1=1,K
  726 A(J1,KP2)=SQRT(A(J1,J1))
      DO 727 J1=1,K
      A(J1,KP1)=A(J1,KP1)/A(J1,KP2)
      DO 727 J2=1,K
  727 A(J1,J2)=A(J1,J2)/(A(J1,KP2)*A(J2,KP2))
  730 FL=FLA/FNU
      GOTO 810
  800 FL=FNU*FL
  810 DO 840 J1=1,K
  820 DO 830 J2=1,KP1
  830 AC(J1,J2)=A(J1,J2)
  840 AC(J1,J1)=AC(J1,J1)+FL
C
C SOLVE CORRECTION EQUATIONS
C
```

```
      DO 930 L1=1,K
      L2=L1+1
      DO 910 L3=L2,KP1
  910 AC(L1,L3)=AC(L1,L3)/AC(L1,L1)
      DO 930 L3=1,K
      IF(L1-L3)920,930,920
  920 DO 925 L4=L2,KP1
  925 AC(L3,L4)=AC(L3,L4)-AC(L1,L4)*AC(L3,L1)
  930 CONTINUE
C
      DN=0.
      DG=0.
      DO 1028 J1=1,K
      AC(J1,KP2)=AC(J1,KP1)/A(J1,KP2)
      J2=KBI1+J1
      P(J2)=AMAX1(BMIN(J1),AMIN1(BMAX(J1),B(J1)+AC(J1,KP2)))
      DG=DG+AC(J1,KP2)*A(J1,KP1)*A(J1,KP2)
      DN=DN+AC(J1,KP2)*AC(J1,KP2)
 1028 AC(J1,KP2)=P(J2)-B(J1)
      COSG=DG/SQRT(DN*GN)
      JGAM=0
      IF(COSG)1100,1110,1110
 1100 JGAM=2
      COSG=-COSG
 1110 CONTINUE
      COSG=AMIN1(COSG,1.0)
      GAMM=ARCOS(COSG)*180./(3.14159265)
      IF(JGAM.GT.0)GAMM=180.-GAMM
 1030 CALL EQN(K,P(KBI1+1),N,P(KZI+1),FV)
 1500 PHI=0.
      DO 1520 J1=1,N
      J2=KZI+J1
 1520 PHI=PHI+(P(J2)-Y(J1))**2
      IF(PHI.LT.1.E-10)GOTO 3000
      IF(I.GT.0)GOTO 1540
 1521 ICON=K
      GOTO 2110
 1540 IF(PHI.GE.PH)GOTO 1530
C
C EPSILON TEST
C
 1200 ICON=0
      DO 1220 J1=1,K
      J2=KBI1+J1
 1220 IF(ABS(AC(J1,KP2))/(TAU+ABS(P(J2))).GT.EPS)ICON=ICON+1
      IF(ICON.EQ.0)GOTO 1400
C
C GAMMA LAMBDA TEST
C
      IF(FL.GT.1.0.AND.GAMM.GT.90.0) ICON=-1
      GOTO 2105
C
```

```
C GAMMA EPSILON TEST
C
 1400 IF(FL.GT.1.0.AND.GAMM.LE.45.0) ICON=-4
      GOTO 2105
C
 1530 IF(I1-2)1531,1531,2310
 1531 I1=I1+1
      GOTO (530,590,800),I1
 2310 IF(FL.LT.1.0E+8)GOTO 800
 1320 ICON=-1
C
 2105 FLA=FL
      DO 2091 J2=1,K
      J3=KBI1+J2
 2091 B(J2)=P(J3)
 2110 DO 2050 J2=1,N
      J3=KZI+J2
 2050 Z(J2)=P(J3)
      PH=PHI
      I=I+1
 2120 RETURN
 3000 ICON=0
      GOTO 2105
C
      END
C
C
      FUNCTION ARCOS(Z)
C
      X=Z
      KEY=0
      IF(X.LT.(-1.))X=-1.
      IF(X.GT.1.)X=1.
      IF(X.GE.(-1.).AND.X.LT.0.)KEY=1
      IF(X.LT.0.)X=ABS(X)
      IF(X.EQ.0.)GOTO 10
      ARCOS=ATAN(SQRT(1.-X*X)/X)
      PIE=3.14159265
      D1=ARCOS
      IF(KEY.EQ.1)ARCOS=PIE-D1
      GOTO 999
 10   ARCOS=1.5707963
C
 999  RETURN
      END
```

C.4 Thermal Conductivity Program

The following program listing of TCCALC.FOR is intended for use in optimizing shape factors in predicting thermal conductivity measurements by the DeVries (1963) method. The program was written for use with the Microsoft Fortran package for IBM PC's or compatibles. The program is interactive to the user.

```
C
C              PROGRAM TCCALC.FOR
C
C  TO MATCH IN-SITU THERMAL CONDUCTIVITY DATA TO THE
C  DEVRIES (1963) MODEL
C
C                    WRITTEN BY
C               ROBERT G. KNOWLTON, JR.
C
C
      DIMENSION DELD1(40),ZZ1(40),TH1(40),TH2(40),
     1      DELD2(40),ZZ2(40),DF(80),DI(80),THI(80),THF(80),
     2      VMI(80),VMF(80),VMP(80),XTP(80),DCALC(80)
      DIMENSION P(400),A(10,10),AC(10,10),X(80)
      DIMENSION B(10),Z(80),Y(80),BV(10),BMIN(10),BMAX(10)
      COMMON X
      CHARACTER*20 FILIN1,FILIN2, FILOUT,FILPLT
      CHARACTER*30 TITLE
      WRITE(*,205)
      WRITE(*,206)
      WRITE(*,*)'GIVE A TITLE (MAX 30 CHARACTERS):'
      READ(*,109)TITLE
  109 FORMAT(A30)
  209 FORMAT(A20)
      WRITE(*,*)'GIVE THE OUTPUT FILE NAME:'
      READ(*,209)FILOUT
      WRITE(*,*)'GIVE THE PLOTTING OUTPUT FILE NAME:'
      READ(*,209)FILPLT
      OPEN(UNIT=22,FILE=FILOUT,STATUS='UNKNOWN')
      OPEN(UNIT=23,FILE=FILPLT,STATUS='UNKNOWN')
C
      WRITE(22,205)
      WRITE(22,206)
  205 FORMAT(/,28X,'PROGRAM TCCALC.FOR',//,12X,
     1      ' TO CALCULATE COEFFICIENTS TO PREDICT THERMAL',1X,
     2      'CONDUCTIVITY',/)
  206 FORMAT(35X,'WRITTEN BY',/,28X,
     1      'ROBERT G. KNOWLTON, JR.',//)
      WRITE(22,109)TITLE
      NN=3
      KK=2
      X(1)=0.0285
      Y(1)=.000878
      X(2)=0.0674
      Y(2)=.0019
      X(3)=0.0883
      Y(3)=.002
      DO 108 I=1,3
      DF(I)=Y(I)
      XTP(I)=X(I)
  108 CONTINUE
C
```

```
C B(1) = ks, B(2) = ka
      BMIN(1)=0
      BMAX(1)=40
      WRITE(*,*)'Give a value for ks: '
      READ(*,*)BWAP1
      B(1)=BWAP1
      BMIN(2)=0
      BMAX(2)=500
      WRITE(*,*)'Give a value for ka: '
      READ(*,*)BWAP2
      B(2)=BWAP2
C
C MARQUARDT SOLUTION
C
C
      FNU=0.0
      FLA=0.0
      TAU=0.0
      EPS=0.0
      PHMIN=0.0
      I=0
      KD=KK
      FV=0.0
      DO 100 J=1,KK
      BV(J)=1
  100 CONTINUE
      ICON=KK
      ITER=0
      WRITE(22,15)
   15 FORMAT(//,10X,'BSOLVE REGRESSION ALGORITHM',//,
     1       ' ITERATION',4X,'ICON',8X,'PH',10X,'B(1)',10X,'B(2)'
     2       ,/,'   NUMBER',/)
  200 CALL BSOLVE(KK,B,NN,Z,Y,PH,FNU,FLA,TAU,EPS,PHMIN,I,ICON,FV,DV,
     1       BV,BMIN,BMAX,P,KD,A,AC,GAMM)
C
      ITER=ITER+1
      WRITE(22,136)ITER,ICON,PH,B(1),B(2)
  136 FORMAT(3X,I3,10X,I3,1X,E14.4,1X,F10.4,1X,F10.4)
      IF(ICON)10,300,200
   10 IF(ICON+1)20,60,200
   20 IF(ICON+2)30,70,200
   30 IF(ICON+3)40,80,200
   40 IF(ICON+4)50,90,200
   50 GO TO 95
   60 WRITE(22,4)
    4 FORMAT(//,2X,'NO FUNCTION IMPROVEMENT POSSIBLE')
      GO TO 300
   70 WRITE(22,5)
    5 FORMAT(//,2X,'MORE UNKNOWNS THAN FUNCTIONS')
      GO TO 300
   80 WRITE(22,6)
    6 FORMAT(//,2X,'TOTAL VARIABLES ARE ZERO')
```

```
      GO TO 300
 90   WRITE(22,7)
 7    FORMAT(//,2X,'CORRECTIONS SATISFY CONVERGENCE'
     1      1X,'REQUIREMENTS BUT LAMDA FACTOR (FLA) STILL LARGE')
      GO TO 300
 95   WRITE(22,8)
 8    FORMAT(//,2X,'THIS IS NOT POSSIBLE')
      GO TO 300
 300  WRITE(22,2)
 2    FORMAT(//,2X,'SOLUTIONS OF THE EQUATIONS')
      DO 400 J=1,KK
      WRITE(22,3)J,B(J)
 3    FORMAT(/,2X,'B(',I2,') = ',E16.8)
 400  CONTINUE
      WRITE(22,23)
C CALCULATE THE FINAL FITTED DATA
      CALL EQN(KK,B,NN,Z,FV,VMI,VMP,VMF,DI)
      SUM=0
C CALCULATE THE SUM OF THE SQUARES OF THE RESIDUALS
      DO 350 I=1,NN
      DCALC(I)=Z(I)
      DMIND=DF(I)-DCALC(I)
      SUM=SUM+(DMIND**2)
      WRITE(22,25)XTP(I),DF(I),DCALC(I),DMIND
      WRITE(23,25)XTP(I),DF(I),DCALC(I),DMIND
 350  CONTINUE
      WRITE(22,26)B(1),B(2)
      WRITE(22,27)SUM
 23   FORMAT(//,' RESULTS OF MODEL FIT FOR THERMAL CONDUCTIVITY',
     1      //,2X,'DEPTH',9X,'δD',
     2      8X,'δD (calc)',5X,'RESIDUAL',/)
 25   FORMAT(F8.4,2X,1P,E10.3,2X,E10.3,2X,E10.3)
 26   FORMAT(//,5X,'ks = ',F10.4,/,5x,'ka = ',f10.4)
 27   FORMAT(5X,'SUM OF THE SQUARES OF THE RESIDUALS = ',
     3      1P,E10.3,//)
 29   FORMAT(F7.1,1X,F7.1,1X,F6.3)
C
      END
C
C SUBROUTINE EQN
C
      SUBROUTINE EQN(KK,B,NN,Z,FV,VMI,VMP,VMF,DI)
      DIMENSION X(80),Z(80),B(10),VMI(80),VMP(80),
     1      VMF(80),DI(80),DCALC(80)
      COMMON X
C
C
      DO 30 I=1,NN
      E1=(B(1)*0.0189)+(X(I)*0.00137)
      E2=B(2)*(0.37-X(I))*0.00006
      E3=X(I)+(B(1)*0.63)+(B(2)*(0.37-X(I)))
      DCALC(I)=(E1+E2)/E3
```

```
 30   CONTINUE
      DO 100 JJ=1,NN
      Z(JJ)=DCALC(JJ)
 100  CONTINUE
C
      RETURN
      END
C
C SUBROUTINE BSOLVE
C
      SUBROUTINE BSOLVE(KK,B,NN,Z,Y,PH,FNU,FLA,TAU,EPS,
     1      PHMIN,I,ICON,FV,DV,BV,BMIN,BMAX,P,KD,
     2      A,AC,GAMM)
      DIMENSION B(10),Z(80),Y(80),BV(10),BMIN(10),BMAX(10)
      DIMENSION P(400),A(10,10),AC(10,10),X(80),FV(10),DV(10)
C
      K=KK
      N=NN
      Y1=Y(1)
      KP1=K+1
      KP2=KP1+1
      KBI1=K*N
      KBI2=KBI1+K
      KZI=KBI2+K
      IF(FNU.LE.0.)FNU=10.0
      IF(FLA.LE.0.)FLA=0.01
      IF(TAU.LE.0.)TAU=0.001
      IF(EPS.LE.0.)EPS=0.00002
      IF(PHMIN.LE.0.)PHMIN=0.0
 120  KE=0
 130  DO 160 I1=1,K
 160  IF(BV(I1).NE.0.)KE=KE+1
      IF(KE.GT.0)GO TO 170
 162  ICON=-3
 163  GO TO 2120
 170  IF(N.GE.KE)GO TO 500
 180  ICON=-2
 190  GO TO 2120
 500  I1=1
 530  IF(I.GT.0)GO TO 1530
 550  DO 560 J1=1,K
      J2=KBI1+J1
      P(J2)=B(J1)
      J3=KBI2+J1
 560  P(J3)=ABS(B(J1))+1.0E-4
      GO TO 1030
 590  IF(PHMIN.GT.PH.AND.I.GT.1)GO TO 625
      DO 620 J1=1,K
      N1=(J1-1)*N
      IF(BV(J1))601,620,605
C 601 CALL DERIV(K,B,N,Z,P(N1+1),FV,DV,J1,JTEST)
 601  WRITE(*,*)'NEED A DERIVATIVE FUNCTION!!!!'
```

```
      IF(JTEST.NE.(-1))GO TO 620
      BV(J1)=1.0
 605  DO 606 J2=1,K
      J3=KBI1+J2
 606  P(J3)=B(J2)
      J3=KBI1+J1
      J4=KBI2+J1
      DEN=0.001*AMAX1(P(J4),ABS(P(J3)))
      IF(P(J3)+DEN.LE.BMAX(J1))GO TO 55
      P(J3)=P(J3)-DEN
      DEN=-DEN
      GO TO 56
 55   P(J3)=P(J3)+DEN
 56   CALL EQN(K,P(KBI1+1),N,P(N1+1),FV,VMI,VMP,VMF,DI)
      DO 610 J2=1,N
      JB=J2+N1
 610  P(JB)=(P(JB)-Z(J2))/DEN
 620  CONTINUE
C
C SET UP CORRECTION EQUATIONS
C
 625  DO 725 J1=1,K
      N1=(J1-1)*N
      A(J1,KP1)=0.
      IF(BV(J1))630,692,630
 630  DO 640 J2=1,N
      N2=N1+J2
 640  A(J1,KP1)=A(J1,KP1)+P(N2)*(Y(J2)-Z(J2))
 650  DO 680 J2=1,K
 660  A(J1,J2)=0.
 665  N2=(J2-1)*N
 670  DO 680 J3=1,N
 672  N3=N1+J3
 674  N4=N2+J3
 680  A(J1,J2)=A(J1,J2)+P(N3)*P(N4)
      IF(A(J1,J1).GT.1.E-20)GO TO 725
 692  DO 694 J2=1,KP1
 694  A(J1,J2)=0.
 695  A(J1,J1)=1.0
 725  CONTINUE
      GN=0.
      DO 729 J1=1,K
 729  GN=GN+A(J1,KP1)**2
C
C SCALE CORRECTION EQUATIONS
C
      DO 726 J1=1,K
 726  A(J1,KP2)=SQRT(A(J1,J1))
      DO 727 J1=1,K
      A(J1,KP1)=A(J1,KP1)/A(J1,KP2)
      DO 727 J2=1,K
 727  A(J1,J2)=A(J1,J2)/(A(J1,KP2)*A(J2,KP2))
```

```
 730  FL=FLA/FNU
      GOTO 810
 800  FL=FNU*FL
 810  DO 840 J1=1,K
 820  DO 830 J2=1,KP1
 830  AC(J1,J2)=A(J1,J2)
 840  AC(J1,J1)=AC(J1,J1)+FL
C
C SOLVE CORRECTION EQUATIONS
C
      DO 930 L1=1,K
      L2=L1+1
      DO 910 L3=L2,KP1
 910  AC(L1,L3)=AC(L1,L3)/AC(L1,L1)
      DO 930 L3=1,K
      IF(L1-L3)920,930,920
 920  DO 925 L4=L2,KP1
 925  AC(L3,L4)=AC(L3,L4)-AC(L1,L4)*AC(L3,L1)
 930  CONTINUE
C
      DN=0.
      DG=0.
      DO 1028 J1=1,K
      AC(J1,KP2)=AC(J1,KP1)/A(J1,KP2)
      J2=KBI1+J1
      P(J2)=AMAX1(BMIN(J1),AMIN1(BMAX(J1),B(J1)+AC(J1,KP2)))
      DG=DG+AC(J1,KP2)*A(J1,KP1)*A(J1,KP2)
      DN=DN+AC(J1,KP2)*AC(J1,KP2)
 1028 AC(J1,KP2)=P(J2)-B(J1)
      COSG=DG/SQRT(DN*GN)
      JGAM=0
      IF(COSG)1100,1110,1110
 1100 JGAM=2
      COSG=-COSG
 1110 CONTINUE
      COSG=AMIN1(COSG,1.0)
      GAMM=ARCOS(COSG)*180./(3.14159265)
      IF(JGAM.GT.0)GAMM=180.-GAMM
 1030 CALL EQN(K,P(KBI1+1),N,P(KZI+1),FV,VMI,VMP,VMF,DI)
 1500 PHI=0.
      DO 1520 J1=1,N
      J2=KZI+J1
 1520 PHI=PHI+(P(J2)-Y(J1))**2
      IF(PHI.LT.1.E-10)GOTO 3000
      IF(I.GT.0)GOTO 1540
 1521 ICON=K
      GOTO 2110
 1540 IF(PHI.GE.PH)GOTO 1530
C
C EPSILON TEST
C
 1200 ICON=0
```

```
      DO 1220 J1=1,K
      J2=KBI1+J1
 1220 IF(ABS(AC(J1,KP2))/(TAU+ABS(P(J2))).GT.EPS)ICON=ICON+1
      IF(ICON.EQ.0)GOTO 1400
C
C GAMMA LAMBDA TEST
C
      IF(FL.GT.1.0.AND.GAMM.GT.90.0) ICON=-1
      GOTO 2105
C
C GAMMA EPSILON TEST
C
 1400 IF(FL.GT.1.0.AND.GAMM.LE.45.0) ICON=-4
      GOTO 2105
C
 1530 IF(I1-2)1531,1531,2310
 1531 I1=I1+1
      GOTO (530,590,800),I1
 2310 IF(FL.LT.1.0E+8)GOTO 800
 1320 ICON=-1
C
 2105 FLA=FL
      DO 2091 J2=1,K
      J3=KBI1+J2
 2091 B(J2)=P(J3)
 2110 DO 2050 J2=1,N
      J3=KZI+J2
 2050 Z(J2)=P(J3)
      PH=PHI
      I=I+1
 2120 RETURN
 3000 ICON=0
      GOTO 2105
C
      END
C
C
      FUNCTION ARCOS(Z)
C
      X=Z
      KEY=0
      IF(X.LT.(-1.))X=-1.
      IF(X.GT.1.)X=1.
      IF(X.GE.(-1.).AND.X.LT.0.)KEY=1
      IF(X.LT.0.)X=ABS(X)
      IF(X.EQ.0.)GOTO 10
      ARCOS=ATAN(SQRT(1.-X*X)/X)
      PIE=3.14159265
      D1=ARCOS
      IF(KEY.EQ.1)ARCOS=PIE-D1
      GOTO 999
 10   ARCOS=1.5707963
```

```
C
 999  RETURN
      END
```

REFERENCES

Allison, G.B. 1982. The relationship between ^{18}O and deuterium in water in sand columns undergoing evaporation. Journal of Hydrology. 55:163-169.

Allison, G.B., C.J.Barnes, and M.W.Hughes 1983. The distribution of deuterium and ^{18}O in dry soils: 2. Experimental. Journal of Hydrology. 64:377-397.

Allison, G.B., C.J.Barnes, M.W.Hughes, and F.W.J.Leaney 1984. The effect of climate and vegetation on oxygen-18 and deuterium profiles in soils. Isotope Hydrology 1983. IAEA, Vienna, 105-124.

Allison, G.B., and M.W.Hughes 1983. The use of natural tracers as indicators of soil-water movement in a temperate semi-arid region. Journal of Hydrology. 60:157-173.

Allison, G.B., W.J.Stone, and M.W.Hughes 1985. Recharge in karst and dune elements of a semi-arid landscape as indicated by natural isotopes and chloride. Journal of Hydrology. 76:1-26.

Barnes, C.J., and G.B.Allison 1983. The distribution of D and ^{18}O in dry soils: 1. Theory. Journal of Hydrology. 60:141-156.

Barnes, C.J., and G.B.Allison 1984. The distribution of deuterium and ^{18}O in dry soils: 3. Theory for non-isothermal water movement. Journal of Hydrology. 74:119-136.

Bath, A.H., W.G.Darline, and A.P.Brunsdon 1982. The stable isotope composition of infiltration moisture in the unsaturated zone of the English Chalk. Stable Isotopes, Proc. Fourth Inter. Conf., Julich, 23-26 March 1981 (Schmidt, H.-L., Forstel, H., and Heinzinger, K., editors), Analytical Chemistry Symposium Series, Vol. II, Elsevier, Amsterdam, p. 161-166.

Bergstrom, R.E., and R.E.Aten 1965. Natural recharge and localization of fresh water in Kuwait. Journal of Hydrology. 2:213-231.

Coleman, M.L., T.J.Shepherd, J.J.Durham, J.E.Rouse, and G.R.Moore 1982. Reduction of water with zinc for hydrogen isotope analysis. Analytical Chemistry. 54:993-995.

Craig, H. 1961. Isotopic variations in meteoric waters. Science. 133:1702-1703.

Dansgaard, W. 1964. Stable isotopes in precipitation. Tellus. 16:436-468.

DeVries, D.A. 1963. Thermal properties of soils. In: Physics of Plant Environment. Editor: W.R.VanWijk. North-Holland Publishing Co., Amsterdam. p. 210-235.

DeVries, D.A. and A.J.Peck 1958a. On the cylindrical probe method of measuring thermal conductivity with special reference to soils, I. Extension of theory and discussion of probe characteristics. Australian Journal of Physics. 11:255-271.

DeVries, D.A. and A.J.Peck 1958b. On the cylindrical probe method of measuring thermal conductivity with special reference to soils, II. Analysis of moisture effects. Australian Journal of Physics. 11:255-271.

DeVries, D.A. and J.R.Philip 1986. Soil heat flux, thermal conductivity, and the null-alignment method. Soil Science Society of America Journal. 50:12-18.

Dincer, T., A.Al-Mugrin, and U.Zimmerman 1974. Study of the infiltration and recharge through the sand dunes in arid zones, with special reference to the stable isotopes and thermonuclear tritium. Journal of Hydrology. 23:79-109.

Epstein, S., and T.Mayeda 1953. Variation of ^{18}O content of waters from natural sources. Geochimica et Cosmochimica Acta. 4:213-224.

Falconer, K.L., L.C.Hull, and S.A.Mizell 1982. A mathematical model for evaluating the suitability of a low-level radioactive waste site. In Waste Management '82 (Post, R.G., editor), Vol. 2, Proceedings of Symposium, Tucson, Arizona, 8-11 March 1982, p.245-258.

Foster, S.S.D., and A.Smith-Carrington 1980. The interpretation of tritium in the Chalk unsaturated zone. Journal of Hydrology. 46:343-364.

Graybill, F.A. 1961. An introduction to linear statistical models. New York: McGraw-Hill.

Grismer, M.E., D.B.McWhorter, and A.Klute 1986. Determination of diffusivity and hydraulic conductivity in soils at low water contents from nondestructive transient flow observations. Soil Science. 141(1): 10-19.

Horton, R. and P.J.Wierenga 1984. The effect of column wetting on soil thermal conductivity. Soil Science. 138(2):102-108.

Jackson, R.D., B.A.Kimball, R.J.Reginato, and F.S.Nakayama 1973. Diurnal Soil-Water Evaporation: Time-Depth-Flux Patterns. Soil Science Society of America Proceedings. 37:505-509.

Jaynes, D.B. and A.S.Rogowski 1983. Applicability of Fick's law to gas diffusion. Soil Science Society of America Journal. 47:425-430.

Kendall, C., and T.B.Coplen 1985. Multisample conversion of water to hydrogen by zinc for stable isotope determination. Analytical Chemistry. June 1985, p.1437-1446.

Kirk-Othmer 1983. Encyclopedia of Chemical Technology. 23:246-273. New York: John Wiley & Sons.

Knowlton, R.G.,Jr., F.M.Phillips, and A.R.Campbell 1989. A stable-isotope investigation of water vapor during ground-water recharge in New Mexico. Technical Completion Report No. 237, New Mexico Water Resources Research Institute, New Mexico State University, Las Cruces, NM, 88p.

Machette, M.N. 1978. Geologic map of the San Acacia quadrangle, Socorro County, New Mexico. U.S. Geological Survey, Geologic Quadrangle Map GQ-1415.

Majoube, M. 1971. Fractionnement en oxygene 18 et en deuterium entre l'eau et sa vapeur. Journal of Chemical Physics. 68:1423-1436.

Mann, J.F., Jr. 1976. Waste waters in the vadose zone of arid regions: Hydrologic interactions. Groundwater. 14:367-372.

Mattick, J.L., F.M.Phillips, and T.A.Duval. 1986. Quantification of ground-water recharge rates in New Mexico using bomb-36Cl and bomb-3H as soil-water tracers, New Mexico Water Resources Research Institute Technical Completion Report No. 220, New Mexico State University, Las Cruces, New Mexico.

Merlivat, L. 1979. Molecular diffusivities of $H_2{}^{16}O$, $HD^{16}O$ and $H_2{}^{18}O$ in gases. Journal Chemical Physics. 69:2864-2871.

Mills, R. 1973. Self diffusion in normal and heavy water in the range 1-45° C. Journal Chemical Physics. 77:685-688.

Philip, J.R. and D.A.de Vries 1957. Moisture movement in porous materials under temperature gradients. Transactions of the American Geophysical Union. 38:222-232.

Phillips, F.M., J.L.Mattick, and T.A.Duval 1988. Chlorine-36 and tritium from nuclear-weapons fallout as tracers for long-term liquid and vapor movement in desert soils. Water Resources Research. 24:1877-1891.

Phillips, F.M., K.N.Trotman, H.W.Bentley, and S.N.Davis 1983. ^{36}Cl, an environmental tracer for soil water. Proceedings of the National Conference on Advances in Infililtration. American Society of Agricultural Engineers, 12-13 December, Chicago.

Phillips, F.M., K.N.Trotman, H.W.Bentley, and S.N.Davis 1984. The bomb-^{36}Cl pulse as a tracer for soil-water movement near Socorro, New Mexico. Selected Papers on Water Quality and Pollution in New Mexico (Stone, W.B., ed.), New Mexico Bureau of Mines and Mineral Resources, Hydrologic Report 7, p.271-280.

Roether, W. 1970. Water-CO_2 exchange set-up for the routine ^{18}oxygen assay of natural waters. International Journal of Applied Radiation and Isotopes. 21:379-387.

Rose, C.W. 1968. Water transport in soil with a daily temperature wave. II. Analysis. Australian Journal of Soil Research. 6:45-47.

Saxena, R.K. 1984. Seasonal variations of oxygen-18 in soil moisture and estimation of recharge in esker and moraine formations. Nordic Hydrology. 15:235-242.

Saxena, R.K., and Z.Dressie 1983. Estimation of ground-water recharge and moisture movement in sandy formations by tracing natural oxygen-18 and injected tritium profiles in the unsaturated zone. Isotope Hydrology 1983. IAEA, Vienna, p.139-150.

Sharma, M.L. and M.W.Hughes 1985. Groundwater recharge estimation using chloride, deuterium and oxygen-18 profiles in the deep coastal sands of western Australia. Journal of Hydrology. 81:93-109.

Snedecor, G.W. and W.G. Cochran 1973. Statistical Methods. 6th edition, Iowa State University Press, Ames, Iowa.

Stephens, D.B. and R.G.Knowlton, Jr. 1986. Soil-water movement and recharge through sand at a semi-arid site in New Mexico. Water Resources Research. 22:881-889.

Stephens, D.B., R.G.Knowlton, Jr., J.McCord, and W.Cox 1985. Field study of natural ground water recharge in a semi arid lowland. New Mexico Water Resources Research Institute Technical Completion Report No. 177, New Mexico State University, Las Cruces, New Mexico.

Stone, W.J., and B.E.McGurk 1985. Ground-water recharge on the southern High Plains, east-central New Mexico. New Mexico Geological Society Guidebook, 36th Field Conference, Santa Rosa. p.331-336.

Taylor, S.A., and J.W.Carey 1964. Linear equations for the simultaneous flow of matter and energy in a continuous soil system. Soil Science Society of America Proceedings. 28:167-172.

Thoma, G., N.Esser, C.Sonntag, W.Weiss, J.Rudolph, and P.Leveque 1979. New techniques of in-situ soil moisture sampling for environmental isotope analysis applied at Pilat sand dune near Bordeaux. Isotope Hydrology Proceedings of the International Symposium. 1978, IAEA, 2:753-768.

Thorstenson,D.C. and D.W.Pollock 1989. Gas transport in unsaturated porous media: the adequacy of Fick's Law. Reviews of Geophysics. 27(1):61-78.

U.S. Department of Agriculture 1972. New Mexico water resources: assessment for planning purposes. 22 maps, Soil Conservation Service.

VanWijk, W.R. and D.A.DeVries 1963. Periodic temperature variations in a homogeneous Soil. In: Physics of Plant Environment. Editor: W.R.VanWijk. North-Holland Publishing Co., Amsterdam. p. 102-143.

Verhagen, B.Th., P.E.Smith, I.McGeorge, and Z.Dziembowski 1979. Tritium profiles in Kalahari sands as a measure of rain-water recharge. Isotope Hydrology, Proceedings of the International Symposium. 1978, IAEA, 2:733-751.

Vuataz, F.D., and F.Goff 1986. Isotope geochemistry of thermal and nonthermal waters in the Valles Caldera, Jemez Mountains, northern New Mexico. Journal of Geophysical Research. 91:1835-1854.

Weast, R.C. 1975. Handbook of Chemistry and Physics. Edited by R.C.Weast, 55th ed., Cleveland, Ohio: Chemical Rubber Company.

Zimmerman, U., D.Enhalt, and K.O.Munnich 1967. Soil-water movement and evapotranspiration: Changes in the isotopic composition of the water. Isotopes in Hydrology, 1966. Proceedings of the IAEA Symposium, Vienna, p.567-584.

This dissertation is accepted on behalf of the faculty of the Institute by the following committee:

Fred M. Phillips
Advisor

Fred M. Phillips

Daniel B. Stephens

Daniel B. Stephens

Andrew Campbell

Andrew Campbell

John L. Wilson

John L. Wilson

May 7, 1990
Date